FORCED CONVECTION HEAT TRANSFER IN PARALLEL PLATE CHANNELS PARTIALLY FILLED WITH POROUS MATERIAL

A THESIS SUBMITTED TO
NATIONAL INSTITUTE OF TECHNOLOGY WARANGAL, (T.S.)
FOR THE AWARD OF THE DEGREE OF

DOCTOR OF PHILOSOPHY
IN
MATHEMATICS

BY
J SHARATH KUMAR REDDY
(ROLL NO: 715079)

UNDER THE SUPERVISION OF
Dr. D. BHARGAVI

DEPARTMENT OF MATHEMATICS

NATIONAL INSTITUTE OF TECHNOLOGY

WARANGAL - 506 004 INDIA

MARCH, 2019

CERTIFICATE

This is to certify that the thesis entitled " **Forced Convection Heat Transfer in Parallel Plate Channels Partially Filled with Porous Material**" submitted to National Institute of Technology Warangal, India for the award of the degree of ***Doctor of Philosophy***, is the bonafide research work done by **Mr. J. SHARATH KUMAR REDDY** under my supervision. The contents of this thesis have not been submitted elsewhere for the award of any degree.

Dr. D. Bhargavi
(Supervisor)
Assistant Professor
Department of Mathematics
National Institute of Technology, Warangal
Telangana State, INDIA - 506004.

Date: 01-03-2019
Place: NIT Warangal

DECLARATION

This is to certify that the work presented in the thesis entitled " **Forced Convection Heat Transfer in Parallel Plate Channels Partially Filled with Porous Material**", is a bonafide work done by me under the supervision of **Dr. D. Bhargavi** and has not been submitted elsewhere for the award of any degree.

I declare that this written submission represents my ideas in my own words and where others' ideas or words have been included, I have adequately cited and referenced the original sources. I also declare that I have adhered to all principles of academic honesty and integrity and have not misrepresented or fabricated or falsified any idea / data / fact /source in my submission. I understand that any violation of the above will be a cause for disciplinary action by the Institute and can also evoke penal action from the sources which have thus not been properly cited or from whom proper permission has not been taken when needed.

J Sharath Kumar Reddy
(Roll No: 715079)
Date: 01-03-2019
Place: NIT Warangal

Dedicated to

my wife and son

Smt. Vishala and Sai Vaasvik Reddy

and

My Parents

ACKNOWLEDGEMENTS

It is a rare privilege and boon that I could associate myself for pursuing my research work with **Dr. D. Bhargavi**, Assistant Professor of Mathematics, National Institute of Technology, Warangal, India. I sincerely record my gratitude for her invaluable guidance and constant encouragement throughout the preparation of this thesis and her involvement and meticulous supervision while my work was in progress. I recall how my mentor persistently motivated me during the difficult moments of my research tenure by her astounding knowledge and sound logical sense. I cherish the kind support of my supervisor, philosopher and guide in all the ways. Her constant and critical evaluation during this period is thankfully acknowledged. I deem it a privilege to have worked under her amiable guidance.

Fellowship provided by GATE, India during the course of my research is gratefully acknowledged.

I thank the Doctoral Scrutiny Committee members, **Prof. J. V. Ramana Murthy, Prof. D. Srinivasacharya,** Department of Mathematics and **Prof. R.L.N. Sai Prasad,** Department of Physics for their constructive criticism at different stages of my research work.

It is a pleasure to express my thanks to **Prof. D. Srinivasacharya,** Head, Department of Mathematics, **Prof. G. Radhakrishnamacharya(Retd.), Prof. Y. N. Reddy, Prof. K. N. S. Kasi Viswanadham, Prof. D. Dutta, Dr. P. Muthu, Dr. A. Benarji Babu, Dr. H. P. Rani, Dr. R. S. Selvaraj, Dr. T. Kurmayya, Dr. J. Pranitha, Dr. Ch. Ram Reddy, Dr. E. Satyanarayana, Dr. Y. Sreenivasa Rao** and non teaching staff of the Department for their valuable suggestions, support and timely help.

I express my sincere thanks to **Dr. Ch. Sudhakar, Associate Professor,** Department of Computer Science Engineering. He generously provided the computational facility needed to carry out my doctoral research. I also thank **Dr. M. Raja**

Vishwanathan, Head, Department of Humanities and Social Sciences for his diligent proof reading of this thesis.

I also express my thanks to my co-research scholars **Dr. K. Appi Reddy, Dr. S. Mallishwar Reddy, Smt. S.V. Kiranmayi Ch, Mr. N.V. Koteswar Rao, Mr. G. Shiva Kumar Reddy, Mr. M. Pavan Kumar Reddy, Mr. I. Sreenath, Mr. P. Jagadeeshwar, Mr. P. Naveen Mr. K. Sita Ramana** and other scholars for their suggestions, technical help and encouragement during my research period. Also express my thanks to my best friends **Mr. P. Srenu, Mr. B. Kala Raman, Mr. P. Santhosh, Mr. B. Rajender, Mr. Nallapu Vijender, Mr. Naresh Yadav, Mr. Chirra Suman**, **Mr. Vijay Vardhan, Mr. G. Sreenivasulu** , **Mr. K. Naga Raju** and all other friends for their continuous support, encouragement to do this research work.

I express my sincere thanks to **Dr. P. Venkat Reddy**, Head, Department of Science and Humanities and Management of Sreenidhi Institute of Science and Technology for grateful support and encouragement for pursuing my Ph.D.

There are no words to express my sincere gratitude to my wife **Smt. Vishala**, loving son **Mr. Sai Vaasvik Reddy** and my parents **Sree Venkat Reddy**, **Smt. Bhagyamma** and all my family members, who supported me a lot throughout my academic career. Yours love and affection are the most important part of my life, which always encourages me to bravely chase my dream. Finally, I would like to take this opportunity to extend my heartfelt thanks to my father in law **Sree Shekar Reddy**, mother in law **Smt. Alivelamma** and other family members for their continuous support, encouragement cooperation to do this research work.

Finally, I bow down before the almighty that has made everything possible.

Place: NIT Warangal
Date: 01-03-2019 (J Sharath Kumar Reddy)

ABSTRACT

The objective of the present study has been to make available hydrodynamic and thermal characteristics of a Newtonian fluid for laminar incompressible flow in channels partially filled with porous material. The given amount of porous material porous layer was distributed equally at the two walls. Porous fraction, γ_p, is defined as the ratio of the porous layer thickness to the distance between the walls of the channel.

Analytical or numerical solutions have been obtained for the following values of the parameters characterizing the different problems studied. Porous fraction γ_p: $0 \le \gamma_p \le 1.0$, Darcy number, *Da*: 0.001 to 1.0. When magnetic field is considered, the Hartman number, *M* is between 1 to 10. When axial conduction is considered, the Peclet number, *Pe* ranges from 5 to 100. When viscous dissipation is included, the Brinkman number *Br* assumes a value between -1.0 and 1.0, i.e., $-1.0 \le Br \le 1.0$. Numerical solutions have been obtained employing Successive Accelerated Replacement scheme after validating the scheme.

As Hartmann number (Magnetic field parameter) *M* increases, the porous channel behaves like a clear fluid channel for all Darcy numbers. The magnetic field parameter is negligible in the fully filled porous region with such high Hartmann number.

Axial conduction effects are significant for *Pe* < 100 and become negligible even near the entry for *Pe* > 100 in channels partially filled with porous material. When viscous dissipation is included, the limiting bulk mean temperature is higher than the wall temperature. The local Nusselt number displays an unbounded swing since the bulk mean temperature reaches the wall temperature and exceeds it because of viscous dissipation.

Limiting temperature and limiting Nusselt number depend on the Brinkman number when the channel walls are subjected to constant wall heat flux. In the case of

constant wall temperate, limiting Nusselt number is independent of Brinkman number for $Br \neq 0$.

Developed flow depends on *Da*, γ_p and developing temperature field depends on *Da*, γ_p, *Pe*, and *Br*. Local Nusselt number, Nu_{px} is significantly large when *Pe* is low. Nu_{px} decreases with increasing X^*. Influence of axial conduction, viscous dissipation and developing thermal field on temperature profiles and local Nusselt number, have been evaluated when different models have been employed. The local Nusselt number attains a minimum for some, $0 < \gamma_p < 1.0$ (subjected to constant wall heat flux). It has been found that minimum value of γ_p is practically independent of the axial location and Peclet number.

Effects of viscous dissipation employing Darcy model and the clear fluid compatible model have been studied. The results include the effects of viscous dissipation on temperature profiles and Nusselt numbers. In general the effects of axial conduction are subdued when viscous dissipation is strong and vice versa.

N O M E N C L A T U R E

A_c	Axial conduction	h_{px}	Local heat transfer coefficient, at the porous wall, W/m^{2}K
A_i	Constants which are given in appendix.	H	Width of the channel, m
$\overline{B}$	Magnetic induction vector, $\left\|\overline{B}\right\| = B_0$, kgs^{-2}A^{-1}	$\overline{J}$	Electric current density, A/m^2
Br	Brinkman number, $Br = \frac{\mu_f u_{ref}{}^2}{qH}$ (subjected to constant wall heat flux), $Br = \frac{\mu_f u_{ref}{}^2}{k_f \left(T_e - T_w\right)}$ (subjected to constant wall temperature)	K	Permeability, m^2
c	Constant less than unity	k_f	Thermal conductivity in fluid region, W/(m. K)
C_p	Specific heat, J / g °C	k_{eff}	Effective thermal conductivity in porous region, $k_{eff} = (1-\varphi)\, k_s + \varphi\, k_f$, W/(m. K)
C_{fp}	Skin friction coefficient	k_s	Thermal conductivity of the solid, W/(m. K)
Da	Darcy number, $Da = K / H^2$	l_p	Thickness of the porous region, m
Fc	Forchheimer number	M	Hartmann number(Magnetic field parameter), $M = \sqrt{\frac{\sigma B_0{}^2 H^2}{\mu_f}}$
F_L	Lorentz forces, $F_L = \overline{J} \times \overline{B}$	MD	Number of divisions in the axial distance (X) direction
G	Acceleration due to gravity, m/s^2	m_1	Slope of the Darcy model
h_p	Heat transfer coefficient, W/m^{2}K	m_2	Slope of the form drag model

m_3	Slope of the clear fluid compatible model	Re	Reynolds number, $Re = \rho u_{ref} H / \mu_f$
N	Grid number in the computational mess corresponding to non-dimensional normal coordinate Y	T_b	Bulk mean temperature, K
ND	Number of divisions in the normal(Y) direction	T_e	Inlet temperature, K
NP	Grid number at the porous-fluid interface	T_i	Interfacial temperature, K
$Nu_{p,CL1}$	Nusselt number due to Darcy model	T_f	Temperature in fluid region, K
$Nu_{p,CL2}$	Nusselt number due to form drag model	T_p	Temperature in porous region, K
$Nu_{p,CL3}$	Nusselt number due to clear fluid compatible model	T_{w1}	Temperature at wall1(at $Y = -H/2$)
Nu_f	Nusselt number in fluid region	T_{w2}	Temperature at wall 2 (at $Y = H/2$)
Nu_p	Nusselt number in porous region	U_f	Non dimensional velocity in the fluid region
Nu_p^M	Nusselt number in porous region with effect of Magnetic field	U_p	Non dimensional velocity in the porous region
Nu_{px}	Local Nusselt number in porous region	U_i	Non-dimensional interfacial velocity
P	Non-dimensional pressure	$\overline{u}_{f,p}$	Velocity vector
p	Pressure, kg $m^{-1}s^{-2}$	u_f	Fluid velocity, m/s
Pe	Peclet number, $Pe = u_{ref} H / \alpha_f$	u_p	Porous velocity, m/s
P_g	$P_g = \frac{dP}{dX}$	u_{ref}	Reference velocity, m/s
P_{gr}	$P_{gr} = Re\frac{dp}{dx}$	u_i	Interfacial velocity, m/s
Q	Volumetric flow rate, m^3/s	x	Longitudinal coordinate, m
q	Constant heat flux, W/m^2	X	Non-dimensional axial distance, x/H

X^*	Normalized non dimensional axial distance, $(= X / Pe)$	φ	Porosity
X^*_{fd}	Normalized fully developed length.	ω	Acceleration factor
y	Transverse coordinate, m	θ_i	Non-dimensional interfacial temperature
Y	Non-dimensional transverse coordínate, y/H	θ_f	Non-dimensional temperature in fluid region
	Greek symbols	θ_p	Non-dimensional temperature in porous region
α_f	Thermal diffusivity in fluid region, m^2/s	θ^*	Non-dimensional bulk mean temperature, $\theta^* = (T_b - T_e) / (qH / k_f)$
α_{eff}	Thermal diffusivity in porous region, m^2/s	$\theta_{f,\,CL1}$	Non-dimensional temperature in fluid region due to Darcy model
η	The ratio between thermal diffusivity in fluid and porous regions, α_f / α_{eff}	$\theta_{f,\,CL2}$	Non-dimensional temperature in fl fluid region due to form drag model
ε	μ_f / μ_{eff}	$\theta_{f,\,CL3}$	Non-dimensional temperature in fl fluid region due to clear fluid compatible model
ε_t	Error tolerance limit	$\theta_{p,\,CL1}$	Non-dimensional temperature in fl porous region due to Darcy model
σ	Electric conductivity, $kg^{-1}m^{-3}s^3A^2$	$\theta_{p,\,CL2}$	Non-dimensional temperature in fl porous region due to from drag model
γ_p	Non-dimensional porous fraction	$\theta_{p,\,CL3}$	Non-dimensional temperature in porous region due to clear fluid compatible model
μ_f	Fluid viscosity, $(N.\ s)/m^2$	θ_{CL}	Non dimensional temperature in the conduction limit for three dissipation
μ_{eff}	Effective viscosity in porous region, $(N.\ s)/m^2$	$\theta^{'}_{CL}$	Non dimensional bulk mean temperature in the conduction limit
ρ	Fluid density, kg/m^3	$\theta^{'}_{CL1}$	Non dimensional bulk mean temperature in the conduction limit for Darcy model

θ_{CL2}	Non dimensional bulk mean temperature in the conduction limit for from drag model	ΔNu^{M}	The net change in the Nusselt number with effect of Magnetic field
θ_{CL3}	Non dimensional bulk mean temperature in the conduction limit for clear fluid compatible model	ΔNu_1	Net change in the Nusselt number for the Darcy model
θ_{w1}	Non-dimensional wall 1(at $Y=-1/2$) temperature	ΔNu_2	Net change in the Nusselt number for the form drag model
θ_{w2}	Non-dimensional wall 2(at $Y=1/2$) temperature	ΔNu_3	Net change in the Nusselt number for the clear fluid compatible model
θ_w	Non-dimensional wall temperature	ΔX^*	grid size in the flow direction=1/*MD*
$\tilde{\theta}_f$	Error in the energy equation in the fluid region	ΔY	grid size in the normal direction=1/*ND*
$\tilde{\theta}_p$	Error in the energy equation in the porous region	ΔX_1^*	First non-uniform grid width defined by, $\Delta X_1^* = c\ \Delta X^*$
ΔNu	The net change Nusselt number	Φ	Dissipation function

Contents

Chapter 1
Introduction

1.1 Introduction

In recent times, several researchers have studied fluid flow and heat transfer in porous media, in view of the significant applications in situations such as enhanced recovery of oil by thermal methods, cooling of electronic components, risk assessment of disposal of nuclear waste, proton exchange membrane (PEM) fuel cells.

It is observed that, in fully filled systems, there is significant pressure drop. Hence, there is necessity for enhancing heat transfer partially in a desirable way. This can even be done by keeping the pumping expense at an appropriate level. The application of convective heat transfer in porous medium, such as solid matrix heat exchangers and thermal insulation, oil recovery, geothermal engineering, heat pipes, chemical reactors, and hydrogeology, has been a topic of interest to mathematicians. Forced convective Nusselt number is higher when ducts have been filled with porous material. Recent applications, where studies on partially filled porous channels can be gainfully employed, include solar absorbers, catalytic and inert packed bed reactors, fuel cells, and compact heat exchangers. Several studies examined the boundary conditions at the porous-fluid interface.

1.2 Brief Review on Flow and Heat Transfer in Laminar Internal Flow Through Parallel Plate Channels

The problem of forced convection in a channel formed by two parallel plates is a classical problem that has been revisited in recent years in connection with the cooling of electronic equipments using materials involving hyper porous media or micro channels. The review presented here describes representative developments, and recent studies that include parallel plates kept at uniform but unequal temperatures and viscous dissipation.

Hatton and Turton [1] obtained series solution in the case of constant, unequal wall temperature boundary condition assuming that the flow is developed and the temperature field is developing. Also, Hatton and Turton[1] results show that the limiting Nusselt number is 4. This Nusselt number is independent of the degree of asymmetry in the wall temperatures. More recently, Mitrovic, Maletic and Baclic [2] addressed the asymmetric Graetz problem for asymmetric isothermal case referred by Nield [3]. Nusselt number under asymmetric isothermal case exhibits an unbounded swing, at the wall kept at lower of the two temperatures. Similarly, when viscous dissipation is included, Barletta [4] found the limiting Nusselt number (=17.5) to be independent of the Brinkman number, for all $Br \neq 0$.

Comprehensive relations for Nusselt numbers for thermally developed duct flows subjected to different boundary conditions have been presented by Sparrow and Patankar

[5]. Pins, Mulder and Schenk [6] obtained the temperature profile for hydrodynamically developed and thermally developing flow, including axial conduction using power series method for flow between parallel plates. Weigand, Kanzamar and Beer [7] studied analytically the influence of axial heat conduction on heat transfer in a circular pipe and in a parallel plate channel with uniform heating of the wall for two cases; of semi infinite length and finite length of the heated section. Cheng and Wu [8] studied the effects of viscous dissipation on convective instability in horizontal parallel plate channel when the fluid is heated from below. The effect is significant for Prandtl number, when $Pr \geq 10$. Barletta [9] investigated the laminar convection in a parallel plate vertical channel by taking into account both viscous dissipation and buoyancy. Nguyen [10] presented the results of numerical studies on hydrodynamically and thermally developing flow at low Reynolds number in the entrance region of a cascade of parallel horizontal plates. Two-dimensional Navier-Stokes and energy equations employed by Nguyen have been solved by ADI [11 and 12] and QUICK [13] methods.

Comprehensive studies on laminar forced convection in hydrodynamically and thermally developing region of parallel plate channels have been presented by Ramjee [14]. The parallel plates have been kept at unequal temperatures. Ramjee and Satyamurty [15] reported basic heat transfer characteristics for the asymmetrically heated channel and introduced a Nusselt number based on the average wall temperature. The limiting Nusselt numbers when viscous dissipation has been included and the channel walls are kept at unequal temperatures are available in Ramjee and Satyamurty [16]. Satyamurty and

Ramjee [17] also developed the superposition relations from which the Nusselt numbers at the two walls of the channel at unequal temperatures can be calculated for any desired degree of asymmetry from the solution of the problem subjected to boundary conditions of first kind, see p. 17 of Shah and London [18].

1.3 Porous Medium

A porous medium may be defined as a solid having holes connected in continuous paths in several directions. Fibrous aggregates, porous or fissured rocks, glass wool and fiberglass are some of the examples of porous material. Studies on flow through porous media date back to the 19^{th} century, the pioneer being Darcy who devoted considerable attention in developing the theory of ground water motion.

The porous matrix is in general characterized by an effective porosity, φ, and permeability, *K*. Pores or fraction of the medium that is filled by the fluid determine effective porosity. To distinguish two porous media having the same porosity, additional characteristic term, called permeability. Permeability is essentially the conductance of the medium defined with direct reference to Darcy's law. The permeability depends on the porosity of the medium and an equivalent diameter of the particle.

1.3.1 Characterization and Governing Equations for Momentum

Darcy Law

Darcy law formulates that the volumetric flow rate, Q, through a porous medium is directly proportional to the hydraulic head difference, h_d, and the cross sectional area, A, and inversely proportional to the length, l, of the porous column. Stated in the form of an equation, Darcy law can be expressed as,

$$Q \propto [(h_d A) / l] \tag{1.1}$$

The hydraulic head difference, h_d can be obtained from the relation below,

$$h_d = z + \frac{p}{\rho g} \tag{1.2}$$

where z denotes the elevation, p, pressure, ρ, the density of the fluid and g is acceleration due to gravity. The Darcian velocity v, is related to the volumetric flow rate by,

$$v = Q/A \tag{1.3}$$

Darcy law can be expressed in a differential form as,

$$v = -\frac{K}{\mu_f}\left(\frac{dp}{dx} - \rho g_x\right) \tag{1.4}$$

In Eq. (1.4), K is the permeability of the medium and μ_f is the viscosity of the fluid

For a three dimensional flow, Eq. (1.4), as given in Stanek and Szekely [19], takes the following form,

$$\vec{V} = -\frac{K}{\mu_f}\left(\nabla p - \rho\vec{g}\right) \tag{1.5}$$

In Eq. (1.5), $\vec{V}$ is the Darcian velocity vector and $\vec{g}$ is the gravity vector. From Eq. (1.5) , it may be noted that Darcy flow does not satisfy the no slip condition at solid boundaries. Modifications to the Darcy description, in general, become necessary when the flow Reynolds number, based on the local velocity and pore diameter, is high.

Non-Darcy Extensions

In order to account for the flow inertia effects and boundary effects, extensions to the Darcy law have been put forth by including classical convective terms, non-linear inertia terms and viscous terms. Methodology to derive the governing equation using the local volume averaging technique can be found in Slattery [20]. The governing equation for conservation of momentum from Catton [21] in vector form can be expressed as,

$$\frac{\mu_f}{K}\vec{V} + \rho\left(\frac{\mu_{eff}}{\mu_f}\right)^2 [\vec{V}.\nabla]\vec{V} + \rho\frac{K'}{K}\left|\vec{V}\right|\vec{V} = -\nabla p + \vec{F} + \mu_{eff}\nabla^2\vec{V} \qquad (1.6)$$

In Eq. (1.6), K' is the Forchheimer coefficient and μ_{eff} is an effective viscosity that takes into account the difference in the resistance offered for the fluid flow, though permeability may remain the same. For high-permeability foam, the effective viscosity can differ from the fluid viscosity by a factor of ten as demonstrated by Givler and Altobellis [22]. At times, the ratio μ_f/μ_{eff} is referred to as porosity in the literature. This terminology is not followed in the present thesis. $\vec{F}$ is the body force vector. In addition, non-dimensionalization of Eq. (1.6) leads to the parameters, *Da*, the Darcy number and *Fc*, the Forchheimer number being defined by,

$$Da = K/H^2 \qquad (1.7)$$

$$Fc = K^{'} / H \qquad (1.8)$$

It has been reported in the literature {see for example, Kaviany [23], Vafai and Kim [24] and Nield, Junqueira, and Lage [25]} that, results very close to the clear fluid flow configurations are obtained when the Darcy number is high.

In Eq. (1.6) the second term on the left hand side is the modified convective term, which includes the permeability and the porosity of the medium. The third term often referred to as Forchheimer non-linear inertial term, accounts for turbulent kinetic energy. The second term on the right hand side is due to Brinkman, which accounts for the boundary effects. Inclusion of Brinkman friction terms enables no-slip velocity boundary condition to be satisfied.

A comprehensive account of the early literature on momentum transfer through fluid saturated porous media is available in Bear [26] and Greenkorn [27]. Early theoretical and experimental studies on convective heat transfer in porous media are due to Rogers, Schilberg and Morrison [28], Wooding [29] and Elder [30 and 31]. Studies reported in [28-31] are devoted to understanding the flow structure when the medium is heated from below. The onset of convection has been theoretically predicted by Lapwood [32] which has been confirmed experimentally by Katto and Masuoka [33].

In general, the literature dealing with flow in porous media uses Eq. (1.6) or simplified forms. The simplified forms include some of the terms of Eq. (1.6), though the

Darcy model is part of all the forms. Many studies have established that the effect of convective terms in the LHS of Eq. (1.6) is not significant, e.g., Kaviany [23], Vafai and Tien [34], Lage [35], Manole and Lage [36].

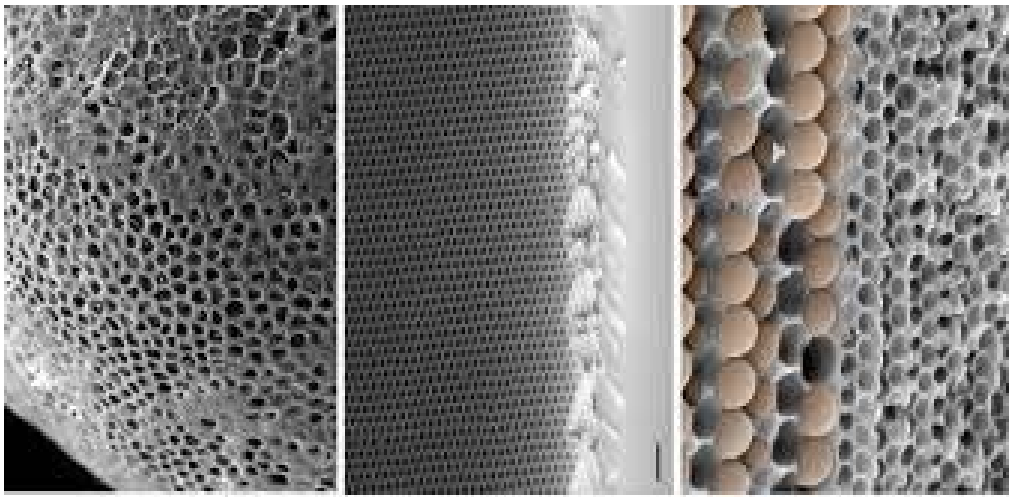

Fig. 1.1: Examples of porous medium.

1.3.2 Interfacial Boundary Conditions

The conditions to be satisfied at the porous-fluid interface for a class of problems studied in the present are dealt with here. Beavers and Joseph [37] addressed this issue when the no-slip assumption is needed to be reviewed for high permeability porous media. Beavers and Joseph postulated that a slip velocity can exist across the interface given by,

$$u_f - u_p = (\sqrt{K} / \alpha') \, u_p \tag{1.9}$$

In Eq. (1.9), u_f and u_p denote velocities on either side of the fluid-porous interface. α' is experimentally determined to be $0.1 \le \alpha' \le 4$. Saffman [38] justified the Beavers and Joseph [37] condition theoretically.

Neale and Nader [39], Vafai and Thiyagaraja [40] and Vafai and Kim [41], proposed that both velocity and shear stress are continuous at the interface.

$$u_f = u_p \tag{1.10}$$

$$\mu_{eff} \frac{du_p}{dy} = \mu_f \frac{du_f}{dy} \tag{1.11}$$

The conditions given Eq. (1.10) and Eq. (1.11) are extensively used by Sahraoui and Kaviany [42], Chandesris and Jamet [43], Prathap Kumar, Umavathi and Chamkha [44] and Bhargavi, Satymurty and Raja Sekhar [45].

1.4 Forced Convection in Porous Material Filled Ducts

Forced convection heat transfer in porous media is an interesting problem, the solution of which is important in several areas of engineering practice, see for e.g. Bejan et al. [46]. Various fluid flow and heat transfer arrangements have been treated both analytically and numerically, see Kaviany [47], Nield and Bejan [48], Bejan [49] and Vafai [50].

1.4.1 Porous Material Filled Pipes and Annuli

Poulikakos and Renken [51] examined the effect of Forchheimer non-linear inertial terms, Brinkman viscous terms and variable porosity on heat transfer through channels and pipes filled with porous materials subjected to constant temperature. Marpu [52] reported numerical results for the local Nusselt number in the entrance region considering two-dimensional descriptions for flow and thermal fields. Momentum equations included

convective terms and non-linear inertial terms due to Forchheimer and Brinkman viscous terms. Axial conduction in the energy equation has also been included.

Recent studies by Mitrovic and Maletic [53] have dealt with forced convection in the entrance region of annuli filled with porous medium where the inner and outer pipes are subjected to unequal temperatures. Mitrovic and Maletic [53] employed fully developed velocity profile though they included axial conduction in the energy equation. Mitrovic and Maletic [53] gave an excellent account of intermediate developments on porous material filled annuli.

1.4.2 Porous Material Filled Channels

Studies on laminar flow through a channel filled with porous material bounded by isothermal parallel plates employing Brinkman extended Darcy flow model along with the classical convective terms for the momentum equation have been reported by Kaviany [23]. Vafai and Kim [24] investigated a fully developed forced convection in a porous material filled channel, both walls subjected to equal heat flux. Satyamurty and Marpu [54] reported numerical results for the porous material filled channels, similar to those in [52] described above for annuli. The study [54] concluded that, when Brinkman extended Darcy model is employed, the local Nusselt number values are significantly lower from the values obtained employing Darcy flow model.

Hwang, Wu and Chao [55] investigated non-Darcian forced convection in an asymmetrically heated sintered porous channel. Nield, Junqueira and Lage [25] analyzed the fully developed forced convection in a fluid-saturated porous material filled channel with isothermal or isoflux boundaries. Xiong and Kuznetsov [56] investigated thermal dispersion and non-Darcian effects with forced convection in a Couette flow in a composite flat conduit. The walls were subjected to constant but different heat fluxes.

Nield, Kuznetsov and Xiong [57] investigated the thermal development of forced convection in parallel plate channel and a circular tube filled by a saturated porous medium, with walls subjected to constant heat flux. Similar studies when the walls were kept at constant temperature are available in [58]. Axial conduction has been neglected in both [57] and [58]. The analyses for various cross sections of conduits with embedded porous media presented by Haji-Sheikh and Vafai [59] gave insight into the effect of the Darcy number on the thermal performance of such ducts. Mitrovic and Maletic [60] dealt with forced convection in the entrance region of porous material filled channel, where the walls are subjected to unequal temperatures. Mitrovic and Maletic [60] employed fully developed velocity profile though included axial conduction, as has been the case in Mitrovic et al. [2]. A summary of additional literature on the subject of flow and heat transfer in porous material filled ducts (pipes, annuli, channels and other cross sections) is given in Table 1.1.

Table 1.1: A Summary of Additional Literature on the Subject of Flow and Heat Transfer in Porous Material Filled Ducts

Sl. No.	Geometry, Flow Field, Thermal Field and other Features in Brief	Boundary Conditions	Reference
1	Rectangular channel and circular duct filled with porous material, fully developed flow with Darcy-Brinkman-Forchheimer model. Developed thermal field.	Constant wall heat flux	Marafie and Vafai [61]
2	Circular tube with porous medium, fully developed flow with Darcy-Brinkman model. Developed thermal field. Analytical solution and numerical solution.	Constant wall heat flux	Hooman and Ranjbar-Kani [62]
3	Parallel plates and circular pipe with porous material, fully developed flow field with Darcy-Brinkman model. Developing thermal field, axial conduction neglected. Analytical solution. Correlations for both local and average heat transfer coefficients have been obtained.	Constant wall temperature	Haji-Sheikh [63]
4	Parallel plates and circular porous passages, fully developed flow with Darcy-Brinkman model. Developing thermal field, axial conduction included.	Constant wall temperature	Minkowycz and Haji-Sheikh[64]
5	Circular tube with porous material, fully developed flow with Darcy-Brinkman-Forchheimer model. Developed thermal field, axial conduction neglected.	Constant wall heat flux	Hooman and Gurgenci [65]
6	Parallel plate channel and circular tube filled by a porous medium saturated by a rarefied gas, fully developed flow with Darcy-Brinkman model. Developing thermal field, axial conduction neglected. Analytical solution.	Constant heat flux	Kuznetsov and Nield [66]

Contd. on next page

Table 1.1 - Contd.

Sl. No.	Geometry, Flow Field, Thermal Field and other Features in Brief	Boundary Conditions	Reference
7	Porous material filled parallel plate channel, hydrodynamics of developing flow field with Darcy-Brinkman model. At the entry three inlet velocity distributions are considered. Analytical solution obtained by using Fourier series.	No slip condition at the walls, and fully developed condition	Huang and Liu [67]
8	Porous material filled parallel plate channel, hydrodynamics of fully developed flow with Darcy's model, Darcy-Forchheimer model, Darcy-Lapwood-Brinkman model.	No slip condition at the walls	Awartani and Hamdan [68]
9	Various rectangular ducts with porous medium, fully developed flow with Darcy-Brinkman model. Developing thermal field. Fourier series solution for fully developed velocity filed, temperature field.	Constant wall temperature, constant wall heat flux	Haji-Sheikh [69]
10	Porous material filled parallel plate channel, fully developed flow with Brinkman-Forchheimer model. Developed thermal field. Analytical solution. Compared with numerical solution.	Constant wall heat flux	Hooman [70]
11	Parallel plate channel and circular duct filled by a porous medium, fully developed flow with Darcy and Brinkman-Forchheimer model. Analytical solution.	uniform temperature and uniform heat flux	Nield and Kuznetsov[71]
12	Circular channel filled with a porous medium saturated using the Darcy extended Brinkman-Forchheimer momentum equation with the entropy generation due to heat transfer, analytical solution. fully developed velocity filed, temperature field.	Constant wall heat flux	Dileep and Vikas[72]

Contd. on next page

Table 1.1 - Contd.

13	Triangular porous passages filled with a porous medium with Darcy Brinkman equation. Weighted residual method is used, a fully developed flow and thermally developing temperature field. Axial conduction is included.	Constant wall heat flux.	Banerjee, Haji-Sheikh, and Seiichi[73]

1.5 Forced Convection in Ducts Partially Filled with Porous Material

Poulikakos and Kazmierczak [74] obtained closed form analytical solutions for parallel plates and circular pipes partially filled with porous material subjected to constant heat flux employing Darcy-Brinkman flow model while numerical results were computed for constant wall temperature. They have shown that the Nusselt number attains a minimum for a certain porous layer thickness, the porous material being attached to the pipe or channel walls.

1.5.1 Channels Partially Filled with Porous Material

Forced convection flow within an asymmetrically heated horizontal double-passage (baffle) channel was studied by Cheng, Kou and Huang [75]. Also, an exact solution for a fully developed flow, between plate and an unbounded porous medium has been obtained by Vafai and Kim [41] who employed continuity of velocity and velocity gradients at the interface. Jang and Chen [76] considered the configuration of a channel, the fluid region being at the core and the porous layers being attached to the walls. Jang and Chen [76]

included the effect of thermal dispersion in the porous matrix. Kuznetsov [77-80] obtained analytical solutions for fluid flow in channels partially filled with a porous medium, employing different flow models to describe the porous region.

Transient forced convection flow in parallel-plate channels partially filled with porous substrate has been reported by Hamdan, Al-Nimr and Alkam [81]. The porous layer has been inserted in the channel core and the porous region is governed by Darcy-Brinkman-Forchheimer model. It has been found that the effect of Darcy number and microscopic inertial coefficient is higher in the developing region. Existence of an optimum porous substrate thickness has been established, for which the Nusselt number attains a maximum. Subsequently Alkam, Al-Nimr and Hamdan [82] examined the efficiency of depositing a given amount of porous material on one wall compared to distributing on both the walls of the channel.

Jen and Yan [83] employed three-dimensional velocity and temperature fields to describe forced convection in a channel partially filled with porous medium. Investigations by Jen and Yan established that, as the porous ratio increases, the flow velocity in the fluid layer increases leading to an increase in the friction factor and Nusselt Number. Additional literature on laminar forced convection in ducts partially filled with porous medium is given in Table 1.2.

Table 1.2: Additional Literature on Laminar Forced Convection in Ducts Partially Filled with Porous Medium

Sl. No.	Geometry, Flow Field, Thermal Field and other Features in Brief Description	Boundary Conditions	Reference
1	Parallel plate channel bounded below by a porous layer of finite thickness and above by an impermeable plate moving with a uniform velocity. Hydrodynamics of fully developed flow employing Poiseuille-Couette flow and Darcy-Brinkman model in fluid and porous regions has been analytically studied.	At one wall no slip, other wall is moving with constant velocity	Rudraiah [84]
2	Flow and heat transfer past a plate with a porous material attached the plate have been studied numerically employing two-dimensional Navier-Stokes and Darcy-Brinkman-Forchheimer model in the fluid and porous regions respectively.	Constant wall temperature	Vafai and Kim [85]
3	Developing, two-dimensional flow and thermal fields including axial conduction have been considered in studying external flow past a plate with alternate porous cavity-block obstacles. Numerical solutions have been obtained employing Navier-Stokes equations and Darcy-Brinkman-Forchheimer model in fluid and porous regions respectively.	Constant wall temperature	Huang and Vafai [86]
4	Existence of optimum porous matrix for parallel plate channel with porous block obstacles on one wall of the channel considering hydrodynamically and thermally developing fields employing two-dimensional description has been established.	Constant wall temperature	Huang and Vafai [87]
5	Flow past a plate with an attached porous substrate, boundary layer approximation has been made and significant reduction in computational time compared to the approach in Sl. No. 2 has resulted.	Constant wall temperature	Huang and Vafai [88]

Contd. on next page

Table 1.2 - Contd.

Sl. No.	Geometry, Flow Field, Thermal Field and other Features in Brief Description	Boundary Conditions	Reference
6	Parallel plate channel with alternate porous cavity-block obstacles on the bottom plate, hydrodynamically developing, two-dimensional flow employing Navier-Stokes equations and Darcy-Brinkman-Forchheimer model in fluid and porous regions respectively. Developing thermal field, axial conduction included. Stream function-vorticity formulation. Numerical solution.	Constant wall temperature	Huang and Vafai [89]
7	Flow over intermittently emplaced porous cavities, two-dimensional hydrodynamically developing flow employing Navier-Stokes equations and Darcy-Brinkman-Forchheimer model in fluid and porous regions respectively. Developing thermal field, axial conduction included. Numerical solution. Stream function-vorticity formulation.	Constant wall temperature	Vafai and Huang [90]
8	Vertical parallel plate channel with porous substrates attached to both the walls, hydrodynamically developing two-dimensional, mixed convection flow employing Navier-Stokes equations and Darcy-Brinkman-Forchheimer model in fluid and porous regions respectively. Developing thermal field, axial conduction included. Numerical solution.	Constant wall temperature	Chang and Chang [91]
9	Pulsating flow through a circular pipe with a porous layer attached to inside of the pipe. Navier-Stokes equations and Darcy-Brinkman-Forchheimer equations have been employed. Axial conduction neglected.	Constant wall heat flux	Guo, Kim and Sung [92]

Contd. on next page

Table 1.2 - Contd.

Sl. No.	Geometry, Flow Field, Thermal Field and other Features in Brief Description	Boundary Conditions	Reference
10	Vertical tube with a porous layer attached to inside of the tube, hydrodynamically developing, two-dimensional, mixed convection flow employing Navier-Stokes equations and Darcy-Brinkman-Forchheimer model in fluid and porous regions respectively. Developing thermal filed, axial conduction included. Numerical solution.	Constant wall temperature	Chang, Dai and Chang [93]
11	Performance enhancement of a double-pipe heat exchanger, by inserting porous substrates at inner and on outer sides of the inner pipe has been numerically studied Navier-Stokes and Darcy-Brinkman-Forchheimer equations.	Constant wall temperature	Alkam and Al-Nimr [94]
12	Circular duct with a porous substrate attached to the duct wall, fully developed flow employing Darcy-Brinkman-Forchheimer model in the region. Developed thermal field. Two boundary conditions have been considered.	Constant wall temperature, constant wall heat flux	Kuznetsov and Xiong [95]
13	Parallel plate channel with porous layer attached to bottom wall. Hydro dynamically and thermally developing flow. Darcy-Brinkman-Forchheimer model in the porous region has been employed. Boundary layer approximation has been made for both flow and thermal fields.	Constant wall temperature	Alkam, Al-Nimr and Hamdan [96]
14	Effect of local inertial term on unsteady fully developed flow through a parallel plate channel with the porous layer attached to top wall has been numerically studied employing, Poiseuille and Darcy-Brinkman Forchheimer descriptions.		Abu-Hijleh and Al-Nimr [97]

Contd. on next page

Table 1.2 - Contd.

Sl. No.	Geometry, Flow Field, Thermal Field and other Features in Brief Description	Boundary Conditions	Reference
15	Circular pipe with a porous layer attached to inside of the pipe. The porous insert is attached at the pipe wall and extends inward, toward the centerline. The flow and thermal field are fully developed. Darcy-Brinkman-Forchheimer equation in the porous region. Numerical solution.	Constant wall heat flux	Habibollah and Hossein [98]
16	Circular pipe with 1) a porous layer attached to the tube wall and 2) placed at the center. Fully developed flow and thermal fields have been assumed in both the regions. Darcy-Brinkman-Forchheimer description has been employed in the porous region. Developed thermal field. Numerical solution.	Constant wall temperature, constant wall heat flux	Kim et al. [99]
17	Multiple porous-covering heated blocks, hydrodynamically developing flow employing Navier-Stokes equations and Darcy-Brinkman-Forchheimer model in fluid and porous regions respectively. Developing thermal field. Stream function-vorticity method. Numerical solution.	Two walls are insulated	Huang et al. [100]
18	Parallel plate channel with porous insert at the entry of the channel, hydrodynamically developing flow employing Navier-Stokes equations and Darcy-Brinkman-model in the fluid and porous regions respectively. Developing thermal field. Numerical solution.	Constant wall temperature	Keyhani, Karimi and Nazari [101]
19	Circular pipe with a porous layer attached to inside of the pipe. The flow in the porous and fluid regions is fully developed. Darcy-Brinkman-Forchheimer equation in the porous region. Developed thermal field. Numerical solution.	Constant wall heat flux	Sayehvand and Shokouhmand [102]

Contd. on next page

Table 1.2 - Contd.

Sl. No.	Geometry, Flow Field, Thermal Field and other Features in Brief Description	Boundary Conditions	Reference
20	Circular channel with i) a porous insert is placed adjacent to the pipe wall, and ii) a cylindrical element of porous material is inserted at the centre. Hydrodynamics of unsteady fully developed flow employing Poiseuille and Darcy-Brinkman equations in the fluid and porous regions respectively has been analytically studied .		Alkam and Al-Nimr [103]
21	Circular pipe with 1) porous material has a cylindrical shape placed at the centerline of the pipe 2) the porous material has an annular shape, 3) a cylindrical shape placed at the pipe inlet. Fully and thermal fields are developing. Darcy-Brinkman-Forchheimer description has been employed in the porous region. Numerical solution.	Constant wall heat flux	Mohamed , Maghlany and Dawood[104]
22	Circular pipe with partially filled with porous media, Brinkman–Forchheimer-extended Darcy model is employed for the region of porous medium. Flow and thermal fields are developing. Numerical solution. The new axisymmetric lattice Boltzmann model is used.	Constant wall temperature	Fumei et al.[105]
23	Two configurations, (1) fully filled with a porous channel, and (2) partially porous channel. Hydrodynamically and Thermally developing. Darcy-Brinkman Forchheimer equation is used in the porous region. Numerical solution.	Lower wall is subjected to constant wall heat flux	Hadim[106]
24	Parallel plate channel partially filled with a porous material with porous insert is placed at bottom wall of the channel walls. Darcy equation in the porous region. The flow and thermal fields are developed. Analytical solution.	Constant wall heat flux	Kuznetsov and Nield[107]

Contd. on next page

Table 1.2 - Contd.

Sl. No.	Geometry, Flow Field, Thermal Field and other Features in Brief Description	Boundary Conditions	Reference
25	Parallel plate channel with 1) porous material is attached to one of the walls of the channel, 2) distributed equally at the two walls, and 3) placed as one insert in the middle of the channel. Flow and thermal fields are developed. Analytical solution.	Constant wall heat flux	Bhargavi and Satyamurty [108]
26	Parallel plate channel partially filled with a porous material with porous insert is placed at the center of the channel. Darcy-Brinkman-Forchheimer equation in the porous region. Flow and thermal fields are developed. Analytical and numerical solutions.	Constant wall heat flux	Cekmer et al. [109]
27	Inclined parallel plate channel partially filled with porous material. Darcy-Brinkman equation in the porous region. Flow and thermal fields are developed. Analytical solution.	Constant different temperatures	Malashetty, Umavathi and Prathap Kumar [110]
28	A three dimensional channel partially filled with porous material. Darcy-Brinkman equation in the porous region Flow and thermal fields are developing. Numerical solution.	Isothermal	Tien and Yan [111]
29	Parallel plate channel with 1) porous material is distributed equally at the two walls, and 2) placed at centre of the channel. Darcy-Forchheimer equation in the porous region. Flow and thermal fields are developing.	Constant wall temperature.	Shokouhmand, Jam and Salimpour [112]
30	Parallel plate channel partially filled with a porous insert with porous insert is attached to the lower plate of the channel. Darcy-Brinkman equation in the porous region. Flow and thermal fields are developing. Numerical solution.	Constant wall temperature	Madera et al. [113]
31	Circular pipe with 1) porous material is inserted at the core of the pipe, and 2) annulus porous material is attached to the inner wall. Darcy-Brinkman-Forchheimer equation in the porous region. Flow and thermal fields are developing. Numerical solution.	1) Constant wall temperature 2)Constant wall heat flux	Maerefat, Mahmoudi and Mazaheri [114]

1.6 Magnetohydrodynamics (MHD)

In recent years, the study of Magnetohydrodynamic (MHD) flow and heat transfer for a viscous incompressible fluid over a plate has immense applications in engineering and industrial problems such as petroleum industries, plasma studies, geothermal energy extractions and many others. Magnetohydrodynamics is a branch of continuum mechanics which deals with the motion of an electrically conducting fluid in the presence of a magnetic field. The motion of conducting material across the magnetic lines of force creates potential differences which in general cause electric currents to flow. The magnetic fields associated with these currents modify the magnetic field which creates them. On the other hand, the flow of electric current across a magnetic field associated with a body force, called Lorentz force, influences the fluid flow.

Raju et al. [115] studied MHD forced convective flow of a viscous fluid of finite depth in a saturated porous medium over a fixed horizontal channel with thermally insulated and impermeable bottom wall in the presence of viscous dissipation and Joule heating. Sharmilaa and Saranya [116] studied the effect of magnetic field in a fully developed forced convection through a porous medium bounded by parallel plate channel, with the inclusion of boundary and inertial effects. The effect of magnetic field on fluid flow through various geometries under different conditions have been studied by several authors, among whom were Kurzweg [117], Gulab Ram and Mishra [118], Raptis and Kafousias [119], Raptis and Perdikis [120], Manju et al. [121] and Vineet Kumar and Amit Kumar [122].

Baoku, Israel-Cookey and Olajuwon [123] studied the effects of thermal radiation, magnetic field and thermal conductivity on Couette flow of a high viscous fluid with temperature dependent viscosity through a porous channel and they obtained numerical solution using finite difference methods. Varshney, Katiyar and Kumar [124] analyzed the effect of the externally applied transverse magnetic field which enhances flow resistance.

Many investigators{Ashish, Satya and Filippov [125], Ghofrani et al. [126], Sheikholeslami, Rashidi and Ganji [127] and Sheikhnejad, Hosseini and Majid Saffar [128], Takhar and Beg [129], Barletta et al. [130], Guven, Aytac and Ibrahim [131], Sahar [132], Srivastava and Satya [133] and Jhankal, Jat and Kumar [134]} studied the interaction of forced convection with porous medium/magnetic field in view of its importance in engineering applications.

1.7 Viscous Dissipation in Flows Through Porous Media

Production of thermal energy through the mechanism of viscous stresses is encountered in both the viscous flow of clear fluids and the fluid flow within porous media. The effect of the heat released by viscous dissipation can be significant when a non-dimensional parameter, the Brinkman number, $Br = (\mu_f \ u_{ref}^2) / (k_f \Delta T)$ is high. Considering that the effective viscosity can be significantly higher {see, Givler and Altobellis [22]} than fluid viscosity when it flows through the porous medium, the Brinkman number shall be

considerably higher compared to that for clear fluid flows. Present day applications involving flow through porous media, call for including viscous dissipation effects in the conservation of energy equation. Some of them may generically be described as internal flows, say, flow through a porous material fully or partially filled pipes, channels and, in general, ducts. If the effective fluid viscosity is high or temperature differences are small or kinetic energy is high, viscous dissipation can be expected to be significant. An account of the importance of dissipation can be found in Vafai [50].

1.7.1 Dissipation Modeling

The form of the dissipation function Φ for flows through porous media is not unique. In deriving the conservation of {as in say, Al-Hadhrami, Elliott and Ingham [135 and 136], or Schlichting and Gersten [137] for more generality} thermal energy equation for clear fluid flows, mechanical energy equation is subtracted from the overall conservation of energy equation. Different models proposed by different researchers/investigators for the dissipation function for porous media, have not always been compatible with the momentum equation actually used in such investigations. The five forms of the dissipation function, Φ, available in the literature for flow through porous media for unidirectional flow are as following.

Bejan [49]: $\Phi = (\mu_f / K)u^2$ (1.12)

Takhar and Beg [129] and Takhar, Soundalgekar and Gupta [138]:

$\Phi = \mu_f (\partial u / \partial y)^2$ (1.13)

Murthy and Singh [139]: $\Phi = u[(\mu_f /\mathrm{K})u + \rho(K^{'} / K)u^2]$ (1.14)

Nield [140]: $\Phi = (\mu_f / K)u^2 - \mu_{eff} u(d^2u / dy^2)$ (1.15)

Al-Hadhrami et al. [135 and 136]: $\Phi = (\mu_f / K)u^2 + \mu_{eff} (du / dy)^2$ (1.16)

1.7.2 Forced Convection in Channels Filled with Porous Material with Viscous Dissipation

A general review of the dissipation models in porous media has been developed and the background is available in Nield and Bejan [48]. When the thermal energy equation includes a viscous dissipation term involving the Brinkman number, Nield [141] termed it as Brinkman-Brinkman problem. The different dissipation functions that have been proposed are given by Eqs. (1.12) to (1.16).

A summary of the literature on convective heat transfer through porous media, including dissipation, along with the model employed is given in Tables 1.3. Dissipation function employed in column number 2 is indicated by the reference number.

Table 1.3: A Summary of Literature on Convective Heat Transfer through Porous Media Including Dissipation

Sl. No.	Geometry, Flow Field, Thermal Field , other Features in Brief and Dissipation Function, Φ	Boundary Conditions	Reference
1	Vertical plate channel. Numerical solution for fully developed free and forced convection flow employing Darcy model. Axial conduction included in the energy equation. [49]	Equal and unequal wall temperature	Ingham and Pop [142]
2	Vertical plate. Steady mixed convection flow employing Darcy-Forchheimer model. Boundary layer approximation has been made in the energy equation. Effect of thermal dispersion and viscous dissipation are studied. [139]	Isothermal wall temperature	Murthy [143]
3	Vertical Plate. Analytical solution for two-dimensional mixed convection employing Darcy-Forchheimer model. Boundary layer approximation has been made in the energy equation. [139]	Isothermal wall temperature	Tashtoush [144]
4	Circular duct filled with porous material, fully developed flow with Darcy Brinkman model. Developing thermal field, including axial conduction. A modified Graetz methodology. Three models have been evaluated. [49], [135 and 136] and [140]	Constant wall temperature	Nield, Kuznetsov and Xiong [145]
5	Vertical plate. Analytical solution for steady free convection employing Darcy model. Boundary layer approximation has been made in the energy equation. [49]	Constant wall temperature	Rees, Magyari and Keller [146]
6	Porous material bounded by parallel plate channel, fully developed flow and thermal fields, with Darcy-Brinkman model. Different dissipation models shown to yield almost the same results for small Darcy number. [49], [135 and 136] and [140]	Constant wall temperature and constant wall heat flux	Nield, Kuznetsov and Xiong [147]

Contd. on next page

Table 1.3 - Contd.

7	Circular pipe filled with porous material, fully developed flow with Darcy-Brinkman model. Developed thermal field. Analytical solution using perturbation method. [49]	Constant wall temperature	Hooman and Ranjbar-Kani [148]
8	Vertical channel. Numerical solution for mixed Convection employing Darcy-Brinkman-Forchheimer model. Boundary layer approximation has been made in the energy equation. [135 and 136]	Isothermal and Isoflux	Umavathi et al. [149]
9	Porous material filled parallel plate channel, fully developed flow with Darcy-Brinkman model. Developed thermal field. Analytical and numerical solutions have been obtained. [49], [135 and 136] and [140]	Unequal Constant wall temperature	Mahmud and Fraser [150]
10	Porous material filled parallel plate channel, fully developed flow with Darcy model. Developed thermal field. The limiting Nusselt number is independent of the Brinkman number. [49]	Constant wall temperature	Hooman and Gorji-Bandpy [151]
11	Pipes and channels partially (porous insert has been placed symmetrically at the center) and fully filled with porous material. Two-dimensional, developing flow field with Darcy-Brinkman-Forchheimer model with convective terms. Developing thermal field included axial conduction. Included viscous dissipation to estimate entropy generation. [139]	Constant wall temperature	Morosuk [152]
12	Circular duct filled porous material, fully developed flow with Darcy Brinkman model. Developing thermal field included axial conduction and viscous dissipation. Analytical solution. [49], [135 and 136] and [140]	Constant wall temperature	Kuznetsov, Xiong and Nield [153]
13	Circular duct filled with porous material, Darcy Brinkman model. Developing thermal field included axial conduction and viscous dissipation. Numerical solution.[49]	Constant wall heat flux	Hooman, Pourshaghaghy and Ejlali [154]

Contd. on next page

Table 1.3 - Contd.

14	Porous material filled parallel plate channel, fully developed flow with Darcy-Brinkman-Forchheimer model. Developing thermal field included axial conduction and viscous dissipation. Three viscous dissipation models are studied. Analytical solution and numerical solution. [49], [135 and 136] and [140]	Constant wall temperature and constant wall heat flux	Hooman and Gurgenci [155]
15	Circular tube filled with porous material parallel plate channel, fully developed flow with Darcy Brinkman model. Developed thermal field included and viscous dissipation. Analytical solution. [129] and [138]	Constant wall heat flux	Shigeru and Koichi Ichimiya [156]
16	Porous material filled parallel plate channel, fully developed flow with Darcy-Brinkman model. Developed field included viscous dissipation. Analytical solution. [129] and [138]	Lower wall with constant heat flux, the upper wall is fixed and adiabatic.	Olaseni and Philip [157]

1.8 Lacunae in the Past Studies on Laminar Forced Convection in Parallel Plate Channels Filled with Porous Material

The focus of the present study has been to examine forced convection through channels partially or fully filled with porous material owing to a number of present day applications such as fuel cells, solar absorbers and catalytic converters. As mentioned earlier, channels partially filled with porous material may be geometry of interest for a device or the porous insert has been included to enhance heat transfer. Forced convection in porous material filled ducts gives an opportunity to enhance heat transfer not only by providing a tortuous path but also by providing a scope to manipulate the effective thermal conductivity. On the basis of earlier studies, {Hamdan, Al-Nimr and Alkam [81], Alkam, Al-Nimr and Hamdan

[82], Huang and Vafai [86 and 87] and Bhargavi, Satyamurty and Raja Sekhar [45], Bhargavi and Satyamurty [108] and Satyamurty and Bhargavi [158]}, partially filled channels leads to higher increase in Nusselt number than fully filled channel compared to clear fluid flow configuration. A cautious interpretation of the improvement or otherwise of heat transfer needs to be made, when effects such as axial conduction and viscous dissipation are included.

The studies available in the literature involving forced convection in porous material filled channels are reasonably comprehensive within the frame work of two-dimensional flow and temperature fields. However, there is no unanimity in viscous dissipation modeling for the flows through porous media. Further, studies that include dissipation in flows through channels partially filled with porous material, to the best knowledge of the author, have not been reported widely, particularly in the context of heat transfer enhancement. Morosuk [152] studied pipes and channels partially (porous insert has been placed symmetrically at the center) and fully filled with porous material. Morosuk [152] included viscous dissipation to estimate entropy generation. In order to fill some of the lacunae, the present investigations have been taken up. Specific aspects investigated in this thesis are given in § 1.10 on the scope and objectives of the present thesis.

1.9 Numerical Method

The studies which are proposed to be undertaken involve obtaining numerical solutions to two-dimensional conservation of energy equation, including axial conduction and viscous

dissipation and these are computationally intensive even within the framework of developed velocity field. When axial conduction is included, the conservation of thermal energy equation is elliptic in nature. Applying the downstream boundary condition at a priori unknown axial distance makes the process of arriving at a solution an iterative process. Some of the numerical techniques that have been employed extensively for the class of internal flows considered are as follows. The energy conservation equation with boundary layer approximation was solved by Habchi and Acharya [159] using implicit finite-difference scheme. Numerical solutions to the full Navier-Stokes and energy equations have been obtained by Naito and Nagano [160] using Successive Over-Relaxation (SOR) method. Nguyen [10 and 161] used Alternating Direction Implicit (ADI) [11 and 12] and Quadratic Upwind Interpolation for Convective Kinematics (QUICK) [13] methods, to solve Navier-Stokes and energy equations in the finite difference form. SIMPLER (Semi-Implicit Method for Pressure Linked Equations-Revised) algorithm [162] with a staggered grid system was employed by Jeng, Chen and Aung [163]. Crank-Nicholson semi-implicit scheme was used by Krishnan and Sastri [164] to solve the energy equation. Discretized momentum and energy equations have been solved by Min et al. [165] using a line-by-line, TDMA, Tri-Diagonal Matrix Algorithm [166] while the pressure equation has been solved using a line SOR.

The Successive Accelerated Replacement (SAR) scheme has been employed successfully for a wide class of problems by a group of researchers at Energy Systems Laboratory, of Mechanical Engineering Department, IIT Kharagpur, India. SAR scheme

is essentially non-linear over relaxation method due to Lew [167], Lieberstein [168] and Dellinger [169]. Lew [167] and Dellinger [169] applied the SAR scheme for solving non-linear ordinary differential equations. Dellinger's scheme differs from the non-linear over relaxation method essentially in choosing the relaxation factor. Satyamurty [170] demonstrated the applicability of the SAR scheme for solving a system of partial differential equations in the study of two-dimensional natural convection heat transfer in porous media. This scheme has been extensively applied by Satyamurty and Marpu [171], Marpu and Satyamurty [172], Satyamurty and Marpu [173], Marpu and Satyamurty [174], Marpu [175], Sharma [176], Prakash Chandra [177] and Satyamurty and Prakash Chandra [178]. More recently the method has been employed for forced convection studies by Ramjee and Satyamurty [15], Satyamurty and Bhargavi [158], and Jagadeesh and Satyamurty [179] SAR scheme has been chosen to obtain numerical solutions to the problems studied in the present thesis.

Philosophy of Successive Accelerated Replacement (SAR)

The basic philosophy of the SAR scheme is to guess a profile for each variable that satisfies the boundary conditions. Let the partial differential equation governing a variable, $\phi(X, Y)$, expressed in finite difference form given by $\bar{\phi}_{M,N} = 0$. (M, N) represent the nodal point when the non-dimensional height and length of the channel are divided into a finite number of intervals *MD* and *ND* respectively. The guessed profile for the variable ϕ at any mesh point, in general, will not satisfy the equation. Let the error in the equation at (M, N) and at k^{th} iteration be $\bar{\phi}^{k}_{M,N}$.

The $(k+1)^{th}$ approximation to the variable ϕ is obtained from,

$$\phi_{M,N}^{k+1} = \phi_{M,N}^{k} - \omega \left\{ \bar{\phi}_{M,N}^{k} \Big/ \left(\partial \bar{\phi}_{M,N}^{k} / \partial \phi_{M,N} \right) \right\} \qquad (1.17)$$

In Eq. (1.17), ω is an acceleration factor which varies between $0 < \omega < 2$. $\omega < 1$ represents under-relaxation and $\omega > 1$ represents over relaxation.

The procedure for correcting the variable ϕ at each mesh point in the entire region of interest is repeated until a convergence criterion is satisfied. The criterion is that the normalized change in the variable at any mesh point between k^{th} and $(k+1)^{th}$ approximation satisfies,

$$\left| 1 - \left(\phi_{M,N}^{k} / \phi_{M,N}^{k+1} \right) \right| < \varepsilon_t \qquad (1.18)$$

where ε_t, the error tolerance limit, is a prescribed small positive number. To correct the guessed profiles, each dependent variable has to be associated with one equation. It is natural to associate the equation that contains the highest order derivative of that variable.

1.10 Scope and Objectives

The objective of the present study is to study laminar forced convection in channels partially filled with porous material. In particular, the effects of axial conduction and viscous dissipation have been evaluated in the thermally developing region of the flow.

The scope includes employing fully developed flow field corresponding to Poiseuille flow in the clear fluid region and Darcy-Brinkman model in the porous region. Thermal field has been considered to be developing and a two-dimensional description has been employed in both the porous and fluid regions. Varying degrees of approximation to describe the temperature field have been made in different studies reported in Chapters 2 to 7. The effects of viscous dissipation on heat transfer have been evaluated considering three dissipation models; those of the Darcy model due to Bejan[49], Eq. (1.12) , form drag model due to Nield [140], Eq. (1.15) and that of clear fluid compatible model given by Al-Hadhrami et al. [135 and 136], Eq. (1.16).

The physical model is that of a channel formed by parallel plates, H distance apart. The fluid enters at an average velocity of u_{ref} and a temperature of T_e. The plates at $y = \pm H/2$ are subjected to constant heat flux, q or constant temperature T_w. The channel is partially filled with a porous material of thickness l_p. The total thickness of the porous material adjacent to the plates is l_p. The porous fraction is defined by $\gamma_p = l_p / H$.

The following topics, which form the subject matter of chapters 2 to 7 of the present thesis, have been studied.

- Analytical investigation of laminar forced convection in a channel partially filled with porous material subjected to constant wall heat flux.
- Analytical study of forced convection in a channel partially filled with porous material with effect of magnetic field subjected to constant wall heat flux.

- Analytical investigation of laminar forced convection with viscous dissipation in parallel plate channels partially filled with a porous material at the conduction limit.
- Effect of heat transfer in the thermally developing region of the channel partially filled with a porous medium: constant wall heat flux.
- Effect of axial conduction in the thermally developing region of the channel partially filled with a porous medium: constant wall heat flux.
- Effect of viscous dissipation and axial conduction in the thermally developing region of the channel partially filled with a porous material subjected to constant wall heat flux.

It has been assumed that the effective and fluid viscosities are equal throughout the studies reported here. Similarly, it has also been assumed that effective thermal conductivity is equal to fluid thermal conductivity. The flow field has been assumed to be fully developed in all the investigations reported in the present thesis. This assumption has been made to facilitate obtaining analytical solutions in certain cases and for ease in obtaining numerical solutions when the thermal field is developing.

Studies on laminar forced convection in hydrodynamically and thermally developed flow between the parallel plates partially filled with the porous medium have been presented in Chapter 2. The given amount of porous material porous layer has been distributed equally at the two walls. The channel walls are subjected to constant heat flux.

A porous material of thickness $l_p/2$ is attached to both the walls of the channel. The problem is characterized by Darcy number, *Da,* Reynolds number, *Re,* and the porous fraction, γ_p. Analytical expressions for the non-dimensional velocity and temperature profiles in the porous and clear fluid regions have been obtained. From the velocity and temperature expressions, the fully developed skin friction coefficients and the Nusselt numbers on the porous wall have been obtained analytically.

Studies on laminar forced convection in hydrodynamically developed and thermally developed flow between the parallel plates partially filled with the porous material have been presented in Chapter 3. The parallel plates have been subjected to uniform heat flux. In addition to the parameters, $\gamma_p = l_p / H$, $Da = K/H^2$ and $Re = \rho u_{ref} H / \mu_f$, the problem is characterized by the Hartmann number, $M = \sqrt{\frac{\sigma B_0{}^2 H^2}{\mu_f}}$. Analytical solution has been obtained and closed form expressions have been derived for velocity, skin friction coefficient and temperature profiles in the porous and fluid regions and for the Nusselt number in the porous region. It has been shown that the analytical expressions yield the standard values for the Hartmann number, $M = 0$ {absence of magnetic field)} for all porous fractions γ_p , $0 \le \gamma_p \le 1.0$.

Enhancement in the fully developed Nusselt number for parallel plate channel flow subjected to constant wall heat flux and constant wall temperature with porous inserts distributed equally at the two walls of the channel for the three dissipation models

has been studied in Chapter 4,. The three dissipation models are 1) the Darcy model, 2) form drag model and 3) clear fluid compatible model in the porous region. Two boundary conditions are considered. Channel walls are subjected to (i) constant wall heat flux and (ii) constant wall temperature. Analytical expressions for limiting temperature profile and limiting Nusselt number plots are obtained. Limiting temperature profile and limiting Nusselt number depend on the Brinkman number for the constant wall heat flux boundary condition. Nusselt numbers in the conduction limit have been found to be independent of the Brinkman number, a feature well reported for clear fluid channels, see Barletta [9] for the constant wall temperature boundary condition.

Studies on laminar forced convection in hydrodynamically developed and thermally developing flow between the parallel plates partially filled with the porous material have been presented in Chapter 5. The parallel plates have been subjected to uniform heat flux. Numerical solutions to the conservation of thermal energy equation without axial conduction in the porous and fluid regions have been obtained for $0 \le \gamma_p \le 1.0$ and Da = 0.001, 0.005, 0.01, 0.05 and 0.1, applying successive acceleration replacement (SAR) scheme [15, 158 and 179]. When axial conduction is neglected Peclet number does not appear explicitly in the conservation of the thermal energy equation expressed in terms of the normalized non-dimensional axial distance X^*.

Extensive numerical trials have been conducted and the following values for the parameters involved have been found to be satisfactory. a) The acceleration factor, 0.5 $\le$

$\omega \leq 1.5$ b) Error tolerance limit, $\varepsilon_t = 10^{-4}$, 10^{-5}, 10^{-6} and 10^{-7} c) Number of divisions in the Y direction, $60 \leq ND \leq 100$ (uniform) and d) Non-uniform divisions in the axial direction, $1000 \leq MD \leq 8000$. The non-uniform grids have been generated in geometric progression.

Based on the numerical trials conducted, the following values for the parameters have been employed in obtaining numerical solutions presented. a) Acceleration factor $\omega \leq 1$ has been determined as per Eqs. (5.17) and (5.20) b) Error tolerance limit, $\varepsilon_t = 10^{-5}$ c) $X^*_{fd} = 0.4$ d) $MD = 1000$ with ΔX^*_M generated in geometric progression with $c = 1/8$ in Eq. (5.51) and e) $ND = 90$ with $\Delta Y = 1/90$.

The values of the local Nusselt numbers when the channel is a clear fluid channel and when the channel is fully filled with a porous material agree well with the values available in Shah and London [18] and Nield et al. [57 and 58]. The local Nusselt number Nu_{px} decreases as X^* increases for all γ_p and Da, and reaches the fully developed values for $X^* = 0.4$. Nu_{px} is a minimum when $\gamma_p \approx 0.6$ at low $Da = 0.005$. Thus, there exists an optimum porous fraction to attain minimum enhancement in the Nusselt numbers.

The effect of axial conduction in hydrodynamically developed and thermally developing region of parallel plate channels partially filled with a porous material has been studied numerically in Chapter 6. The parallel plates have been subjected to constant heat flux. In addition to the parameters, γ_p, Da and $Re = (u_{ref} H)/\nu$, the problem is

characterized by the Peclet number, $Pe = u_{ref} H / \alpha_f$, where α_f is the thermal diffusivity of the fluid. Numerical solutions to the conservation of thermal energy equation with axial conduction in the porous and fluid regions have been obtained for $0 \leq \gamma_p \leq 1.0$, $5 \leq Pe \leq 100$ and Da = 0.001, 0.005, 0.01, 0.05 and 0.1, applying the Successive Acceleration Replacement (SAR) scheme [15, 158 and 179]. When axial conduction is neglected, the Peclet number does not appear explicitly and this case is denoted by $A_c = 0$.

It has been concluded that the non-dimensional temperature profiles become independent of the Peclet number for $Pe \geq 100$ indicating that the effect of axial conduction has become negligible. The downstream condition satisfied by the clear fluid ducts $\partial\theta_b / \partial X^* \rightarrow 0$, has been found to be valid for parallel plate channels partially filled with porous material also. This feature assumes importance since the flow and thermal fields are not symmetric when the channel is partially filled with porous material. Non-dimensional bulk mean temperature excess of wall temperature, $\theta_w - \theta^*$, increases as X^* increases. $\theta_w - \theta^*$ decreases as Peclet number decreases. This indicates that a stronger axial conduction effect present at lower Peclet numbers makes the fluid less heated or less cooled compared to when axial conduction is neglected. The local Nusselt number Nu_{px} decreases as X^* increases for all γ_p and reaches the fully developed values for $X^* \geq 0.4$.

Laminar forced convection including viscous dissipation in the thermally developing region of parallel plate channels partially filled with porous material, when the parallel plates have been subjected to constant wall heat flux, has been numerically investigated employing the SAR scheme [15, 158 and 179] in Chapter 7. The two dissipation models have been employed in the porous region. $Br > 0$ represents fluid getting cooled and $Br < 0$ shows fluid getting heated. Two dissipation models, namely, a) Darcy model due to Bejan [49] and b) clear fluid compatible model due to Al-Hadhrami et al. [135 and 136] have been employed in the porous region. The conventional dissipation function {see, Schlichting and Gersten [137]} has been employed in the fluid region. Numerical solutions have been obtained neglecting axial conduction and including axial conduction terms in the energy equation for $Pe = 5$, 25 and 100. Ranges for the other parameters are, $0 \leq \gamma_p \leq 1.0$, $0.005 \leq Da \leq 0.01$ and $-1.0 \leq Br \leq 1.0$.

Nusselt number displays an unbounded swing at some $X^* = X^*_{sw}$ when $Br < 0$. X^*_{sw}, decreases as Br decreases, i.e., for larger negative values of Br. The limiting values of the Nusselt numbers (for large X^*) on the fluid and porous sides, Nu_{px} are dependent on Br for all $Br \neq 0$ in the developing region also. These limiting values depend on the porous fraction too. Nu_{px}, decreases as X^* increases for all porous fractions when $Br > 0$. In chapter 8, we have given conclusions of all chapters.

A summary of the studies presented and the important conclusions drawn from the present studies have been recorded in Chapter 8.

Chapter 2

Analytical Investigation of Laminar Forced Convection In a Channel Partially Filled with Porous Material Subjected to Constant Wall Heat Flux

2.1 Introduction

Fluid flow and heat transfer in channels partially filled with porous media mainly depend on the porous fraction, permeability, porosity (or the ratio of effective viscosity in the porous region to the fluid viscosity), the flow (fully developed or developing), the thermal boundary conditions at the channel walls, and the interfacial boundary conditions.

The objective of the present chapter is to study the hydrodynamic and thermal field characteristics for flow through a channel partially filled with a porous material. The flow in the porous material is described by the Brinkman–extended Darcy equation. The problem is characterized by the porous fraction and Darcy number. The objectives have been set to examine the establish the optimum porous fraction for maximum enhancement in the Nusselt number. In the present chapter, it is assumed that both the flow and the thermal fields are developed and the channel walls are subjected to constant heat flux. These assumptions enable obtaining analytical solutions for the flow and temperature fields.

2.2 Mathematical Formulation

The physical model and the coordinate system, of a channel formed by parallel plates, H distance apart, are shown in Fig. 2.1. x is the axial distance and y is normal to the flow direction measured from the center line of the channel. As per the coordinate system, the plates are at $y = \pm H/2$. The total thickness of the porous material, adjacent to the plates at $y = \pm H/2$, is l_p. It is assumed that the flow and thermal fields are fully developed and the fluid enters the channel with a uniform temperature of T_e. The parallel plates have been subjected to a constant heat flux, q. The problem has been studied assuming laminar, steady, incompressible flow of a Newtonian fluid. The fluid and the porous matrix are in local thermal equilibrium. The porous medium is homogeneous and isotropic. Further, it is assumed that the pressure work is negligible and the thermo-physical properties are constant. The flow in the fluid region is assumed to be governed by Poiseuille description, and in the porous region by Brinkman extended non-Darcy flow.

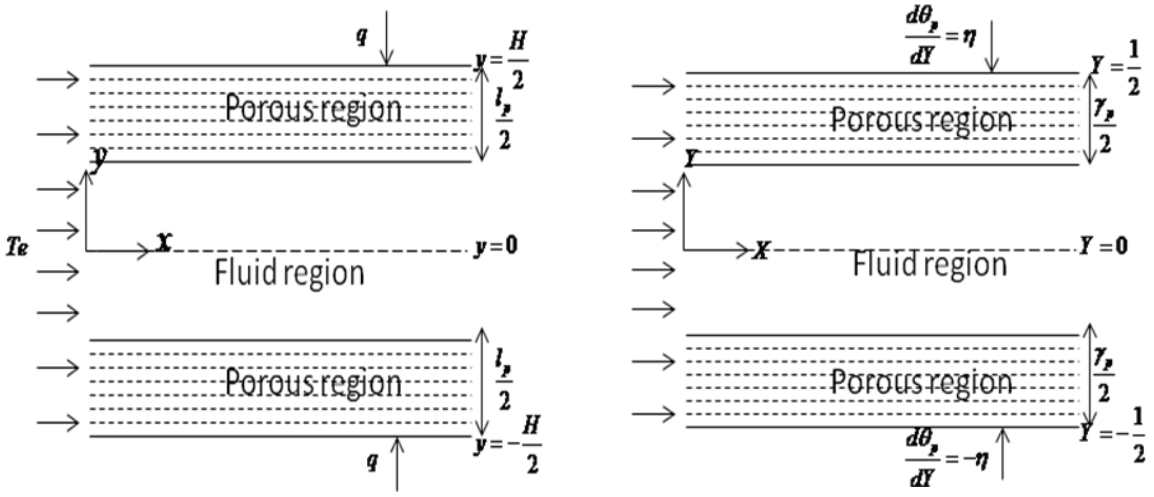

(a) Dimensional (b) Non Dimensional

Fig. 2.1: Physical Model and Coordinate System.

Governing Equations

Momentum Equation in Fluid Region :

$$\frac{d^2u_f}{dy^2} = \frac{1}{\mu_f}\frac{dp}{dx} \tag{2.1}$$

In Eq. (2.1), p is the pressure, μ_f is the dynamic viscosity and u_f is the velocity in the fluid region.

Energy Equation in Fluid Region :

$$\rho C_p\left(u_f\frac{\partial T_f}{\partial x}\right) = k_f\left(\frac{\partial^2 T_f}{\partial y^2}\right) \tag{2.2}$$

In Eq. (2.2), T_f is the temperature in the fluid region ρ, C_p and k_f are the density, the specific heat and the thermal conductivity of the fluid respectively.

Momentum Equation in Porous Region :

$$u_p = -\frac{K}{\mu_f}\frac{dp}{dx} + K\frac{\mu_{eff}}{\mu_f}\frac{d^2u_p}{dy^2} \tag{2.3}$$

In Eq. (2.3), u_p is the velocity in the porous region, K is the permeability of the porous medium, μ_{eff} is the effective viscosity associated with the Brinkman viscous term which may differ from μ_f, the fluid viscosity.

Energy Equation in Porous Region :

$$\rho C_p\left(u_p\frac{\partial T_p}{\partial x}\right) = k_{eff}\left(\frac{\partial^2 T_p}{\partial y^2}\right) \tag{2.4}$$

In Eq. (2.4), T_p is the temperature in the porous region and k_{eff} is the effective thermal conductivity of the porous medium. k_{eff} can be calculated from Catton [21] as

$$k_{eff} = (1-\varphi)\, k_s + \varphi\, k_f \tag{2.5}$$

In Eq. (2.5), φ is the porosity and k_s is the thermal conductivity of the solid in the porous matrix.

Eqs. (2.1) and (2.2) , applicable for the fluid region and Eqs. (2.3) and (2.4) for the porous region, are subjected to the following boundary and interfacial conditions.

Boundary and Interfacial Conditions

$$u_p = 0\,, \quad -k_{eff}\frac{dT_p}{dy} = q \quad \text{at} \quad y = -H/2 \tag{2.6}$$

$$u_f = u_p = u_i \quad , \quad \mu_{eff}\frac{du_p}{dy} = \mu_f \frac{du_f}{dy} \qquad \text{at interface} \quad y = -\frac{H}{2} + \frac{l_p}{2} \tag{2.7}$$

$$T_f = T_p = T_i\,, \qquad k_f\left(dT_f/dy\right) = k_{eff}\left(dT_p/dy\right) \quad \text{at interface} \quad y = -\frac{H}{2} + \frac{l_p}{2} \tag{2.8}$$

$$\frac{du_f}{dy} = 0,\ \frac{dT_f}{dy} = 0 \quad \text{at} \quad y = 0 \quad \{\text{Symmetry boundary conditions}\} \tag{2.9}$$

It may be noted that the boundary conditions given by Eqs. (2.6) to (2.9) for Fig. 2.1, are written for the half channel, making use of the symmetry.

Non-dimensionalization

Governing equations {Eqs. (2.1) to (2.4)} are rendered non-dimensional by introducing the following non-dimensional variables.

$$\left.\begin{aligned} &X = x/H\,,\ Y = y/H\,,\ U_f = u_f/u_{ref}\,,\ U_i = u_i/u_{ref}\,,\ U_p = u_p/u_{ref}\,,\ P = p/\rho\, u_{ref}^2\,, \\ &\theta_f = (T_f - T_e)/(qH/k_f)\,,\ \theta_p = (T_p - T_e)/(qH/k_f) \end{aligned}\right\} \tag{2.10}$$

In Eq. (2.10), X and Y are the non-dimensional coordinates. U and P are the non-dimensional velocity, and pressure. The subscripts f and p refer to fluid and porous regions. θ,{ θ_f in the fluid region and θ_p in the porous region}, is the non-dimensional temperature. u_{ref} is the average velocity through the channel. u_{ref} is related to u_p and u_f by,

$$\frac{2}{H}\left[\int_{-H/2}^{-\frac{H}{2}+\frac{l_p}{2}} u_p dy + \int_{-\frac{H}{2}+\frac{l_p}{2}}^{0} u_f dy\right] = u_{ref} \tag{2.11}$$

In addition, the non-dimensional porous layer thickness γ_p, which shall be referred to as porous fraction is defined by,

$$\gamma_p = l_p / H \tag{2.12}$$

On introducing the non-dimensional variables given by Eq. (2.10), the governing equations for conservation of momentum and energy applicable in the fluid {Eqs. (2.1) and (2.2) }and porous {Eqs. (2.3) and (2.4) } regions in non-dimensional form become,

Fluid Region:

$$\frac{d^2U_f}{dY^2} = Re\frac{dP}{dX} \tag{2.13}$$

$$U_f \frac{\partial\theta_f}{\partial X} = \frac{1}{Pe}\frac{\partial^2\theta_f}{\partial Y^2} \tag{2.14}$$

In Eq. (2.13), *Re*, the Reynolds number and in Eq. (2.14), *Pe*, the Peclet number are defined by,

$$Re = \rho u_{ref} H / \mu_f \tag{2.15}$$

$$Pe = u_{ref} H / \alpha_f \tag{2.16}$$

Porous Region :

$$U_p = -ReDa\frac{dP}{dX} + \frac{Da}{\varepsilon}\frac{d^2U_p}{dY^2} \tag{2.17}$$

$$U_p \frac{\partial \theta_p}{\partial X} = \frac{1}{\eta\, Pe}\frac{\partial^2 \theta_p}{\partial Y^2} \tag{2.18}$$

In Eq. (2.17), *Da*, the Darcy number is defined by,

$$Da = K / H^2 \tag{2.19}$$

In Eqs. (2.17) and (2.18) , ε and η are defined by,

$$\varepsilon = \mu_f / \mu_{eff} \tag{2.20}$$

$$\eta = k_f / k_{eff} \tag{2.21}$$

Non-dimensional Boundary Conditions

The boundary and interfacial conditions given by Eqs. (2.6) to (2.9) take the following non-dimensional form {using Eq. (2.10)}

$$U_p = 0\,,\ \left(\frac{d\theta_p}{dY}\right) = -\eta \qquad \text{at} \quad Y = -1/2 \tag{2.22}$$

$$U_f = U_p = U_i\,,\ \frac{1}{\varepsilon}\frac{dU_p}{dY} = \frac{dU_f}{dY} \quad \text{at the interface} \quad Y = -\frac{1}{2} + \frac{\gamma_p}{2} \tag{2.23}$$

$$\theta_f = \theta_p = \theta_i, \quad \eta\left(\frac{d\theta_f}{dY}\right) = \left(\frac{d\theta_p}{dY}\right) \quad \text{at the interface} \quad Y = -\frac{1}{2} + \frac{\gamma_p}{2} \tag{2.24}$$

$$\frac{dU_f}{dY} = 0, \quad \frac{d\theta_f}{dY} = 0 \qquad \text{at} \qquad Y = 0 \tag{2.25}$$

2.3 Expressions for Non-dimensional Velocity and Skin Friction Coefficient

2.3.1. Non-dimensional velocity Profiles

Fluid Region:

Upon solving Eq. (2.13) along with the boundary conditions given by Eq. (2.23) and (2.25) velocity in the fluid region is obtained thus:

$$U_f(Y) = \frac{1}{8}\left\{8U_i + \left[4Y^2 - \left(-1+\gamma_p\right)^2\right]P_{gr}\right\} \tag{2.26}$$

where

$$U_i = \frac{-\sqrt{Da}\left[e^{\frac{\gamma_p}{2}\sqrt{\frac{\varepsilon}{Da}}} - 1\right]\left\{2\sqrt{Da}\left[e^{\frac{\gamma_p}{2}\sqrt{\frac{\varepsilon}{Da}}} - 1\right] - \left[1 + e^{\frac{\gamma_p}{2}\sqrt{\frac{\varepsilon}{Da}}}\right]\sqrt{\varepsilon}\left(\gamma_p - 1\right)\right\}P_{gr}}{2\left(1 + e^{\gamma_p\sqrt{\frac{\varepsilon}{Da}}}\right)} \tag{2.27}$$

and

$$P_{gr} = Re\frac{dp}{dx} = \frac{12\left(1+e^{\gamma_p\sqrt{\frac{\varepsilon}{Da}}}\right)\sqrt{\varepsilon}}{\left\{\begin{array}{l} 24Da^{3/2}\left(e^{\gamma_p\sqrt{\frac{\varepsilon}{Da}}}-1\right)-6\sqrt{Da}\left(e^{\gamma_p\sqrt{\frac{\varepsilon}{Da}}}-1\right)\varepsilon\left(\gamma_p-1\right)^2+\left(1+e^{\gamma_p\sqrt{\frac{\varepsilon}{Da}}}\right)\sqrt{\varepsilon}\left(\gamma_p-1\right)^3+ \\ 12Da\sqrt{\varepsilon}\left[e^{\gamma_p\sqrt{\frac{\varepsilon}{Da}}}\left(\gamma_p-2\right)-4e^{\frac{\gamma_p}{2}\sqrt{\frac{\varepsilon}{Da}}}\left(\gamma_p-1\right)+\gamma_p-2\right] \end{array}\right\}} \quad (2.28)$$

Porous Region:

Similarly, upon solving Eq. (2.17) along with the boundary conditions given by Eq. (2.22) and (2.23), velocity in the porous region is obtained as

$$U_p(Y) = \frac{e^{-Y\sqrt{\frac{\varepsilon}{Da}}}\left[e^{\frac{(1+2Y)}{2}\sqrt{\frac{\varepsilon}{Da}}}-1\right]\left\{U_i e^{\frac{\gamma_p}{2}\sqrt{\frac{\varepsilon}{Da}}}\left[e^{\frac{-1}{2}\sqrt{\frac{\varepsilon}{Da}}}+e^{Y\sqrt{\frac{\varepsilon}{Da}}}\right]-Da\left[e^{Y\sqrt{\frac{\varepsilon}{Da}}}\left(1-e^{\frac{\gamma_p}{2}\sqrt{\frac{\varepsilon}{Da}}}\right)-e^{\frac{-1}{2}\sqrt{\frac{\varepsilon}{Da}}}\left(e^{\frac{\gamma_p}{2}\sqrt{\frac{\varepsilon}{Da}}}-e^{\gamma_p\sqrt{\frac{\varepsilon}{Da}}}\right)\right]P_{gr}\right\}}{\left(e^{\gamma_p\sqrt{\frac{\varepsilon}{Da}}}-1\right)} \quad (2.29)$$

where U_i and P_{gr} are given Eqs. (2.27) and (2.28).

2.3.2 Skin friction coefficient

Skin friction coefficient C_{fp} at the walls $Y = -\frac{1}{2}$ is defined as

$$C_{fp} = \left\{\mu_{eff}\left.\frac{du_p}{dy}\right|_{y=\frac{-H}{2}}\right\} / \rho u_{ref}{}^2 \quad (2.30)$$

by using Eq. (2.10), we get

$$C_{fp} = \frac{1}{\varepsilon Re}\left.\frac{dU_p}{dY}\right|_{Y=\frac{-1}{2}} \quad (2.31)$$

where Re and ε are given in Eqs. (2.15) and (2.20).

Using Eqs. (2.27) and (2.28) to simplify U_p in Eq.(2.29), then substitute simplified U_p in Eq. (2.31), ReC_{fp} is obtained as

$$ReC_{fp} = \frac{6\left[-2\sqrt{Da}\left(e^{\gamma_p\sqrt{\frac{\varepsilon}{Da}}}-1\right)+2e^{\gamma_p\sqrt{\frac{\varepsilon}{Da}}}\sqrt{\varepsilon}\left(\gamma_p-1\right)\right]}{\left\{\begin{array}{l}24Da^{3/2}\left(e^{\gamma_p\sqrt{\frac{\varepsilon}{Da}}}-1\right)-6\sqrt{Da}\left(e^{\gamma_p\sqrt{\frac{\varepsilon}{Da}}}-1\right)\varepsilon\left(\gamma_p-1\right)^2+\left(1+e^{\gamma_p\sqrt{\frac{\varepsilon}{Da}}}\right)\sqrt{\varepsilon}\left(\gamma_p-1\right)^3\\ +12Da\sqrt{\varepsilon}\left[e^{\gamma_p\sqrt{\frac{\varepsilon}{Da}}}\left(\gamma_p-2\right)-4e^{\frac{\gamma_p}{2}\sqrt{\frac{\varepsilon}{Da}}}\left(\gamma_p-1\right)+\gamma_p-2\right]\end{array}\right\}} \quad (2.32)$$

2.4 Expressions for Non-dimensional Temperature and Nusselt Number

2.4.1 Non-dimensional temperature

It may be noted that, when the thermal field is fully developed, $\partial T / \partial X$ = Constant = constant= dT_b / dX when the channel walls are subjected to constant heat flux. where T_b is bulk mean temperature and defined by

$$T_b = \frac{2\left(\int_{\frac{-H}{2}}^{\frac{-H}{2}+\frac{l_p}{2}} \mathrm{u}_p\ \mathrm{T}_p\ dy + \int_{\frac{-H}{2}+\frac{l_p}{2}}^{0} u_f\ \mathrm{T}_f\ dy\right)}{2\left(\int_{\frac{-H}{2}}^{\frac{-H}{2}+\frac{l_p}{2}} u_p dy + \int_{\frac{-H}{2}+\frac{l_p}{2}}^{0} u_f dy\right)} \quad (2.33)$$

Peclet number appearing in Eqs. (2.14) and (2.18) can be absorbed by defining

$$X^* = X / Pe \quad (2.34)$$

Eqs. (2.14) and (2.18) take the form,

$$U_f \frac{\partial \theta_f}{\partial X^*} = \frac{\partial^2 \theta_f}{\partial Y^2} \tag{2.35}$$

$$U_p \frac{\partial \theta_p}{\partial X^*} = \frac{1}{\eta} \frac{\partial^2 \theta_p}{\partial Y^2} \tag{2.36}$$

Noting that the derivatives, $(\partial \theta_f / \partial X^*)$ and $(\partial \theta_p / \partial X^*)$ are constant, Eqs. (2.35) and (2.36) can be rewritten as,

$$U_f \ \lambda = \frac{d^2 \theta_f}{dY^2} \tag{2.37}$$

$$U_p \ \lambda = \frac{1}{\eta} \frac{d^2 \theta_p}{dY^2} \tag{2.38}$$

where, the constant, λ is used to denote,

$$\lambda = \left(\partial \theta_f / \partial X^*\right) = \left(\partial \theta_p / \partial X^*\right) = \left(d\theta^* / dX^*\right) \tag{2.39}$$

In Eq. (2.39), θ^* is the non-dimensional bulk mean temperature denoted by

$$\theta^* = \frac{T_b - T_e}{\left(qH / k_f\right)} \tag{2.40}$$

and defined as (since from Eq. (2.33)),

$$\theta^* = \frac{2\left(\int_{\frac{-1}{2}}^{\frac{-1}{2}+\frac{\gamma_p}{2}} U_p\ \theta_p\ dY + \int_{\frac{-1}{2}+\frac{\gamma_p}{2}}^{0} U_f\ \theta_f\ dY\right)}{2\left(\int_{\frac{-1}{2}}^{\frac{-1}{2}+\frac{\gamma_p}{2}} U_p dY + \int_{\frac{-1}{2}+\frac{\gamma_p}{2}}^{0} U_f dY\right)} \tag{2.41}$$

Therefore

$$\theta_{w1} - \theta^* = 2\left(\int_{\frac{-1}{2}}^{\frac{-1}{2}+\frac{\gamma_p}{2}} U_p\ (\theta_{w1} - \theta_p)\ dY + \int_{\frac{-1}{2}+\frac{\gamma_p}{2}}^{0} U_f\ (\theta_{w1} - \theta_f)\ dY\right) \tag{2.42}$$

The constant $\lambda (= \partial\theta_f / \partial X^* = \partial\theta_p / \partial X^* = d\theta^* / dX^*)$ can be evaluated by making energy balance on an element.

$$\rho\ C_p\ H\ u_{ref}\ (dT_b / dx) = 2\ q \tag{2.43}$$

Introducing the non-dimensional bulk mean temperature, θ^*, defined by Eq.(2.39), it can be readily shown that,

$$Pe(d\theta^* / dX) = \lambda = 2 = Pe(\partial\theta_f / \partial X^*) = Pe(\partial\theta_p / \partial X^*) \tag{2.44}$$

Using Eqs. (2.26) and (2.29) for U_f and U_p and the boundary conditions given by Eqs. (2.22),(2.24) and (2.25) , the problems have been solved. Since the boundary condition is of Neumann type, Eqs. (2.22) and (2.25) have been solved in terms of temperature difference between the fluid and one of the walls. Let the temperature at wall 1 (at $Y = -H/2$) be T_{w1} and at wall 2 (at $Y = H/2$) be T_{w2}. The corresponding non-dimensional wall temperatures, θ_{w1} and θ_{w2} are now expressed as,

$$\theta_{w1} = \left(T_{w1} - T_e\right) / \left(qH / k_f\right);\ \theta_{w2} = \left(T_{w2} - T_e\right) / \left(qH / k_f\right) \tag{2.45}$$

The solutions to Eqs. (2.37) and (2.38), for $\theta_f(Y)$ and $\theta_p(Y)$ contain θ_{w1}. The temperature profiles in the fluid and porous regions are expressed relative to θ_{w1}.

$[\theta_{w1} - \theta_f(Y)]$ and $[\theta_{w1} - \theta_p(Y)]$ are obtained as,

Fluid Region:

On solving Eq. (2.37) along with the boundary conditions given by Eq. (2.24) and (2.25) , temperature in the fluid region is obtained as

$$\theta_{w1} - \theta_f(Y) = -\frac{\lambda\left\{\begin{array}{l}\varepsilon\left[48DaA_1^2 + A_2\left(5(\gamma_p - 1)^2 - 4Y^2\right) - 24(Da\varepsilon)^{1/2}A_3(\gamma_p - 1)\right]\left[\left((\gamma_p - 1)^2 - 4Y^2\right)\right] \\ +8\eta\left[\begin{array}{l}(\gamma_p - 1)\left(24Da^{3/2}A_3\varepsilon^{1/2} + 6A_3Da^{1/2}\varepsilon^{3/2}(\gamma_p - 1) - A_2\gamma_p\varepsilon(\gamma_p - 1)^2\right) - 48Da^2A_1^2 \\ -6Da\varepsilon\gamma_p\left(3\gamma_p - 4A_4(\gamma_p - 1) - 4 + A_5\left(3\gamma_p - 4\right)\right)\end{array}\right]\end{array}\right\}}{\left\{32\varepsilon^{1/2}\left(\begin{array}{l}24A_3Da^{3/2} - 6A_3\varepsilon Da^{1/2} + A_2\varepsilon^{1/2}(\gamma_p - 1)^3 \\ +12Da\varepsilon^{1/2}\left((\gamma_p - 2)(A_5 + 1) - 4A_4(\gamma_p - 1)\right)\end{array}\right)\right\}} \tag{2.46}$$

Porous Region:

Similarly, on solving Eq. (2.38) along with the boundary conditions given by Eq. (2.22) and (2.24) , temperature in the porous region is obtained as

$$\theta_{w1}-\theta_p(Y)=\frac{-\left\{e^{-Y\sqrt{\frac{\varepsilon}{Da}}}A_6\eta\lambda\left[\begin{array}{l} 6Da\left(\begin{array}{l} e^{Y\sqrt{\frac{\varepsilon}{Da}}}(A_7+A_8)(1+2Y)\varepsilon\gamma_p(\gamma_p-1-2Y) \\ -2A_9e^{Y\sqrt{\frac{\varepsilon}{Da}}}(1+2Y)+ \\ +8Da\left(\begin{array}{l} e^{Y\sqrt{\frac{\varepsilon}{Da}}}(A_7+A_8)(1+2Y-\gamma_p) \\ +e^{2Y\sqrt{\frac{\varepsilon}{Da}}}A_{10}\gamma_p+A_5\gamma_p \end{array}\right) \end{array}\right)+4\sqrt{Da}\sqrt{\varepsilon}(\gamma_p-1)\left(\begin{array}{l} e^{Y\sqrt{\frac{\varepsilon}{Da}}}(A_7-A_8)(1+2Y) \\ -A_4\gamma_p+e^{2Y\sqrt{\frac{\varepsilon}{Da}}}A_{10}A_4\gamma_p \end{array}\right) \\ +A_7(1+2Y)\left[\begin{array}{l} -48Da^2A_1^2+24Da^{3/2}A_3\sqrt{\varepsilon}(\gamma_p-1)+6\sqrt{Da}A_3\varepsilon^{3/2}(\gamma_p-1)^2\gamma_p \\ -A_2\varepsilon(\gamma_p-1)^3\gamma_p-6Da\varepsilon\gamma_p\left(3\gamma_p+A_5(-4+3\gamma_p)-4-4A_4(\gamma_p-1)\right) \end{array}\right] \end{array}\right]\right\}}{\left\{4\sqrt{\varepsilon}\gamma_p\left[\begin{array}{l} 24Da^{3/2}A_3-6\sqrt{Da}A_3\varepsilon(\gamma_p-1)^2+A_2\sqrt{\varepsilon}(\gamma_p-1)^3 \\ +12Da\sqrt{\varepsilon}\left(A_5(\gamma_p-2)-4A_4(\gamma_p-1)+\gamma_p-2\right) \end{array}\right]\right\}} \tag{2.47}$$

2.4.2 Nusselt numbers

The heat transfer coefficient h_p, at the plate $y=-H/2$ adjacent to the porous medium is defined by

$$-k_{eff}\frac{dT_p}{dy}\Big|_{y=-\frac{H}{2}}=h_p(T_{w1}-T_b) \tag{2.48}$$

Upon non-dimensionalizing (using Eq. (2.10)), the Nusselt number at $Y=-1/2$. Nu_p is given by

$$Nu_p=\frac{h_p(2H)}{k_f}=\frac{2}{\theta_{w1}-\theta^*} \tag{2.49}$$

Therefore using Eq. (2.42), Nu_p is given by

$$Nu_p = \frac{140\left[A_{11} - 6\sqrt{Da}A_{12} + A_{13} + 12Da\sqrt{\varepsilon}A_{14}\right]^2}{\left(\begin{array}{l} A_{15}\eta\left(\begin{array}{l} 480Da^{5/2}A_{16} + A_{11}\times A_5 \times A_{17}e^{\frac{1}{2}\sqrt{\frac{\varepsilon}{Da}}}(\gamma_p - 1) - \\ A_5 \times A_2{}^2 e^{\frac{\sqrt{\varepsilon}}{2\sqrt{Da}}}\varepsilon^{3/2}(\gamma_p - 2)(\gamma_p - 1)^3\gamma_p - 2\sqrt{Da}e^{\frac{1}{2}\sqrt{\frac{\varepsilon}{Da}}}(A_5 - A_5{}^3)\varepsilon(\gamma_p - 1)^2 A_{18} - \\ 96Da^2 A_5 e^{\frac{1}{2}\sqrt{\frac{\varepsilon}{Da}}}\sqrt{\varepsilon}A_{19} - 4Da\sqrt{\varepsilon}\left(\begin{array}{l} -2e^{\frac{1}{2}\sqrt{\frac{\varepsilon}{Da}}}(\gamma_p - 1)A_{18}(A_4^3 - A_4^5) + 2e^{\frac{1}{2}\sqrt{\frac{\varepsilon}{Da}}}A_5^2(2\ \gamma_p - (1)^3 + \\ \varepsilon(6 - 9\gamma_p^2 + 5\gamma_p^3)) + e^{\frac{1}{2}\sqrt{\frac{\varepsilon}{Da}}}A_{20}(A_5 + A_5^3) \end{array}\right) \end{array}\right) \\ +(\gamma_p - 1)\left(\begin{array}{l} 1680Da^2 A_1{}^2\eta A_{21} - 840Da^{3/2}A_3\sqrt{\varepsilon}\eta A_{22}(\gamma_p - 1) + \\ 420\,DaA_3{}^2\varepsilon^2(\gamma_p - 1)^3(1 + (3\eta - 1)\gamma_p) - \\ 84\sqrt{Da}A_3\varepsilon^{3/2}(\gamma_p - 1)\left(\begin{array}{l} A_2(\gamma_p - 1)^3(2 + (5\eta - 2)\gamma_p) + \\ 5Da\left(\begin{array}{l} A_{23} - 8A_4(\gamma_p - 1)(1 + (3\eta - 1)\gamma_p) + \\ A_5 \times A_{23} \end{array}\right) \end{array}\right) + \\ \varepsilon\left(\begin{array}{l} A_2{}^2(\gamma_p - 1)^5(17 + (35\eta - 17)\gamma_p) + 42DaA_2(\gamma_p - 1)^2 \times \\ \left(\begin{array}{l} A_{24} - 8A_4(\gamma_p - 1)\times \\ (2 + (5\eta - 2)\gamma_p) + A_5 \times A_{24} \end{array}\right) + 840Da^2 A_1{}^2\left(\begin{array}{l} A_{25} + 4A_4(\gamma_p - 1)(\gamma_p - 1 - 3\eta) + \\ A_5 \times A_{25} \end{array}\right) \end{array}\right) \end{array}\right) \end{array}\right)} \tag{2.50}$$

Where A_i , i = 1, 2,....25 are constants given in appendix.

2.5 Results and Discussion

In this section, velocity profiles and skin friction coefficient for flow through the channel partially filled with porous material have been discussed. It has been assumed that $\varepsilon = \mu_f /\mu_{eff} = 1$ and $\eta = k_f/ k_{eff} = 1$. The channel is referred to as the clear fluid channel here when $\gamma_p = 0$. Similarly, when $\gamma_p = 1.0$, the geometry shall be referred to as channel fully filled with the porous material. When the porous fraction is $0 < \gamma_p < 1.0$, the channel is referred to as channel partially filled with the porous material.

2.5.1 Limiting Cases

Clear Fluid Channel:

By setting γ_p = 0, in Eqs. (2.26), and by using Eqs. (2.27) and (2.28) and (2.32), U_f and C_{ff}, for the clear fluid reduce to,

$$U_f[Y] = \frac{3}{2}\left(1 - 4Y^2\right) \tag{2.51}$$

$$C_{ff} = 6/Re \tag{2.52}$$

when the porous fraction γ_p = 0, in Eqs. (2.46) and (2.50), $\theta_{w1} - \theta_f(Y)$ and Nu_f for the clear fluid reduces to,

$$\theta_{w1} - \theta_f(Y) = \frac{1}{16}\left(5 - 24Y^2 + 16Y^4\right) \tag{2.53}$$

and

$$Nu_f = 140/17 \tag{2.54}$$

Further, when γ_p = 0, Eqs. (2.51) to (2.54) correspond to the exact solutions for the velocity, skin friction coefficient, temperature and the fully developed Nusselt number available in, say, Shah and London [18], p.153 and p.157.

channel fully filled with the porous material:

Similarly the porous fraction γ_p = 1 analytical expressions for U_p, $\theta_{w1} - \theta_p(Y)$, C_{fp} and Nu_p, given by Eqs. (2.29),(2.47),(2.32) and (2.50) reduces respectively,

$$U_p[Y]=\frac{\left[\cosh\left(\frac{\sqrt{\varepsilon}}{2\sqrt{Da}}\right)-\cosh\left(\frac{Y\sqrt{\varepsilon}}{\sqrt{Da}}\right)\right]\sqrt{\varepsilon}}{\sqrt{\varepsilon}\cosh\left(\frac{\sqrt{\varepsilon}}{2\sqrt{Da}}\right)-2\sqrt{Da}\sinh\left(\frac{\sqrt{\varepsilon}}{2\sqrt{Da}}\right)} \tag{2.55}$$

$$\theta_{w1}-\theta_p[Y]=\frac{-\left(1+e^{\frac{\sqrt{\varepsilon}}{\sqrt{Da}}}\right)\left(-8Da+(-1+4Y^2)\varepsilon\right)+16Dae^{\frac{\sqrt{\varepsilon}}{2\sqrt{Da}}}\cosh\left(\frac{Y\sqrt{\varepsilon}}{\sqrt{Da}}\right)}{4\left[2\sqrt{Da}+e^{\frac{\sqrt{\varepsilon}}{\sqrt{Da}}}\left(-2\sqrt{Da}+\sqrt{\varepsilon}\right)+\sqrt{\varepsilon}\right]\sqrt{\varepsilon}} \tag{2.56}$$

$$ReC_{fp}=\frac{1}{\sqrt{Da\ \varepsilon}\coth\left(\frac{\sqrt{\varepsilon}}{2\sqrt{Da}}\right)-2Da} \tag{2.57}$$

When the present coordinate system is used the expression available in Haji-Sheikh and Vafai [59] for U_p reduces to Eq. (2.55).

$$Nu_p=\frac{-24\sqrt{\varepsilon}\left[\sqrt{\varepsilon}\cosh\left(\frac{\sqrt{\varepsilon}}{2\sqrt{Da}}\right)-2\sqrt{Da}\sinh\left(\frac{\sqrt{\varepsilon}}{2\sqrt{Da}}\right)\right]^2}{\sqrt{\varepsilon}(-36Da+\varepsilon)+\sqrt{\varepsilon}(-24Da+\varepsilon)\cosh\left(\frac{\sqrt{\varepsilon}}{\sqrt{Da}}\right)+60Da^{3/2}\sinh\left(\frac{\sqrt{\varepsilon}}{\sqrt{Da}}\right)} \tag{2.58}$$

Eq. (2.58) for Nu_p has been verified to be equivalent to the result given in Nield et al. [25].

Variation of the product (ReC_{fp}) {given by Eq. (2.57)} with the Darcy number is shown in Fig. 2.2(a). For large values of *Da*, $(ReC_{fp})\rightarrow 6$ [see, Eq. (2.52)], as the porous material filled channel approaches the behavior of clear fluid channel, a feature that has been documented.

Variation of the fully developed Nusselt number Nu_p with *Da* is shown in Fig. 2.2(b). Nu_p decreases with *Da*. For large *Da*, i.e. ≥ 1.0, $Nu_p \rightarrow 8.23529$ (= 140/17), which is the value for clear fluid channel, see, Shah and London [18], p. 157 and also in Nield et al. [25].

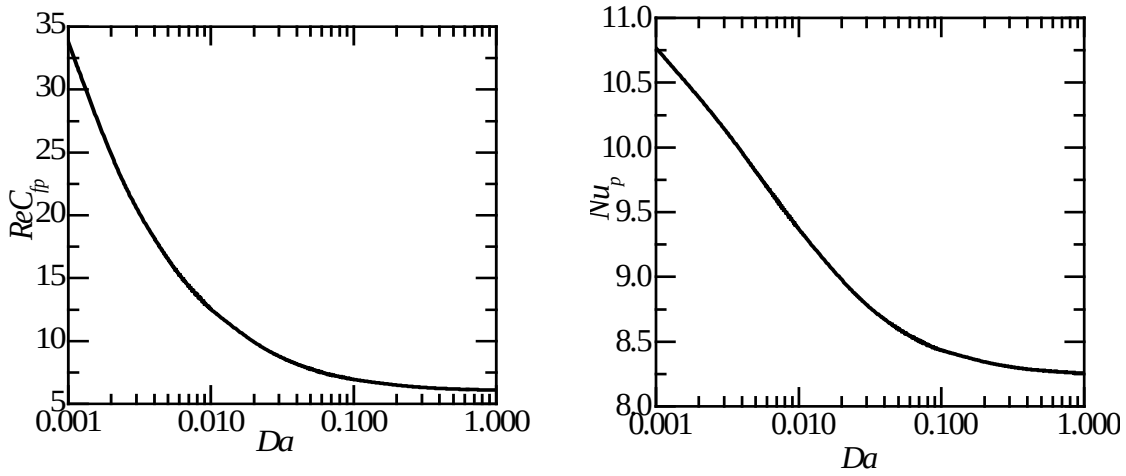

(a) (b)

Fig. 2.2: Variation of (a) skin friction coefficient and (b) Nusselt number with Darcy number in the porous material-filled channel $\gamma_p = 1.0$.

2.5.2 Hydrodynamics

Velocity profiles:

Non-dimensional velocity profiles for different *Da*, for porous layer thickness, γ_p = 0, 0.2, 0.4, 0.6, 0.8 and 1.0 are shown in Figs. 2.3(a) to 2.3(f). As the porous fraction increases, the maximum velocity, which occurs in the fluid region, increases for $\gamma_p < 1.0$. Also, plots are given with different scales on the *X*-axis. Velocity in the porous region U_p is higher at higher Darcy number, whereas, in the fluid region, U_f, is lower at higher *Da*. As can be expected, this is due to the porous region behaving like a clear fluid region as Darcy

number increases. This is evident from the non-dimensional velocity approaching a maximum of 1.5 even at Da = 0.1. Also, the maximum value of the velocity occurs in the fluid region for all porous fractions and this maximum value is even higher than 1.5. It can be noticed from Fig. 2.3(e) that when γ_p = 0.8, the increase in the velocity in the fluid region becomes profound since the resistance in the porous region at the high porous fraction further decelerates the flow resulting in a consequent further increase in the fluid region.

Skin Friction Coefficient:

ReC_{fp} has been evaluated using Eqs. (2.27), (2.28), (2.29) and (2.31). Variation of the product ReC_{fp} with γ_p is shown in Fig. 2.4 for Darcy numbers, Da = 0.001, 0.005, 0.01, 0.05 and 0.1. ReC_{fp} increases with Da for $\gamma_p \leq 0.7$. However, this trend of monotonic variation changes at higher γ_p, which becomes pronounced at γ_p = 0.8. This is due to the channel partially filled with porous material approaching the behavior of a channel fully filled with porous material for which ReC_{fp} decreases with Da, as can be seen in Fig. 2.4, this is a consequence of higher resistance offered with increasing porous fraction which again is a consequence of higher resistance offered with increasing porous fraction.

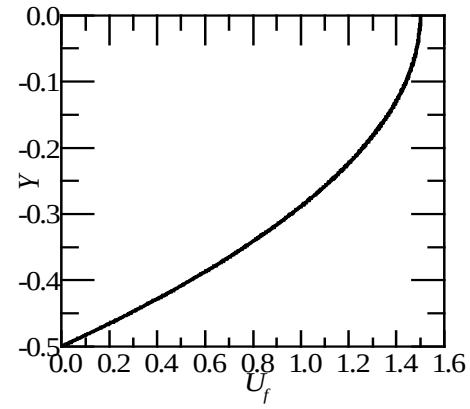

(a) $\gamma_p = 0$

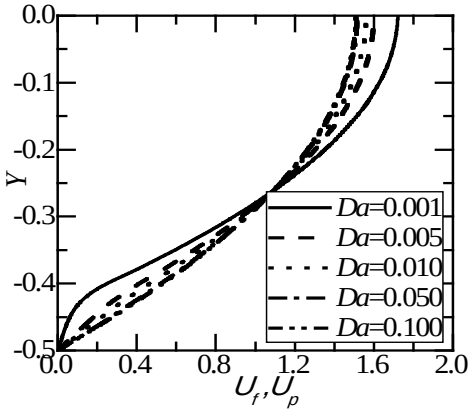

(b) $\gamma_p = 0.2$

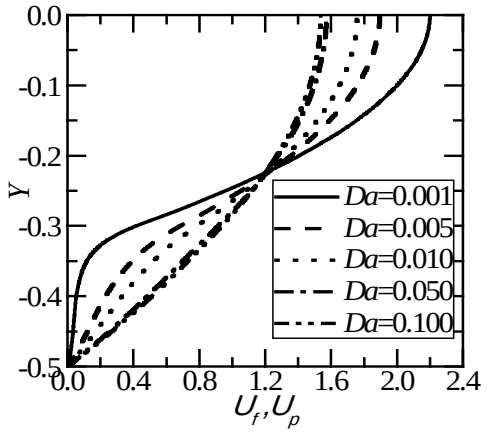

(c) $\gamma_p = 0.4$

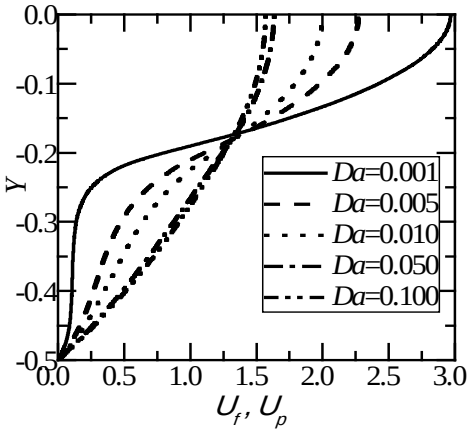

(d) $\gamma_p = 0.6$

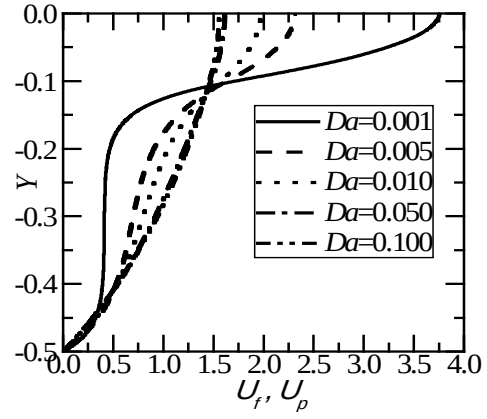

(e) $\gamma_p = 0.8$

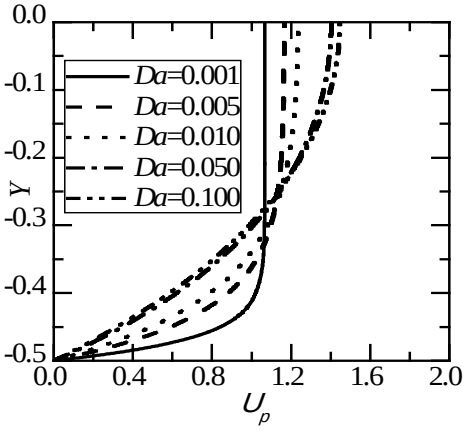

(f) $\gamma_p = 1.0$

Fig. 2.3: Variation of velocity profiles for different values of Darcy numbers, *Da* for (a) $\gamma_p = 0$ (b) $\gamma_p = 0.2$ (c) $\gamma_p = 0.4$ (d) $\gamma_p = 0.6$ (e) $\gamma_p = 0.8$ and (f) $\gamma_p = 1.0$.

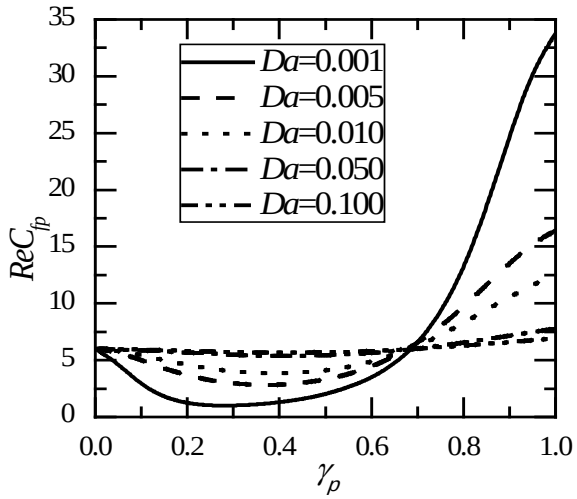

Fig. 2.4: Variation of ReC_{fp} with porous fraction γ_p at different values of Darcy number.

2.5.3 Thermal Field

Profiles of the non-dimensional temperature in excess of the wall temperature, $(\theta_{w1} - \theta_p)$, $(\theta_{w1} - \theta_f)$ are shown in Figs. 2.5(a) to 2.5(f) for γ_p = 0, 0.2, 0.4, 0.6, 0.8 and 1.0 for different Darcy numbers. From Figs. 2.5(b) to 2.5(e), the effect of porous fraction on $(\theta_{w1} - \theta_p)$, $(\theta_{w1} - \theta_f)$ can be assessed. Maximum in $(\theta_{w1} - \theta)$ occurs closer to the wall at Y = 0. This is commensurate with the acceleration associated with the fluid in the fluid region at higher γ_p. It may also be noticed that $(\theta_{w1} - \theta)$ is lower for higher Darcy number for all $0 < \gamma_p \leq 1.0$.

In contrast, the profiles shown in Fig. 2.5(a) and Fig. 2.5(f) for γ_p = 0 and 1.0 are symmetric about Y = 0. The profile in Fig. 2.5(a) is independent of the Darcy number and is also very close to the profile in Fig. 2.5(f) for Da = 0.1, the highest Darcy number depicted in Fig. 2.5. Indeed, the porous material filled channel behaves like the clear fluid channel at higher Da, which is also noticeable in Figs. 2.5(b) to 2.5(c) as well, even though these two profiles pertain to a partially filled channel.

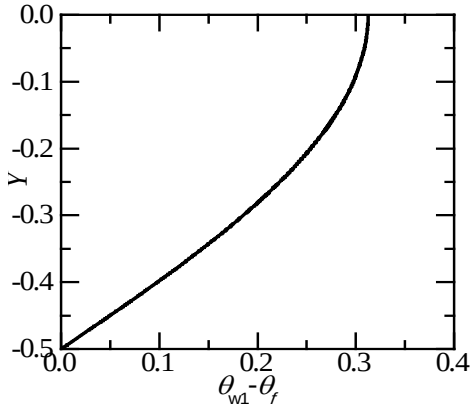

(a) $\gamma_p = 0$

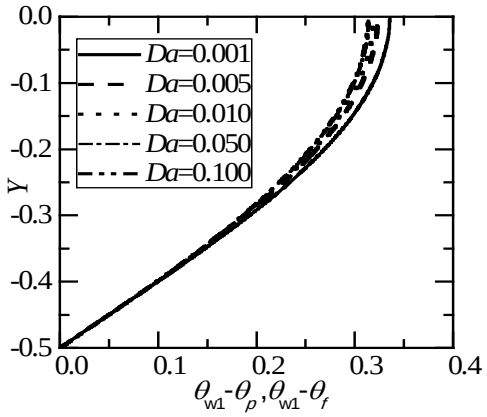

(b) $\gamma_p = 0.2$

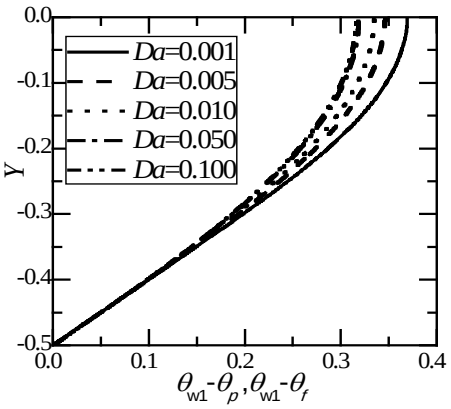

(c) $\gamma_p = 0.4$

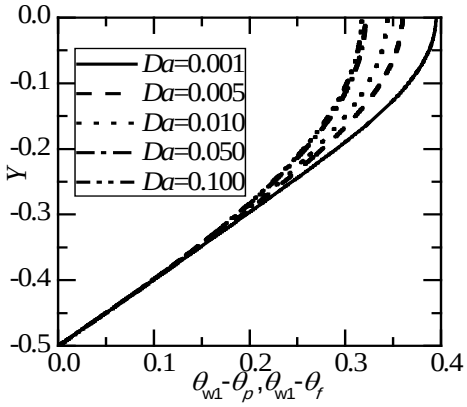

(d) $\gamma_p = 0.6$

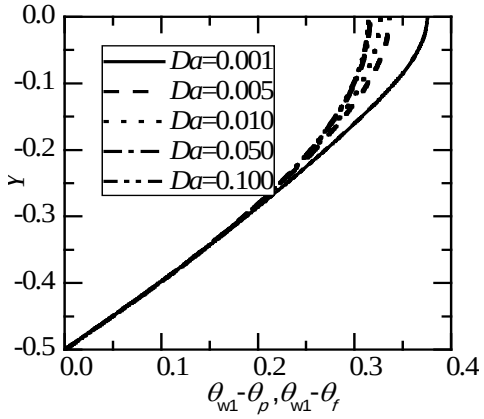

(e) $\gamma_p = 0.8$

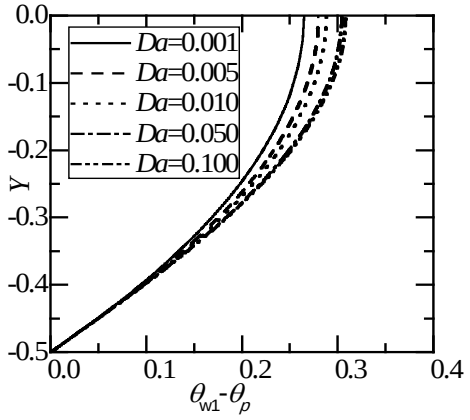

(f) $\gamma_p = 1.0$

Fig. 2.5: Variation of $\theta_{w1} - \theta_p$, $\theta_{w1} - \theta_f$ profiles for different values of Darcy numbers, *Da* for (a) $\gamma_p = 0$ (b) $\gamma_p = 0.2$ (c) $\gamma_p = 0.4$ (d) $\gamma_p = 0.6$ (e) $\gamma_p = 0.8$ and (f) $\gamma_p = 1.0$.

Fully Developed Nusselt Number:

Variation of fully developed Nusselt number on the fluid side, (i.e., at $Y = -1/2$, the lower plate which is adjacent to the porous region), Nu_p, with the porous fraction γ_p for different Darcy numbers is shown in Fig. 2.6(a). Nu_f displays minimum for $0 < \gamma_p < 1.0$. The $\gamma_p(Nu_{p\min}) \rightarrow 140/17$ as *Da* increases which signifies that the flow approaches that of a clear fluid channel flow. $\gamma_p(Nu_{p\min})$ decreases with increasing *Da*.

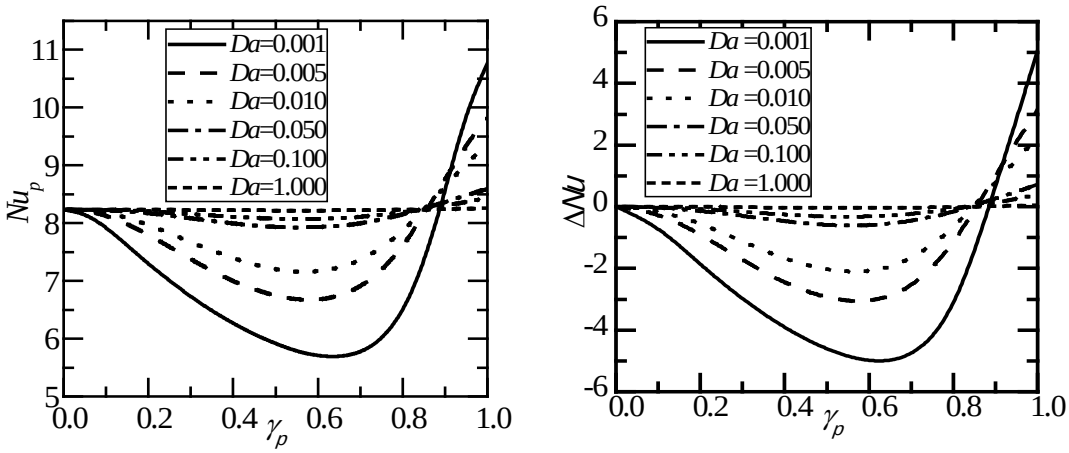

(a) Nu_p (b) ΔNu

Fig. 2.6: Variation of (a) Nu_p and (b) ΔNu with porous fraction γ_p at different values of Darcy number, *Da*.

The net change, ΔNu, is shown in Eq. (2.59), in comparison with the fully developed clear fluid channel value and this is given below

$$\Delta Nu = 2\left[Nu_p|_{\gamma_p} - (140/17)\right] \tag{2.59}$$

Variation of ΔNu with γ_p for different *Da* is shown in Fig. 2.6(b). It is clear from Fig. 2.6(b) that ΔNu is negative for γ_p say, < 0.9 with a minimum for some $0 < \gamma_p < 0.9$.

ΔNu is > 0 for higher $\gamma_p > 0.9$. ΔNu reaches a limit, a possible maximum in general, at $\gamma_p = 1.0$, which is equal to the difference in the Nusselt number values corresponding to a porous material filled channel and a clear channel. Enhancement in the Nusselt number when porous material of thickness $l_p/2$ is attached to each of the two walls of the channel is low, compared to the enhancement when the channel is fully filled with porous material. The value of ΔNu is maximum at $\gamma_p = 1.0$.

2.6 Conclusions

Fluid flow and heat transfer in parallel plate channels partially filled with porous medium have been studied assuming fully developed flow and temperature fields. The given amount of porous material in the porous layer has been distributed equally at the two walls. The channel walls are subjected to constant heat flux.

The problem is characterized by Darcy number, *Da,* Reynolds number, *Re,* and the porous fraction, γ_p. Analytical expressions for the non-dimensional velocity and temperature profiles in the porous and clear fluid regions have been obtained. From the velocity and temperature expressions, the fully developed skin friction coefficients and the Nusselt numbers on the porous wall has been obtained analytically. It has been shown that the analytical expressions yield the standard values for a clear fluid channel and for fully porous material filled channels when the porous fraction γ_p is set equal to 0 and 1.0 respectively. The value of the porous fraction where the minimum value of Nusselt number occurs, decreases as Darcy number increases.

Chapter 3

Analytical Study of Forced Convection In a Channel Partially Filled with Porous Material with Effect of Magnetic Field Subjected to Constant Wall Heat Flux

3.1 Introduction

The objective of the present chapter is to study the effect of magnetic field on Newtonian fluid flow in a parallel plate channel partially filled with fluid saturated porous medium. The channel walls are subjected to constant wall heat flux. The fluid flow is taken to be fully developed. Analytical solutions have been obtained. Following the analysis of chapter 2, analytical solutions have been obtained. Closed form expressions for flow variables such as velocity, skin friction coefficient, temperature and Nusselt number have been obtained and the effects of various relevant parameters such as Darcy number *Da*, porous fraction γ_p, Hartmann number, *M* and the flow variables have been studied.

3.2 Mathematical Formulation

The physical model and the coordinate system, that of a channel formed by parallel plates, *H* distance apart, are shown in Fig. 3.1. *x* is the flow direction and *y* is normal to the flow direction measured from the center of the channel. As per the coordinate system, the plates are at $y = \pm H/2$. The thickness of the porous medium, adjacent to the plates at

$y = \pm H/2$, is l_p. It is assumed that the flow and thermal fields are fully developed and the fluid enters the channel with a uniform temperature T_e. The parallel plates have been subjected to constant heat flux, q. The problem has been studied by assuming steady, laminar, incompressible flow of a Newtonian fluid. The fluid and the porous matrix are in local thermal equilibrium. The porous medium is homogeneous and isotropic. Further, it is assumed that the thermo-physical properties are constant.

A transverse magnetic field of uniform intensity is applied. The Magnetic Reynolds number is assumed to be very small and there is no external electric field so that the induced current is very small and hence it can be neglected. The flow in the fluid region is assumed to be governed by Poiseuille description, and in the porous region by Brinkman extended non-Darcy flow with effect of the magnetic field.

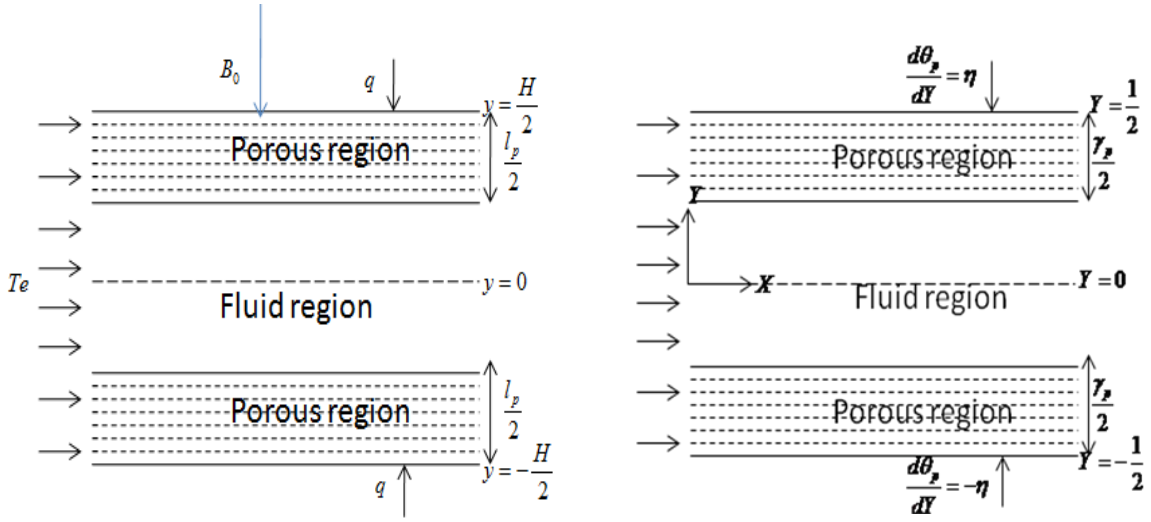

(a) Dimensional (b) Non Dimensional

Fig. 3.1: Physical Model and Coordinate System.

The governing equation for the flow in the fluid region can be expressed by

$$\mu_f \frac{d^2 u_f}{dy^2} + \bar{J} \times \bar{B} = \frac{dp}{dx} \tag{3.1}$$

Also the flow in the porous region can be expressed by

$$\mu_{eff} \frac{d^2 u_p}{dy^2} - \frac{\mu_f}{K} u_p + \bar{J} \times \bar{B} = \frac{dp}{dx} \tag{3.2}$$

Eqs. (3.1) and (3.2) were taken from the literature Ashish, Satya and Filippov [125].

In Eq. (3.1), p is the pressure, μ_f is the dynamic viscosity and u_f is the velocity in the fluid region. In Eq. (3.2), u_p is the velocity in the porous region, K is the permeability of the porous medium, μ_{eff} is the effective viscosity associated with the Brinkman viscous term which may differ from μ_f, the fluid viscosity. In Eqs. (3.1) and (3.2), $\bar{J}$ is the electric current density and $\bar{B}$ is the magnetic induction vector of applied uniform magnetic field. Assume that external electric field is absent and internal causes such as separation of charges or polarization do not cause an induced electric field, $\bar{J} = \sigma\left(\bar{u}_{f,p} \times \bar{B}\right)$, where σ is electric conductivity. Therefore Lorentz forces $F_L = \bar{J} \times \bar{B}$ and velocity vector $\bar{u}_{f,p}$ are collinear and opposite in direction. Hence $F_L = \bar{J} \times \bar{B} = -\sigma B_0^{\,2} u_{f,p}$, where $B_0 = \left|\bar{B}\right|$. Therefore, the governing equations given in Eqs. (3.1) and (3.2) are reduced to,

Momentum equation in fluid region:

$$\mu_f \frac{d^2 u_f}{dy^2} - \sigma {B_0}^2 u_f = \frac{dp}{dx} \tag{3.3}$$

Momentum equation in porous region:

$$\mu_{eff} \frac{d^2 u_p}{dy^2} - \frac{\mu_f}{K} u_p - \sigma {B_0}^2 u_p = \frac{dp}{dx} \tag{3.4}$$

Energy Equation in Fluid Region :

$$\rho C_p \left(u_f \frac{\partial T_f}{\partial x} \right) = k_f \left(\frac{\partial^2 T_f}{\partial y^2} \right) \tag{3.5}$$

In Eq. (3.5), T_f is the temperature in the fluid region ρ, C_p and k_f are the density, the specific heat and the thermal conductivity of the fluid respectively.

Energy Equation in Porous Region :

$$\rho C_p \left(u_p \frac{\partial T_p}{\partial x} \right) = k_{eff} \left(\frac{\partial^2 T_p}{\partial y^2} \right) \tag{3.6}$$

In Eq. (3.6), T_p is the temperature in the porous region and k_{eff} is the effective thermal conductivity of the porous medium. k_{eff} can be calculated from Catton [21] as,

$$k_{eff} = (1-\varphi)\, k_s + \varphi k_f \tag{3.7}$$

In Eq. (3.7), φ is the porosity and k_s is the thermal conductivity of the solid in the porous matrix.

Eqs. (3.3) and (3.5) , applicable for the fluid region and Eqs. (3.4) and (3.6) for the porous region, are subjected to the following boundary and interfacial conditions.

Boundary and Interfacial Conditions

$$u_p = 0, \quad -k_{eff}\frac{dT_p}{dy} = q \quad \text{at} \quad y = -H/2 \tag{3.8}$$

$$u_f = u_p = u_i \quad , \quad \mu_{eff}\frac{du_p}{dy} = \mu_f \frac{du_f}{dy} \qquad \text{at interface} \quad y = -\frac{H}{2} + \frac{l_p}{2} \tag{3.9}$$

$$T_f = T_p = T_i, \qquad k_f\left(dT_f/dy\right) = k_{eff}\left(dT_p/dy\right) \quad \text{at interface} \quad y = -\frac{H}{2} + \frac{l_p}{2} \tag{3.10}$$

$$\frac{du_f}{dy} = 0, \; \frac{dT_f}{dy} = 0 \quad \text{at} \quad y = 0 \quad \{\text{Symmetry boundary conditions}\} \tag{3.11}$$

It may be noted that the boundary conditions given by Eqs. (3.8) to (3.11) for Fig. 3.1, are written for half channel, making use of the symmetry.

Non-dimensionalization:

The governing equations {Eqs. (3.3) to (3.6)} are rendered non-dimensional by introducing the following non-dimensional variables.

$$\left.\begin{aligned} &X = \frac{x}{H}, \;\; Y = \frac{y}{H}, \;\; U_f = u_f/u_{ref}, \;\; U_i = u_i/u_{ref}, \; U_p = u_p/u_{ref}, \; P = \frac{p}{\mu_f \; u_{ref}/H}, \\ &\theta_f = (T_f - T_e)/(qH/k_f), \;\; \theta_p = (T_p - T_e)/(qH/k_f), \;\; M = \sqrt{\frac{\sigma B_0{}^2 H^2}{\mu_f}} \end{aligned}\right\} \tag{3.12}$$

In Eq. (3.12), X and Y are non-dimensional coordinates. U and P are non-dimensional velocity, and pressure. The subscripts f and p refer to fluid and porous regions. θ,{ θ_f in

the fluid region and θ_p in the porous region}, is the non-dimensional temperature. u_{ref} is the average velocity through the channel. u_{ref} is related to u_p and u_f by

$$\frac{2}{H}\left[\int_{-H/2}^{-\frac{H}{2}+\frac{l_p}{2}} u_p dy + \int_{-\frac{H}{2}+\frac{l_p}{2}}^{0} u_f dy\right] = u_{ref} \tag{3.13}$$

In addition, the non-dimensional porous layer thickness γ_p, which shall be referred to as porous fraction is defined by,

$$\gamma_p = l_p / H \tag{3.14}$$

On introducing the non-dimensional variables given by Eq. (3.12), the governing equations for conservation of momentum and energy applicable in the fluid {Eqs. (3.3) and (3.5)}and porous {Eqs. (3.4)and (3.6) } regions in non-dimensional form become,

Fluid Region:

$$\frac{d^2U_f}{dY^2} - M^2U_f = \frac{dP}{dX} \tag{3.15}$$

$$U_f \frac{\partial\theta_f}{\partial X} = \frac{1}{Pe}\frac{\partial^2\theta_f}{\partial Y^2} \tag{3.16}$$

In Eq. (3.15), *M*, the Hartmann number (Magnetic field parameter) and in Eq. (3.16), *Pe*, the Peclet number is defined by,

$$Pe = u_{ref} H / \alpha_f \tag{3.17}$$

Porous Region:

$$\frac{d^2U_p}{dY^2} - \varepsilon\left(\frac{1}{Da} + M^2\right)U_p = \varepsilon\frac{dP}{dX} \tag{3.18}$$

$$U_p\frac{\partial\theta_p}{\partial X} = \frac{1}{\eta\, Pe}\frac{\partial^2\theta_p}{\partial Y^2} \tag{3.19}$$

In Eq. (3.18), *Da*, the Darcy number is defined by,

$$Da = K / H^2 \tag{3.20}$$

In Eqs. (3.18) and (3.19) , ε and η are defined by,

$$\varepsilon = \mu_f / \mu_{eff} \tag{3.21}$$

$$\eta = k_f / k_{eff} \tag{3.22}$$

Non-dimensional Boundary Conditions

The boundary and interfacial conditions given by, Eqs. (3.8) to (3.11) take the following non-dimensional form {using Eq. (3.12)}

$$U_p = 0\,, \left(\frac{d\theta_p}{dY}\right) = -\eta \quad \text{at} \quad Y = -1/2 \tag{3.23}$$

$$U_f = U_p = U_i\,, \ \frac{1}{\varepsilon}\frac{dU_p}{dY} = \frac{dU_f}{dY} \quad \text{at the interface} \quad Y = -\frac{1}{2} + \frac{\gamma_p}{2} \tag{3.24}$$

$$\theta_f = \theta_p = \theta_i\,, \ \eta\left(\frac{d\theta_f}{dY}\right) = \left(\frac{d\theta_p}{dY}\right) \quad \text{at the interface} \quad Y = -\frac{1}{2} + \frac{\gamma_p}{2} \tag{3.25}$$

$$\frac{dU_f}{dY} = 0\ , \frac{d\theta_f}{dY} = 0 \qquad \text{at} \qquad Y = 0 \tag{3.26}$$

3.3 Expressions for Non-dimensional Velocity and Skin Friction

3.3.1 Non-dimensional velocity profiles

Fluid Region:

On solving Eq. (3.15) along with the boundary conditions given by Eq. (3.24) and Eq. (3.26), the velocity in the fluid region is obtained as

$$U_f(Y) = \frac{e^{-MY}\left(U_i e^{\frac{M}{2}(\gamma_p - 1)}\left(1 + e^{2MY}\right)M^2 + \left(e^{\frac{M}{2}(\gamma_p - 1)} - e^{M(Y+\gamma_p - 1)} + e^{\frac{M}{2}(4Y+\gamma_p - 1)} - e^{MY}\right)\right)}{\left(1 + e^{M(\gamma_p - 1)}\right)M^2} \tag{3.27}$$

Porous Region:

Similarly, on solving Eq. (3.18) along with the boundary conditions given by Eqs. (3.23) and (3.24), velocity in the porous region is obtained as

$$\begin{aligned} U_p(Y) = {} & e^{-Y\sqrt{\frac{\varepsilon(1+DaM^2)}{Da}}}\left(e^{\frac{(1+2Y)}{2}\sqrt{\frac{\varepsilon(1+DaM^2)}{Da}}} - 1\right) \\ & \left(U_i\left(A_{26}e^{-\frac{1}{2}\sqrt{\frac{\varepsilon(1+DaM^2)}{Da}}} + A_{27}e^{Y\sqrt{\frac{\varepsilon(1+DaM^2)}{Da}}}\right)\left(1 + DaM^2\right)\right. \\ & -Da\left(e^{Y\sqrt{\frac{\varepsilon(1+DaM^2)}{Da}}} - A_{27}\left(e^{-\frac{1}{2}\sqrt{\frac{\varepsilon(1+DaM^2)}{Da}}} + e^{Y\sqrt{\frac{\varepsilon(1+DaM^2)}{Da}}}\right)\right.\right. \\ & \left.\left. + A_{26}e^{-\frac{1}{2}\sqrt{\frac{\varepsilon(1+DaM^2)}{Da}}}\right)p_g\Bigg) \\ & /\,(A_{26} - 1)(1 + DaM^2) \end{aligned} \tag{3.28}$$

where

$$U_i = \frac{p_g\left(\frac{\sqrt{Da}\,\tanh\left[\frac{\gamma_p}{4}\sqrt{\frac{\varepsilon(1+DaM^2)}{Da}}\right]}{\sqrt{\varepsilon\left(1+DaM^2\right)}}+\frac{\tanh\left[M\left(\gamma_p-1\right)/2\right]}{M}\right)}{\left(M\,\tanh\left[\frac{M}{2}\left(\gamma_p-1\right)\right]\right)-\left(\frac{\sqrt{1+DaM^2}\,\coth\left(\frac{\gamma_p}{2}\sqrt{\frac{\varepsilon(1+DaM^2)}{Da}}\right)}{\sqrt{Da\varepsilon}}\right)} \tag{3.29}$$

and

$$p_g = \frac{dP}{dX} = \frac{1}{\left\{Da\left(\frac{2(A_{27}-1)^3(1+A_{27})A_{28}-A_{29}(A_{30}+A_{31})+(A_{26}-1)M(A_{32}-2A_{26}(A_{33}+A_{34}))}{\left((A_{26}-1)M(1+DaM^2)^{3/2}\sqrt{\varepsilon}(A_{35}+A_{36})\right)}\right)+\left(\frac{(-1-DaM^2)A_{37}+A_{38}+(1+DaM^2)A_{39}+A_{40}}{M^3(1+DaM^2)(A_{41}+A_{42})}\right)\right\}} \tag{3.30}$$

Where U_i and P_g are given Eqs. (3.29) and (3.30).

3.3.2 Skin friction coefficient

Skin friction coefficient C_{fp} at the walls $Y=-1/2$ is defined as,

$$C_{fp} = \left\{\mu_{eff}\,\frac{du_p}{dy}\Big|_{y=\frac{-H}{2}}\right\}/\rho u_{ref}{}^2 \tag{3.31}$$

by using Eq. (3.12), we get

$$C_{fp} = \frac{1}{\varepsilon Re}\frac{dU_p}{dY}\Big|_{Y=\frac{-1}{2}} \tag{3.32}$$

Using Eqs. (3.29) and (3.30) to simplify U_p in Eq. (3.28), substitute simplified U_p in Eq. (3.32), ReC_{fp} is obtained as

$$ReC_{fp} = \frac{1}{\sqrt{\varepsilon}}\left(e^{\frac{1}{2}\sqrt{\frac{\varepsilon}{Da}(1+DaM^2)}} \left(A_{44} - DaA_{43}\right)\right) \qquad (3.33)$$

$$/\left(\frac{\left(\begin{array}{l} Da\left(\begin{array}{l} 2(A_{27}-1)^3(A_{27}+1)A_{28} - A_{29}(A_{30}+A_{31}) \\ -(A_{26}-1)M\left(\begin{array}{l}(A_{26}{}^2+1)\gamma_p\sqrt{(1+DaM^2)\varepsilon} \\ +2A_{26}(A_{33}+A_{34})\end{array}\right)\end{array}\right)\end{array}\right)}{(A_{26}-1)M(1+DaM^2)^{3/2}\sqrt{\varepsilon}(A_{35}+A_{36})} + \left(\frac{A_{37}+A_{38}+A_{39}+A_{40}}{M^3(1+DaM^2)(A_{41}-A_{42})}\right)\Bigg)$$

3.4 Expressions for Non-dimensional Temperature and Nusselt Number

3.4.1 Non-dimensional temperature

It may be noted that, when the thermal field is fully developed, $\partial T / \partial X$ =constant= dT_b / dX when the channel walls are subjected to constant heat flux. Peclet number appearing in Eqs. (3.16) and (3.19) can be absorbed by defining

$$X^* = X / Pe \qquad (3.34)$$

Eqs. (3.16) and (3.19) take the form,

$$U_f \frac{\partial \theta_f}{\partial X^*} = \frac{\partial^2 \theta_f}{\partial Y^2} \qquad (3.35)$$

$$U_p \frac{\partial \theta_p}{\partial X^*} = \frac{1}{\eta}\frac{\partial^2 \theta_p}{\partial Y^2} \qquad (3.36)$$

Noting that the derivatives, $(\partial \theta_f / \partial X^*)$ and $(\partial \theta_p / \partial X^*)$ are constant, Eqs. (3.35) and (3.36) can be rewritten as,

$$U_f \;\lambda = \frac{d^2\theta_f}{dY^2} \tag{3.37}$$

$$U_p \;\lambda = \frac{1}{\eta}\frac{d^2\theta_p}{dY^2} \tag{3.38}$$

where, the constant λ is used to denote,

$$\lambda = \left(\partial\theta_f / \partial X^*\right) = \left(\partial\theta_p / \partial X^*\right) = \left(d\theta^* / dX^*\right) \tag{3.39}$$

In Eq. (3.39), θ^* is the non-dimensional bulk mean temperature denoted by

$$\theta^* = \frac{T_b - T_e}{\left(qH / k_f\right)} \tag{3.40}$$

and defined as,

$$\theta^* = \frac{2\left(\int_{\frac{-1}{2}}^{\frac{-1}{2}+\frac{\gamma_p}{2}} U_p\;\theta_p\;dY + \int_{\frac{-1}{2}+\frac{\gamma_p}{2}}^{0} U_f\;\theta_f\;dY\right)}{2\left(\int_{\frac{-1}{2}}^{\frac{-1}{2}+\frac{\gamma_p}{2}} U_p dY + \int_{\frac{-1}{2}+\frac{\gamma_p}{2}}^{0} U_f dY\right)} \tag{3.41}$$

Therefore

$$\theta_{w1} - \theta^* = 2\left(\int_{\frac{-1}{2}}^{\frac{-1}{2}+\frac{\gamma_p}{2}} U_p\;(\theta_{w1} - \theta_p)\,dY + \int_{\frac{-1}{2}+\frac{\gamma_p}{2}}^{0} U_f\;(\theta_{w1} - \theta_f)\,dY\right) \tag{3.42}$$

The constant $\lambda(=\partial\theta_f / \partial X^* = \partial\theta_p / \partial X^* = d\theta^* / dX^*)$ can be evaluated by making energy balance on an element.

$$\rho\, C_p\, H\, u_{ref}\,(dT_b / dx) = 2\, q \tag{3.43}$$

Introducing the non-dimensional bulk mean temperature, θ^*, defined by Eq. (3.39), it can be readily shown that,

$$Pe(d\theta^* / dX) = \lambda = 2 = Pe(\partial\theta_f / \partial X^*) = Pe(\partial\theta_p / \partial X^*) \tag{3.44}$$

Using Eqs. (3.27) and (3.28) for U_f and U_p and the boundary conditions given by Eqs. (3.23),(3.25) and (3.26) , energy Eqs. (3.37) and (3.38) have been solved. Since the boundary condition is of Neumann type, Eqs. (3.23) and (3.26) have been solved in terms of temperature difference between the fluid and one of the walls. Let the temperature at wall 1 (at $Y = -H/2$) be T_{w1} and at wall 2 (at $Y = H/2$) be T_{w2}. The corresponding non-dimensional wall temperatures, θ_{w1} and θ_{w2} are now expressed as,

$$\theta_{w1} = \left(T_{w1} - T_e\right) / (qH / k_f);\ \theta_{w2} = \left(T_{w2} - T_e\right) / (qH / k_f) \tag{3.45}$$

The solutions to Eqs. (3.37) and (3.38), for $\theta_f(Y)$ and $\theta_p(Y)$ contain θ_{w1}. The temperature profiles in the fluid and porous regions are expressed relative to θ_{w1}.

Porous Region:

Solving Eq. (3.38) along with the boundary conditions given by Eqs. (3.23) and (3.25), the temperature in the porous region is obtained as

$$\theta_{w1}-\theta_p(Y)=-\frac{\eta\lambda}{2(A_{26}-1)^2A_{27}}e^{-\frac{(2Y-1)}{2}\sqrt{\frac{\varepsilon}{Da}(1+DaM^2)}} \tag{3.46}$$

$$\times\left\{\begin{array}{l}2Da(A_{26}-1)U_i\left(\left(e^{2Y\sqrt{\frac{\varepsilon}{Da}(1+DaM^2)}}-e^{-\sqrt{\frac{\varepsilon}{Da}(1+DaM^2)}}\right)A_{26}\gamma_p\right)\\+U_i\left(A_{27}-A_{27}{}^3\right)e^{\frac{(Y-1)}{2}\sqrt{\frac{\varepsilon}{Da}(1+DaM^2)}}(1+2Y)(2Da(A_{26}-1)+A_{45}\sqrt{Da})\\+\frac{1}{(1+DaM^2)^2\varepsilon Da(A_{26}-1)}(Da(A_{46}+8e^{2Y\sqrt{\frac{\varepsilon}{Da}(1+DaM^2)}}(A_{26}-A_{27})\\+e^{\frac{(2Y-1)}{2}\sqrt{\frac{\varepsilon}{Da}(1+DaM^2)}}(A_{27}-A_{27}{}^3)\left[8+\left[M^2(1+2Y)\varepsilon(1+2Y-\gamma_p)\right]\right])\\+(A_{27}-A_{27}{}^3)\varepsilon e^{\frac{(2Y-1)}{2}\sqrt{\frac{\varepsilon}{Da}(1+DaM^2)}}(1+2Y)(1+2Y-\gamma_p))p_g\\+(A_{26}-1)\left(A_{27}-A_{27}{}^3\right)e^{\frac{(Y-1)}{2}\sqrt{\frac{\varepsilon}{Da}(1+DaM^2)}}(1+2Y)(A_{47}+A_{48})\end{array}\right\}$$

Fluid Region:

Similarly, solving Eq. (3.37) along with the boundary conditions given by Eqs. (3.25) and (3.26), the temperature in the fluid region is obtained as

$$\theta_{w1}-\theta_f(Y)=-\frac{e^{-MY}\lambda}{8\left[1+e^{M(\gamma_p-1)}\right]} \tag{3.47}$$

$$\times\left\{\begin{array}{l}\dfrac{-8U_i\left(e^{MY}-e^{\frac{M}{2}(\gamma_p-1)}+e^{M(\gamma_p+Y-1)}-e^{\frac{M}{2}(\gamma_p+4Y-1)}\right)}{M^2}\\-\dfrac{4\eta U_i\sqrt{Da}\left(e^{MY}+e^{M(\gamma_p+Y-1)}\right)\left(\begin{array}{l}-2\sqrt{Da}(A_{26}-1)\sqrt{1+DaM^2}\\+(1+DaM^2)\end{array}\right)(1+A_{27})\gamma_p\sqrt{\varepsilon}}{(A_{26}-1)(1+DaM^2)^{3/2}\varepsilon}\\+\left(\dfrac{8e^{\frac{M}{2}(\gamma_p-1)}+8e^{\frac{M}{2}(\gamma_p+4Y-1)}+e^{MY}A_{49}}{M^4}\right)p_g-\left(e^{MY}+e^{M(\gamma_p+Y-1)}\right)\eta\gamma_p(A_{47}-A_{48})\end{array}\right\}$$

Where A_i , i = 26, 27, ...53 are constants given in appendix.

3.4.2 Nusselt numbers

The heat transfer coefficient h_p, at the plate $y = -H/2$ adjacent to the porous medium is defined by

$$-k_{eff}\frac{dT_p}{dy}\Big|_{y=-\frac{H}{2}} = h_p(T_{w1} - T_b) \tag{3.48}$$

Upon non-dimensionalizing {using Eq. (3.12)}, the Nusselt number at $Y = -1/2$, Nu_p^M is given by

$$Nu_p^M = \frac{h_p(2H)}{k_f} = \frac{2}{\theta_{w1} - \theta^*} \tag{3.49}$$

Therefore using Eq. (3.42), Nu_p^M in Eq. (3.49) is obtained. Because of lengthy expression, only numerical results are given in plots.

3.5 Results and Discussion

It has been assumed that $\varepsilon = \mu_f / \mu_{eff} = 1$ and $\eta = k_f / k_{eff} = 1$. Here, when $\gamma_p = 0$, the channel is referred to as clear fluid channel. Similarly, when $\gamma_p = 1.0$, the channel is referred to as channel fully filled with the porous medium. When the porous fraction is $0 < \gamma_p < 1.0$, the channel is treated as partially filled with the porous material.

3.5.1 Limiting Cases

Clear Fluid Channel:

By setting γ_p = 0, in Eq. (3.27), and by using Eqs. (3.29) and (3.30) , U_f for the clear fluid reduces to,

$$U_f(Y) = \frac{e^{M\left(\frac{1}{2}-Y\right)}\left\{U_i(1+e^{2MY})M^2 - \left[e^{M\left(Y-\frac{1}{2}\right)} - e^{2MY} + e^{M\left(\frac{1}{2}+Y\right)} - 1\right]p_g\right\}}{(1+e^M)M^2} \tag{3.50}$$

when the porous fraction γ_p = 0, in Eq. (3.47) , $\theta_{w1} - \theta_f(Y)$ for the clear fluid reduces to,

$$\theta_{w1} - \theta_f(Y) = \frac{e^{-MY}\left\{8e^{\frac{M}{2}} + 8e^{\frac{M}{2}(1+4Y)} + (e^{MY} + e^{M(1+Y)})\left[M^2(1-4Y^2) - 8\right]\right\}}{8M\left[2 + e^M(M-2) + M\right]} \tag{3.51}$$

Further, when γ_p = 0, substituting M = 0 in Eqs. (3.50) and (3.51), the expressions reduce to the equations given in chapter 2, § 2.5, which are available in Shah and London [18], p.153 and p.157.

channel fully filled with the porous material:

Similarly, for the porous fraction γ_p = 1.0 analytical expressions for U_p, $\theta_{w1} - \theta_p(Y)$ are given by Eqs. (3.28) and (3.46), which reduce respectively,

$$U_p(Y) = e^{-Y\sqrt{\frac{\varepsilon}{Da}(1+DaM^2)}}\left(e^{\frac{(1+2Y)}{2}\sqrt{\frac{\varepsilon}{Da}(1+DaM^2)}}-1\right) \tag{3.52}$$
$$\times\left\{\begin{array}{l} U_i\left(1+e^{\frac{(1+2Y)}{2}\sqrt{\frac{\varepsilon}{Da}(1+DaM^2)}}\right)(1+DaM^2) \\ +Da\left(e^{\sqrt{\frac{\varepsilon}{Da}(1+DaM^2)}}-1\right)\left(e^{Y\sqrt{\frac{\varepsilon}{Da}(1+DaM^2)}}-1\right)P_g \end{array}\right\} / \left(e^{\sqrt{\frac{\varepsilon}{Da}(1+DaM^2)}}-1\right)(1+DaM^2)$$

$$\theta_{w1}-\theta_p(Y) = e^{-Y\sqrt{\frac{\varepsilon}{Da}(1+DaM^2)}} \tag{3.53}$$
$$\times\left\{\begin{array}{l} A_{50}e^{-Y\sqrt{\frac{\varepsilon}{Da}(1+DaM^2)}}(4Y^2-1)+Da\left[\begin{array}{l} A_{51}-8e^{2Y\sqrt{\frac{\varepsilon}{Da}(1+DaM^2)}}\left(\begin{array}{l} e^{\frac{1}{2}\sqrt{\frac{\varepsilon}{Da}(1+DaM^2)}} \\ -8e^{\frac{3}{2}\sqrt{\frac{\varepsilon}{Da}(1+DaM^2)}} \end{array}\right) \\ +A_{52}e^{Y\sqrt{\frac{\varepsilon}{Da}(1+DaM^2)}}\left(M^2\varepsilon(1-4Y^2)-8\right) \end{array}\right] \end{array}\right\}$$
$$/\,8A_{53}\left[e^{\sqrt{\frac{\varepsilon}{Da}(1+DaM^2)}}-1\right]\sqrt{1+DaM^2}$$

Substituting M = 0 in Eqs. (3.52) and (3.53), the expressions reduce to the equations given in Haji-Sheikh and Vafai [59] and chapter 2, § 2.5. In the presence of the magnetic field, for γ_p = 0, the present results are agreeing with the results in Chorlton [180], for γ_p =1.0, the present results are compared with the coordinate system in the paper published by Raju et al. [115]. It is found to be good agreement. Variation of velocity profiles with different Darcy numbers, *Da*, for channels fully filled with porous medium ($\gamma_p = 1.0$) are shown in Fig. 3.2. For large values of *Da*, the porous material

filled channel approaches the behavior of clear fluid channel, a feature that has been reported in literature Bhargavi, Satyamurty and Raja Sekhar[45].

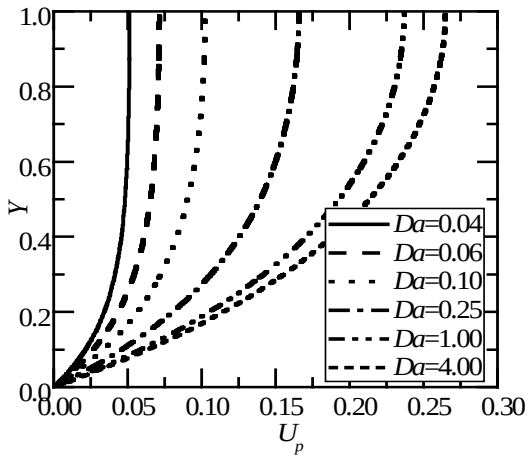

Fig. 3.2: Variation of velocity profiles for different Darcy numbers, *Da* and for *M* = 2.0 for $\gamma_p = 1.0$.

3.5.2 Hydrodynamics

Velocity Profiles:

Non-dimensional velocity profiles for different Hartmann numbers are *M* = 1, 2, 5 and 10 for a typical Darcy number *Da* =0.005 and, for porous layer thickness, γ_p = 0, 0.2, 0.4, 0.6, 0.8 and 1.0, as shown in Figs. 3.3(a) to 3.3(f). The flow behavior for the present geometry in the absence of magnetic field parameter (*M* = 0) has already been discussed in chapter 2, § 2.5. For clear fluid channel γ_p = 0, the maximum velocity decreases as Hartmann number *M* increases at the centre of the channel {Chorlton [180], Baoku et al. [123]}. This is due to the magnetic field parameter (*M*), which depicts the ratio of magnetic induction to the viscous force. Hence, an increase in the magnetic field parameter reduces the viscosity of the fluid. It means magnetic field is limited to retardation. Velocity in the porous region increases, as Hartmann number *M* increases and velocity in the fluid region decreases as Hartmann number *M*, increases for all porous

fractions $0 < \gamma_p < 1.0$. The maximum velocity is occurs in the fluid region at $Y = 0$. As Hartmann number M increases, the porous channel behaves like a clear fluid channel for all Darcy numbers. It means presence of the magnetic field parameter is negligible in the fully filled porous region with such high Hartmann number. This fact can be observed from the profiles of Fig. 3.3(f).

Skin friction Coefficient:

ReC_{fp} has been evaluated using Eqs. (3.28), (3.29), (3.30) and (3.32). Variation of the product ReC_{fp} with γ_p is shown in Fig. 3.4 for different Hartmann numbers, M = 1, 2, 5 and 10. As Hartmann number, M increases, ReC_{fp} increases for all porous fractions, γ_p. In the absence of the magnetic parameter (M =0), $ReC_{fp} \to 6$ as mentioned in Chapter 2, § 2.5.

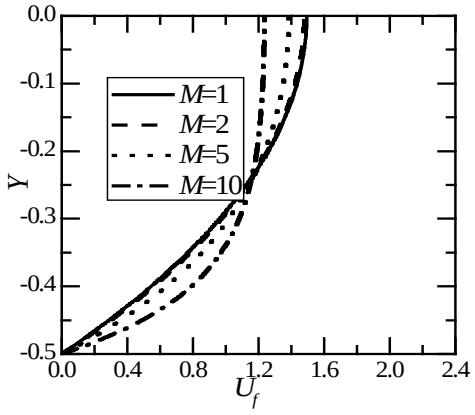

(a) $\gamma_p = 0$

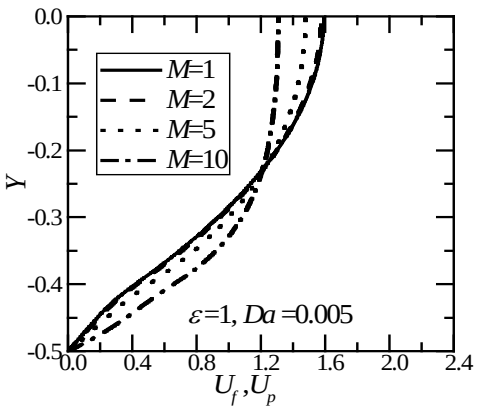

(b) $\gamma_p = 0.2$

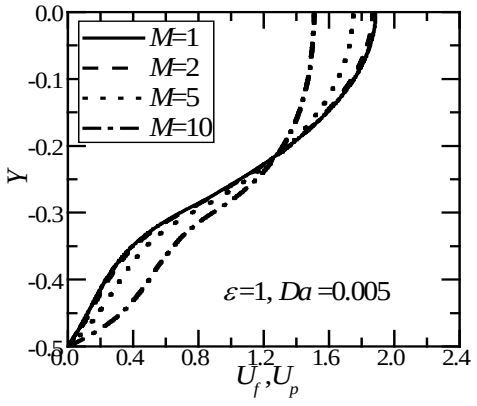

(c) $\gamma_p = 0.4$

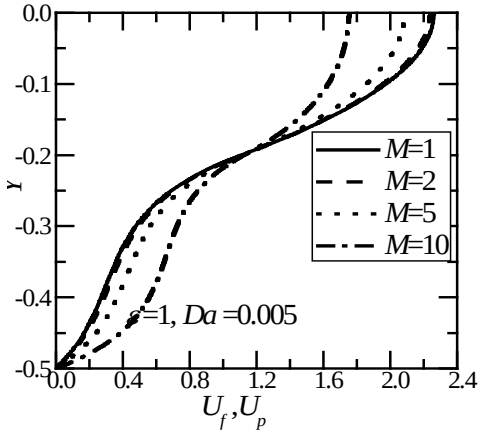

(d) $\gamma_p = 0.6$

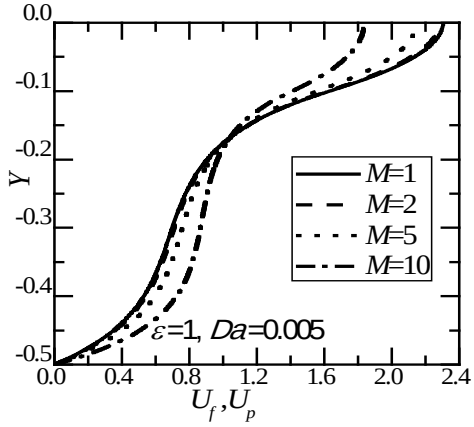

(e) $\gamma_p = 0.8$

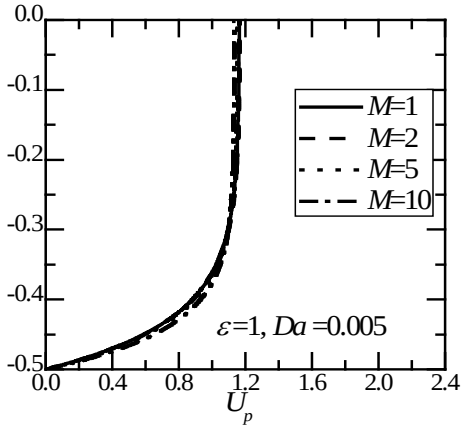

(f) $\gamma_p = 1.0$

Fig. 3.3: Variation of velocity profiles for different values of Hartmann number, *M* for *Da* = 0.005 for (a) $\gamma_p = 0$ (b) $\gamma_p = 0.2$ (c) $\gamma_p = 0.4$ (d) $\gamma_p = 0.6$ (e) $\gamma_p = 0.8$ and (f) $\gamma_p = 1.0$.

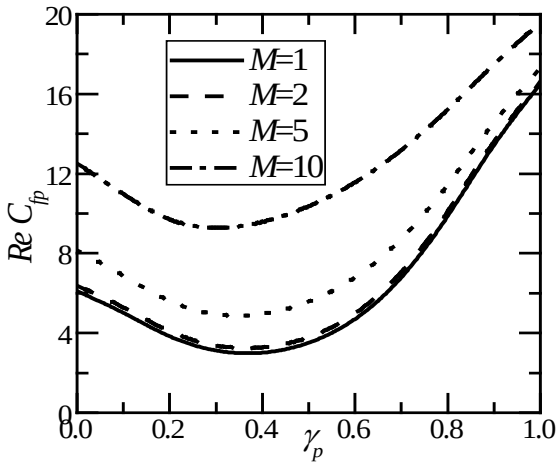

Fig. 3.4: Variation of ReC_{fp} with porous fraction γ_p at different values Hartmann number.

3.5.3 Thermal Field

Non-dimensional temperature profiles in excess of the wall temperature, $(\theta_{w1}-\theta_p)$, $(\theta_{w1}-\theta_f)$ are shown in Figs. 3.5(a) to 3.5(f) for different Hartmann numbers, M = 1,2,5 and 10, for Da = 0.005 and for porous layer thickness, γ_p = 0, 0.2, 0.4, 0.6, 0.8 and 1.0. The flow behavior in the absence of magnetic field parameter (M = 0) is already discussed in chapter 2, § 2.5. From Figs. 3.5(b) to 3.5(e), the effect of porous fraction, γ_p on $(\theta_{w1}-\theta_p)$, $(\theta_{w1}-\theta_f)$ can be assessed in the presence of magnetic parameter Hartmann number, M. The maximum value in $(\theta_{w1}-\theta)$ occurs closer to the wall at Y = 0. It may also be noticed that $(\theta_{w1}-\theta)$ is lower for higher Hartmann number, M for all porous fraction, $0\leq \gamma_p \leq 1.0$. In contrast with the profiles shown in Figs. 3.5(b) to 3.5(e), the profiles shown in Figs. 3.5(a) and 3.5(f) for γ_p = 0 and 1.0 are symmetric about Y = 0. The profiles in Fig. 3.5(a) are very close to the profiles in Fig. 3.5(f) for large Hartmann number, say M = 10. For the profile in Fig. 3.5(f) where γ_p =1.0 for a fully porous

channel, we observe that the effect of magnetic field parameter is not felt much. This behavior is same for all Darcy numbers.

Fully Developed Nusselt Numbers:

Variation of fully developed Nusselt number on the porous side, (i.e., at $Y = -1/2$, the lower plate which is adjacent to the porous region), Nu_p^M, with the porous fraction γ_p for different Hartmann numbers, M = 1, 2, 5 and 10 and for Da = 0.005 is shown in Fig. 3.6. As Hartmann number increases, the Nusselt number also increases for all porous fractions and for all Darcy numbers. Also, the minimum value of Nu_p^M at $0.55 \le \gamma_p \le 0.6$ for all Hartmann numbers, which is also the same for $M = 0$ given in chapter 2, § 2.5.

The net change, ΔNu^M, is defined relative to the fully developed Nusselt number value in the porous region in the absence of magnetic field ($M = 0$),

$$\Delta Nu^M = 2\left[Nu_p^M - Nu_P^{M=0}\right] \tag{3.54}$$

Variation of ΔNu^M with M for different porous fractions $\gamma_p = 0.2$ and $\gamma_p = 0.8$ for Da = 0.005 is shown in Fig. 3.7. As Hartmann number, M increases ΔNu^M is also increases for $\gamma_p = 0.2$ and $\gamma_p = 0.8$. Also, it can be observe that as the porous fraction, γ_p, increases, ΔNu^M decreases for all Hartmann numbers. This implies that as porous fraction increases, the effect of magnetic field decreases.

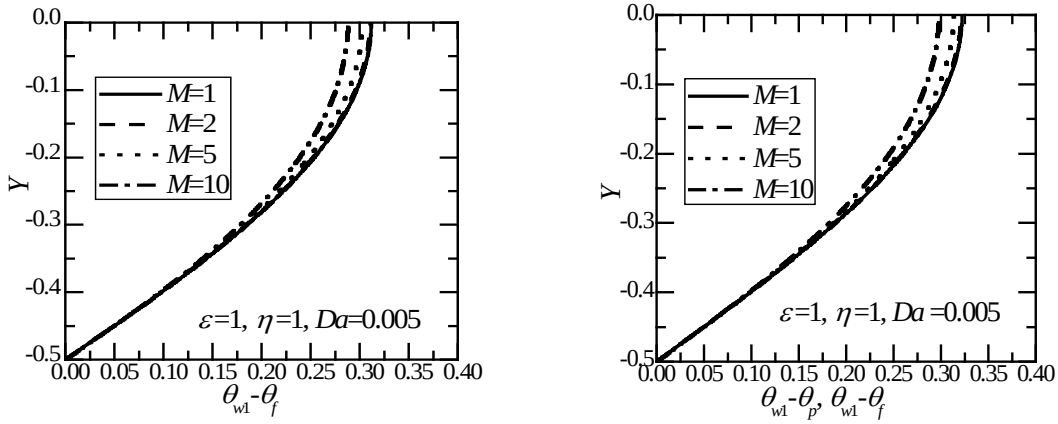

(a) $\gamma_p = 0$ (b) $\gamma_p = 0.2$

(c) $\gamma_p = 0.4$ (d) $\gamma_p = 0.6$

(e) $\gamma_p = 0.8$ (f) $\gamma_p = 1.0$

Fig. 3.5: Variation of $\theta_{w1} - \theta_p$, $\theta_{w1} - \theta_f$ profiles for different values of Hartmann number, *M* for *Da* =0.005 for (a) $\gamma_p = 0$ (b) $\gamma_p = 0.2$ (c) $\gamma_p = 0.4$ (d) $\gamma_p = 0.6$ (e) $\gamma_p = 0.8$ and (f) $\gamma_p = 1.0$.

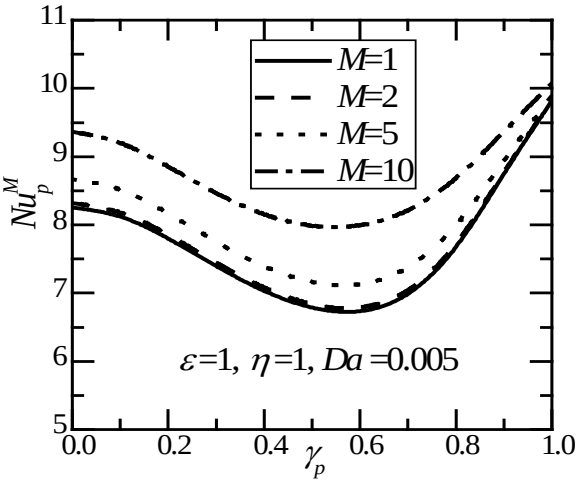

Fig. 3.6: Variation of Nu_p^M with porous fraction γ_p at different values of Hartmann number, *M* for Darcy number, *Da*=0.005.

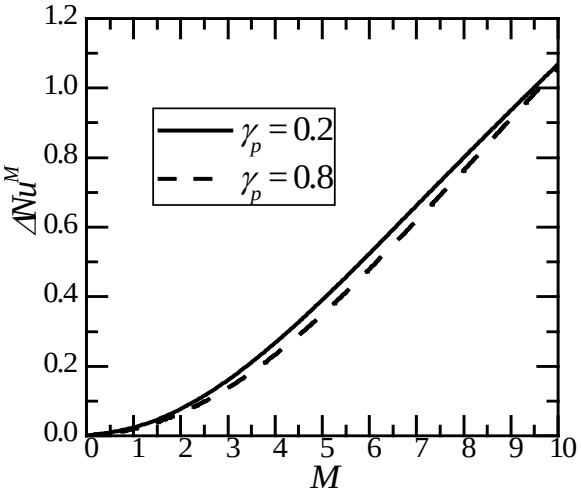

Fig. 3.7: Variation of ΔNu^M for porous fractions $\gamma_p = 0.2$ and $\gamma_p = 0.8$ with Hartmann number, *M* for Darcy number, *Da*=0.005.

3.6 Conclusions

The effects of forced convection and magnetic field for a fully developed flow of Newtonian fluid in a parallel plate channel partially filled with porous material have been studied. Analytical solution has been obtained and closed form expressions have been derived for velocity, skin friction coefficient and temperature profiles in the porous and

fluid regions and the Nusselt number has also been obtained for the porous region. The effects of relevant parameters such as Darcy number, *Da*, Hartmann number, *M*, and the porous fraction, γ_p have been studied graphically. It has been shown that analytical expressions yield standard values for the Hartmann number, $M = 0$ {absence of the magnetic field)} for all porous fractions γ_p , $0 \leq \gamma_p \leq 1.0$ {Chapter 2, § 2.5}.

Some important conclusions are

- Nusselt number and the net change in the Nusselt number increase with Hartmann number, *M* for all porous fractions, γ_p. Hence the effect of the magnetic field can be considered to enhance the heat transfer in the channels partially filled with porous medium.

- Further, it is also observed that Nusselt number and the net change in the Nusselt number decrease with porous fraction, γ_p and then increase with porous fraction, γ_p. Hence, optimal value for the porous fraction to decrease the Nusselt number in the presence of magnetic field is around 0.6.

Chapter 4

Analytical Investigation of Laminar Forced Convection with Viscous Dissipation in Parallel Plate Channels Partially Filled with a Porous Material at the Conduction Limit

4.1 Introduction

A general review of the dissipation models in porous media is available in Nield and Bejan [48], but none of those models deal with the effect of viscous dissipation at the conduction limit. Viscous dissipation effects are to be included in the energy equation when *Br* (Characterized by viscous dissipation) is large, for a flow through a porous medium. Though the problem of flow in porous media with dissipation have been studied by several researchers{ Nield and Bejan [48], Murthy [143 and 181], Hooman and Gorji-Bandpy [151], Hooman, Pourshaghaghy and Ejlali [154] and Ramjee and Satyamurty [182] etc.}, the effect of viscous dissipation at conduction limit (neglecting the convective terms in the energy equation and hence, it is a balance of conduction and dissipation terms) has not received sufficient attention. Since the conduction limit (i.e., neglecting convection terms in the energy equation), since $\partial T/\partial x = \partial T_b/\partial x = 0$, the condition $\frac{\partial}{\partial x^*}\left(\frac{T-T_{ref}}{T_b-T_{ref}}\right)=0$ is not violated for say $T_{ref}=T_e$ for constant flux boundary condition and $T_{ref}=T_w$ for constant wall boundary condition. Also, $\frac{\partial}{\partial x^*}\left(\frac{T-T_{ref}}{T_b-T_{ref}}\right)=0$ also implies no further net heat transfer to the fluid. There is heat transfer after the Nusselt number reached the fully developed value, until when $T=T_b=T_w$ which occurs at the same X^*. Thus the difference between the fully developed Nusselt number and the limiting Nusselt number is that, heat transfer continues to take place after attaining the

fully developed value, whereas, after the limiting value is reached, the net heat transfer is zero.

In view of the above, in this chapter, a laminar forced convection in parallel plate channels partially filled with a porous medium has been investigated. Three dissipation models in the energy equation at the conduction limit, namely, the Darcy model due to Bejan [49] , form drag model due to Nield [140] and the clear fluid compatible model due to Al-Hadhrami, Elliott and Ingham [135 and 136] have been considered. Further, it is assumed that the flow field is fully developed. Two types of boundary conditions are considered. They are (i) constant wall heat flux and (ii) constant wall temperature. Based on the analysis of chapter 2, for fluid flow, analytical solutions have been obtained for energy equations. Further expressions for temperature, bulk mean temperature and Nusselt number at the conduction limit have been derived for both the cases of the boundary conditions. The effect of important relevant parameters on them, have been investigated.

4.2 Mathematical Formulation

The physical model and the coordinate system, that of a channel formed by parallel plates, H distance apart, partially filled with porous material shown in Fig. 4.1. Two porous materials, each of thickness $l_p/2$, attached to both the walls. x is the axial distance and y is normal to flow direction measured from center of the channel. As per the coordinate system the walls are at $y = \pm H/2$. The fluid enters the channel at inlet temperature T_e. It has been assumed that the parallel plates of the channel have been subjected to uniform heat flux, q or constant wall temperature, $T=T_w$. The flow in the fluid region is assumed to be governed by Poiseuille description, and by Brinkman

extended non-Darcy flow in the porous region. The problem has been studied on the assumptions, that the flow is steady, incompressible and fully developed. The fluid and the porous matrix are in local thermal equilibrium. The porous medium is homogeneous and isotropic and the fluid properties are assumed to be constant.

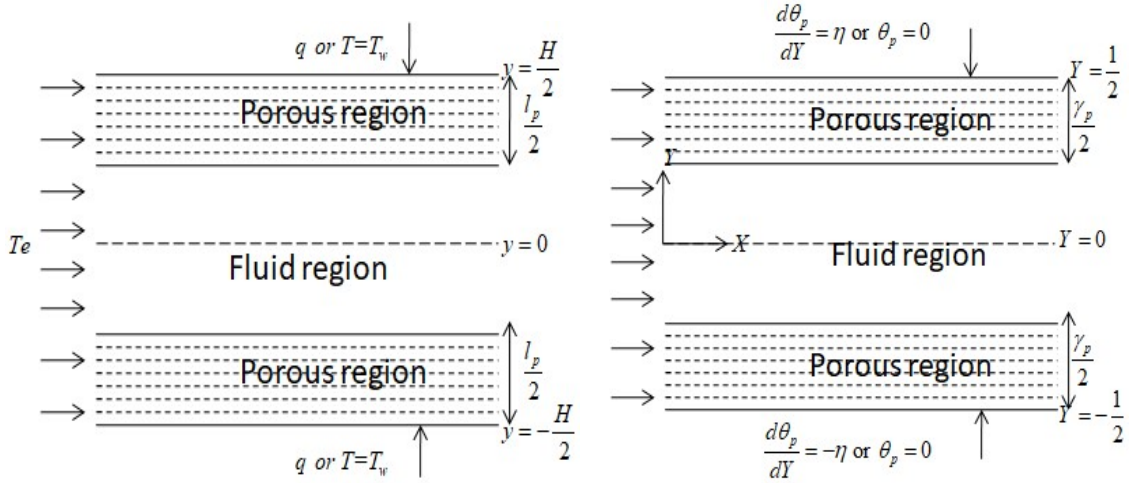

(a) Dimensional (b) Non Dimensional

Fig. 4.1: Physical Model and the Coordinate System.

Governing Equations:

Momentum Equation in Fluid Region :

$$\frac{d^2u_f}{dy^2} = \frac{1}{\mu_f}\frac{dp}{dx} \tag{4.1}$$

In Eq. (4.1), p is the pressure, μ_f is the dynamic viscosity and u_f is the velocity in the fluid region.

Energy Equation in the Conduction Limit:

The governing equation in the conduction limit is obtained by neglecting the convective term in the energy equation and hence, it is a balance of conduction and dissipation terms.

$$k_f \frac{d^2 T_f}{dy^2} + \mu_f \left(\frac{du_f}{dy} \right)^2 = 0 \tag{4.2}$$

In Eq. (4.2), T_f is the temperature in fluid region, k_f is the thermal conductivity in fluid region.

Momentum Equation in Porous Region :

$$u_p = -\frac{K}{\mu_f} \frac{dp}{dx} + K \frac{\mu_{eff}}{\mu_f} \frac{d^2 u_p}{dy^2} \tag{4.3}$$

Energy Equations in the Conduction Limit:

$$k_{eff} \frac{d^2 T_p}{dy^2} + \Phi_i = 0 \tag{4.4}$$

$$k_{eff} = (1-\varphi)\, k_s + \varphi\, k_f \tag{4.5}$$

In Eq. (4.5), φ is the porosity and k_s is the thermal conductivity of the solid in the porous matrix.

In Eq. (4.4), Φ_i is dissipation models, 1) the Darcy model due to Bejan [49], 2) form drag model due to Nield [140] and 3) the clear fluid compatible model due to Al-Hadhrami et al. [135 and 136].

Darcy model:

$$\Phi_1 = \frac{\mu_f}{K} u_p^{\,2} \tag{4.6}$$

Form drag model:

$$\Phi_2 = \frac{\mu_f}{K} u_p^{\,2} - \mu_{eff} u_p \frac{d^2 u_p}{dy^2} \tag{4.7}$$

Clear fluid compatible model:

$$\Phi_3 = \frac{\mu_f}{K} u_p{}^2 + \mu_f \left(\frac{du_p}{dy} \right)^2 \tag{4.8}$$

Boundary and Interfacial Conditions:

$$\left.\begin{array}{l} u_p = 0 \ , \ -k_{eff} \dfrac{dT_p}{dy} = q \quad \text{at} \quad y = -H/2 \ \{\text{subjected to constant wall heat flux}\} \\ u_p = 0 \ , \ T = T_w \quad \text{at} \quad y = -H/2 \ \{\text{subjected to constant wall temperature}\} \end{array}\right\} \tag{4.9}$$

$$u_f = u_p = u_i \quad , \quad \mu_{eff} \frac{du_p}{dy} = \mu_f \frac{du_f}{dy} \qquad \text{at interface} \quad y = -\frac{H}{2} + \frac{l_p}{2} \tag{4.10}$$

$$T_f = T_p = T_i , \qquad k_f \left(dT_f / dy \right) = k_{eff} \left(dT_p / dy \right) \text{ at interface } \quad y = -\frac{H}{2} + \frac{l_p}{2} \tag{4.11}$$

$$\frac{du_f}{dy} = 0, \ \frac{dT_f}{dy} = 0 \quad \text{at} \quad y = 0 \tag{4.12}$$

It may be noted that the boundary conditions given by Eqs. (4.9) to (4.12) for Fig. 4.1 are written for the half channel, making use of the symmetry. These interface conditions have been taken from Mahmoudi, Karimi and Mazaheri [183] and Mahmoudi and Karimi [184].

Non-dimensionalization:

Governing equations {Eqs. (4.1) to (4.4)} are rendered non-dimensional by introducing the following non-dimensional variables.

$$\left.\begin{array}{l} X = x/H \ , \ Y = y/H \ , \ U_f = u_f / u_{ref} \ , \ U_i = u_i / u_{ref} \ , \ U_p = u_p / u_{ref} \ , \ P = p/\rho u_{ref}^2 \ , \\ \theta_f = (T_f - T_e)/(qH/k_f) \ , \theta_p = (T_p - T_e)/(qH/k_f) \ \{ \text{here } \theta_f \text{ and } \theta_p \text{ are subjected} \\ \text{to constant wall heat flux} \} \end{array}\right\} \tag{4.13}$$

$\theta_f = (T_f - T_w)/(T_e - T_w)$, $\theta_p = (T_p - T_w)/(T_e - T_w)$ { here θ_f and θ_p are subjected to constant wall temperature}

In Eq. (4.13), X and Y are non-dimensional coordinates. U and P are non-dimensional velocity and pressure. The subscripts f and p refer to fluid and porous regions. θ,{ θ_f in the fluid region and θ_p in the porous region}, is non-dimensional temperature. u_{ref} is average velocity through the channel. u_{ref} is related to u_p and u_f by,

$$\frac{2}{H}\left[\int_{-H/2}^{-\frac{H}{2}+\frac{l_p}{2}} u_p dy + \int_{-\frac{H}{2}+\frac{l_p}{2}}^{0} u_f dy\right] = u_{ref} \tag{4.14}$$

In addition, the non-dimensional porous layer thickness γ_p, which is referred to as porous fraction is defined by,

$$\gamma_p = l_p / H \tag{4.15}$$

On introducing non-dimensional variables given in Eq. (4.13), the governing equations for conservation of momentum and energy equation applicable in the fluid {Eqs. (4.1) and (4.2) } and porous {Eqs. (4.3) and (4.4) } regions in non-dimensional form become,

Non dimensional governing equations:

Fluid region:

$$0 = -\frac{dP}{dX} + \frac{1}{Re}\frac{d^2U_f}{dY^2} \tag{4.16}$$

$$\frac{d^2\theta_f}{dY^2} + Br\left(\frac{dU_f}{dY}\right)^2 = 0 \tag{4.17}$$

In Eq. (4.16) and Eq. (4.17), *Re* , the Reynolds number and *Br*, The Brinkman number are defined by

$$Re = \frac{\rho u_{ref} H}{\mu_f} \tag{4.18}$$

$$\left.\begin{aligned} Br &= \frac{\mu_f u_{ref}^{\ 2}}{qH} \ \{\text{here } Br \text{ is subjected to constant wall heat flux}\} \\ Br &= \frac{\mu_f u_{ref}^{\ 2}}{k_f \left(T_e - T_w\right)} \ \{\text{here } Br \text{ is subjected to constant wall temperature}\} \end{aligned}\right\} \tag{4.19}$$

Porous region:

$$U_p = -ReDa\frac{dP}{dX} + \frac{Da}{\varepsilon}\frac{d^2U_p}{dY^2} \tag{4.20}$$

In Eq. (4.20), *Da*, the Darcy number and ε are defined as,

$$Da = K / H^2 \text{ and} \tag{4.21}$$

$$\varepsilon = \mu_f / \mu_{eff} \tag{4.22}$$

$$\frac{d^2\theta_p}{dY^2} + \Psi_i = 0 \tag{4.23}$$

In Eq. (4.23), Ψ_i is non-dimensional dissipation model is given by,

Darcy model:

$$\Psi_1 = \frac{\eta Br}{Da} U_p^{\ 2} \tag{4.24}$$

Form drag model:

$$\Psi_2 = \eta Br U_p \left(\frac{U_p}{Da} - \frac{1}{\varepsilon}\frac{d^2U_p}{dY^2}\right) \tag{4.25}$$

Clear fluid compatible model :

$$\Psi_3 = \eta Br\left(\frac{U_p^{\,2}}{Da} + \left(\frac{dU_p}{dY}\right)^2\right) \tag{4.26}$$

In Eqs. (4.24) to (4.26),

$$\eta = k_f / k_{eff} \tag{4.27}$$

$Br > 0$ represents, the fluid is getting cooled and $Br < 0$ represents the fluid is getting heated.

Non-dimensional Boundary Conditions:

The boundary and interfacial conditions given by, Eqs. (4.9) to (4.12) take the following non-dimensional form {using Eq.(4.13)}

$$\left.\begin{aligned} &U_p = 0\,, \left(\frac{d\theta_p}{dY}\right) = -\eta \quad \text{at} \quad Y = -1/2 \quad \{\text{subjected to constant wall heat flux}\} \\ &U_p = 0\,, \quad \theta_p = 0 \qquad \text{at} \quad Y = -1/2 \quad \{\text{subjected to constant wall temperature}\} \end{aligned}\right\} \tag{4.28}$$

$$U_f = U_p = U_i\,, \;\; \frac{1}{\varepsilon}\frac{dU_p}{dY} = \frac{dU_f}{dY} \quad \text{at the interface} \quad Y = -\frac{1}{2} + \frac{\gamma_p}{2} \tag{4.29}$$

$$\theta_f = \theta_p = \theta_i\,, \;\; \eta\left(\frac{d\theta_f}{dY}\right) = \left(\frac{d\theta_p}{dY}\right) \quad \text{at interface} \quad Y = -\frac{1}{2} + \frac{\gamma_p}{2} \tag{4.30}$$

$$\frac{dU_f}{dY} = 0, \; \frac{d\theta_f}{dY} = 0 \quad \text{at} \quad Y = 0 \tag{4.31}$$

Analytical expressions for velocity in fluid and porous regions are available in chapter 2, § 2.3.

4.3 Non-dimensional Limiting Temperature Profiles and Nusselt Number

4.3.1 Case(i): Subjected to constant wall heat flux

4.3.1.1 Limiting temperature profiles

The limiting temperature profiles have been taken using $U_p(Y)$ and $U_f(Y)$ taken from chapter 2, § 2.3 and boundary conditions given by Eqs. (4.28), (4.30) and (4.31). Since the boundary condition is of Neumann type, Eqs. (4.28) and (4.31) have been solved in terms of temperature difference between the fluid and one of the walls. Let the temperature at wall 1 (at $Y=-H/2$) be T_{w1} and at wall 2 (at $Y=H/2$) be T_{w2}. The corresponding non-dimensional wall temperatures, θ_{w1} and θ_{w2} are now expressed as,

$$\theta_{w_1}=\left(T_{w1}-T_e\right)/\left(qH/k_f\right);\ \theta_{w_2}=\left(T_{w2}-T_e\right)/\left(qH/k_f\right) \tag{4.32}$$

The solutions to Eq. (4.17) and Eq. (4.23) for three dissipation models given in Eq.(4.24), (4.25) and (4.26), for $\theta_f(Y)$ and $\theta_p(Y)$ contain θ_{w1}. The limiting temperature profiles in the fluid and porous regions are expressed relative to θ_{w1}. Since $\theta_f(Y)$ and $\theta_p(Y)$ have the function of Brinkman number *Br*. Therefore limiting temperature profiles expressed as, $\left[\theta_{w1}-\theta_{f,CL}(Y)\right]/Br$ and $\left[\theta_{w1}-\theta_{p,CL}(Y)\right]/Br$ for three dissipation models are obtained at the conduction limit. This above procedure is adopted from a study on convective heat and mass transfer by Kays et al. [185].

Darcy model:

Solving Eqs. (4.17) and (4.23) with boundary conditions given by Eqs. (4.28), (4.30) and (4.31) for $\Psi_1 = \frac{\eta Br}{Da} U_p{}^2$, the expressions of $\left[\theta_{w1} - \theta_{f,CL1}(Y)\right] / Br$ and $\left[\theta_{w1} - \theta_{p,CL1}(Y)\right] / Br$ are as follows

$$\frac{\theta_{w1} - \theta_{f,CL1}(Y)}{Br} = \left\{ \begin{array}{l} \dfrac{3A_{54}{}^2 \varepsilon\left(-16Y^4 + (\gamma_p - 1)^4\right)}{24\left[\left(24Da^{3/2} - 6\sqrt{Da}\varepsilon(\gamma_p - 1)^2\right)A_{55} + A_{54}\sqrt{\varepsilon}(\gamma_p - 1)^3 + 12Da\sqrt{\varepsilon}A_{56}\right]^2} \\ + \dfrac{3\eta\gamma_p\left[A_{54}{}^2\varepsilon(\gamma_p - 1)^3 - \dfrac{3}{\gamma_p}\left(-4Da^2 A_{57} + 8Da^{3/2}A_{58} - A_{59} + \sqrt{Da}A_{55}A_{60} - Da\varepsilon A_{61}\right)\right]}{\left[\left(24Da^{3/2} - 6\sqrt{Da}\varepsilon(\gamma_p - 1)^2\right)A_{55} + A_{54}\sqrt{\varepsilon}(\gamma_p - 1)^3 + 12Da\sqrt{\varepsilon}A_{56}\right]^2} \end{array} \right\} \quad (4.33)$$

$$\frac{\theta_{w1}-\theta_{p,CL1}(Y)}{Br}=\left\{-3\eta\left[\begin{array}{l}-A_{54}{}^2(1+2Y)\varepsilon(\gamma_p-1)^3A_{62}{}^2+\frac{3}{\gamma_p}e^{-(1+2Y)\sqrt{\frac{\varepsilon}{Da}}}(1+2Y)\left(\begin{array}{l}e^{(1+2Y)\sqrt{\frac{\varepsilon}{Da}}}\left(\begin{array}{l}576Da^3A_{63}+12\sqrt{Da}A_{64}\\+576Da^{5/2}A_{65}\end{array}\right)\\+e^{(1+2Y)\sqrt{\frac{\varepsilon}{Da}}}\left(\begin{array}{l}A_{54}{}^2\varepsilon(\gamma_p-1)^6\\+12Da(1+2Y)\varepsilon(\gamma_p-1)^3A_{66}\\-144Da^2A_{67}\end{array}\right)\end{array}\right)\left(\begin{array}{l}-4Da^2A_{68}\\+A_{69}+\sqrt{Da}A_{70}\\-Da\varepsilon A_{71}\end{array}\right)\\-\frac{3}{\gamma_p}e^{-(1+2Y)\sqrt{\frac{\varepsilon}{Da}}}A_{62}\left(\begin{array}{l}e^{\frac{(1+2Y)}{2}\sqrt{\frac{\varepsilon}{Da}}}(1+2Y)(\gamma_p-1-2Y)\left(2\sqrt{Da}A_{72}+e^{(1+2Y+\gamma_p)\sqrt{\frac{\varepsilon}{Da}}}A_{73}\right)\\+4Da^2\left(\begin{array}{l}16(1+2Y)\left(e^{(2+4Y+\gamma_p)\sqrt{\frac{\varepsilon}{Da}}}+e^{\frac{(2+4Y+3\gamma_p)}{2}\sqrt{\frac{\varepsilon}{Da}}}\right)-2e^{(1+2Y+\gamma_p)\sqrt{\frac{\varepsilon}{Da}}}(9+\varepsilon+2Y(9+\varepsilon)-8\gamma_p)\\+e^{(1+2Y)\sqrt{\frac{\varepsilon}{Da}}}\left(1+e^{2\gamma_p\sqrt{\frac{\varepsilon}{Da}}}\right)(-7+\varepsilon)(1+2Y-\gamma_p)\\-8\gamma_p\left(\begin{array}{l}e^{\frac{3(1+2Y)}{2}\sqrt{\frac{\varepsilon}{Da}}}+e^{\frac{(1+2Y+2\gamma_p)}{2}\sqrt{\frac{\varepsilon}{Da}}}\\+e^{\frac{(3+6Y+2\gamma_p)}{2}\sqrt{\frac{\varepsilon}{Da}}}+e^{\frac{(1+2Y+4\gamma_p)}{2}\sqrt{\frac{\varepsilon}{Da}}}\end{array}\right)\gamma_p(1+\varepsilon)\left(e^{2(1+2Y)\sqrt{\frac{\varepsilon}{Da}}}+e^{2\gamma_p\sqrt{\frac{\varepsilon}{Da}}}\right)\end{array}\right)\\+Da\varepsilon\left(\begin{array}{l}(1+\varepsilon)(\gamma_p-1)^2\gamma_pe^{\gamma_p\sqrt{\frac{\varepsilon}{Da}}}\left(1+e^{(2+4Y)\sqrt{\frac{\varepsilon}{Da}}}\right)\\+(1+2Y)(4(1+Y)\gamma_p-3\gamma_p{}^2-1-\varepsilon(\gamma_p-1)^2)e^{(1+2Y)\sqrt{\frac{\varepsilon}{Da}}}\left(1+e^{4\gamma_p\sqrt{\frac{\varepsilon}{Da}}}\right)\\-2e^{(1+2Y+\gamma_p)\sqrt{\frac{\varepsilon}{Da}}}(1+2Y-\gamma_p)(-2(1+4Y)\gamma_p-\gamma_p{}^2-1-\varepsilon(1-4(1+Y)\gamma_p{}^2)\end{array}\right)\\-4Da^{3/2}\sqrt{\varepsilon}(1+\gamma_p)\left(\begin{array}{l}e^{(1+2Y)\sqrt{\frac{\varepsilon}{Da}}}\left(\begin{array}{l}-4(1+2Y)\left(e^{\gamma_p\sqrt{\frac{\varepsilon}{Da}}}-1\right)-(1+\varepsilon)(2+4Y-\gamma_p)\left(\begin{array}{l}e^{\frac{\gamma_p}{2}\sqrt{\frac{\varepsilon}{Da}}}\\-e^{\frac{3\gamma_p}{2}\sqrt{\frac{\varepsilon}{Da}}}\end{array}\right)\end{array}\right)\\+(1+\varepsilon)\gamma_pe^{\frac{3}{2}\sqrt{\frac{\varepsilon}{Da}}}-4\gamma_p\left(\begin{array}{l}e^{\frac{(1+2Y)}{2}\sqrt{\frac{\varepsilon}{Da}}}\left(e^{\frac{\gamma_p}{2}\sqrt{\frac{\varepsilon}{Da}}}+e^{\frac{3\gamma_p}{2}\sqrt{\frac{\varepsilon}{Da}}}\right)-\left(\begin{array}{l}e^{3(1+2Y+\gamma_p)\sqrt{\frac{\varepsilon}{Da}}}\\+e^{\frac{(3+6Y+2\gamma_p)}{2}\sqrt{\frac{\varepsilon}{Da}}}\end{array}\right)\end{array}\right)\end{array}\right)\end{array}\right)\end{array}\right]}{\left[\left(24Da^{3/2}-6\sqrt{Da}\varepsilon(\gamma_p-1)^2\right)A_{55}+A_{54}\sqrt{\varepsilon}(\gamma_p-1)^3+12Da\sqrt{\varepsilon}A_{56}\right]^4}\right. \tag{4.34}$$

Form drag model Dissipation model:

Solving Eqs. (4.17) and (4.23) with boundary conditions given by Eqs. (4.28), (4.30) and (4.31) for $\Psi_2=\eta BrU_p\left(\frac{U_p}{Da}-\frac{1}{\varepsilon}\frac{d^2U_p}{dY^2}\right)$, the expressions of $\left[\theta_{w1}-\theta_{f,CL2}(Y)\right]/Br$ and $\left[\theta_{w1}-\theta_{p,CL2}(Y)\right]/Br$ are as follows

$$\frac{\theta_{w1}-\theta_{f,CL2}(Y)}{Br}=\left\{\begin{array}{l}\dfrac{3{A_{54}}^2\varepsilon\left(-16Y^2+(\gamma_p-1)^4\right)}{4\left[\left(24Da^{3/2}-6\sqrt{Da}\varepsilon(\gamma_p-1)^2\right)A_{55}+A_{54}\sqrt{\varepsilon}(\gamma_p-1)^3+12Da\sqrt{\varepsilon}A_{56}\right]^2}\\ +\dfrac{3\eta A_{54}\left[-A_{54}\varepsilon(\gamma_p-1)^3\gamma_p-6DaA_{74}\right]}{\left[\left(24Da^{3/2}-6\sqrt{Da}\varepsilon(\gamma_p-1)^2\right)A_{55}+A_{54}\sqrt{\varepsilon}(\gamma_p-1)^3+12Da\sqrt{\varepsilon}A_{56}\right]^2}\end{array}\right\} \quad (4.35)$$

$$\frac{\theta_{w1}-\theta_{p,CL2}(Y)}{Br}=\left\{\begin{array}{l}-3e^{-(1+2Y)\sqrt{\frac{\varepsilon}{Da}}}\eta\\ \dfrac{+6Da\left[\begin{array}{l}e^{\frac{(1+2Y)}{2}\sqrt{\frac{\varepsilon}{Da}}}\left((1+2Y)A_{75}-6Da(1+2Y)A_{54}A_{74}\right)\\ +6Da\left(\begin{array}{l}e^{(1+2Y)\sqrt{\frac{\varepsilon}{Da}}}(1+2Y)A_{76}+8DaA_{54}\left(\begin{array}{l}-2(1+2Y)e^{\frac{(1+2Y+\gamma_p)}{2}\sqrt{\frac{\varepsilon}{Da}}}\\ +(1+2Y-\gamma_p)\left(\begin{array}{l}e^{(1+2Y)\sqrt{\frac{\varepsilon}{Da}}}\\ +e^{\frac{(1+2Y+2\gamma_p)}{2}\sqrt{\frac{\varepsilon}{Da}}}\end{array}\right)\\ +\gamma_p\left(e^{(1+2Y)\sqrt{\frac{\varepsilon}{Da}}}+e^{\gamma_p\sqrt{\frac{\varepsilon}{Da}}}\right)\end{array}\right)\\ +4\sqrt{Da\varepsilon}(\gamma_p-1)\left(\begin{array}{l}(1+2Y)e^{\frac{(1+2Y)}{2}\sqrt{\frac{\varepsilon}{Da}}}\left(\begin{array}{l}\left(1-e^{2\gamma_p\sqrt{\frac{\varepsilon}{Da}}}\right)\\ -\gamma_p\left(e^{\frac{\gamma_p}{2}\sqrt{\frac{\varepsilon}{Da}}}+e^{\frac{3\gamma_p}{2}\sqrt{\frac{\varepsilon}{Da}}}\right)\end{array}\right)\\ +\gamma_p e^{(1+2Y)\sqrt{\frac{\varepsilon}{Da}}}\left(e^{\frac{\gamma_p}{2}\sqrt{\frac{\varepsilon}{Da}}}+e^{\frac{3\gamma_p}{2}\sqrt{\frac{\varepsilon}{Da}}}\right)\end{array}\right)\end{array}\right)\end{array}\right]}\\ \gamma_p\left[\left(24Da^{3/2}-6\sqrt{Da}\varepsilon(\gamma_p-1)^2\right)A_{55}+A_{54}\sqrt{\varepsilon}(\gamma_p-1)^3+12Da\sqrt{\varepsilon}A_{56}\right]^2\end{array}\right\} \quad (4.36)$$

Clear fluid compatible model:

Solving Eqs. (4.17) and (4.23) with boundary conditions given by Eqs. (4.28), (4.30) and (4.31) for $\Psi_3=\eta Br\left(\frac{{U_p}^2}{Da}+\left(\frac{dU_p}{dY}\right)^2\right)$. Then the expressions of $\left[\theta_{w1}-\theta_{f,CL3}(Y)\right]/Br$ and $\left[\theta_{w1}-\theta_{p,CL3}(Y)\right]/Br$ are as follows

$$\frac{\theta_{w1}-\theta_{f,CL3}(Y)}{Br}=\left\{\frac{-3\left[\begin{array}{l}A_{54}{}^{2}\varepsilon(-16Y^{4}+(\gamma_p-1)^{4})-4A_{54}{}^{2}\varepsilon\eta(\gamma_p-1)^{3}\gamma_p\\+12e^{-\sqrt{\frac{\varepsilon}{Da}}\gamma_p}\eta\left(\begin{array}{l}e^{\sqrt{\frac{\varepsilon}{Da}}\gamma_p}\left(4Da^{2}A_{77}+8Da^{3/2}\sqrt{\varepsilon}A_{78}-Da\varepsilon A_{79}\right)\\+e^{2\sqrt{\frac{\varepsilon}{Da}}\gamma_p}(\varepsilon-1)\varepsilon^{2}(\gamma_p-1)^{2}\gamma_p{}^{2}-\sqrt{Da}\varepsilon^{3/2}(\gamma_p-1)\gamma_pA_{80}\end{array}\right)\end{array}\right]}{4\left[\left(24Da^{3/2}-6\sqrt{Da}\varepsilon(\gamma_p-1)^{2}\right)A_{55}+A_{54}\sqrt{\varepsilon}(\gamma_p-1)^{3}+12Da\sqrt{\varepsilon}A_{56}\right]^{2}}\right\} \quad (4.37)$$

$$\frac{\theta_{w1}-\theta_{p,CL3}(Y)}{Br}=\left\{\begin{array}{l}-3e^{-(1+2Y)\sqrt{\frac{\varepsilon}{Da}}}\eta\left\{\begin{array}{l}-(1+2Y)e^{(1+2Y)\sqrt{\frac{\varepsilon}{Da}}}A_{81}+\left[\frac{\left(e^{\sqrt{\frac{\varepsilon}{Da}}\gamma_p}\left(4Da^{2}A_{88}+8Da^{3/2}\sqrt{\varepsilon}A_{89}-Da\varepsilon A_{82}\right)+A_{90}-\sqrt{Da}\varepsilon^{3/2}(\gamma_p-1)\gamma_pA_{91}\right)}{\left[\left(24Da^{3/2}-6\sqrt{Da}\varepsilon(\gamma_p-1)^{2}\right)A_{55}+A_{54}\sqrt{\varepsilon}(\gamma_p-1)^{3}+12Da\sqrt{\varepsilon}A_{56}\right]^{2}}\right]\\-3\left\{\begin{array}{l}2\sqrt{Da}e^{(1+2Y)\sqrt{\frac{\varepsilon}{Da}}}(1+2Y)_p(-\gamma_p+1+2Y)A_{92}+(1+2Y)(-\gamma_p+1+2Y)e^{(1+2Y)\sqrt{\frac{\varepsilon}{Da}}}A_{93}\\+4Da^{2}\left(\begin{array}{l}16(1+2Y)\left(e^{\frac{(2+4Y+\gamma_p)}{2}\sqrt{\frac{\varepsilon}{Da}}}-e^{\frac{(2+4Y+3\gamma_p)}{2}\sqrt{\frac{\varepsilon}{Da}}}\right)-2e^{(1+2Y+\gamma_p)\sqrt{\frac{\varepsilon}{Da}}}(9+18Y-8\gamma_p)\\-7e^{(1+2Y)\sqrt{\frac{\varepsilon}{Da}}}(1+2Y-\gamma_p)-7e^{(1+2Y+2\gamma_p)\sqrt{\frac{\varepsilon}{Da}}}\\-8\gamma_p{}^{2}\left(\begin{array}{l}e^{\frac{3(1+2Y)}{2}\sqrt{\frac{\varepsilon}{Da}}}+e^{\frac{(1+2Y+2\gamma_p)}{2}\sqrt{\frac{\varepsilon}{Da}}}\\+e^{\frac{(3+6Y+2\gamma_p)}{2}\sqrt{\frac{\varepsilon}{Da}}}+e^{\frac{(1+2Y+4\gamma_p)}{2}\sqrt{\frac{\varepsilon}{Da}}}\end{array}\right)\left(e^{2(1+2Y)\sqrt{\frac{\varepsilon}{Da}}}+e^{2\gamma_p\sqrt{\frac{\varepsilon}{Da}}}\right)\end{array}\right)\\-4Da^{3/2}\sqrt{\varepsilon}(\gamma_p-1)\left(\begin{array}{l}-4(1+2Y)\left(e^{(1+2Y+\gamma_p)\sqrt{\frac{\varepsilon}{Da}}}-e^{(1+2Y)\sqrt{\frac{\varepsilon}{Da}}}\right)+(2+4Y-\gamma_p)e^{\frac{(2+4Y+3\gamma_p)}{2}\sqrt{\frac{\varepsilon}{Da}}}\\+\gamma_pe^{\frac{3}{2}\sqrt{\frac{\varepsilon}{Da}}}-4\gamma_p\left(\begin{array}{l}e^{\frac{(1+2Y+\gamma_p)}{2}\sqrt{\frac{\varepsilon}{Da}}}-e^{3(1+2Y+\gamma_p)\sqrt{\frac{\varepsilon}{Da}}}-e^{\frac{(3+6Y+2\gamma_p)}{2}\sqrt{\frac{\varepsilon}{Da}}}\\+e^{\frac{(1+2Y+3\gamma_p)}{2}\sqrt{\frac{\varepsilon}{Da}}}\end{array}\right)\\-e^{\frac{(4+8Y+\gamma_p)}{2}\sqrt{\frac{\varepsilon}{Da}}}+e^{\frac{(2+4Y+\gamma_p)}{2}\sqrt{\frac{\varepsilon}{Da}}}(-2+4Y+\gamma_p)\end{array}\right)\\+Da\varepsilon\left(\begin{array}{l}(\gamma_p-1)^{2}\gamma_p\left(e^{\gamma_p\sqrt{\frac{\varepsilon}{Da}}}+e^{(2+4Y+\gamma_p)\sqrt{\frac{\varepsilon}{Da}}}\right)\\+(1+2Y)(4(1+Y)\gamma_p-3\gamma_p{}^{2}-1)\left(e^{(1+2Y)\sqrt{\frac{\varepsilon}{Da}}}+e^{(1+2Y+4\gamma_p)\sqrt{\frac{\varepsilon}{Da}}}\right)\\+2(16Y^{2}\gamma_p-(\gamma_p-1)(\gamma_p+1)^{2}\\+4(2+12\gamma_p-6\gamma_p{}^{2}))e^{(1+2Y+\gamma_p)\sqrt{\frac{\varepsilon}{Da}}}\end{array}\right)\end{array}\right\}\end{array}\right\}}{\gamma_p\left[\left(24Da^{3/2}-6\sqrt{Da}\varepsilon(\gamma_p-1)^{2}\right)A_{55}+A_{54}\sqrt{\varepsilon}(\gamma_p-1)^{3}+12Da\sqrt{\varepsilon}A_{56}\right]^{2}}\right\} \quad (4.38)$$

Where A_i , i = 54, 55, ...95 are constants given in appendix.

4.3.1.2 Limiting Nusselt number

The present investigation is concerned with determining optimum configuration for Nusselt number augmentation. It is straightforward, though cumbersome, to apply the procedure available in chapter 2, to obtain the expressions for the Nusselt numbers. In general, *h*, the heat transfer coefficient at a wall is evaluated from the defining equation,

$$-k_f \frac{dT}{dy}\Big|_w = h(T_w - T_b) \tag{4.39}$$

where, k_f is the thermal conductivity of the fluid. T_w is the wall temperature and T_b is the bulk mean temperature. On non-dimensionalizing, the Nusselt number *Nu*, based on the hydraulic diameter, 2H.

Let T_b is bulk mean temperature, is defined by

$$T_b = \frac{2\left(\int_{\frac{-H}{2}}^{\frac{-H}{2}+\frac{l_p}{2}} \mathrm{u}_p \, \mathrm{T}_p \, dy + \int_{\frac{-H}{2}+\frac{l_p}{2}}^{0} u_f \, \mathrm{T}_f \, dy\right)}{2\left(\int_{\frac{-H}{2}}^{\frac{-H}{2}+\frac{l_p}{2}} u_p dy + \int_{\frac{-H}{2}+\frac{l_p}{2}}^{0} u_f dy\right)} \tag{4.40}$$

θ^* is the non-dimensional bulk mean temperature denoted by

$$\theta^* = \frac{T_b - T_e}{\left(qH / k_f\right)} \tag{4.41}$$

and defined as (Using Eqs. (4.40), (4.41) and (4.13))

$$\theta^* = \frac{2\left(\int_{\frac{-1}{2}}^{\frac{-1}{2}+\frac{\gamma_p}{2}} U_p\ \theta_p\ dY + \int_{\frac{-1}{2}+\frac{\gamma_p}{2}}^{0} U_f\ \theta_f\ dY\right)}{2\left(\int_{\frac{-1}{2}}^{\frac{-1}{2}+\frac{\gamma_p}{2}} U_p dY + \int_{\frac{-1}{2}+\frac{\gamma_p}{2}}^{0} U_f dY\right)} \tag{4.42}$$

Therefore

$$\theta_{w1} - \theta^* = 2\left(\int_{\frac{-1}{2}}^{\frac{-1}{2}+\frac{\gamma_p}{2}} U_p\ (\theta_{w1} - \theta_p)\ dY + \int_{\frac{-1}{2}+\frac{\gamma_p}{2}}^{0} U_f\ (\theta_{w1} - \theta_f)\ dY\right) \tag{4.43}$$

Since

$$2\left(\int_{\frac{-1}{2}}^{\frac{-1}{2}+\frac{\gamma_p}{2}} U_p dY + \int_{\frac{-1}{2}+\frac{\gamma_p}{2}}^{0} U_f dY\right) = 1 \tag{4.44}$$

The heat transfer coefficient h_p, at the plate $y = -H/2$ adjacent to the porous medium is defined by

$$-k_{eff}\frac{dT_p}{dy}\Big|_{y=-\frac{H}{2}} = h_p(T_{w1} - T_b) \tag{4.45}$$

Upon non-dimensionalizing (using Eq. (4.13)), The Nusselt number at $Y = -1/2$, $Nu_{p,CL}$ is given by

$$Nu_{p.CL} = \frac{h_p(2H)}{k_f} = \frac{2}{\theta_{w1} - \theta^*} \tag{4.46}$$

The expressions for Nusselt number were arrived at with product of Brinkman number *Br*, for different dissipation models using Eq. (4.46) and denoted as $BrNu_{p,CL1}$(

using Eqs. (4.33),(4.34) and (4.43)), $BrNu_{p,CL2}$ (using Eqs. (4.35),(4.36) and (4.43)) and $BrNu_{p,CL3}$ (using Eqs. (4.37),(4.38) and (4.43)) . The numerical results of Nusselt number with product of Brinkman *Br*, for different dissipation models are given graphically.

Net change in the Nusselt number:

The net change, ΔNu for the three dissipation models is defined, in comparison with fully developed clear fluid channel value, as follows

$$\Delta Nu_1 = 2\left[Br\ Nu_{p,CL} - Br\ Nu_{p,CL}\,|_{\gamma_p=0} \right] \tag{4.47}$$

Darcy model:

$$\Delta Nu_1 = 2\left[Br\ Nu_{p,CL1} - \left(-\frac{35}{12} \right) \right] \tag{4.48}$$

Form drag model:

$$\Delta Nu_2 = 2\left[Br\ Nu_{p,CL2} - \left(-\frac{35}{12} \right) \right] \tag{4.49}$$

Clear fluid compatible model:

$$\Delta Nu_3 = 2\left[Br\ Nu_{p,CL3} - \left(-\frac{35}{12} \right) \right] \tag{4.50}$$

4.3.2 Case(ii): Subjected to constant wall temperature

4.3.2.1 Non-dimensional limiting temperature profiles

The limiting temperature profiles are obtained using $U_p(Y)$ and $U_f(Y)$ taken from chapter 2, § 2.3 and the boundary conditions given by Eqs. (4.28), (4.30) and (4.31). The solutions to Eq. (4.17) and Eq. (4.23) for three dissipation models are supplied by Eqs.

(4.24) to (4.26) for $\theta_f(Y)$ and $\theta_p(Y)$. Since $\theta_f(Y)$ and $\theta_p(Y)$ are functions of Brinkman number *Br*, it leads to limiting temperature profiles expressed, $\theta_{f,CL}(Y)/Br$ and $\theta_{p,CL}(Y)/Br$ for three dissipation models are obtained.

Darcy model:

Solving Eqs. (4.17) and (4.23) with boundary conditions given by Eqs. (4.28), (4.30) and (4.31) for $\Psi_1 = \frac{\eta Br}{Da} U_p^{\,2}$. Then the expressions of $\theta_{f,CL1}(Y)/Br$ and $\theta_{p,CL1}(Y)/Br$ become

$$\frac{\theta_{f,CL1}(Y)}{Br} = \frac{1}{192}\left\{\left((\gamma_p - 1)^4 - 16Y^4\right) p_{gr}^{\,2} + \frac{4\eta}{Da\varepsilon\left(e^{\gamma_p\sqrt{\frac{\varepsilon}{Da}}} - 1\right)^2}\left[A_{96} + A_{97} + A_{98}\right]\right\} \tag{4.51}$$

$$\frac{\theta_{p,CL1}(Y)}{Br}=\frac{e^{-(2Y+\gamma_p)\sqrt{\frac{\varepsilon}{Da}}}\eta}{8Da\left(e^{\gamma_p\sqrt{\frac{\varepsilon}{Da}}}-1\right)^2\varepsilon\gamma_p}\left\{\begin{array}{l}2U_iDa\left[\begin{array}{l}-e^{\frac{1}{2}(4Y+3\gamma_p)\sqrt{\frac{\varepsilon}{Da}}}(1+2Y)(1+2Y-\gamma_p)A_{99}\\ -3(1+2Y)\left(e^{(2Y+\gamma_p)\sqrt{\frac{\varepsilon}{Da}}}+e^{(2Y+3\gamma_p)\sqrt{\frac{\varepsilon}{Da}}}\right)+A_{100}\\ -\gamma_p\left(e^{(1+4Y+2\gamma_p)\sqrt{\frac{\varepsilon}{Da}}}+e^{\left(\frac{4Y+3\gamma_p}{2}\right)\sqrt{\frac{\varepsilon}{Da}}}\right)\\ +2Da\left(\begin{array}{l}+4\gamma_p\left(\begin{array}{l}e^{\frac{1}{2}(2Y+3\gamma_p-1)\sqrt{\frac{\varepsilon}{Da}}}-e^{\frac{1}{2}(6Y+3\gamma_p+1)\sqrt{\frac{\varepsilon}{Da}}}\\ -e^{\frac{1}{2}(2Y+5\gamma_p-1)\sqrt{\frac{\varepsilon}{Da}}}+e^{\frac{1}{2}(6Y+5\gamma_p+1)\sqrt{\frac{\varepsilon}{Da}}}\end{array}\right)\\ +\gamma_p\left(e^{\frac{1}{2}(8Y+3\gamma_p+2)\sqrt{\frac{\varepsilon}{Da}}}-e^{\frac{1}{2}(4Y+5\gamma_p)\sqrt{\frac{\varepsilon}{Da}}}\right)\\ +2e^{2(Y+\gamma_p)\sqrt{\frac{\varepsilon}{Da}}}(3+6Y+\gamma_p)\end{array}\right)\end{array}\right]p_{gr}\\ +A_{101}\left[\begin{array}{l}A_{102}\left(e^{\frac{1}{2}(1+2Y)\sqrt{\frac{\varepsilon}{Da}}}-1\right)\left(\begin{array}{l}7\left(e^{\frac{1}{2}(2Y+2\gamma_p+1)\sqrt{\frac{\varepsilon}{Da}}}-e^{(1+2Y)\sqrt{\frac{\varepsilon}{Da}}}\right)\\ +8\left(e^{\frac{1}{2}(2Y+\gamma_p+1)\sqrt{\frac{\varepsilon}{Da}}}-e^{\frac{1}{2}(4Y+\gamma_p+2)\sqrt{\frac{\varepsilon}{Da}}}\right)\\ +e^{\frac{3}{2}(2Y+1)\sqrt{\frac{\varepsilon}{Da}}}-e^{\gamma_p\sqrt{\frac{\varepsilon}{Da}}}\end{array}\right)\\ -e^{(\gamma_p+2Y)\sqrt{\frac{\varepsilon}{Da}}}(1+2Y)(1+2Y-\gamma_p)A_{103}\end{array}\right]\gamma_p p_{gr}^{\ 2}\\ +2\left[\begin{array}{l}U_i^2\left(\begin{array}{l}e^{2(\gamma_p+Y)\sqrt{\frac{\varepsilon}{Da}}}(1+2Y)(1+2Y-\gamma_p)\gamma_p+Da\left(\begin{array}{l}(1+2Y)\left(\begin{array}{l}e^{(\gamma_p+2Y)\sqrt{\frac{\varepsilon}{Da}}}\\ +e^{(3\gamma_p+2Y)\sqrt{\frac{\varepsilon}{Da}}}\end{array}\right)\\ -\gamma_p\left(\begin{array}{l}e^{(2\gamma_p+1)\sqrt{\frac{\varepsilon}{Da}}}\\ +e^{(1+2\gamma_p+4Y)\sqrt{\frac{\varepsilon}{Da}}}\end{array}\right)\\ +e^{2(\gamma_p+Y)\sqrt{\frac{\varepsilon}{Da}}}(2\gamma_p-4Y-2)\end{array}\right)\end{array}\right)\\ +\frac{1}{12}e^{(\gamma_p+2Y)\sqrt{\frac{\varepsilon}{Da}}}(1+2Y)\left(A_{96}+A_{97}+A_{98}\right)\end{array}\right]\end{array}\right\} \tag{4.52}$$

Form drag Model:

Solving Eqs. (4.17) and (4.23) with boundary conditions given by Eqs. (4.28), (4.30) and (4.31) for $\Psi_2 = \eta Br U_p \left(\frac{U_p}{Da} - \frac{1}{\varepsilon} \frac{d^2 U_p}{dY^2} \right)$. Then the expressions of $\theta_{f,CL2}(Y)/Br$ and $\theta_{p,CL2}(Y)/Br$ are as follows

$$\frac{\theta_{f,CL2}(Y)}{Br} = \frac{p_{gr}}{192} \left\{ \left((\gamma_p - 1)^4 - 16Y^4 \right) p_{gr} + \frac{4\eta}{\varepsilon \left(e^{\gamma_p \sqrt{\frac{\varepsilon}{Da}}} - 1 \right)} \left[24 U_i A_{104} + A_{105} p_{gr} \right] \right\} \tag{4.53}$$

$$\frac{\theta_{p,CL2}(Y)}{Br} = \frac{e^{-\left(\frac{1+2Y}{2}\right)\sqrt{\frac{\varepsilon}{Da}}} \eta p_{gr}}{48 \left(e^{\gamma_p \sqrt{\frac{\varepsilon}{Da}}} - 1 \right) \varepsilon \gamma_p} \left\{ \begin{array}{l} 48 U_i Da \left[\left((1+2Y) e^{\left(\frac{1+2Y}{2}\right)\sqrt{\frac{\varepsilon}{Da}}} \left(1 - e^{\gamma_p \sqrt{\frac{\varepsilon}{Da}}} \right) - e^{\frac{\gamma_p}{2}\sqrt{\frac{\varepsilon}{Da}}} \left(1 - e^{(1+2Y)\sqrt{\frac{\varepsilon}{Da}}} \right) \gamma_p \right) \right] \\ +6Da \left[\begin{array}{l} 8Da \left(\begin{array}{l} e^{\left(\frac{1+2Y}{2}\right)\sqrt{\frac{\varepsilon}{Da}}} - e^{(1+2Y)\sqrt{\frac{\varepsilon}{Da}}} + e^{\frac{\gamma_p}{2}\sqrt{\frac{\varepsilon}{Da}}} - e^{\gamma_p \sqrt{\frac{\varepsilon}{Da}}} \\ -e^{\frac{1}{2}(4Y+\gamma_p+2)\sqrt{\frac{\varepsilon}{Da}}} + e^{\frac{1}{2}(2Y+2\gamma_p+1)\sqrt{\frac{\varepsilon}{Da}}} \end{array} \right) \gamma_p p_{gr} \\ -e^{\left(\frac{1+2Y}{2}\right)\sqrt{\frac{\varepsilon}{Da}}} \left(1 - e^{\gamma_p \sqrt{\frac{\varepsilon}{Da}}} \right) (1+2Y) \varepsilon (1+2Y-\gamma_p) \end{array} \right] \\ -e^{\left(\frac{1+2Y}{2}\right)\sqrt{\frac{\varepsilon}{Da}}} (1+2Y) \left[24 U_i A_{104} + A_{105} p_{gr} \right] \end{array} \right\} \tag{4.54}$$

Clear fluid compatible model :

Solving Eqs. (4.17) and (4.23) with boundary conditions given by Eqs. (4.28), (4.30) and (4.31) for $\Psi_3 = \eta Br \left(\frac{{U_p}^2}{Da} + \left(\frac{dU_p}{dY} \right)^2 \right)$. Then the expressions of $\theta_{f,CL3}(Y)/Br$ and $\theta_{p,CL3}(Y)/Br$ become

$$\frac{\theta_{f,CL3}(Y)}{Br} = \frac{1}{192} \left\{ \left((\gamma_p - 1)^4 - 16Y^4 \right) {p_{gr}}^2 - 8\eta\gamma_p \left[A_{106} + A_{107} + A_{108} + A_{109} \right] \right\} \tag{4.55}$$

$$\frac{\theta_{p,CL3}(Y)}{Br}=\frac{e^{-(1+2Y)\sqrt{\frac{\varepsilon}{Da}}}\eta}{8Da\left(e^{\gamma_p\sqrt{\frac{\varepsilon}{Da}}}-1\right)^2\varepsilon\gamma_p}\left\{\begin{array}{l}2U_iDa\left[\begin{array}{l}e^{\frac{1}{2}(2+4Y+\gamma_p)\sqrt{\frac{\varepsilon}{Da}}}(1+2Y)(1+2Y-\gamma_p)A_{99}\\+2Da\left(\begin{array}{l}(\varepsilon-3)(1+2Y)\left(e^{(1+2Y)\sqrt{\frac{\varepsilon}{Da}}}+e^{(1+2Y+2\gamma_p)\sqrt{\frac{\varepsilon}{Da}}}\right)\\+4\gamma_p\left(\begin{array}{l}e^{\frac{1}{2}(2Y+\gamma_p+1)\sqrt{\frac{\varepsilon}{Da}}}+e^{\frac{3}{2}(2Y+\gamma_p+1)\sqrt{\frac{\varepsilon}{Da}}}\\-e^{\frac{1}{2}(6Y+\gamma_p+3)\sqrt{\frac{\varepsilon}{Da}}}-e^{\frac{1}{2}(2Y+3\gamma_p+1)\sqrt{\frac{\varepsilon}{Da}}}\end{array}\right)\\+A_{110}-(1+\varepsilon)\gamma_p\left(\begin{array}{l}e^{\frac{1}{2}(4Y+\gamma_p+2)\sqrt{\frac{\varepsilon}{Da}}}+e^{(2+4Y+\gamma_p)\sqrt{\frac{\varepsilon}{Da}}}\\-e^{\frac{1}{2}(8Y+\gamma_p+4)\sqrt{\frac{\varepsilon}{Da}}}+e^{\frac{1}{2}(4Y+3\gamma_p+2)\sqrt{\frac{\varepsilon}{Da}}}\end{array}\right)\\+2e^{(1+2Y+\gamma_p)\sqrt{\frac{\varepsilon}{Da}}}\left(3-2Y(\varepsilon-3)+\varepsilon(\gamma_p-1)+\gamma_p\right)\end{array}\right)\end{array}\right]p_{gr}\\-Da^2\left[\begin{array}{l}2Da\left(\begin{array}{l}8\left(\begin{array}{l}e^{\frac{1}{2}(6Y+\gamma_p+3)\sqrt{\frac{\varepsilon}{Da}}}+e^{\frac{1}{2}(2Y+2\gamma_p+1)\sqrt{\frac{\varepsilon}{Da}}}+e^{\frac{1}{2}(6Y+2\gamma_p+3)\sqrt{\frac{\varepsilon}{Da}}}\\-e^{\frac{3(1+2Y)}{2}\sqrt{\frac{\varepsilon}{Da}}}-e^{\frac{1}{2}(2Y+\gamma_p+1)\sqrt{\frac{\varepsilon}{Da}}}-e^{\frac{3(1+2Y+\gamma_p)}{2}\sqrt{\frac{\varepsilon}{Da}}}\\-e^{\frac{1}{2}(2Y+4\gamma_p+1)\sqrt{\frac{\varepsilon}{Da}}}+e^{\frac{1}{2}(2Y+3\gamma_p+1)\sqrt{\frac{\varepsilon}{Da}}}\end{array}\right)\\-(\varepsilon-7)\left(e^{(1+2Y)\sqrt{\frac{\varepsilon}{Da}}}+e^{(1+2Y+2\gamma_p)\sqrt{\frac{\varepsilon}{Da}}}\right)\\+(1+\varepsilon)\left(\begin{array}{l}e^{2(1+2Y)\sqrt{\frac{\varepsilon}{Da}}}+A_{111}+2e^{\frac{1}{2}(4Y+\gamma_p+2)\sqrt{\frac{\varepsilon}{Da}}}\\+e^{(2+4Y+\gamma_p)\sqrt{\frac{\varepsilon}{Da}}}-2e^{\frac{1}{2}(8Y+\gamma_p+4)\sqrt{\frac{\varepsilon}{Da}}}\\+2e^{\frac{1}{2}(4Y+3\gamma_p+2)\sqrt{\frac{\varepsilon}{Da}}}\end{array}\right)\\-2(9+\varepsilon)e^{(1+2Y+\gamma_p)\sqrt{\frac{\varepsilon}{Da}}}\end{array}\right)\\-e^{(1+2Y)\sqrt{\frac{\varepsilon}{Da}}}(1+2Y)(1+2Y-\gamma_p)A_{112}\end{array}\right]\gamma_p p_{gr}^2\\+2\left[\begin{array}{l}U_i^2\left(\begin{array}{l}e^{(1+\gamma_p+2Y)\sqrt{\frac{\varepsilon}{Da}}}(1+2Y)(\varepsilon-1)(\gamma_p-1-2Y)\varepsilon\gamma_p\\+Da(1+\varepsilon)\left(\begin{array}{l}(1+2Y)\left(e^{(1+2Y)\sqrt{\frac{\varepsilon}{Da}}}+e^{(1+2\gamma_p+2Y)\sqrt{\frac{\varepsilon}{Da}}}\right)\\-\gamma_p\left(e^{\gamma_p\sqrt{\frac{\varepsilon}{Da}}}+e^{(2+\gamma_p+4Y)\sqrt{\frac{\varepsilon}{Da}}}\right)\\+e^{2(1+\gamma_p+2Y)\sqrt{\frac{\varepsilon}{Da}}}(2\gamma_p-4Y-2)\end{array}\right)\end{array}\right)\\-\frac{1}{6}Dae^{(1+2Y)\sqrt{\frac{\varepsilon}{Da}}}\left(e^{\gamma_p\sqrt{\frac{\varepsilon}{Da}}}-1\right)^2(1+2Y)\varepsilon\gamma_p\left(\begin{array}{l}A_{106}+A_{107}\\+A_{108}+A_{109}\end{array}\right)\end{array}\right]\end{array}\right\} \tag{4.56}$$

It is clear from Eqs. (4.51) to (4.56) that θ_{CL} varies linearly with Br. Thus,

$$\theta_{CL} = m_{1,2,3}(Y, Da)Br \tag{4.57}$$

where m_1 is a slope for Darcy model, m_2 is a slope for form drag model and m_3 is a slope for clear fluid compatible model.

4.3.2.2 Limiting Nusselt Numbers

The heat transfer coefficient h_p , at the plate Y = -H/2 adjacent to the porous medium is defined by

$$-k_{eff}\frac{dT_p}{dy}\Big|_{y=-\frac{H}{2}} = h_p(T_w - T_b) \tag{4.58}$$

T_w is the wall temperature and T_b is the bulk mean temperature, is defined by

$$T_b = \frac{2\left(\int_{\frac{-H}{2}}^{\frac{-H}{2}+\frac{l_p}{2}} \mathrm{u}_p\ \mathrm{T}_p\ dy + \int_{\frac{-H}{2}+\frac{l_p}{2}}^{0} u_f\ \mathrm{T}_f\ dy\right)}{2\left(\int_{\frac{-H}{2}}^{\frac{-H}{2}+\frac{l_p}{2}} u_p dy + \int_{\frac{-H}{2}+\frac{l_p}{2}}^{0} u_f dy\right)} \tag{4.59}$$

On non-dimensionalizing, the limiting Nusselt number based on the hydraulic diameter, 2H, it is given by

$$Nu_{p,CL} = \frac{h_p(2H)}{k_{eff}} = \frac{2\left(\frac{d\theta_p}{dY}\right)_{Y=-1/2}}{\theta^*} \tag{4.60}$$

In Eq. (4.60), θ^* is the non-dimensional bulk mean temperature defined by,

$$\theta^* = \frac{T_b - T_w}{T_e - T_w} \tag{4.61}$$

and evaluated using,

$$\theta^* = \frac{2\left(\int_{\frac{-1}{2}}^{\frac{-1}{2}+\frac{\gamma_p}{2}} U_p\ \theta_p\ dY + \int_{\frac{-1}{2}+\frac{\gamma_p}{2}}^{0} U_f\ \theta_f\ dY\right)}{2\left(\int_{\frac{-1}{2}}^{\frac{-1}{2}+\frac{\gamma_p}{2}} U_p dY + \int_{\frac{-1}{2}+\frac{\gamma_p}{2}}^{0} U_f dY\right)} \tag{4.62}$$

The limiting Nusselt number expressions for three models are (using Eqs. (4.52), (4.54), (4.56) and (4.60))

Darcy model

$$Nu_{p,CL1} = -\frac{1120 e^{-(\gamma_p-1)\sqrt{\frac{\varepsilon}{Da}}}\sqrt{\varepsilon}\eta A_{113}\left(A_{114}+A_{115}\right)}{\left\{Da\left(e^{\gamma_p\sqrt{\frac{\varepsilon}{Da}}}-1\right)^2\left[1/\left(e^{\gamma_p\sqrt{\frac{\varepsilon}{Da}}}-1\right)^2 1680\eta\left(\begin{array}{l}4U_i^2\left(2Da^{3/2}A_{116}-2Da\sqrt{\varepsilon}A_{117}+A_{118}\right)\\ -8U_i\left(e^{\frac{\gamma_p}{2}\sqrt{\frac{\varepsilon}{Da}}}-1\right)\left(\begin{array}{l}6Da^{3/2}A_{119}-A_{120}\\ +3\sqrt{Da}A_{121}-2DaA_{122}\end{array}\right)p_{gr}\\ -Da\left(e^{\frac{\gamma_p}{2}\sqrt{\frac{\varepsilon}{Da}}}-1\right)^2\left(\begin{array}{l}80Da^{5/2}A_{123}-4\sqrt{Da}A_{124}\\ +12Da^{3/2}A_{125}+A_{126}\\ -8Da^2\sqrt{\varepsilon}A_{127}-4Da\sqrt{\varepsilon}A_{128}\end{array}\right)p_{gr}^{\ 2}\end{array}\right)\right.\right.\\ \left.\left.+\varepsilon^{3/2}(\gamma_p-1)\left(\begin{array}{l}-21A_{129}(\gamma_p-1)^4 p_{gr}^{\ 2}+A_{130}-1/105Da\left(e^{\gamma_p\sqrt{\frac{\varepsilon}{Da}}}-1\right)^2\varepsilon\times\\ A_{129}\left(\begin{array}{l}48U_i^2\eta A_{131}-48U_iDa\left(e^{\frac{\gamma_p}{2}\sqrt{\frac{\varepsilon}{Da}}}-1\right)\eta A_{132}p_{gr}\\ +Da\left(e^{\frac{\gamma_p}{2}\sqrt{\frac{\varepsilon}{Da}}}-1\right)^2\sqrt{\varepsilon}\left(A_{133}+\sqrt{\varepsilon}A_{134}\right)p_{gr}^{\ 2}\end{array}\right)\\ +1/35\left(Da\varepsilon\left(e^{\gamma_p\sqrt{\frac{\varepsilon}{Da}}}-1\right)^2\right)\left(e^{\gamma_p\sqrt{\frac{\varepsilon}{Da}}}+1\right)(\gamma_p-1)^2\\ \times\left(\begin{array}{l}48U_i^2\eta A_{131}-48U_iDa\left(e^{\frac{\gamma_p}{2}\sqrt{\frac{\varepsilon}{Da}}}-1\right)\eta A_{132}p_{gr}\\ +Da\left(e^{\frac{\gamma_p}{2}\sqrt{\frac{\varepsilon}{Da}}}-1\right)^2\sqrt{\varepsilon}\left(\begin{array}{l}144Da^{3/2}\left(e^{\gamma_p\sqrt{\frac{\varepsilon}{Da}}}-1\right)\eta\gamma_p\\ +\sqrt{\varepsilon}A_{134}\end{array}\right)p_{gr}^{\ 2}\end{array}\right)\end{array}\right)\right]\right\}} \tag{4.63}$$

Form drag model:

$$Nu_{p,CL2} = -\frac{64\sqrt{\varepsilon}\eta A_{135}}{\left\{\begin{array}{l}\left[\begin{array}{l}\left(6\left(e^{\gamma_p\sqrt{\frac{\varepsilon}{Da}}}+1\right)\sqrt{\varepsilon}A_{136}(\gamma_p-1)^5/5A_{137}\right)+\left(6\left(e^{\gamma_p\sqrt{\frac{\varepsilon}{Da}}}+1\right)^2\sqrt{\varepsilon}(\gamma_p-1)^7/7A_{137}\right)\\ -\left(6A_{138}(\gamma_p-1)(A_{139}+A_{140})/A_{107}\right)+\left(2\left(e^{\gamma_p\sqrt{\frac{\varepsilon}{Da}}}+1\right)(\gamma_p-1)^3(A_{139}+A_{140})/5A_{137}\right)\end{array}\right]\\ \left[96Dae^{-\left(\frac{1+2\gamma_p}{2}\right)\sqrt{\frac{\varepsilon}{Da}}}\eta\left(\begin{array}{l}A_{141}\left(A_{142}+A_{143}+A_{144}\right)\\ +\left(e^{\gamma_p\sqrt{\frac{\varepsilon}{Da}}}+1\right)\left(A_{145}+A_{146}+A_{147}+A_{148}+A_{149}+A_{150}\right)\end{array}\right)\right]\end{array}\right\}} \tag{4.64}$$

Clear fluid compatible model:

$$Nu_{p,CL3} = \frac{1120\sqrt{\varepsilon}\eta A_{113}\left(A_{151}+A_{152}\right)}{\left\{Da\left(e^{\gamma_p\sqrt{\frac{\varepsilon}{Da}}}-1\right)^2\left[\begin{array}{l}1/\left(e^{\gamma_p\sqrt{\frac{\varepsilon}{Da}}}-1\right)^2 1680\eta\left(e^{-\frac{(2+3\gamma_p)}{2}\sqrt{\frac{\varepsilon}{Da}}}-1\right)\left(\begin{array}{l}4U_i^2\left(\begin{array}{l}2Da^{3/2}\left(e^{\frac{(2+3\gamma_p)}{2}\sqrt{\frac{\varepsilon}{Da}}}-1\right)\left(e^{\gamma_p\sqrt{\frac{\varepsilon}{Da}}}-1\right)A_{153}\\ +3\sqrt{Da}A_{154}+A_{155}+A_{156}\end{array}\right)\\ +8U_iDa\left(\begin{array}{l}A_{157}-A_{158}+3\sqrt{Da}\varepsilon\gamma_pA_{159}\\ +2Da\sqrt{\varepsilon}A_{160}\end{array}\right)p_{gr}\\ +Da\left(\begin{array}{l}16Da^{5/2}A_{161}+4\sqrt{Da}A_{162}-A_{163}\\ +12Da^{3/2}\varepsilon\gamma_pA_{164}-4Da\sqrt{\varepsilon}A_{165}\\ +8Da^2\sqrt{\varepsilon}A_{166}\end{array}\right)p_{gr}{}^2\end{array}\right)\\ +\varepsilon^{3/2}(\gamma_p-1)\left(\begin{array}{l}-21A_{129}(\gamma_p-1)^4p_{gr}{}^2+A_{130}+1/105Da\left(e^{\gamma_p\sqrt{\frac{\varepsilon}{Da}}}-1\right)^2\varepsilon\times\\ A_{129}\left(\begin{array}{l}-48U_i^2\eta A_{167}+48U_iDa\left(e^{\frac{\gamma_p}{2}\sqrt{\frac{\varepsilon}{Da}}}-1\right)\eta A_{168}p_{gr}\\ +Da\left(e^{\frac{\gamma_p}{2}\sqrt{\frac{\varepsilon}{Da}}}-1\right)^2\sqrt{\varepsilon}\left(A_{169}-\sqrt{\varepsilon}A_{134}\right)p_{gr}{}^2\end{array}\right)\\ -1/35\left(Da\varepsilon\left(e^{\gamma_p\sqrt{\frac{\varepsilon}{Da}}}-1\right)^2\right)\times\\ \left(e^{\gamma_p\sqrt{\frac{\varepsilon}{Da}}}+1\right)(\gamma_p-1)^2\left(\begin{array}{l}-48U_i^2\eta A_{167}-48U_iDa\left(e^{\frac{\gamma_p}{2}\sqrt{\frac{\varepsilon}{Da}}}-1\right)\eta A_{170}p_{gr}\\ +Da\left(e^{\frac{\gamma_p}{2}\sqrt{\frac{\varepsilon}{Da}}}-1\right)^2\sqrt{\varepsilon}\left(A_{169}-\sqrt{\varepsilon}A_{134}\right)p_{gr}{}^2\end{array}\right)\end{array}\right)\end{array}\right]\right\}} \tag{4.65}$$

Where A_i , i = 96, 97, ...170 are constants given in appendix.

4.4 Result and Discussion

In this section, temperature profiles and Nusselt number for flow through the channel partially filled with porous material is discussed. We have assumed that $\varepsilon = \mu_f / \mu_{eff} = 1$ and $\eta = k_f / k_{eff} = 1$. When $\gamma_p = 0$, the channel referred to is clear fluid channel. Similarly, when $\gamma_p = 1.0$, the channel referred to fully filled with the porous medium. When the porous fraction is $0 < \gamma_p < 1.0$, the channel is referred to as channel partially filled with the porous material.

4.4.1 Case(i): Subjected to constant wall heat flux

4.4.1.1 Limiting Cases

$\gamma_p = 0$, for the clear fluid channel, substituting in Eqs. (4.33), (4.35) and (4.37), the temperature profile reduces to

$$\left[\theta_{w1} - \theta_{f,CL}(Y)\right] / Br = 12Y^4 - (3/4) \tag{4.66}$$

Similarly, $\gamma_p = 1.0$ is substituted for the fully filled with the porous medium in Eqs. (4.34), (4.36) and (4.38), the temperature profiles for fully porous channel for three dissipation models reach the following form

Darcy model:

$$\frac{\theta_{w1} - \theta_{p,CL1}(Y)}{Br} = \frac{e^{-(1+2Y)\sqrt{\frac{\varepsilon}{Da}}}\left(\begin{array}{l} 2Da\left(\begin{array}{l} e^{2\sqrt{\frac{\varepsilon}{Da}}} + 16e^{2(1+2Y)\sqrt{\frac{\varepsilon}{Da}}} + 7\left(e^{(1+2Y)\sqrt{\frac{\varepsilon}{Da}}} + e^{(3+2Y)\sqrt{\frac{\varepsilon}{Da}}}\right) \\ -8\left(\begin{array}{l} e^{3(1+2Y)\sqrt{\frac{\varepsilon}{Da}}} + e^{\frac{(3+2Y)}{2}\sqrt{\frac{\varepsilon}{Da}}} \\ +e^{\frac{(5+2Y)}{2}\sqrt{\frac{\varepsilon}{Da}}} + e^{\frac{(5+6Y)}{2}\sqrt{\frac{\varepsilon}{Da}}} \end{array}\right) + e^{2(1+Y)\sqrt{\frac{\varepsilon}{Da}}} \end{array}\right)\eta \\ +\left(4e^{2(1+Y)\sqrt{\frac{\varepsilon}{Da}}} + e^{(1+2Y)\sqrt{\frac{\varepsilon}{Da}}} + e^{(3+2Y)\sqrt{\frac{\varepsilon}{Da}}}\right)(-1+4Y^2)\varepsilon \end{array}\right)}{8DaA_{94}{}^2} \tag{4.67}$$

Form drag model:

$$\frac{\theta_{w1}-\theta_{p,CL2}(Y)}{Br}=\frac{e^{-Y\sqrt{\frac{\varepsilon}{Da}}}\left(1+e^{\sqrt{\frac{\varepsilon}{Da}}}\right)\left(-8Da\left(\begin{array}{l}e^{\frac{1}{2}\sqrt{\frac{\varepsilon}{Da}}}-e^{Y\sqrt{\frac{\varepsilon}{Da}}}-e^{(1+Y)\sqrt{\frac{\varepsilon}{Da}}}+e^{\frac{(1+4Y)}{2}\sqrt{\frac{\varepsilon}{Da}}}\\+e^{Y\sqrt{\frac{\varepsilon}{Da}}}\left(1+e^{\sqrt{\frac{\varepsilon}{Da}}}\right)(-1+4Y^2)\varepsilon\end{array}\right)\right)\eta}{8DaA_{94}{}^2} \tag{4.68}$$

Clear fluid compatible model:

$$\frac{\theta_{w1}-\theta_{p,CL3}(Y)}{Br}=\frac{e^{-(1+2Y)\sqrt{\frac{\varepsilon}{Da}}}\left((-1+4Y^2)\varepsilon e^{(1+2Y)\sqrt{\frac{\varepsilon}{Da}}}A_{95}+2Da\left(\begin{array}{l}16e^{2(1+Y)\sqrt{\frac{\varepsilon}{Da}}}8\left(\begin{array}{l}e^{3\frac{(1+2Y)}{2}\sqrt{\frac{\varepsilon}{Da}}}+e^{\frac{(3+2Y)}{2}\sqrt{\frac{\varepsilon}{Da}}}\\+e^{(5+2Y)\sqrt{\frac{\varepsilon}{Da}}}+e^{\frac{(5+6Y)}{2}\sqrt{\frac{\varepsilon}{Da}}}\end{array}\right)\\-\left(e^{(1+2Y)\sqrt{\frac{\varepsilon}{Da}}}+e^{(3+2Y)\sqrt{\frac{\varepsilon}{Da}}}\right)(-7+\varepsilon)\\+\left(e^{2\sqrt{\frac{\varepsilon}{Da}}}+e^{2(1+2Y)\sqrt{\frac{\varepsilon}{Da}}}\right)(1+\varepsilon)\end{array}\right)\right)\eta}{8DaA_{94}{}^2} \tag{4.69}$$

4.4.1.2 Thermal Field

Darcy model:

The ratio between the non-dimensional limiting temperature excess of wall temperature to Brinkman number, $\left(\theta_{w1}-\theta_{p,CL1}\right)/Br$, $\left(\theta_{w1}-\theta_{f,CL1}\right)/Br$ is shown in Figs. 4.2(a) to 4.2(f) for γ_p = 0, 0.2, 0.4, 0.6, 0.8 and 1.0 for different Darcy numbers, *Da* = 0.001,0.005,0.01,0.05 and 0.1 for the Darcy Model. From Figs. 4.2(b) to 4.2(e), the effect of porous fraction on $\left(\theta_{w1}-\theta_{p,CL1}\right)/Br$, $\left(\theta_{w1}-\theta_{f,CL1}\right)/Br$ can be assessed. The maximum value of $\left|\left(\theta_{w1}-\theta_{p,f,CL}\right)\right|/Br$ occurs at the centre of the channel at $Y=0$ for all Darcy numbers where the fluid is placed. The maximum value of $\left|\left(\theta_{w1}-\theta_{p,f,CL}\right)\right|/Br$ at

$Y = 0$ is decreasing with the increasing Darcy number for a porous fraction. This is commensurate with acceleration associated with the fluid in the fluid region at higher γ_p. It is apparent too that the value of $|(\theta_{w1} - \theta_{p,f,CL})|/Br$ is minimum other than at centre of the channel for higher Darcy number, say $Da = 0.1$ for all $0 < \gamma_p \leq 1.0$. This implies that the porous medium tends to behave almost like a clear fluid channel.

The profiles shown in Figs. 4.2(a) and 4.2(f) for $\gamma_p = 0$ and 1.0 are clear fluid channel and fully filled with porous material. The profile in Fig. 4.2 (f) is very close to the profile in Fig. 4.2 (a){ for $\gamma_p = 0$} for $Da = 0.1$. Indeed, the porous material filled channel behaves like the clear fluid channel at higher Da which is also evident in Figs. 4.2(b) to 4.2(c) as well, even though these two profiles pertain to a channel containing partially filled porous medium.

Form drag model:

The ratio between the non-dimensional limiting temperature excess of wall temperature to Brinkman number, $(\theta_{w1} - \theta_{p,CL2})/Br$, $(\theta_{w1} - \theta_{f,CL2})/Br$ is featured in Figs. 4.3(a) to 4.3(f) for $\gamma_p = 0$, 0.2, 0.4, 0.6, 0.8 and 1.0 for different Darcy numbers, Da=0.001,0.005,0.01,0.05 and 0.1 for the Form drag model. From Figs. 4.3(b) to 4.3(e), the effect of porous fraction on $(\theta_{w1} - \theta_{p,CL2})/Br$, $(\theta_{w1} - \theta_{f,CL2})/Br$ can be assessed. The maximum value $|(\theta_{w1} - \theta_{p,f,CL})|/Br$ occurs at the centre of the channel at $Y = 0$ for all Darcy numbers where the fluid is placed. The maximum value of $|(\theta_{w1} - \theta_{p,f,CL})|/Br$ at $Y = 0$ is decreasing with increasing Darcy number for a porous fraction. This aligns

with the acceleration associated with the fluid in the fluid region at higher γ_p. It may also be noticed that the value of $|(\theta_{w1} - \theta_{p,f,CL})|/Br$ is minimum except at the centre of the channel for higher Darcy number, say $Da = 0.1$ for all $0 < \gamma_p \leq 1.0$. This indicates that the porous medium behaves as if it were a clear fluid channel.

The profiles shown in Figs. 4.3(a) and 4.3(f) for $\gamma_p = 0$ and 1.0 are clear fluid channel and fully filled with porous material. The profile in Fig. 4.3(f) nearly approximate the profile in Fig. 4.3 (a){ for $\gamma_p = 0$} for $Da = 0.1$. Indeed, the porous material filled channel behaves like the clear fluid channel at higher Da, which is clearly seen in Figs. 4.3(b) to 4.3(c) as well, even though these two profiles pertain to a channel partially filled porous medium.

Clear fluid compatible model:

The ratio between the non-dimensional limiting temperature which is in excess of wall temperature to Brinkman number, $(\theta_{w1} - \theta_{p,CL3})/Br$, $(\theta_{w1} - \theta_{f,CL3})/Br$ is featured in Figs. 4.4(a) to 4.4(f) for $\gamma_p = 0$, 0.2, 0.4, 0.6, 0.8 and 1.0 for different Darcy numbers, Da=0.001,0.005,0.01,0.05 and 0.1 for the clear fluid compatible model. From Figs. 4.4(b) to 4.4(e), the effect of porous fraction on $(\theta_{w1} - \theta_{p,CL3})/Br$, $(\theta_{w1} - \theta_{f,CL3})/Br$ can be assessed. The maximum value of $|(\theta_{w1} - \theta_{p,f,CL})|/Br$ occurs at the centre of the channel at $Y = 0$ for all Darcy numbers, where the fluid is placed. The maximum value of $|(\theta_{w1} - \theta_{p,f,CL})|/Br$ at $Y = 0$ is decreasing with the increasing Darcy number for a porous fraction. This is commensurate with the acceleration associated with the fluid in the fluid

region at higher γ_p. It may also be noticed that the value of $|(\theta_{w1} - \theta_{p,f,CL})|/Br$ is minimum other than at the centre of the channel for higher Darcy number, say Da = 0.1 for all $0 < \gamma_p \leq 1.0$. It means that the porous medium is behaving almost like a clear fluid channel.

The profiles shown in Figs. 4.4(a) and 4.4(f) for γ_p = 0 and 1.0 are clear fluid channel and fully filled with porous material. The profile in Fig. 4.4 (f) is very close to the profile in Fig. 4.4 (a){ for γ_p = 0} for Da = 0.1. Indeed, the porous material filled channel behaves like the clear fluid channel at higher Da which is also noticeable in Figs. 4.4(b) to 4.4(c) as well, even though these two profiles pertain to a channel that has partially filled porous medium.

4.4.1.3 Limiting Nusselt Number

Variation of product of Brinkman number and the Nusselt number with porous fraction, γ_p for the three dissipation models are shown in Figs. 4.5(a) to 4.5(c) for different Darcy numbers, Da = 0.001, 0.005, 0.01, 0.05 and 0.1. From Figs. 4.5(a) to 4.5(c), $Br\ Nu_{p,CL1,2,3}$ decreases as Darcy number increases and tends to the value of -35/12, which is the value for the clear fluid channel. As porous fraction increases $Br\ Nu_{p,CL1,2,3}$ increases for all Darcy numbers. But for higher Da = 0.05 and 0.1 $Br\ Nu_{p,CL1,2}$ exhibits a minimum value of γ_p. This may due to the fluid region being more compared to the porous region. From Figs. 4.5(a) to 4.5(c), limiting Nusselt number can be calculated for any Brinkman number value for all the dissipation models. For small Darcy number, say Da = 0.001, the

difference between these models in limiting Nusselt number is negligible, but for larger Darcy number, say $Da = 0.05$, the difference is significant (Nield et al. [58]).

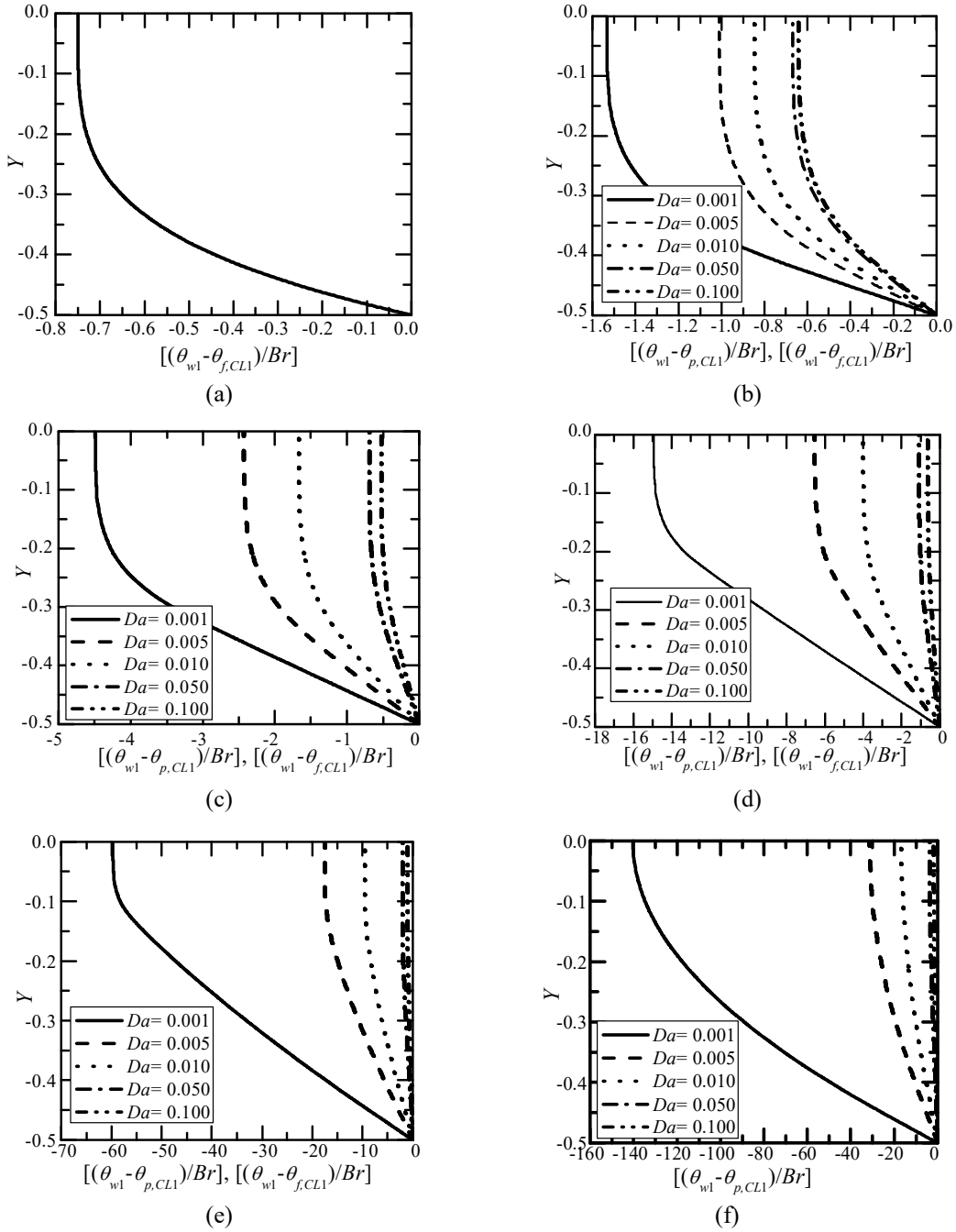

Fig. 4.2 : Variation of limiting temperature profiles for (a) $\gamma_p = 0$ (b) $\gamma_p = 0.2$ (c) $\gamma_p = 0.4$ (d) $\gamma_p = 0.6$ (e) $\gamma_p = 0.8$ (f) $\gamma_p = 1.0$ for different Darcy number for Darcy model.

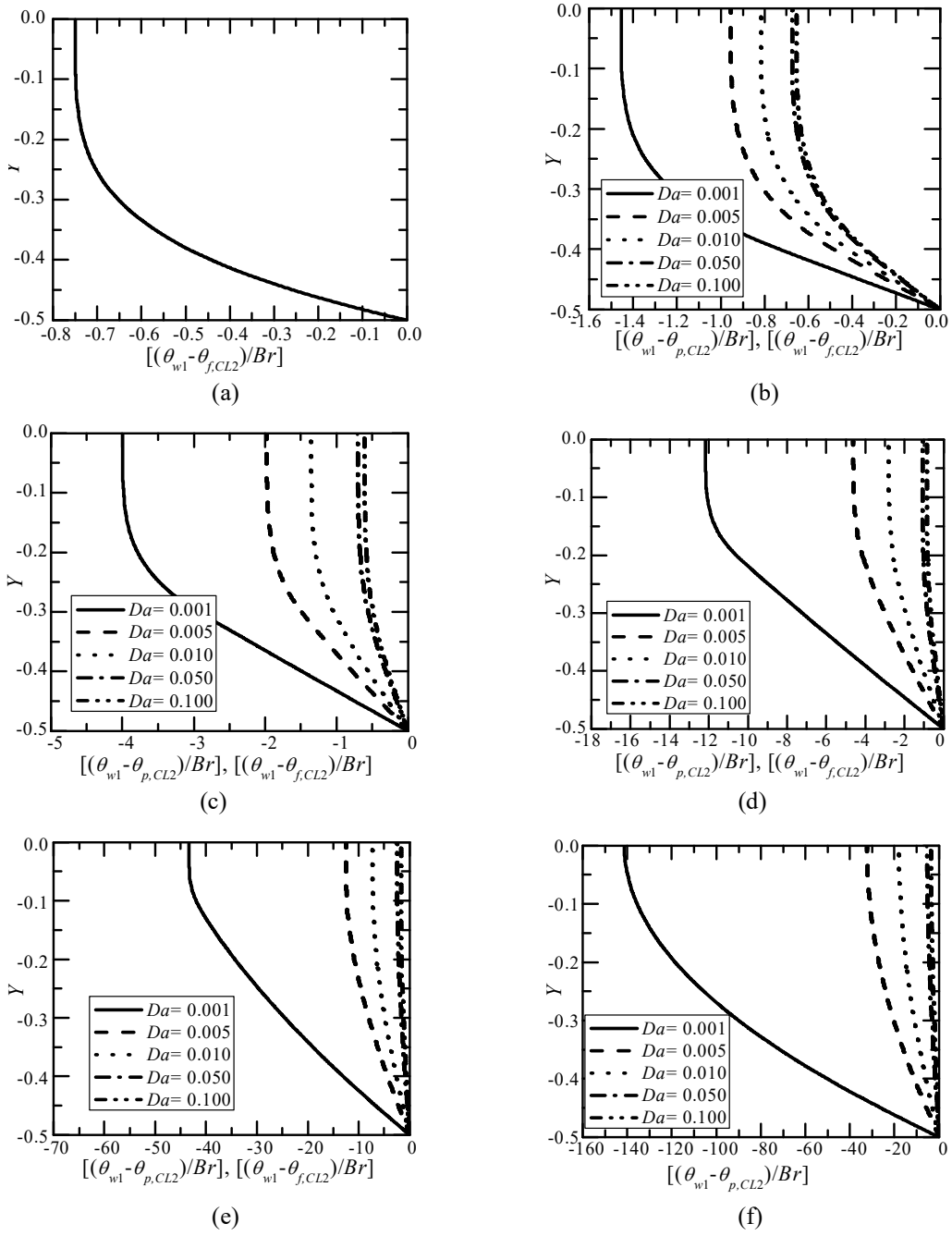

Fig. 4.3: Variation of limiting temperature profiles for (a) $\gamma_p = 0$ (b) $\gamma_p = 0.2$ (c) $\gamma_p = 0.4$ (d) $\gamma_p = 0.6$ (e) $\gamma_p = 0.8$ (f) $\gamma_p = 1.0$ for different Darcy number for Form drag model.

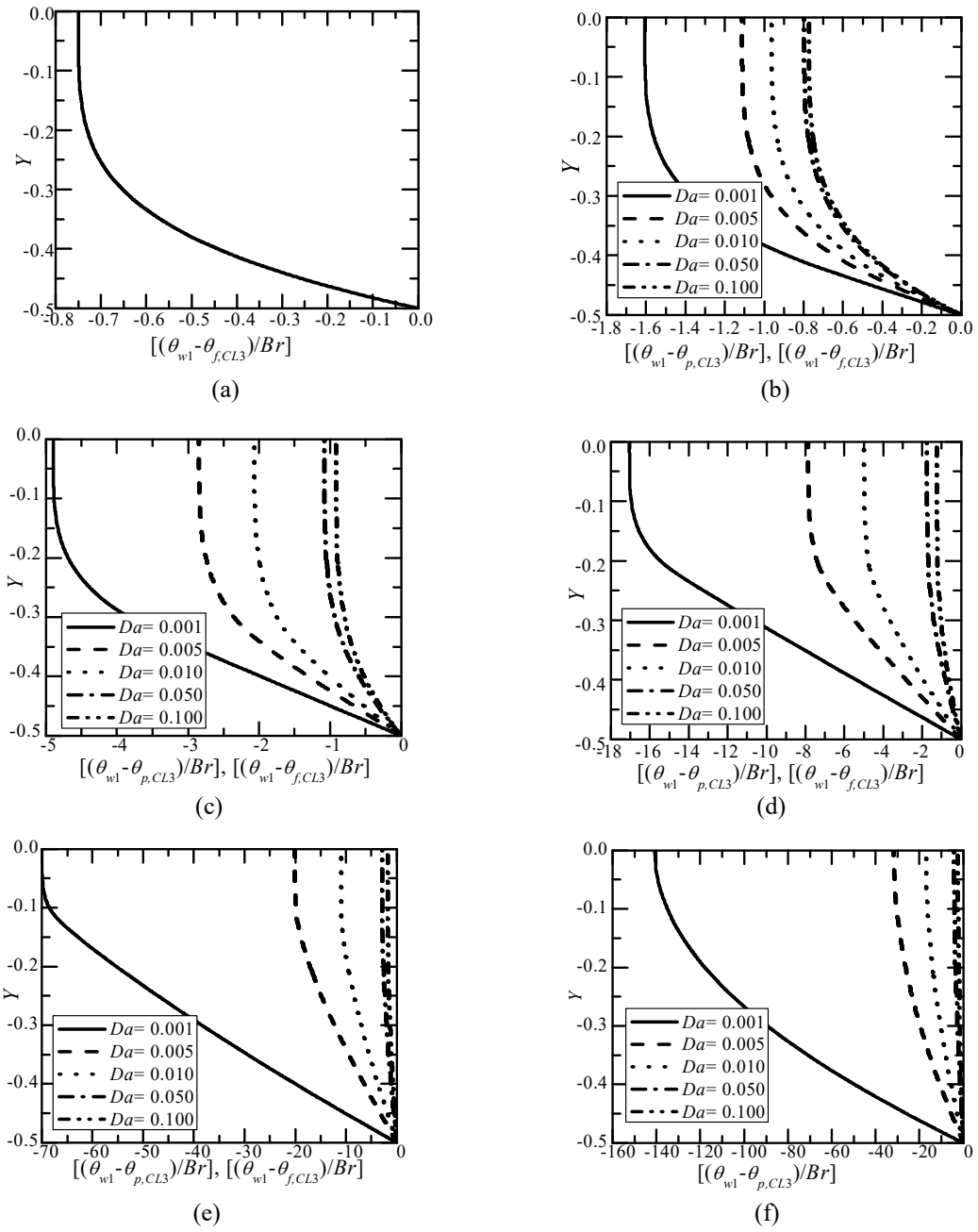

Fig. 4.4: Variation of limiting temperature profiles for (a) $\gamma_p = 0$ (b) $\gamma_p = 0.2$ (c) $\gamma_p = 0.4$ (d) $\gamma_p = 0.6$ (e) $\gamma_p = 0.8$ (f) $\gamma_p = 1.0$ for different Darcy number for Clear fluid compatible model.

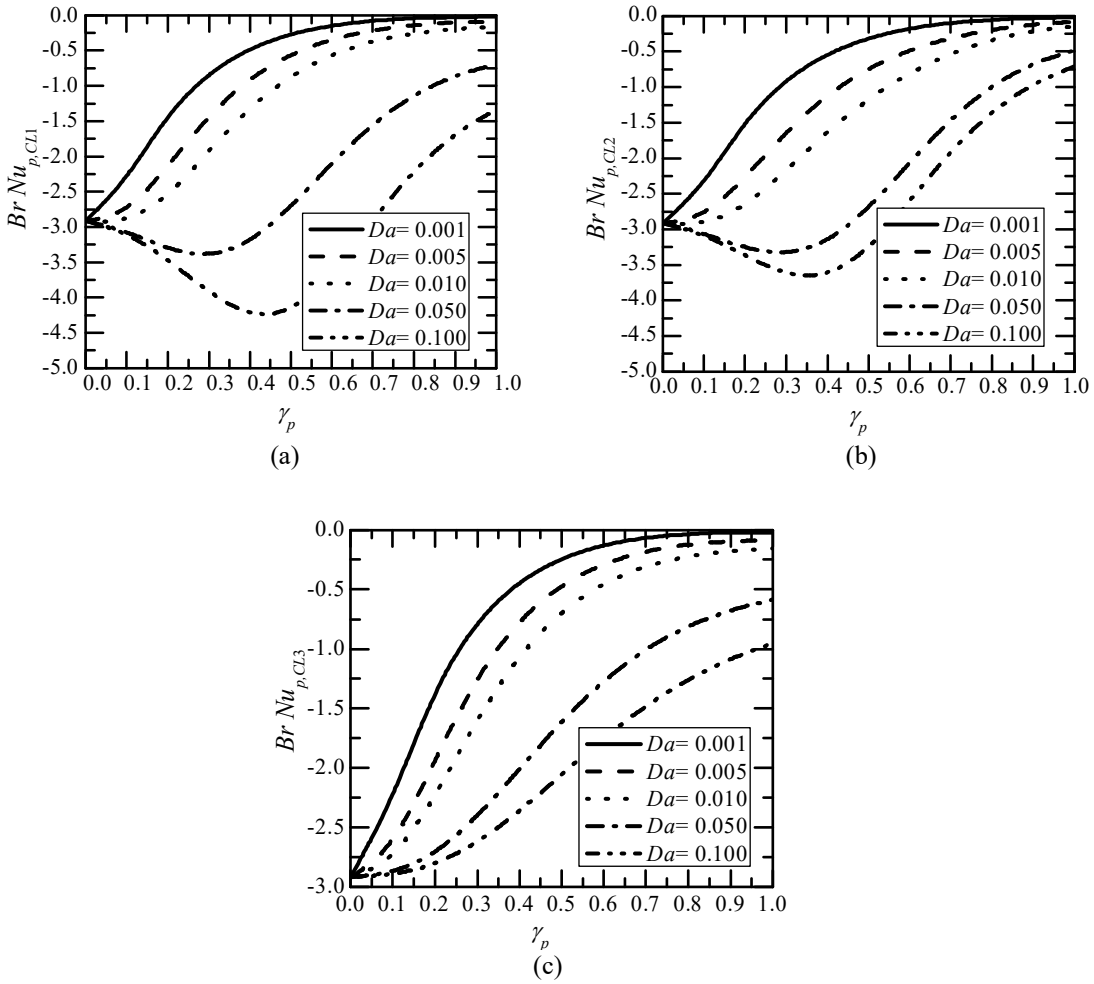

Fig. 4.5: Variation of (a) $Br\ Nu_{p,CL1}$ {the Darcy model } (b) $Br\ Nu_{p,CL2}$ {form drag model} (c) $Br\ Nu_{p,CL3}$ {clear fluid compatible model} with porous fraction, γ_p for different Darcy numbers.

Net change in the Nusselt number:

Variation of (a) ΔNu_1 {the Darcy model}(b) ΔNu_2 {form drag model}(c) ΔNu_3 {clear fluid compatible model} with porous fraction, γ_p for different Darcy numbers, Da = 0.001, 0.005, 0.01, 0.05 and 0.1 is depicted in Figs. 4.6(a) to 4.6(c). Enhancement in the Nusselt number when porous material of thickness l_p is attached to both the walls of the channel, is lower than a the channel fully filled with porous material, when dissipation is

included. In the case of clear fluid compatible model, dissipation effect is more as compared to the Darcy model and form drag model.

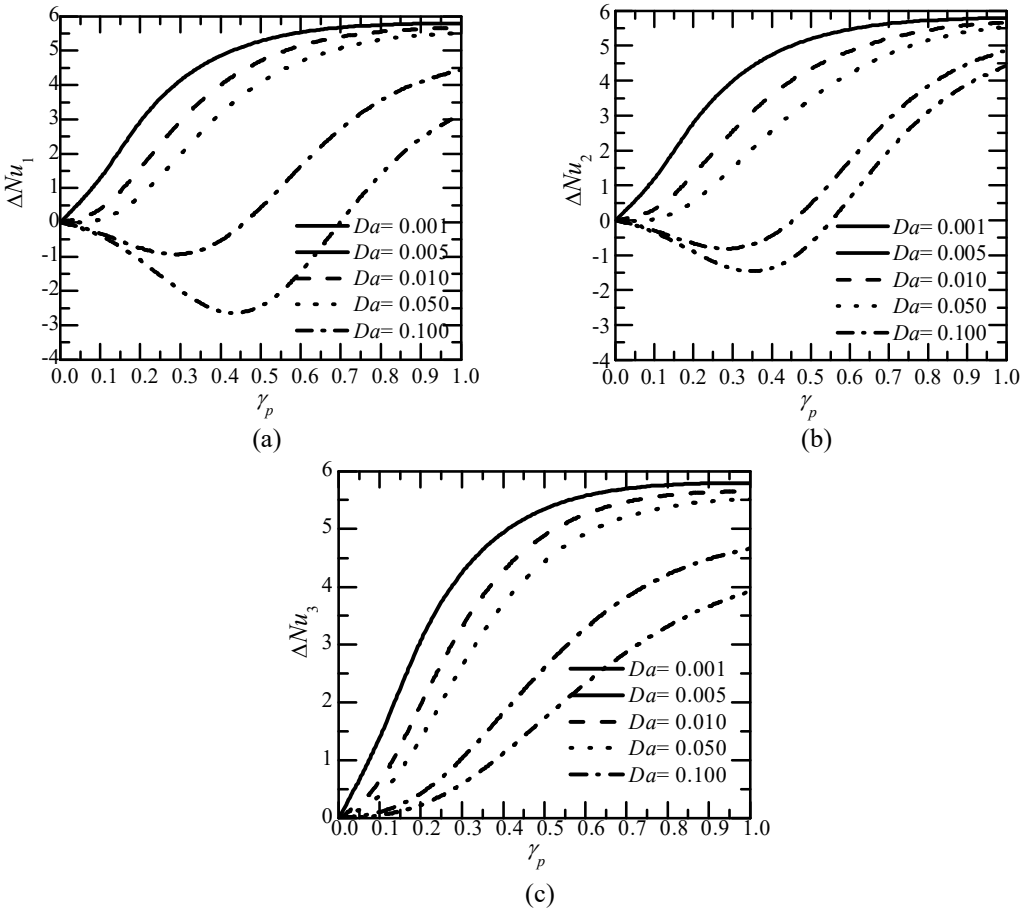

Fig. 4.6 : Variation of (a) ΔNu_1 (b) ΔNu_2 and (c) ΔNu_3 with porous fraction, γ_p for different Darcy numbers.

4.4.2 Case(ii): Subjected to constant wall temperature

4.4.2.1 Limiting cases

Substituting $\gamma_p = 0$ for the clear fluid channel, in Eqs. (4.51), (4.53), (4.55),(4.63), (4.64) and (4.65), the temperature profile and the Nusselt number reduce to

$$\frac{\theta_{f,CL}(Y)}{Br} = \frac{3}{4} - 12Y^4 \tag{4.70}$$

$$Nu_{f,CL} = 17.5 \tag{4.71}$$

These are standard results available in Ramjee and Satyamurty[182] and Barletta [4].

The values of $(\theta_{CL}^{\gamma_p=1.0} / Br)$ obtained with Darcy model due to Bejan [49], form drag model due to Nield [140] and clear fluid compatible model due to Al-Hadhrami, Elliott and Ingham[135 and 136] are designated respectively by $(\theta_{CL1}^{\gamma_p=1.0} / Br)$, $(\theta_{CL2}^{\gamma_p=1.0} / Br)$ and $(\theta_{CL3}^{\gamma_p=1.0} / Br)$. Substituting γ_p = 1.0 for fully filled porous medium in Eqs. (4.52), (4.54), (4.56), (4.63), (4.64) and (4.65), the expressions for $(\theta_{CL1}^{\gamma_p=1.0} / Br)$, $(\theta_{CL2}^{\gamma_p=1.0} / Br)$ and $(\theta_{CL2}^{\gamma_p=1.0} / Br)$ and the limiting Nusselt numbers for three dissipation models are as follows,

Darcy model:

$$\frac{\theta_{CL1}^{\gamma_p=1.0}}{Br} = \frac{-e^{-2Y\sqrt{\frac{\varepsilon}{Da}}}\eta\left[2Da\left(\begin{array}{l} e^{\sqrt{\frac{\varepsilon}{Da}}} + 7\left(e^{2Y\sqrt{\frac{\varepsilon}{Da}}} + e^{2(1+Y)\sqrt{\frac{\varepsilon}{Da}}}\right) - 8\left(\begin{array}{l} e^{\frac{(1+2Y)}{2}\sqrt{\frac{\varepsilon}{Da}}} + e^{\frac{3(1+2Y)}{2}\sqrt{\frac{\varepsilon}{Da}}} \\ +e^{\frac{(3+2Y)}{2}\sqrt{\frac{\varepsilon}{Da}}} + e^{\frac{(1+6Y)}{2}\sqrt{\frac{\varepsilon}{Da}}} \end{array}\right) \\ +16e^{(1+2Y)\sqrt{\frac{\varepsilon}{Da}}} + e^{(1+4Y)\sqrt{\frac{\varepsilon}{Da}}} \end{array}\right)\right.}{\left. +e^{2Y\sqrt{\frac{\varepsilon}{Da}}}(4Y^2-1)\varepsilon\left(1+4e^{\sqrt{\frac{\varepsilon}{Da}}} + e^{2\sqrt{\frac{\varepsilon}{Da}}}\right)\right]} \\ 8Da\left[-2\sqrt{Da}\left(e^{\sqrt{\frac{\varepsilon}{Da}}} - 1\right) + \left(e^{\sqrt{\frac{\varepsilon}{Da}}} + 1\right)\sqrt{\varepsilon}\right]^2 \tag{4.72}$$

$$Nu_{p,CL1}=\frac{12\left(\begin{array}{l}-2\sqrt{Da}\left(e^{\sqrt{\frac{\varepsilon}{Da}}}-1\right)\\+\left(e^{\sqrt{\frac{\varepsilon}{Da}}}+1\right)\sqrt{\varepsilon}\end{array}\right)\left(\begin{array}{l}-3\sqrt{Da}\left(e^{2\sqrt{\frac{\varepsilon}{Da}}}-1\right)\\+\left(1+4e^{\sqrt{\frac{\varepsilon}{Da}}}+e^{2\sqrt{\frac{\varepsilon}{Da}}}\right)\sqrt{\varepsilon}\end{array}\right)\sqrt{\varepsilon}}{Da^{3/2}\left(\begin{array}{l}153\left(e^{2\sqrt{\frac{\varepsilon}{Da}}}-e^{\sqrt{\frac{\varepsilon}{Da}}}\right)\\+89\left(e^{3\sqrt{\frac{\varepsilon}{Da}}}-1\right)\end{array}\right)-3Da\left(\begin{array}{l}59\left(e^{2\sqrt{\frac{\varepsilon}{Da}}}+e^{\sqrt{\frac{\varepsilon}{Da}}}\right)\\+11\left(e^{3\sqrt{\frac{\varepsilon}{Da}}}+1\right)\sqrt{\varepsilon}\end{array}\right)+\left(\begin{array}{l}5\left(e^{2\sqrt{\frac{\varepsilon}{Da}}}+e^{\sqrt{\frac{\varepsilon}{Da}}}\right)\\+e^{3\sqrt{\frac{\varepsilon}{Da}}}+1\end{array}\right)\varepsilon^{3/2}} \tag{4.73}$$

Form drag model:

$$\frac{\theta_{CL2}^{\gamma_p=1.0}}{Br}=\frac{e^{-Y\sqrt{\frac{\varepsilon}{Da}}}\left(e^{\sqrt{\frac{\varepsilon}{Da}}}+1\right)\eta\left[\begin{array}{l}-8Da\left(e^{\frac{1}{2}\sqrt{\frac{\varepsilon}{Da}}}-e^{Y\sqrt{\frac{\varepsilon}{Da}}}-e^{(1+Y)\sqrt{\frac{\varepsilon}{Da}}}+e^{\frac{(1+4Y)}{2}\sqrt{\frac{\varepsilon}{Da}}}\right)\\+e^{Y\sqrt{\frac{\varepsilon}{Da}}}\left(e^{\sqrt{\frac{\varepsilon}{Da}}}+1\right)(4Y^2-1)\varepsilon\end{array}\right]}{8Da\left[-2\sqrt{Da}\left(e^{\sqrt{\frac{\varepsilon}{Da}}}-1\right)+\left(e^{\sqrt{\frac{\varepsilon}{Da}}}+1\right)\sqrt{\varepsilon}\right]^2} \tag{4.74}$$

$$Nu_{p,CL2}=\frac{12\left(-2\sqrt{Da}\left(e^{\sqrt{\frac{\varepsilon}{Da}}}-1\right)+\left(e^{\sqrt{\frac{\varepsilon}{Da}}}+1\right)\sqrt{\varepsilon}\right)^2\sqrt{\varepsilon}}{60Da^{3/2}\left(e^{2\sqrt{\frac{\varepsilon}{Da}}}-1\right)-24Da\left(1+3e^{\sqrt{\frac{\varepsilon}{Da}}}+e^{2\sqrt{\frac{\varepsilon}{Da}}}\right)\sqrt{\varepsilon}+\left(1+e^{\sqrt{\frac{\varepsilon}{Da}}}\right)^2\varepsilon^{3/2}} \tag{4.75}$$

Clear fluid compatible model:

$$\frac{\theta_{CL3}^{\gamma_p=1.0}}{Br}=\frac{e^{-2Y\sqrt{\frac{\varepsilon}{Da}}}\eta\left[\begin{array}{l}2Da\left(\begin{array}{l}16e^{(1+2Y)\sqrt{\frac{\varepsilon}{Da}}}-8\left(\begin{array}{l}e^{\frac{(1+2Y)}{2}\sqrt{\frac{\varepsilon}{Da}}}+e^{\frac{3(1+2Y)}{2}\sqrt{\frac{\varepsilon}{Da}}}\\+e^{\frac{(3+2Y)}{2}\sqrt{\frac{\varepsilon}{Da}}}+e^{\frac{(1+6Y)}{2}\sqrt{\frac{\varepsilon}{Da}}}\end{array}\right)\\-(\varepsilon-7)\left(e^{2Y\sqrt{\frac{\varepsilon}{Da}}}+e^{2(1+Y)\sqrt{\frac{\varepsilon}{Da}}}\right)+(\varepsilon+1)\left(e^{\sqrt{\frac{\varepsilon}{Da}}}+e^{(1+4Y)\sqrt{\frac{\varepsilon}{Da}}}\right)\end{array}\right)\\+e^{2Y\sqrt{\frac{\varepsilon}{Da}}}(4Y^2-1)\varepsilon\left(1+e^{2\sqrt{\frac{\varepsilon}{Da}}}-2e^{\sqrt{\frac{\varepsilon}{Da}}}(\varepsilon-2)\right)\end{array}\right]}{8Da\left[-2\sqrt{Da}\left(e^{\sqrt{\frac{\varepsilon}{Da}}}-1\right)+\left(e^{\sqrt{\frac{\varepsilon}{Da}}}+1\right)\sqrt{\varepsilon}\right]^2} \tag{4.76}$$

It is clear from Eqs. (4.72), (4.74) and (4.76) that $\theta_{CL}^{\gamma_p=1.0}$ varies linearly with *Br*. Thus,

$$\theta_{CL}^{\gamma_p=1.0}=m_{1,2,3}(Y,Da)Br \tag{4.77}$$

where m_1 is a slope for the Darcy model, m_2 is a slope for form drag model and m_3 is a slope for the clear fluid compatible model.

$$Nu_{p,CL3}=\frac{12\left(\begin{array}{l}-2\sqrt{Da}\left(e^{\sqrt{\frac{\varepsilon}{Da}}}-1\right)\\+\left(e^{\sqrt{\frac{\varepsilon}{Da}}}+1\right)\sqrt{\varepsilon}\end{array}\right)\left(\begin{array}{l}-\sqrt{Da}\left(e^{2\sqrt{\frac{\varepsilon}{Da}}}-1\right)(\varepsilon-3)\\+\left(2(\varepsilon-2)e^{\sqrt{\frac{\varepsilon}{Da}}}-e^{2\sqrt{\frac{\varepsilon}{Da}}}-1\right)\sqrt{\varepsilon}\end{array}\right)\sqrt{\varepsilon}}{Da^{3/2}\left(e^{\sqrt{\frac{\varepsilon}{Da}}}-1\right)\left(\begin{array}{l}(7\varepsilon-89)\left(1+e^{2\sqrt{\frac{\varepsilon}{Da}}}\right)\\+e^{\sqrt{\frac{\varepsilon}{Da}}}(46\varepsilon-242)\end{array}\right)-3Da\left(e^{\sqrt{\frac{\varepsilon}{Da}}}+1\right)\sqrt{\varepsilon}\left(\begin{array}{l}(\varepsilon-11)\left(e^{2\sqrt{\frac{\varepsilon}{Da}}}+1\right)\\+8e^{\sqrt{\frac{\varepsilon}{Da}}}(\varepsilon-6)\end{array}\right)-\left(e^{\sqrt{\frac{\varepsilon}{Da}}}+1\right)\left(\begin{array}{l}1+e^{2\sqrt{\frac{\varepsilon}{Da}}}\\-2e^{\sqrt{\frac{\varepsilon}{Da}}}(\varepsilon-2)\end{array}\right)\varepsilon^{3/2}} \tag{4.78}$$

These results for γ_p = 1.0 are standard results available in Bhargavi [186] thesis for the Darcy model and clear fluid compatible model.

4.4.2.2 Thermal Field

Darcy model:

Non dimensional temperature profiles $\theta_{p,CL1}(Y)/Br,\ \theta_{f,CL1}(Y)/Br$ at the conduction limit are shown in Figs. 4.7(a) to 4.7(f) for porous fraction, γ_p = 0, 0.2, 0.4, 0.6, 0.8 and 1.0 for different Darcy numbers for Darcy model. From Figs. 4.7(a) to 4.7(f), the effect of porous fraction on $\theta_{p,CL1}(Y)/Br, \theta_{f,CL1}(Y)/Br$ can be assessed. Maximum value of $\theta_{p,CL1}(Y)/Br,\ \theta_{f,CL1}(Y)/Br$ occurs at the centre of the channel at Y = 0 for all Darcy numbers where fluid is placed. Maximum value of $\theta_{p,CL1}(Y)/Br,\ \theta_{f,CL1}(Y)/Br$ at Y = 0 is decreasing with the increasing Darcy number for all porous fractions. This is commensurate with the acceleration associated with the fluid in the fluid region at higher γ_p. As porous fraction, γ_p increases, the maximum value of $\theta_{p,CL1}(Y)/Br,\ \theta_{f,CL1}(Y)/Br$ increases for all Darcy numbers.

The profiles shown in Figs. 4.7(a) and 4.7(f) for γ_p = 0 and 1.0 are for clear fluid channel and fully filled with a porous material. The profile in Fig. 4.7(f) is very close to the profile in Fig. Fig. 4.7(a) for Da = 0.1. Indeed, the porous material filled channel behaves like clear fluid channel at higher Da. Which is also noticeable in Figs. 4.7(b) and 4.7(c) as well, even though these two profiles pertain to a channel partially filled with a porous medium.

Form drag model:

Non dimensional temperature profiles $\theta_{p,CL2}(Y)/Br$, $\theta_{f,CL2}(Y)/Br$ at the conduction limit are shown in Figs. 4.8(a) to 4.8(f) for porous fraction, γ_p = 0, 0.2, 0.4, 0.6, 0.8 and 1.0 for different Darcy numbers for form drag model. From Figs. 4.8(a) to 4.8(f), the effect of porous fraction on $\theta_{p,CL2}(Y)/Br$, $\theta_{f,CL2}(Y)/Br$ can be assessed. Maximum value of $\theta_{p,CL2}(Y)/Br$, $\theta_{f,CL2}(Y)/Br$ occurs at the centre of the channel at Y = 0 for all Darcy numbers where the fluid is placed. The maximum value of $\theta_{p,CL2}(Y)/Br$, $\theta_{f,CL2}(Y)/Br$ at Y = 0 is decreasing with the increasing Darcy number for all porous fractions. This is commensurate with the acceleration associated with the fluid in the fluid region at higher γ_p. As porous fraction, γ_p increases, the maximum value of $\theta_{p,CL2}(Y)/Br$, $\theta_{f,CL2}(Y)/Br$ increases for all Darcy numbers.

The profiles shown in Figs. 4.8(a) and 4.8(f) for γ_p = 0 and 1.0 are clear fluid channel and fully filled with a porous material. The profile in Fig. 4.8(f) is very close to the profile in Fig. 4.8(a) for *Da* = 0.1. Indeed, the porous material filled channel behaving like the clear fluid channel at higher *Da*. Which is also noticeable in Figs 4.8(b) and 4.8(c) as well, even though these two profiles pertain to a channel partially filled with a porous medium.

Clear fluid compatible model:

Non dimensional temperature profiles $\theta_{p,CL3}(Y)/Br$, $\theta_{f,CL3}(Y)/Br$ at the conduction limit are shown in Figs. 4.9(a) to 4.9(f) for porous fraction, γ_p = 0, 0.2, 0.4, 0.6, 0.8 and

1.0 for different Darcy numbers for clear fluid compatible model. From Figs 4.9(a) to 4.9(f), the effect of porous fraction on $\theta_{p,CL3}(Y)/Br, \theta_{f,CL3}(Y)/Br$ can be assessed. Maximum value of $\theta_{p,CL3}(Y)/Br$, $\theta_{f,CL3}(Y)/Br$ occurs at the centre of the channel at Y = 0 for all Darcy numbers where fluid is placed. Maximum value of $\theta_{p,CL3}(Y)/Br$, $\theta_{f,CL3}(Y)/Br$ at Y = 0 is decreasing with the increasing Darcy number for all porous fractions. This is in line with the acceleration associated with the fluid in the fluid region at higher γ_p. As porous fraction, γ_p increases, the maximum value of $\theta_{p,CL3}(Y)/Br$, $\theta_{f,CL3}(Y)/Br$ increases for all Darcy numbers.

The profiles shown in Figs. 4.9(a) and 4.9(f) for γ_p = 0 and 1.0 are clear fluid channels and fully filled with a porous material. The profile in Fig. 4.9(f) is indeed close to the profile in Fig. 4.9(a) for Da = 0.1. Indeed, the porous material filled channel is known to behave like clear fluid channel at higher Da. This fact is also noticeable in Figs. 4.9(b) and 4.9(c) as well, even though these two profiles pertain to a channel partially filled with a porous medium.

The values of m_1 , m_2 and m_3 in Eq. (4.77), for the three dissipation models for γ_p = 1.0 have also been given in Figs. 4.7(f), 4.8(f) and 4.9(f).

Observations from Figs. 4.7 (a) and 4.7(f) , Fig. 4.8(a) and 4.8(f) and Fig. 4.9(a) and 4.9(f) lead us to the following conclusions.

a) m_1, m_2 and m_3 values for the three models are close to each other at lower Da has been observed already (γ_p = 1.0).

b) Of course, m_1, m_2 and m_3 are not dependent on Da for both the models for $\gamma_p = 0$.

c) m_1 , m_2 and m_3 decrease with increase in Da for a given γ_p and Y for both the models.

The difference between the Darcy model and the clear fluid compatible model is brought out in Fig. 4.10, where the variation of $[(\theta_{CL3}^{\gamma_p=1.0}/Br)-(\theta_{CL1}^{\gamma_p=1.0}/Br)]$ with Y has been given for different Da. It is evident that $(\theta_{CL1}^{\gamma_p=1.0}/Br)$ values are closer to the values of $(\theta_{CL3}^{\gamma_p=1.0}/Br)$ at lower Da. At the lowest considered, Da = 0.001, $[(\theta_{CL3}^{\gamma_p=1.0}/Br)$ − $(\theta_{CL1}^{\gamma_p=1.0}/Br)] \approx 0.28$, which is less than 2.5% considering that $(\theta_{CL}^{\gamma_p=1.0}/Br)$ is of the order of 140. At the highest Da, $[(\theta_{CL3}^{\gamma_p=1.0}/Br)-(\theta_{CL1}^{\gamma_p=1.0}/Br)] \approx 0.65$, where $(\theta_{CL}^{\gamma_p=1.0}/Br)$ is of the order of 2.5. The difference in the values of $(\theta_{CL}^{\gamma_p=1.0}/Br)$ for the two models is less than 30% for $Da < 0.05$.

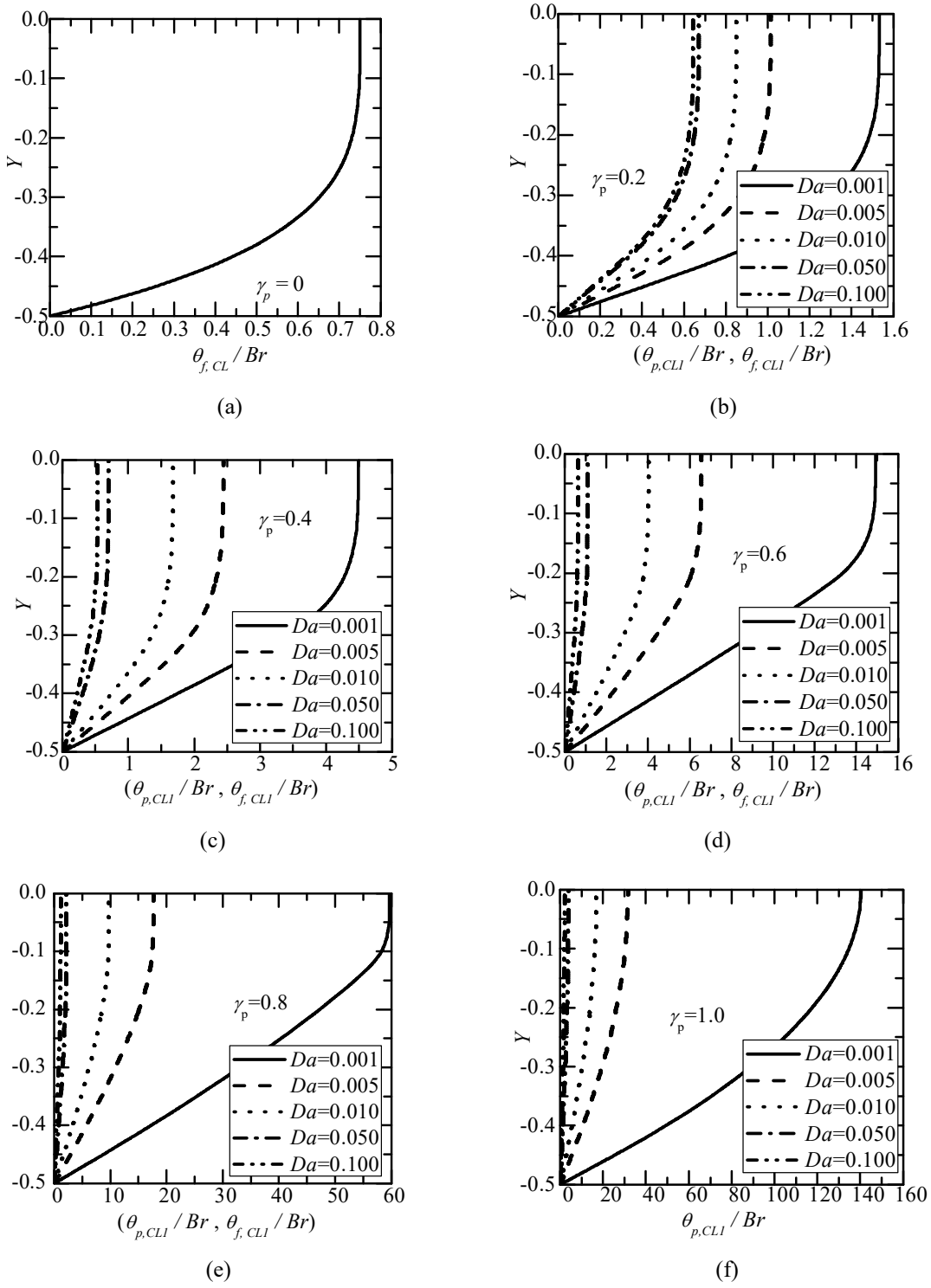

Fig. 4.7: Variation of limiting temperature profiles for (a) $\gamma_p = 0$ (b) $\gamma_p = 0.2$ (c) $\gamma_p = 0.4$ (d) $\gamma_p = 0.6$ (e) $\gamma_p = 0.8$ and (f) $\gamma_p = 1.0$ for different Darcy numbers for Darcy model.

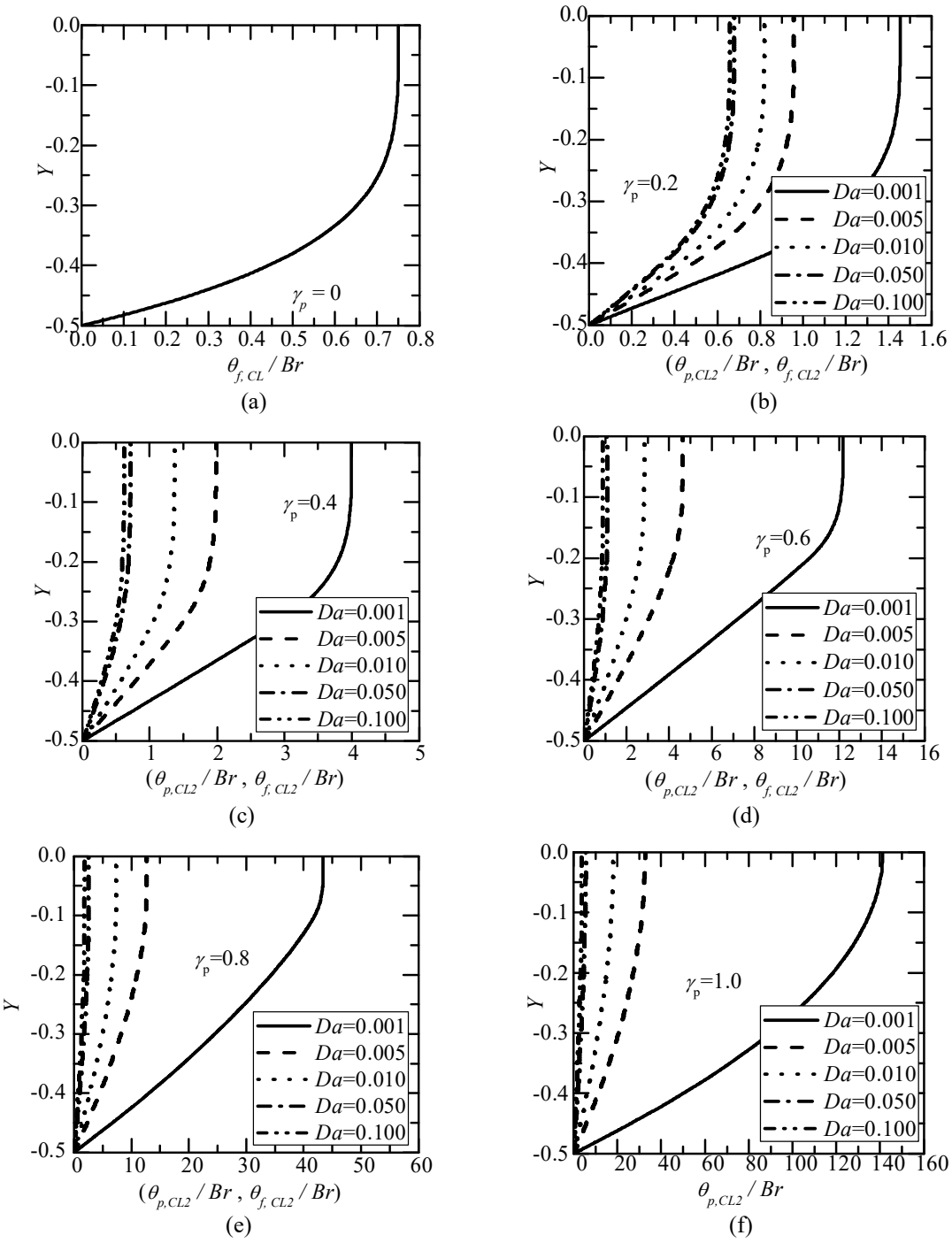

Fig. 4.8: Variation of limiting temperature profiles for (a) $\gamma_p = 0$ (b) $\gamma_p = 0.2$ (c) $\gamma_p = 0.4$ (d) $\gamma_p = 0.6$ (e) $\gamma_p = 0.8$ and (f) $\gamma_p = 1.0$ for different Darcy numbers for form drag model.

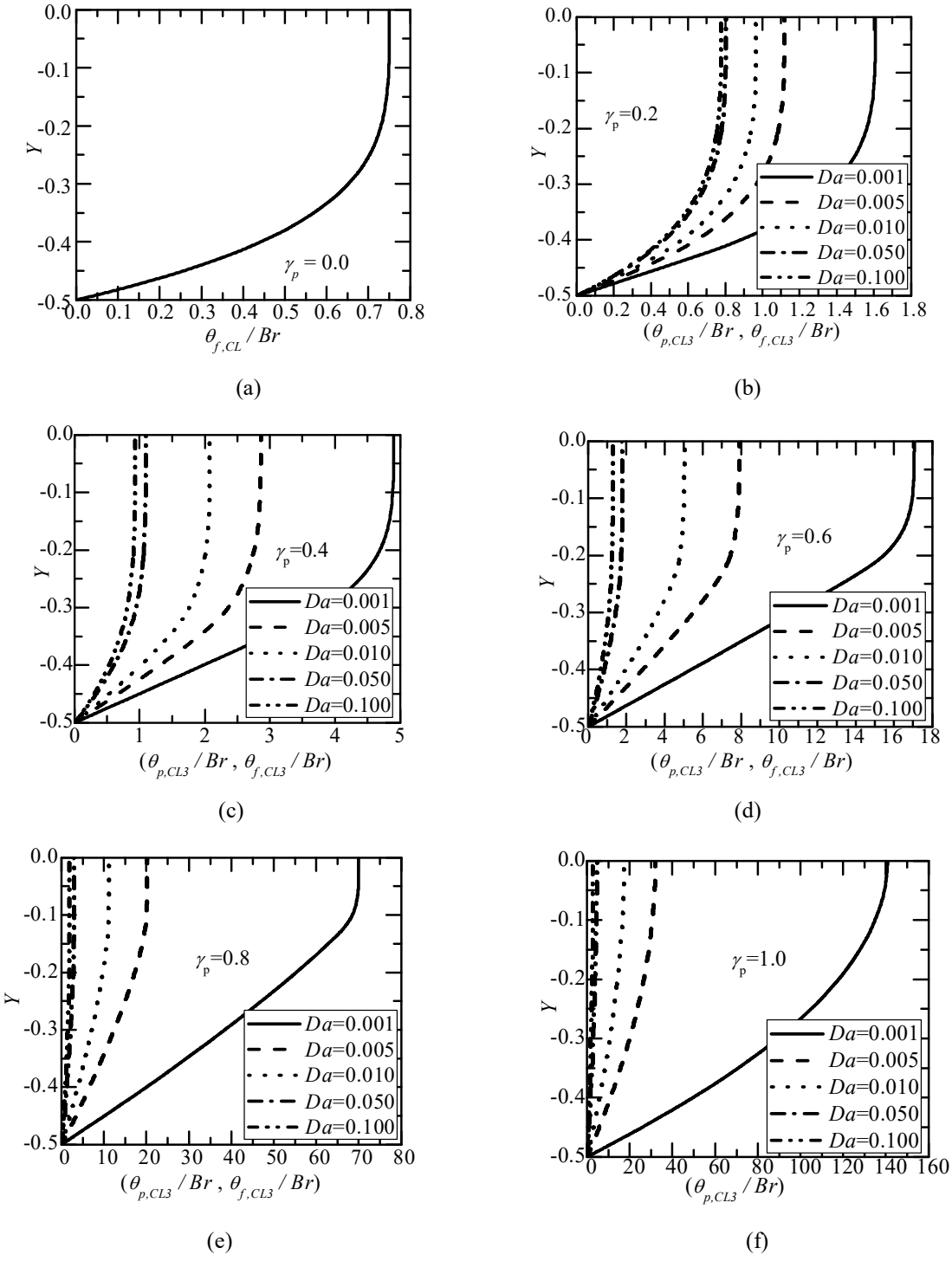

Fig. 4.9: Variation of limiting temperature profiles for (a) $\gamma_p = 0$ (b) $\gamma_p = 0.2$ (c) $\gamma_p = 0.4$ (d) $\gamma_p = 0.6$ (e) $\gamma_p = 0.8$ and (f) $\gamma_p = 1.0$ for different Darcy numbers for the clear fluid compatible model.

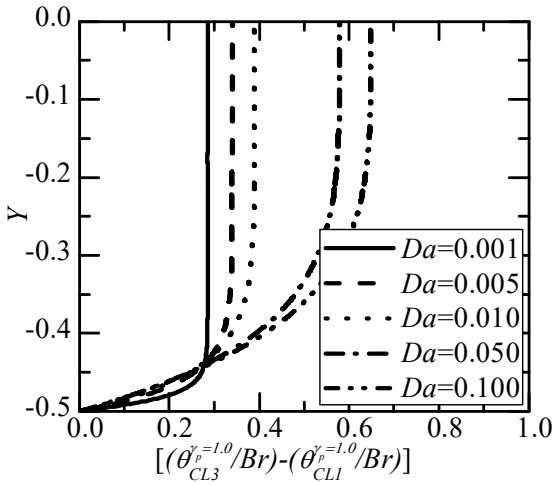

Fig. 4.10: Variation of $[(\theta_{CL3}^{\gamma_p=1.0} / Br) - (\theta_{CL1}^{\gamma_p=1.0} / Br)]$ for different Darcy numbers for γ_p = 1.0.

Bulk mean temperature:

θ_{CL}^* varies linearly with *Br*, since θ_{CL}^* is defined in terms of θ_{CL}. Variation of θ_{CL1}^* / Br, θ_{CL2}^* / Br and θ_{CL3}^* / Br with porous fraction, γ_p for different Darcy numbers is shown in Figs. 4.11(a), 4.11(b) and 4.11(c) for the Darcy model, form drag model and the clear fluid compatible model respectively. As porous fraction, γ_p increases θ_{CL}^* / Br increases for all Darcy numbers for both the models. As Darcy number increases θ_{CL}^* / Br decreases with porous fraction for both the models. For higher Darcy number (say *Da* =1.0), θ_{CL}^* / Br is almost constant with porous fraction.

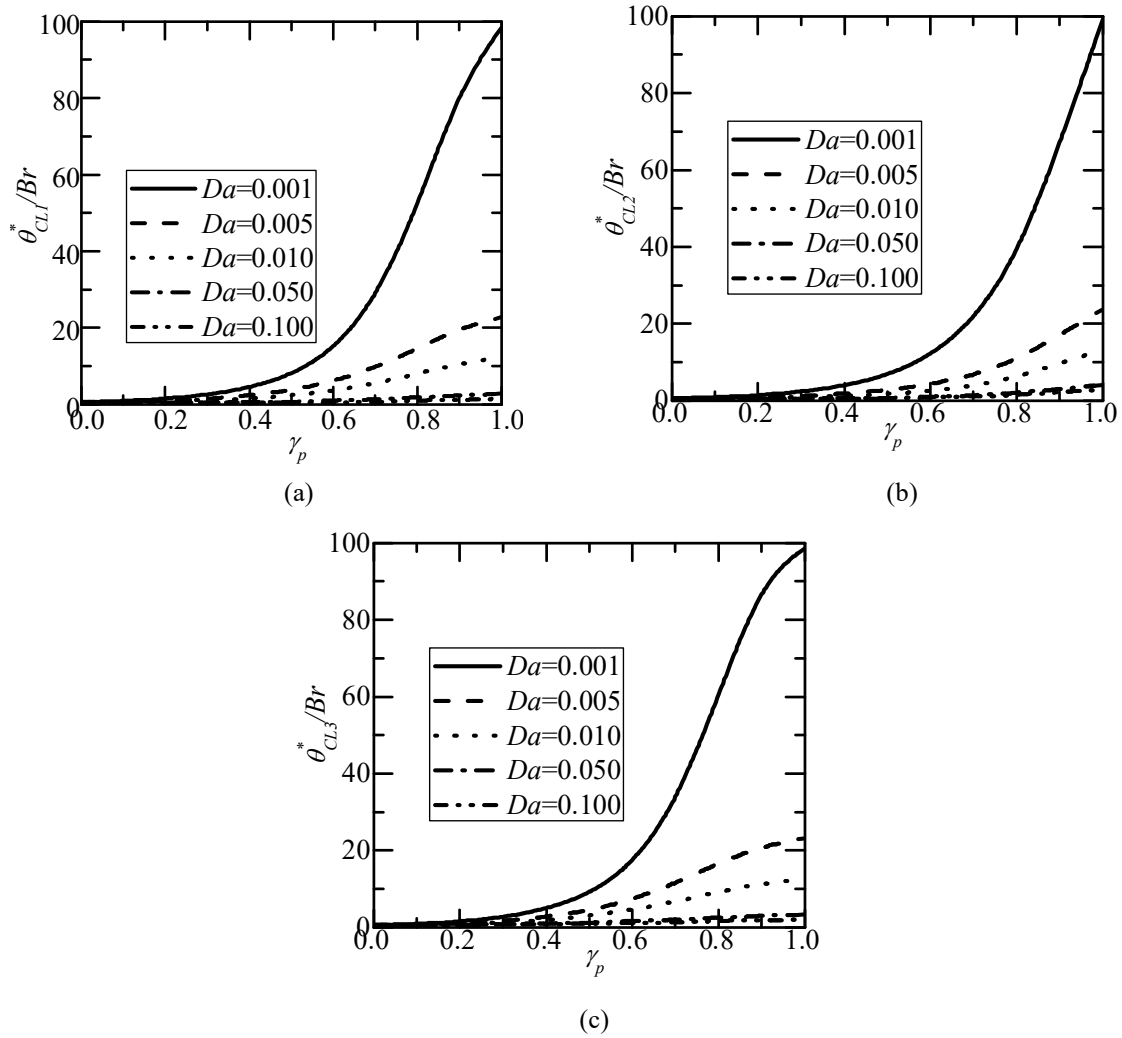

Fig. 4.11: Variation of (a) θ^*_{CL1} / Br {the Darcy model } (b) θ^*_{CL2} / Br {the form drag model} (c) θ^*_{CL3} / Br {clear fluid compatible model}with porous fraction, γ_p for different Darcy numbers.

4.4.2.3 Limiting Nusselt Numbers

Limiting Nusselt numbers $Nu_{p,CL1}$, $Nu_{p,CL2}$ and $Nu_{p,CL3}$ for the three models, {Eq. (4.63), (4.64) and Eq. (4.65)} are independent of the Brinkman number. Variations of limiting Nusselt number with porous fraction, γ_p for the two dissipation models are shown in Figs. 4.12(a), 4.12(b) and 4.12(c) for different Darcy numbers, *Da* = 0.001, 0.005, 0.01, 0.05 and 0.1. From Eqs. (4.63), (4.64) and (4.65), the limiting Nusselt numbers for three

models are independent of *Br*, for all $Br \neq 0$, a feature widely reported in the literature for clear fluid flow channels, by Barletta [4]. From Figs. 4.12(a), 4.12(b) and 4.12(c), $Nu_{p,CL1}$, $Nu_{p,CL2}$ and $Nu_{p,CL3}$ decrease up to a certain porous fraction and then increase for all Darcy numbers. This may due to the fluid region being low compared to the porous region. From Figs. 4.12(a) and 4.12(b) , as Darcy number increases, $Nu_{p,CL1}$ and $Nu_{p,CL2}$ increases up to certain porous fraction then decreases with porous fraction, γ_p. From Fig. 4.12(c), as the Darcy number increases $Nu_{p,CL3}$ increases up to a certain porous fraction then declines with porous fraction, γ_p. It is true that for small Darcy numbers(say, $Da <$ 0.01), $Nu_{p,CL3}$ always increases with porous fraction for higher Darcy numbers(say, $Da \geq 0.01$). From this it may be concluded that as Darcy number increases, porous region starts to behave like a clear fluid region for clear fluid compatible model but it is not true in the case of Darcy model and form drag model. For small Darcy number, say $Da = 0.001$, the difference between these three models in limiting Nusselt number is negligible, but for larger Darcy number, say $Da = 0.05$ the difference becomes significant{ Nield, Kuznetsov and Xioang [58] }. From, Fig. 4.12, it is a foregone conclusion that the limiting Nusselt number differs significantly and even in qualitative behavior for the two dissipation models. Also, these values differ significantly from 17.5 { Ramjee and Satyamurty [182] and Barletta [4] }. Further, it is clear from Figs. 4.12(a), 4.12(b) and 4.12(c) that the values of $Nu_{p,CL}$ at $\gamma_p = 0$ are independent of the dissipation models; the dissipation function is unique.

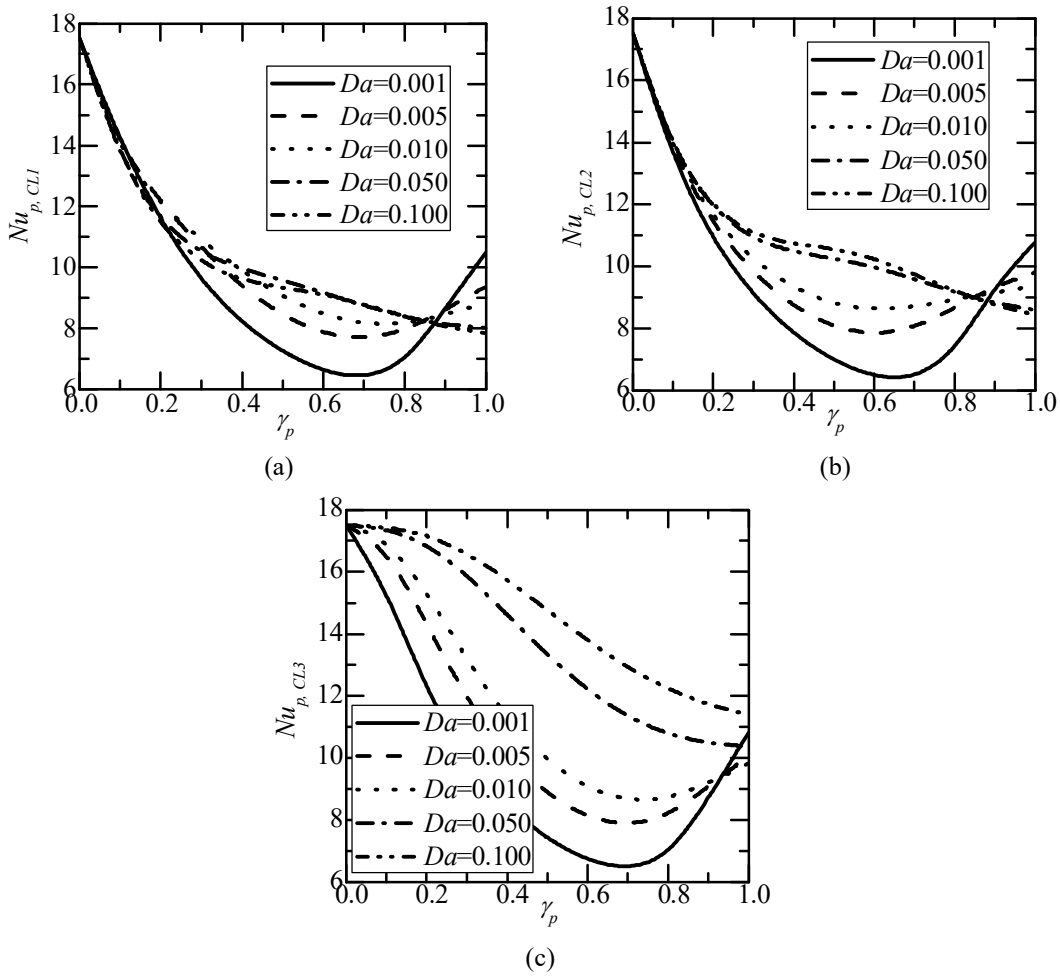

Fig. 4.12: Variation of (a) $Nu_{p,CL1}$ {the Darcy model } (b) $Nu_{p,CL2}$ {form drag model (c) $Nu_{p,CL3}$ {clear fluid compatible model} with porous fraction, γ_p for different Darcy numbers.

Net change in the Nusselt number:

The net change, ΔNu for the three dissipation models is defined, in comparison to the fully developed clear fluid channel value as,

Darcy model:

$$\Delta Nu_1 = 2\left[Nu_{p,CL1} - \left(\frac{35}{2}\right)\right] \tag{4.79}$$

Form drag model:

$$\Delta Nu_2 = 2\left[Nu_{p,CL2} - \left(\frac{35}{2}\right)\right] \tag{4.80}$$

Clear fluid compatible model:

$$\Delta Nu_3 = 2\left[Nu_{p,CL3} - \left(\frac{35}{2}\right)\right] \tag{4.81}$$

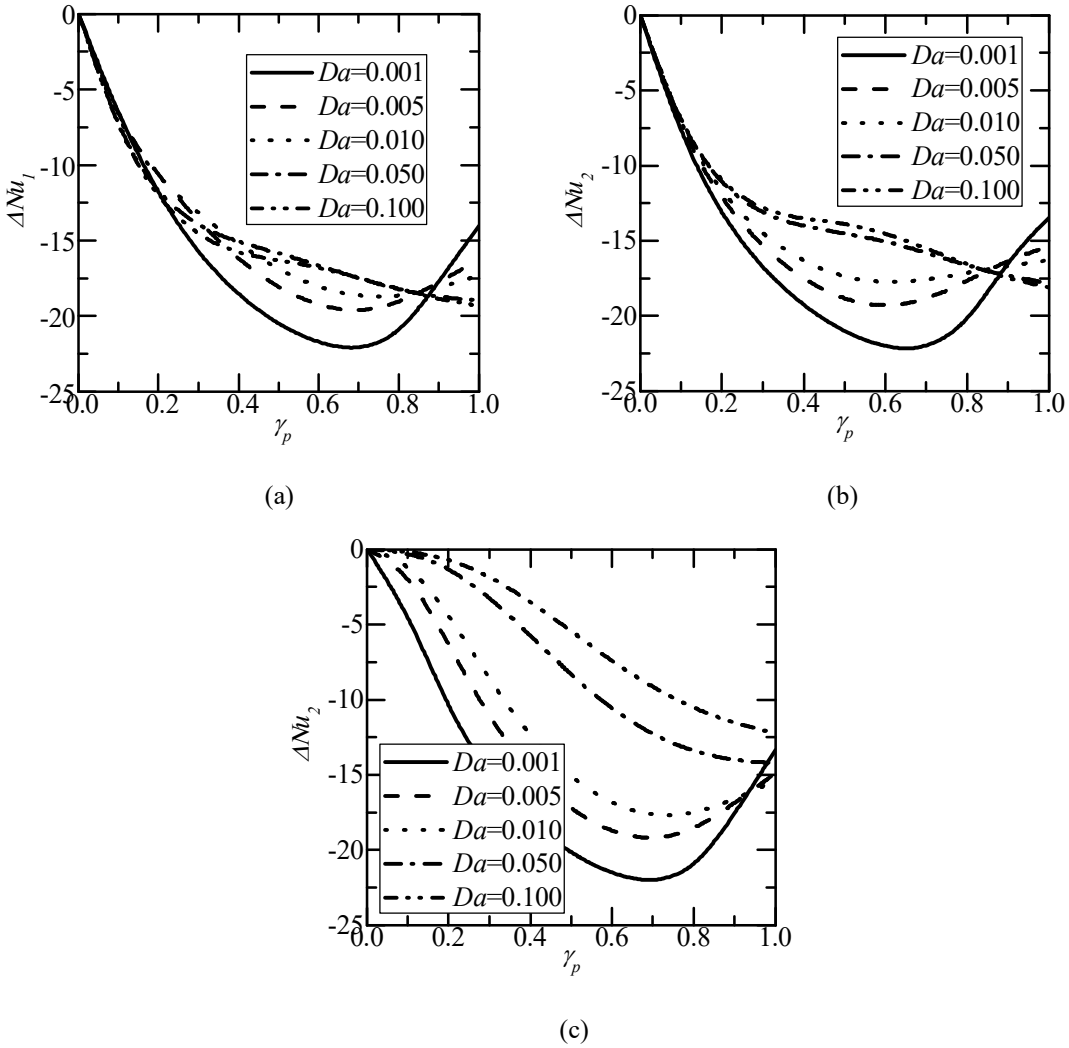

Fig. 4.13: Variation of (a) ΔNu_1 {the Darcy model } (b) ΔNu_2 {form drag model}(c) ΔNu_3 {clear fluid compatible model} with porous fraction, γ_p for different Darcy numbers.

Variation of (a) ΔNu_1 {the Darcy model}(b) ΔNu_2 {form drag model} (c) ΔNu_3 {clear fluid compatible model} with porous fraction, γ_p for different Darcy numbers, Da = 0.001, 0.005, 0.01, 0.05 and 0.1 is shown in Figs. 4.13(a), 4.13(b) and 4.13(c). Enhancement in the Nusselt number when porous material of thickness l_p is attached to both the walls of the channel, is lower than for the channel fully filled with a porous material, when dissipation is included.

4.5 Conclusions

Enhancement in the fully developed Nusselt number for a parallel plate channel flow subjected to (i) constant wall heat flux and (ii) constant wall temperature with porous inserts distributed equally at the two walls of the channel for the three dissipation models, has been studied. Three dissipations models, namely, the Darcy model due to Bejan[49], form drag mode due to Nield [140] and the clear fluid compatible model due to Al-Hadhrami, Elliott and Ingham [135 and 136] are used in the conservation of thermal energy equation. Using the fully developed velocity profiles, as obtained in Chapter 2, § 2.3, the limiting temperature profile and the limiting Nusselt number at the conduction limit have been obtained for porous fraction $0 \le \gamma_p \le 1.0$. The viscous dissipation is characterized by Brinkman number. Both the wall heating and wall cooling cases can be examined from the given plots for all values of Brinkman numbers.

Case (i): constant wall heat flux

Limiting temperature profile and limiting Nusselt number plots are given and are depend on the Brinkman number. The maximum in the value of Nusselt number and net change

in the Nusselt number occurs only at $\gamma_p = 1.0$. For small Darcy numbers, the difference between these models in limiting temperatures and limiting Nusselt numbers is negligible, but for larger Darcy number, the difference is significant. $Br\ Nu_{1,2}$ attains minimum value at certain porous fraction, $\gamma_p \approx 0.4$ for higher *Da*, whereas $Br\ Nu_3$ is always increases as porous fraction increases for all Darcy numbers. Hence heat transfer enhancement is better in clear fluid compatible model compared with Darcy and form drag model.

Case (i): constant wall temperature

It has been found that the non-dimensional temperature and the bulk mean temperature when viscous dissipation is included are linearly proportional to Brinkman number at the conduction limit.

Nusselt numbers in the conduction limit have been found to be independent of the Brinkman number, a feature reported for clear fluid channels, see, Barletta [4]. The three models that describe dissipation yield comparable to Nusselt number values when *Da* is small (say $Da < 0.01$), for the channel partially filled with a porous material also. This feature has been reported by Nield, Kuznetsov and Xioang [58], for channels fully filled with a porous material. The Nusselt number in the conduction limit monotonically increases as *Da* increases for three models up to certain porous fraction. In Darcy model, and form drag model, Nusselt number becomes minimum at higher Darcy number when $\gamma_p = 1.0$, whereas, for the clear fluid compatible model, Nusselt number displays a minimum at $Da \approx 0.015$ when $\gamma_p = 1.0$.

Chapter 5

Effect of Heat Transfer in the Thermally Developing Region of the Channel Partially Filled with a Porous Medium: Constant Wall Heat Flux

5.1 Introduction

In recent times, several authors have studied forced convection in the porous medium and channel partially filled with a porous medium and different conditions, but aspects such as bulk mean temperature and wall temperature as a function of axial distance have not been addressed in any of these investigations. Fully developed forced convection in a parallel plate channel with a centered porous layer was studied by Cekmer et al. [109]. Bhargavi and Satyamurty [108] studied optimum porous insert configurations for enhanced heat transfer in channels. However, the problem of a thermally developing region in a channel partially filled with a porous material and without using the boundary layer approximation has not received enough attention. Since many of the researchers have not discussed about the wall temperature which is unknown temperature profiles for an excess of wall temperature for different porous fractions and fully developed condition in items of the wall temperature when channel walls are subjected to constant wall heat flux.

In the studies reported in the present chapter, it is assumed that the velocity field is fully developed while the temperature field is developing in the channel partially filled

with the porous medium. The walls of the channel are subjected to constant heat flux. The objective of the present chapter is to examine the existence of optimal porous fraction and its dependence on the axial location. The other parameters, the Darcy number and the porous fraction are common to thermal and flow fields. Analytical expressions for momentum equations are available in Chapter 2, § 2.3. Numerical solutions using finite difference successive accelerated replacement (SAR) scheme (Ramjee and Satyamurty [15] and Satyamurty and Bhargavi [158]) have been obtained for energy equations in both the regions. The effects of important relevant parameters on temperature, bulk mean temperature and Nusselt number have been studied.

5.2 Mathematical Formulation

The physical model and the coordinate system, that of a channel formed by two parallel plates, H distance apart, is shown in Fig. 5.1. Let x be the axial distance and y be normal to the flow direction measured from the center of the channel. As per the coordinate system, the plates are at $y = \pm H/2$. The total thickness of a porous medium, adjacent to the plates at $y = \pm H/2$, is l_p. It is assumed that the flow field is fully developed, while the thermal field is developing while the axial conduction is negligible. The fluid enters the channel with a uniform temperature of T_e. The parallel plates are subjected to a constant heat flux q. The problem has been studied assuming steady, laminar, incompressible flow of a Newtonian fluid. The porous and fluid matrix are in local thermal equilibrium. The porous material is homogeneous and isotropic. Further, it is assumed that all the thermo-physical properties are constant. The flow in the fluid region

is assumed to be governed by Poiseuille description and in the porous region, by Darcy-Brinkman equation.

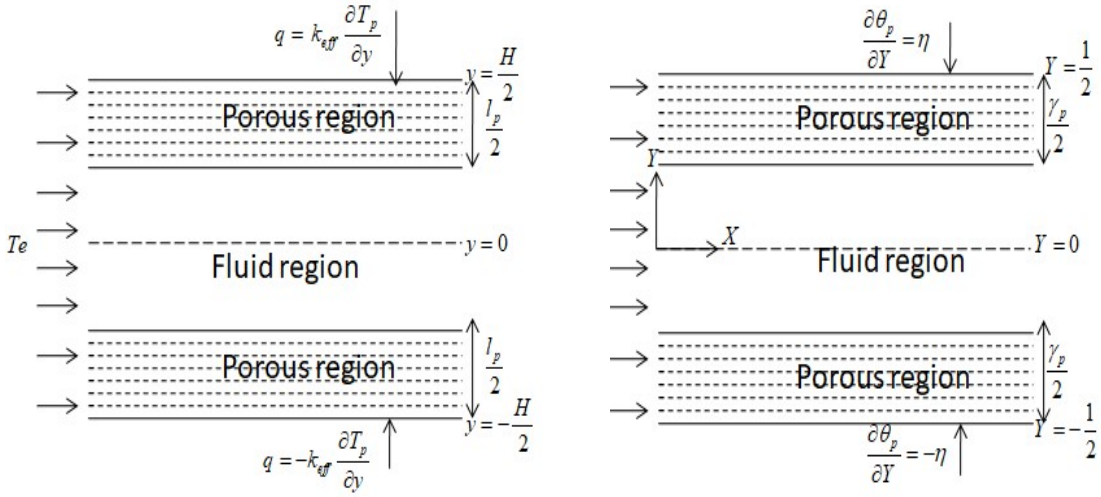

(a) Dimensional (b) Non Dimensional

Fig. 5.1: Physical Model and Coordinate System.

Generalized Governing Equations

Fluid Region:

Momentum Equation:

$$\mu_f \frac{d^2 u_f}{dy^2} = \frac{dp}{dx} \tag{5.1}$$

In Eq. (5.1), p is the pressure, μ_f is the dynamic viscosity and u_f is the velocity in the fluid region.

Conservation of Thermal Energy Equation:

$$\rho C_p u_f \frac{\partial T_f}{\partial x} = k_f \left(F_1 \frac{\partial^2 T_f}{\partial x^2} + \frac{\partial^2 T_f}{\partial y^2} \right) + F_2 \mu_f \left(\frac{du_f}{dy} \right)^2 \tag{5.2}$$

In Eq. (5.2), T_f is the temperature in the fluid region ρ, C_p and k_f are the density, the specific heat and the thermal conductivity of the fluid respectively.

Porous Region:

Momentum Equation:

$$\mu_{eff}\frac{d^2u_p}{dy^2}-\frac{\mu_f}{K}u_p=\frac{dp}{dx} \tag{5.3}$$

In Eq. (5.3), u_p is the velocity in the porous region, K is the permeability of the porous medium, μ_{eff} is the effective viscosity.

Conservation of Thermal Energy Equation:

$$\rho C_p u_p\frac{\partial T_p}{\partial x}=k_{eff}\left(F_1\frac{\partial^2 T_p}{\partial x^2}+\frac{\partial^2 T_p}{\partial y^2}\right)+F_2\Phi_i \tag{5.4}$$

In Eq. (5.2) and Eq. (5.4), F_1 is a constant associated with the axial conduction term and F_2 is a constant associated with the viscous dissipation. In Eq. (5.4), Φ_i is dissipation model, for i = 1, the Darcy model due to Bejan [49], for i = 2, clear fluid compatible model due to Al-Hadhrami et al. [135 and 136] given by,

Darcy model:

$$\Phi_1=\frac{\mu_f}{K}u_p{}^2 \tag{5.5}$$

Clear fluid compatible model:

$$\Phi_2=\frac{\mu_f}{K}u_p{}^2+\mu_f\left(\frac{du_p}{dy}\right)^2 \tag{5.6}$$

In Eq. (5.4), T_p is the temperature in the porous region and k_{eff} is the effective thermal conductivity of the porous medium. k_{eff} can be calculated from Catton [21] as,

$$k_{eff}=(1-\varphi)\,k_s+\varphi\,k_f \tag{5.7}$$

In Eq. (5.7), φ is the porosity and k_s is the thermal conductivity of the solid in the porous matrix. Eqs. (5.1) and (5.2), applicable for the fluid region and Eqs. (5.3) and (5.4) for the porous region.

In the present Chapter, the effects of axial conduction (F_1) and the viscous dissipation (F_2) are neglected. i.e., $F_1 = 0$ and $F_2 = 0$. Then the governing Eq. (5.2) and Eq. (5.4) in fluid and porous regions respectively, become,

Conservation of thermal energy in fluid region:

$$u_f \frac{\partial T_f}{\partial x} = \frac{k_f}{\rho C_p}\left(\frac{\partial^2 T_f}{\partial y^2}\right) \tag{5.8}$$

Conservation of thermal energy in porous region:

$$u_p \frac{\partial T_p}{\partial x} = \frac{k_{eff}}{\rho C_p}\left(\frac{\partial^2 T_p}{\partial y^2}\right) \tag{5.9}$$

Boundary and Interfacial Conditions

$$T_p = T_e \quad \text{at} \quad x = 0\ , \quad -\frac{H}{2} \le y \le -\frac{H}{2} + \frac{l_p}{2} \tag{5.10}$$

$$T_f = T_e \quad \text{at} \quad x = 0\ , \quad -\frac{H}{2} + \frac{l_p}{2} \le y \le 0 \tag{5.11}$$

$$u_p = 0\ , \quad -k_{eff}\frac{\partial T_p}{\partial y} = q \quad \text{at} \quad y = -H/2 \tag{5.12}$$

$$u_f = u_p = u_i\ , \quad \mu_{eff}\frac{du_p}{dy} = \mu_f \frac{du_f}{dy} \quad \text{at interface} \quad y = -\frac{H}{2} + \frac{l_p}{2} \tag{5.13}$$

$$T_f = T_p = T_i\ , \quad k_f\left(\partial T_f / dy\right) = k_{eff}\left(\partial T_p / dy\right) \quad \text{at interface} \quad y = -\frac{H}{2} + \frac{l_p}{2} \tag{5.14}$$

$$\frac{du_f}{dy}=0,\ \frac{\partial T_f}{\partial y}=0 \quad \text{at} \quad y=0 \quad \{\text{Symmetry boundary conditions}\} \tag{5.15}$$

Non-dimensionalization

The governing equations are rendered non-dimensional by introducing the following non-dimensional variables.

$$\left.\begin{aligned} &X=x/H,\ Y=y/H,\ U_f=u_f/u_{ref},\ U_i=u_i/u_{ref},\ U_p=u_p/u_{ref},\ P=p/\rho\, u_{ref}^2, \\ &\theta_f=(T_f-T_e)/(qH/k_f),\theta_p=(T_p-T_e)/(qH/k_f) \end{aligned}\right\} \tag{5.16}$$

In Eq. (5.16), X and Y are non-dimensional coordinates. U and P are the non-dimensional velocity and pressure. The subscripts f and p refer to fluid and porous regions. $\theta\{\theta_f$ in the fluid region and θ_p in the porous region$\}$, is the non-dimensional temperature. u_{ref} is the average velocity through the channel. u_{ref} is related to u_p and u_f by,

$$\frac{2}{H}\left[\int_{-H/2}^{-\frac{H}{2}+\frac{l_p}{2}} u_p dy+\int_{-\frac{H}{2}+\frac{l_p}{2}}^{0} u_f dy\right]=u_{ref} \tag{5.17}$$

The non-dimensional porous layer thickness γ_p, which shall be referred to as porous fraction is defined by,

$$\gamma_p=l_p/H \tag{5.18}$$

when the channel walls are subjected to constant heat flux, Peclet number can be absorbed by defining

$$X^*=X/Pe \tag{5.19}$$

On introducing the non-dimensional variables given by Eq. (5.16), the governing equations for conservation of momentum and energy applicable in the fluid {Eqs. (5.1) and (5.8)} and porous {Eqs. (5.3) and (5.9) } regions in non-dimensional form become,

Fluid Region

$$\frac{d^2U_f}{dY^2} = Re\ \frac{dP}{dX} \tag{5.20}$$

$$U_f \frac{\partial \theta_f}{\partial X^*} = \frac{\partial^2 \theta_f}{\partial Y^2} \tag{5.21}$$

In Eq. (5.20), *Re*, the Reynolds number and in Eq. (5.21), *Pe*, the Peclet number are defined by,

$$Re = \rho u_{ref} H / \mu_f \ , Pe = u_{ref} H / \alpha_f \tag{5.22}$$

Porous Region

$$\frac{d^2U_p}{dY^2} - \frac{\varepsilon}{Da} U_p = \varepsilon\ Re \frac{dP}{dX} \tag{5.23}$$

$$U_p \frac{\partial \theta_p}{\partial X^*} = \frac{1}{\eta} \frac{\partial^2 \theta_p}{\partial Y^2} \tag{5.24}$$

In Eq. (5.23), *Da*, the Darcy number is defined by,

$$Da = K / H^2 \tag{5.25}$$

In Eqs. (5.23) and (5.24) , ε and η are defined by,

$$\varepsilon = \mu_f / \mu_{eff} \ , \ \eta = k_f / k_{eff} \tag{5.26}$$

Non-dimensional Boundary Conditions

The boundary and interfacial conditions given by, Eqs. (5.10) to (5.15) take the following non-dimensional form (using Eq. (5.16))

$$\theta_p(0, Y) = 0 \quad \text{for} \ -\frac{1}{2} \le Y \le -\frac{1}{2} + \frac{\gamma_p}{2} \tag{5.27}$$

$$\theta_f(0, Y) = 0 \quad \text{for} \ -\frac{1}{2} + \frac{\gamma_p}{2} \le Y \le 0 \tag{5.28}$$

$$\frac{dU_f}{dY}=0,\ \frac{\partial\theta_f}{\partial Y}=0 \quad \text{at} \quad Y=0 \tag{5.29}$$

$$U_f=U_p=U_i,\ \ \frac{dU_f}{dY}=\frac{1}{\varepsilon}\frac{dU_p}{dY} \quad \text{at the interface} \quad Y=-\frac{1}{2}+\frac{\gamma_p}{2} \tag{5.30}$$

$$\theta_f=\theta_p=\theta_i,\ \ \frac{\partial\theta_f}{\partial Y}=\frac{1}{\eta}\frac{\partial\theta_p}{\partial Y} \quad \text{at the interface} \quad Y=-\frac{1}{2}+\frac{\gamma_p}{2} \tag{5.31}$$

$$U_p=0,\ \ \frac{\partial\theta_p}{\partial Y}=-\eta \quad \text{at} \quad Y=-1/2 \tag{5.32}$$

5. 3 Expressions for velocity

5.3.1 Non Dimensional Velocity Profiles

Fluid Region:

On solving Eq. (5.20) along with the boundary conditions given in Eq. (5.29) and Eq. (5.30), velocity in the fluid region is obtained as

$$U_f[Y]=\frac{1}{8}\left\{8U_i+\left[4Y^2-\left(\gamma_p-1\right)^2\right]P_{gr}\right\} \tag{5.33}$$

Porous Region:

Similarly, on solving Eq. (5.23) along with the boundary conditions given in Eq. (5.30) and Eq. (5.32), velocity in the porous region is obtained as

$$U_p[Y]=\frac{e^{\frac{-Y\sqrt{\varepsilon}}{\sqrt{Da}}}\left[e^{\frac{(1+2Y)\sqrt{\varepsilon}}{2\sqrt{Da}}}-1\right]\left\{U_i e^{\frac{\gamma_p\sqrt{\varepsilon}}{2\sqrt{Da}}}\left[e^{\frac{-\sqrt{\varepsilon}}{2\sqrt{Da}}}+e^{\frac{Y\sqrt{\varepsilon}}{\sqrt{Da}}}\right]-Da\left[\begin{matrix}e^{\frac{Y\sqrt{\varepsilon}}{\sqrt{Da}}}\left(1-e^{\frac{\gamma_p\sqrt{\varepsilon}}{2\sqrt{Da}}}\right)\\ -e^{\frac{-\sqrt{\varepsilon}}{2\sqrt{Da}}}\left(e^{\frac{\gamma_p\sqrt{\varepsilon}}{2\sqrt{Da}}}-e^{\frac{\gamma_p\sqrt{\varepsilon}}{\sqrt{Da}}}\right)\end{matrix}\right]P_{gr}\right\}}{e^{\frac{\gamma_p\sqrt{\varepsilon}}{\sqrt{Da}}}-1} \tag{5.34}$$

where

$$U_i = -\sqrt{Da}\left[e^{\frac{\gamma_p\sqrt{\varepsilon}}{2\sqrt{Da}}}-1\right]\left\{2\sqrt{Da}\left[e^{\frac{\gamma_p\sqrt{\varepsilon}}{2\sqrt{Da}}}-1\right]-\left[1+e^{\frac{\gamma_p\sqrt{\varepsilon}}{2\sqrt{Da}}}\right]\sqrt{\varepsilon}\left(\gamma_p-1\right)\right\}P_{gr} \tag{5.35}$$

$P_{gr} = Re\dfrac{dp}{dx}$ and obtained as using non dimensional form of Eq. (5.17)

$$P_{gr} = \frac{12\left(1+e^{\frac{\gamma_p\sqrt{\varepsilon}}{\sqrt{Da}}}\right)\sqrt{\varepsilon}}{\left\{\begin{array}{l}\left(e^{\frac{\gamma_p\sqrt{\varepsilon}}{\sqrt{Da}}}-1\right)\left(24Da^{3/2}-6\sqrt{Da}\varepsilon\left(\gamma_p-1\right)^2\right)+\left(1+e^{\frac{\gamma_p\sqrt{\varepsilon}}{\sqrt{Da}}}\right)\sqrt{\varepsilon}\left(\gamma_p-1\right)^3\\ +12Da\sqrt{\varepsilon}\left[e^{\frac{\gamma_p\sqrt{\varepsilon}}{\sqrt{Da}}}\left(\gamma_p-2\right)-4e^{\frac{\gamma_p\sqrt{\varepsilon}}{2\sqrt{Da}}}\left(\gamma_p-1\right)+\gamma_p-2\right]\end{array}\right\}} \tag{5.36}$$

5.3.2 Numerical Scheme: Successive Accelerated Replacement (SAR)

Application of the SAR Scheme (Ramjee and Satyamurty [15] and Satyamurty and Bhargavi [158])**:** Let *MD* and *ND* be the number of divisions in *X* and *Y* direction and ΔX^* and ΔY be the width in *X* and *Y* direction respectively. When the terms in energy Eqs. (5.21) and (5.24) are expressed in finite difference form, the errors $\tilde{\theta}_f, \tilde{\theta}_p$ in fluid and porous regions respectively, are given by,

Discretization of the governing equations {Eq. (5.21) and Eq. (5.24)} have been done using uniform grid in the *X* and *Y* directions bring us the equations given below:

$$\tilde{\theta}_f(M,N) = U_f(N)\left[\frac{\theta_f(M,N)-\theta_f(M-1,N)}{\Delta X^*}\right]-\left[\frac{\theta_f(M,N+1)-2\theta_f(M,N)+\theta_f(M,N-1)}{(\Delta Y)^2}\right] \tag{5.37}$$

$$\tilde{\theta}_p(M,N) = \eta\, U_p(N)\left[\frac{\theta_p(M,N)-\theta_p(M-1,N)}{\Delta X^*}\right]-\left[\frac{\theta_p(M,N+1)-2\theta_p(M,N)+\theta_p(M,N-1)}{(\Delta Y)^2}\right] \quad (5.38)$$

where ΔX^* is the uniform grid size in the X-direction, defined by,

$$\Delta X^* = X^*_{fd} / MD \quad (5.39)$$

where X^*_{fd} is the normalized fully developed length.

$$\Delta Y = 1 / ND \quad (5.40)$$

To correct the profile for θ_f and θ_p , the following derivatives become necessary

$$\frac{\partial \tilde{\theta}_f(M,N)}{\partial \theta_f(M,N)} = \frac{U_f(N)}{\Delta X^*} + \frac{2}{(\Delta Y)^2} \quad (5.41)$$

$$\frac{\partial \tilde{\theta}_p(M,N)}{\partial \theta_p(M,N)} = \frac{\eta\, U_p(N)}{\Delta X^*} + \frac{2}{(\Delta Y)^2} \quad (5.42)$$

Discretization of the governing equations {Eq. (5.21) and Eq. (5.24)} using non-uniform grids in the X-direction and uniform grid in the Y direction:

$$\tilde{\theta}_f(M,N) = U_f(N)\left[\frac{\theta_f(M,N)-\theta_f(M-1,N)}{X(M)-X(M-1)}\right]-\left[\frac{\theta_f(M,N+1)-2\theta_f(M,N)+\theta_f(M,N-1)}{(\Delta Y)^2}\right] \quad (5.43)$$

$$\tilde{\theta}_p(M,N) = \eta\, U_p(N)\left[\frac{\theta_p(M,N)-\theta_p(M-1,N)}{X(M)-X(M-1)}\right]-\left[\frac{\theta_p(M,N+1)-2\theta_p(M,N)+\theta_p(M,N-1)}{(\Delta Y)^2}\right] \quad (5.44)$$

To correct the profile for θ_f and θ_p, the following derivatives become necessary

$$\frac{\partial \tilde{\theta}_f(M,N)}{\partial \theta_f(M,N)} = \frac{U_f(N)}{X(M)-X(M-1)} + \frac{2}{(\Delta Y)^2} \tag{5.45}$$

$$\frac{\partial \tilde{\theta}_p(M,N)}{\partial \theta_p(M,N)} = \frac{\eta\, U_p(N)}{X(M)-X(M-1)} + \frac{2}{(\Delta Y)^2} \tag{5.46}$$

Discretised boundary conditions

$$\theta_p(0,N) = 0 \qquad \text{for} \qquad 1 \le N \le \left(\frac{\gamma_p}{2}\right) ND + 1 \tag{5.47}$$

$$\theta_f(0,N) = 0 \qquad \text{for} \qquad \left(\frac{\gamma_p}{2}\right) ND + 1 \le N \le \frac{ND}{2} + 1 \tag{5.48}$$

$$\theta_f(M,N) = \frac{4\theta_f(M,N-1) - \theta_f(M,N-2)}{3} \qquad \text{at} \qquad N = \frac{ND}{2} + 1 \tag{5.49}$$

$$\theta_p(M,N) = \frac{2\eta\,\Delta Y - \theta_p(M,N+2) + 4\theta_p(M,N+1)}{3} \qquad \text{at} \quad N = 1 \tag{5.50}$$

Let *NP* be a grid number corresponding to the interface. It is assumed that the interface coincides with one of the grid planes in the *Y* direction. When large numbers of *ND* are used, the error involved is not likely to be significant even if the interface does not exactly correspond to an integer *NP*. Boundary conditions given by Eq. (5.31) and on θ_f and θ_p in finite difference form become,

$$\theta_f(M,NP) = \theta_p(M,NP) \qquad \text{at} \quad NP = \left(\frac{\gamma_p}{2}\right) ND + 1 \tag{5.51}$$

$$\theta_f(M,NP) = \theta_f(M,NP-1) + \frac{1}{\eta}\left[\theta_p(M,NP+1) - \theta_p(M,NP)\right] \text{at} \quad NP = \left(\frac{\gamma_p}{2}\right) ND + 1 \tag{5.52}$$

5.3.3 Numerical Trial

In order to obtain satisfactory numerical solutions, suitable values for the parameters that yield converged solutions need to be determined. The parameters are, the acceleration factor, ω, error tolerance limit, ε_t, and the number of divisions *MD* and *ND* in X^* and Y directions.

Numerical trials have been made employing Eqs. (5.21) and (5.24), along with the boundary conditions {Eqs. (5.27) to (5.32)}. Eqs. (5.21) and (5.24), are parabolic and the solutions can be obtained with ease. The finite difference expressions, which are needed to apply in SAR (Ramjee and Satyamurty [15] and Satyamurty and Bhargavi [158]) scheme, are given by Eqs. (5.37) and (5.38) have been used for fixed $Da = 0.005$, and a porous fraction of $\gamma_p = 0.4$. Numerical trials have been conducted with $0.5 \le \omega \le 1.5$, $\varepsilon_t = 10^{-4}, 10^{-5}, 10^{-6}$ and 10^{-7}, $1000 \le MD \le 8000$ and $60 \le ND \le 100$.

Generation of the non uniform grids(given in Bhargavi[186])

Uniform grids are generated by using the formula

$$X(i) = (i-1)\Delta X^* \tag{5.53}$$

Non uniform grids are generated by increasing the axial distance following a geometric progression. Let ΔX_M^* be the increase in geometric progression with a common ratio of (1+*r*). ΔX_M^* is related to the common ratio and the first term of the geometric progression, ΔX_1^* by,

$$\Delta X_M^* = \left(1+r\right)^{(M-1)} \Delta X_1^* \tag{5.54}$$

Let ΔX_1^* be the first non-uniform grid width defined by,

$$\Delta X_1^* = c\ \Delta X^* \tag{5.55}$$

where c is a constant less than unity and ΔX^* is uniform cell width.

Common ratio of (1+r). can be evaluated by,

$$X_{fd}^* = \Delta X_1^* \left(\frac{(1+r)^{MD} - 1}{r} \right) \tag{5.56}$$

Number of Grids, Uniform Spacing

Numerical trials have been made to determine the suitable number of grids in X^* and Y directions for fixed $\varepsilon_t = 10^{-5}$. MD and ND have been varied between $1000 \leq MD \leq 8000$ and $60 \leq ND \leq 100$. Values of Nu_{px} at different values of X^* for ND = 60, 70, 80, 90 and 100 with MD = 1000, 2000, 4000, 6000 and 8000 are given in Table 5.1. The value of Nu_{px} = 7.0065 with ND = 90 obtained in the present numerical trails for grid independence test, shown in Table 5.1 at X^* = 0.4, agree well with the corresponding fully developed values of 6.9962 obtained analytically in chapter 2. It appears that ND = 90 grids is suitable. If uniform grids are employed, ND = 90 and MD = 8000 appear to yield satisfactory local Nusselt number values that do not change significantly with further increase in ND and MD.

Table 5.1: Grid Independence Test, Uniform Mesh: Nu_{px} at Different X^* for $\gamma_p = 0.4$, $Da = 0.005$, $\varepsilon_t = 10^{-5}$ and $\omega = 0.8$(NI = No. of Iterations).

ND	MD	X^*									NI
		0.0016	**0.0050**	**0.0100**	**0.0300**	**0.1000**	**0.150**	**0.2000**	**0.3000**	**0.4000**	
60	1000	15.9547	10.9527	9.2407	7.5155	7.0056	6.9975	6.9968	6.9962	6.9960	4756
	2000	15.7035	11.0186	9.2177	7.5096	7.0054	6.9975	6.9967	6.9962	6.9961	4941
	4000	15.5801	10.9904	9.2062	7.5066	7.0052	6.9975	6.9967	6.9961	6.9959	5311
	6000	15.5394	10.9810	9.2024	7.5057	7.0052	6.9975	6.9967	6.9961	6.9961	5661
	8000	15.5191	10.9764	9.2005	7.5052	7.0052	6.9975	6.9967	6.9961	6.9961	5974
70	1000	15.9005	10.9376	9.2335	7.5136	7.0053	7.0051	7.0052	7.0050	7.0007	6167
	2000	15.6521	11.0032	9.2105	7.5077	7.0050	7.0049	7.0043	7.0039	7.0005	6350
	4000	15.5301	10.9752	9.1991	7.5048	7.0049	7.0044	7.0040	7.0025	7.0004	6722
	6000	15.4898	10.9659	9.1953	7.5038	7.0049	7.0045	7.0043	7.0022	7.0002	7085
	8000	15.4697	10.9612	9.1934	7.5033	7.0048	7.0041	7.0039	7.0038	7.0007	7429
80	1000	15.8641	10.9276	9.2287	7.5124	7.0051	7.0051	7.0050	7.0048	7.0004	7747
	2000	15.6177	10.9929	9.2058	7.5065	7.0048	7.0045	7.0041	7.0043	7.0024	7927
	4000	15.4966	10.9650	9.1944	7.5035	7.0047	7.0042	7.0042	7.0039	7.0025	8300
	6000	15.4566	10.9558	9.1906	7.5025	7.0047	7.0042	7.0041	7.0038	7.0025	8667
	8000	15.4366	10.9512	9.1887	7.5021	7.0046	7.0046	7.0046	7.0046	7.0025	9025
90	1000	15.8385	10.9205	9.2253	7.5115	7.0050	7.0048	7.0047	7.0046	7.0042	9492
	2000	15.5934	10.9857	9.2025	7.5056	7.0047	7.0046	7.0044	7.0044	7.0040	9669
	4000	15.4730	10.9580	9.1911	7.5027	7.0046	7.0044	7.0044	7.0044	7.0041	10041
	6000	15.4332	10.9487	9.1873	7.5017	7.0045	7.0044	7.0043	7.0040	7.0042	10411
	8000	15.4134	10.9441	9.1854	7.5012	7.0075	7.0070	7.0068	7.0065	7.0065	10774
100	1000	15.8198	10.9154	9.2229	7.5109	7.0049	7.0047	7.0047	7.0046	7.0034	11397
	2000	15.5758	10.9805	9.2001	7.5050	7.0046	7.0040	7.0039	7.0038	7.0036	11571
	4000	15.4559	10.9528	9.1887	7.5020	7.0045	7.0042	7.0040	7.0039	7.0039	11941
	6000	15.4262	10.9436	9.1849	7.5010	7.0044	7.0043	7.0044	7.0044	7.0066	12312
	8000	15.4234	10.9541	9.1954	7.5013	7.0075	7.0070	7.0068	7.0065	7.0065	12679

For a chosen value of c, X^*_{fd} = 0.4 and MD, r can be calculated using Eq. (5.56). X^*_{fd} = 0.4 and MD = 2000, with uniform grid size of ΔX^* = 0.0002 yielded satisfactory solution. If the first non-uniform grid ΔX^*_1 = 0.0002 has been chosen, for X^*_{fd} = 0.4, the constant c values and r values are given in Table 5.2 for MD = 500, 1000 and 2000.

Table 5.2: The constant values of c and r for MD = 500, 1000 and 2000.

c	values of r for MD is		
	500	1000	2000
1/4	0.004691189370	0.002341121189	0.001169445089
1/8	0.006660863418	0.003322638941	0.001658206827
1/16	0.008505441991	0.004240980432	0.002117565251

From, Table 5.2, the value of c chooses as 1/8. Non-uniform grids are generated by using the formula Eq. (5.54).

ΔX^*_M, the grids in geometric progression have been generated as described above. Values of Nu_{px} for γ_p = 0.4 and Da = 0.005 at different X^* are given in Table 5.3. Values of Nu_{px} obtained with 8000 uniform grids also are given in Table 5.3. The values of Nu_{px} at different X^* obtained with non-uniform grids generated in geometric progression with MD = 1000 are very close to the values obtained with 8000 uniform grids. It is concluded that non-uniform grids generated in geometric progression with MD = 1000 are suitable to obtain the accuracy comparable to that obtained with 8000 uniform grids. The reduction in computational time is substantial.

Table 5.3: Comparison of Nu_{px} at Different X^* Values for Uniform and Non-uniform Grids, ND = 90, ε_t = 10^{-5}, Da = 0.005, ω = 0.8 for γ_p = 0.4, using GP.

MD	*Nu*$_{px}$ at different X^* values										*NI*
	CPU Time	**0.0016**	**0.0050**	**0.0100**	**0.0300**	**0.1000**	**0.150**	**0.2000**	**0.3000**	**0.4000**	
500 Non-uniform	0m 51s	15.2924	10.9267	9.1686	7.5001	7.0047	6.9970	6.9965	6.9968	7.0066	11318
1000 Non-Uniform	1m 40s	15.3458	10.9113	9.1738	7.5010	7.0045	6.9970	6.9964	6.9967	7.0065	11250
2000 Non-Uniform	3m 18s	15.3242	10.9310	9.1765	7.4991	7.0045	6.9970	6.9965	6.9967	7.0065	11195
8000 Non-Uniform	11m 10s	15.4134	10.9441	9.1854	7.5012	7.0075	7.0070	7.0068	7.0065	7.0065	12679

Based on the numerical trials conducted, the following values for the parameters have been employed in obtaining numerical solutions presented. a) Acceleration factor $\omega \leq 1$ has been determined as per Eqs. (5.21) and (5.24), b) Error tolerance limit, $\varepsilon_t = 10^{-5}$, c) $X^*_{fd} = 0.4$, d) $MD = 1000$ with ΔX^*_M generated in geometric progression with $c = 1/8$ in Eq. (5.55), e) $ND = 90$ with $\Delta Y = 1/90$.

However, no converged solution could be obtained for $\omega \geq 1.2$. A smaller value of ω may ensure convergence but requires larger number of iterations. Similarly, a larger value of ω may result in an advantage of faster convergence; when the solution converges. The acceleration factor is obtained from,

$$\omega = (\varepsilon_t / \bar{\phi}^k_{M,N})\ \phi^k_{M,N}\ (\partial \bar{\phi}^k_{M,N} / \partial \phi_{M,N}) \tag{5.57}$$

In order to ensure convergence, under relaxation is preferred. As adapted by Dellinger [169] and more recently in [15 and 158], the acceleration factor ω is chosen according to,

$$\omega = \omega, \text{ if } \omega < 1 \text{ and; } \omega = 1 \text{ if } \omega \geq 1 \tag{5.58}$$

This ensures that the correction to a variable is never greater than ε_t (error tolerance limit) times the previous magnitude of the variable.

5.3.4 Local Nusselt Numbers

The heat transfer coefficient h_{px}, at the plate $y = -H/2$ adjacent to the porous medium is defined by

$$-k_{eff}\frac{\partial T_p}{\partial y}\Big|_{y=-\frac{H}{2}} = h_{px}(T_w - T_b) \tag{5.59}$$

Upon non-dimensionalizing (using Eq. (5.16)), The Nusselt number at $Y = -1/2$, Nu_{px} is given by

$$Nu_{px} = \frac{h_{px}(2H)}{k_f} = -\frac{2\left(\partial\theta_p / \partial Y\right)|_{Y=-1/2}}{\eta\left[\theta_w - \theta^*(X)\right]} = \frac{2}{\theta_w - \theta^*(X)} \tag{5.60}$$

5.4 Result and Discussion

It has been assumed that $\varepsilon = \mu_f/\mu_{eff} = 1$, $\eta = k_f/k_{eff} = 1$, $c = 1/8$, $X^*_{fd} = 0.4$ and $MD = 1000$ and $ND = 90$. The channel is referred to as the clear fluid channel here when $\gamma_p = 0$. Similarly, when $\gamma_p = 1.0$, the geometry shall be referred to as channel filled with a porous medium fully. When the porous fraction is $0 < \gamma_p < 1.0$, the channel is referred as a channel partially filled with a porous medium.

5.4.1 Thermal Field: For *Da* = 0.005 and *Da* = 0.050

Non-dimensional temperature profiles for an excess of wall temperature $\theta_w - \theta_p$, $\theta_w - \theta_f$ for porous fractions $\gamma_p = 0$, 0.2, 0.4, 0.6, 0.8 and 1.0 at different values of X^* are shown in Figs. 5.2(a) to 5.2(f) for Da = 0.005 and Figs. 5.3(a) to 5.3(f) for Da = 0.050 respectively. These values of X^* correspond to the entrance region and to near fully developed region. As X^* increases, $\theta_w - \theta_p$, $\theta_w - \theta_f$ increase in both the fluid and porous regions for all porous fractions. If X^* is larger (say, = 0.4) $\theta_w - \theta_p$, $\theta_w - \theta_f$ tend to have fully developed profiles for all porous fractions and Darcy numbers, which are given in chapter 2, § 2.3. From Figs. 5.2(a){for $\gamma_p = 0$} and 5.2(f) {for $\gamma_p = 1.0$} and Figs. 5.3(a){for $\gamma_p = 0$} and 5.3(f) {for $\gamma_p = 1.0$} for large X^* (say = 0.4), $\theta_w - \theta_f$ becomes a fully developed profile, as given in Kays et al. [185] and $\theta_w - \theta_p$ tends to the fully developed profiles given in Nield et al. [57]. As Darcy number increases, the porous region behaves like a clear fluid region for all porous fractions. This fact is recorded in the literature.

5.4.2 Non dimensional bulk mean temperature

Non-dimensional bulk mean temperature excess of wall temperature , $\theta_w - \theta^*$ profiles with X^*, for $\gamma_p = 0$, 0.2, 0.4, 0.6, 0.8 and 1.0 and for different Darcy numbers, Da = 0.001, 0.005, 0.010, 0.050 and 0.100, are shown in Figs. 5.4(a) to 5.4(f). As X^* increases, $\theta_w - \theta^*$ increases for all Darcy numbers. From Figs. 5.4(a) to 5.4(e), as Darcy number increases, $\theta_w - \theta^*$ decreases for all X^* values. This fact is reported in Satyamurty and Bhargavi [158]. From Figs. 5.4(a) and 5.4(f), as Darcy number is large, the porous region behaves like a clear fluid region. This fact features reported in the literature. Comparison between analytical and numerical values of bulk mean temperature in excess of wall temperature $\theta_w - \theta^*$ is shown in Table 5.4 for all porous fractions and for Da = 0.005 and 0.050. From Table 5.4, it is seen that the results are in good agreement, with the available literature for $\gamma_p = 0$ and $\gamma_p = 1.0$ (Satyamurty and Bhargavi [158] and chapter 2, § 2.5).

Table 5.4: Comparison of Numerical Values of $\theta_w - \theta^*$ with Analytical Values (Chapter 2) of $\theta_w - \theta^*$ at Fully Developed Length X^* = 0.4.

γ_p	Da = 0.005		Da = 0.050	
	Numerical value	Analytical value	Numerical value	Analytical value
0.0	0.2425	0.2428	0.2425	0.2428
0.2	0.2562	0.2566	0.2444	0.2447
0.4	0.2853	0.2858	0.2498	0.2501
0.6	0.2993	0.2999	0.2519	0.2522
0.8	0.2632	0.2636	0.2451	0.2454
1.0	0.2039	0.2037	0.2325	0.2326

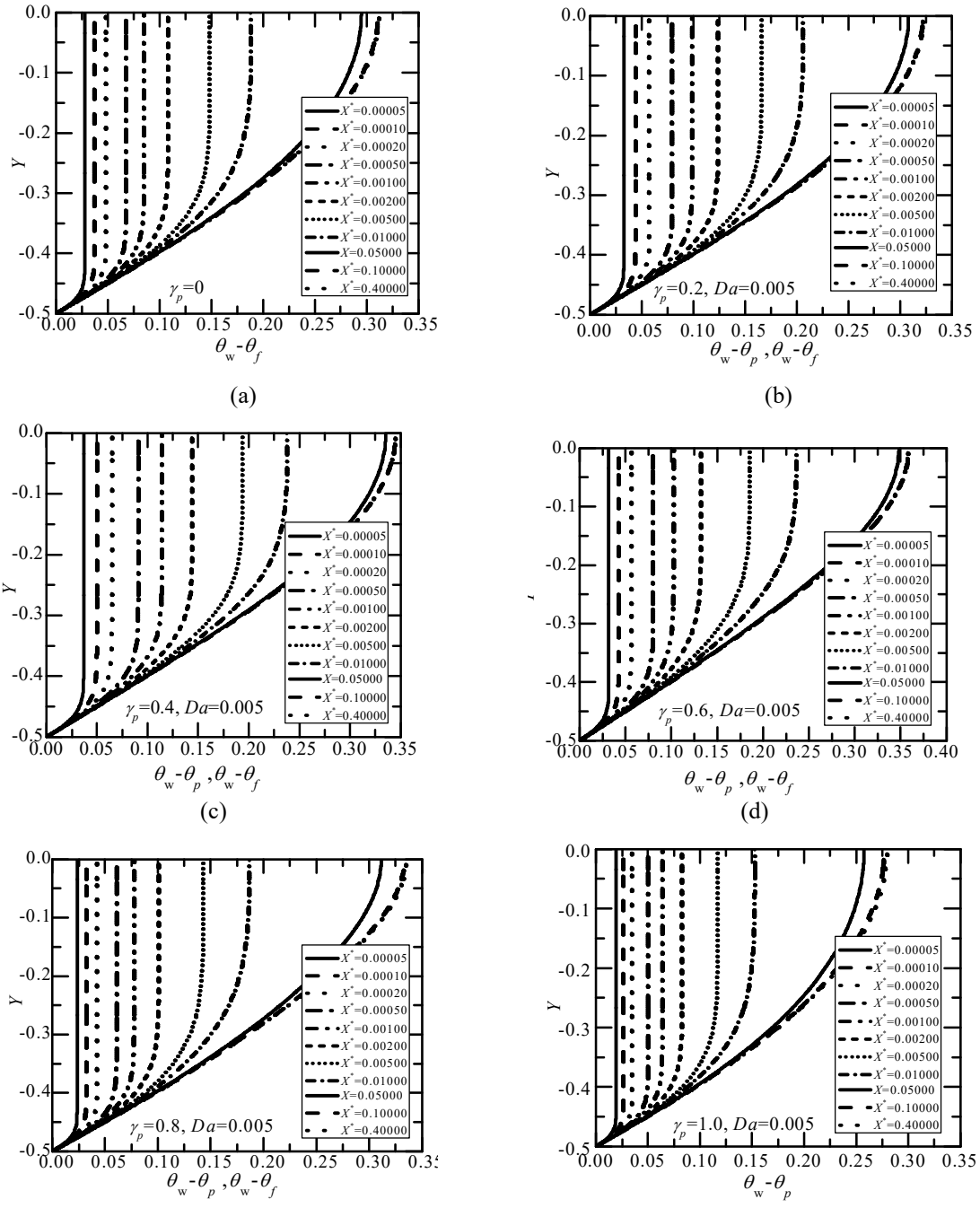

Fig. 5.2: Variation of $\theta_w-\theta_p$, $\theta_w-\theta_f$ profiles for different X^* for Da = 0.005 for (a) $\gamma_p=0$ (b) $\gamma_p=0.2$ (c) $\gamma_p=0.4$ (d) $\gamma_p=0.6$ (e) $\gamma_p=0.8$ and (f) $\gamma_p=1.0$.

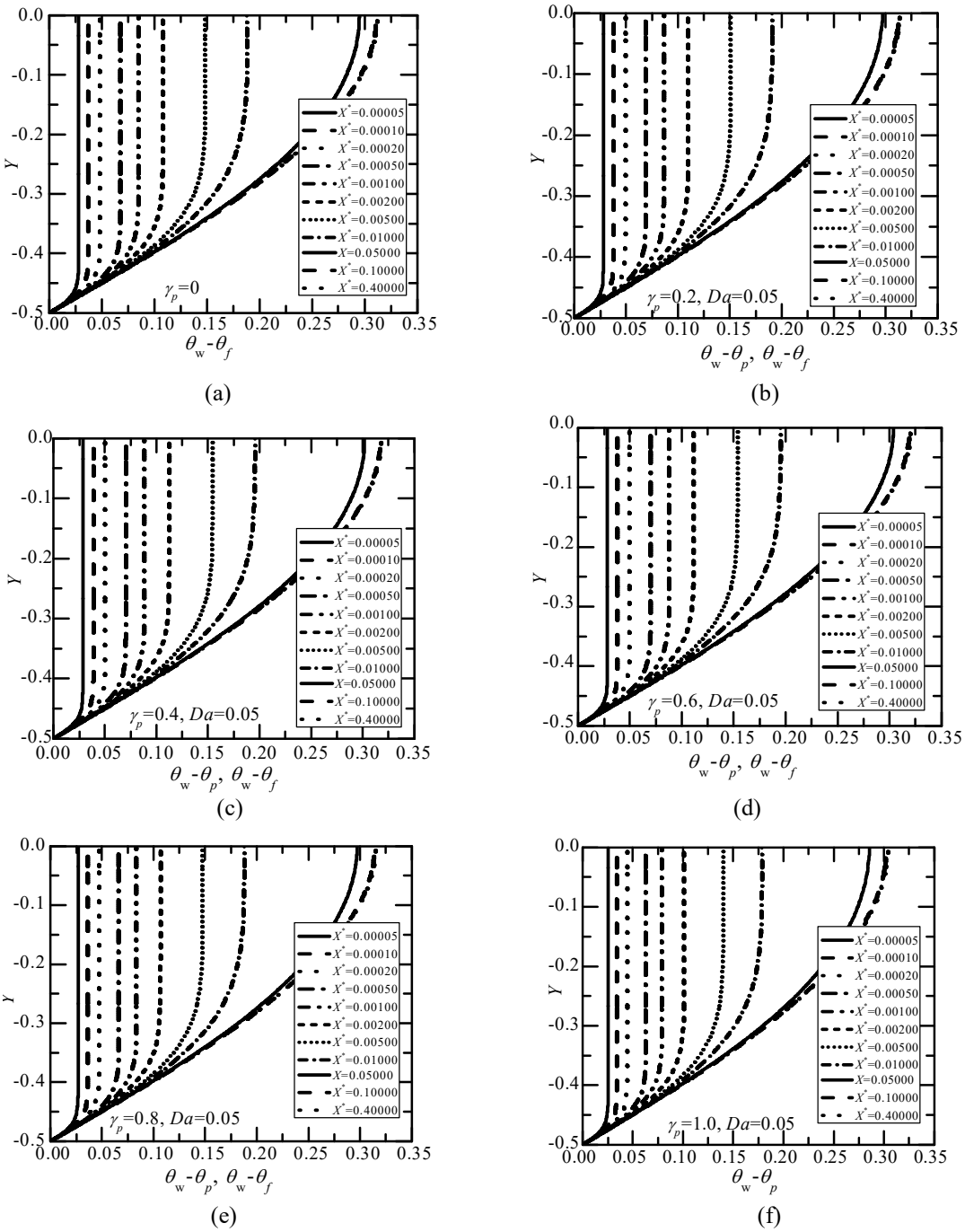

Fig. 5.3: Variation of $\theta_w - \theta_p$, $\theta_w - \theta_f$ profiles for different X^* for Da = 0.05 for (a) $\gamma_p = 0$ (b) $\gamma_p = 0.2$ (c) $\gamma_p = 0.4$ (d) $\gamma_p = 0.6$ (e) $\gamma_p = 0.8$ and (f) $\gamma_p = 1.0$.

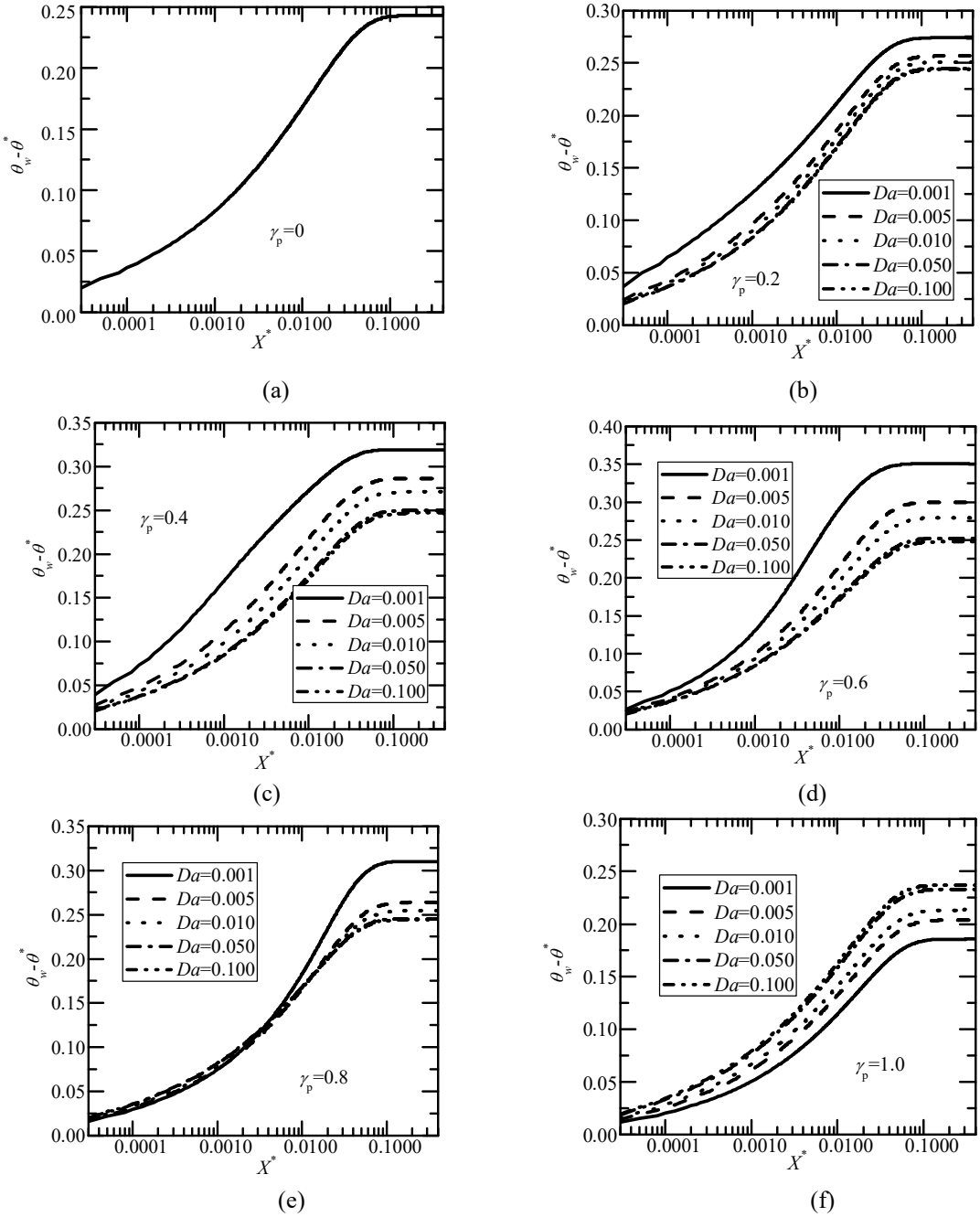

Fig. 5.4: Variation of the non dimensional bulk mean temperature excess of wall temperature $\theta_w - \theta^*$ with X^* for different Darcy numbers, *Da* for (a) $\gamma_p = 0$ (b) $\gamma_p = 0.2$ (c) $\gamma_p = 0.4$ (d) $\gamma_p = 0.6$ (e) $\gamma_p = 0.8$ and (f) $\gamma_p = 1.0$.

Plots of non dimensional wall temperature θ_w against porous fraction γ_p for X^*= 0.00005, 0.00500, 0.05000, 0.10000 and 0.20000 is shown in Figs. 5.5(a) and 5.5(b) for Da = 0.005 and Da = 0.050 respectively. From Figs. 5.5(a) and 5.5(b), θ_w increases as X^* increases, for all porous fractions and for all Darcy numbers. From, Figs. 5.5(a) and 5.5(b), it is observed that non dimensional wall temperature θ_w, increases up to a certain porous fraction and then it decreases for all X^* values. It is true for both the Darcy numbers Da = 0.005 and 0.05. As Darcy number increases, non dimensional wall temperature θ_w is almost constant with porous fraction, γ_p for all X^* values, which can be observed from Fig. 5.5(b).

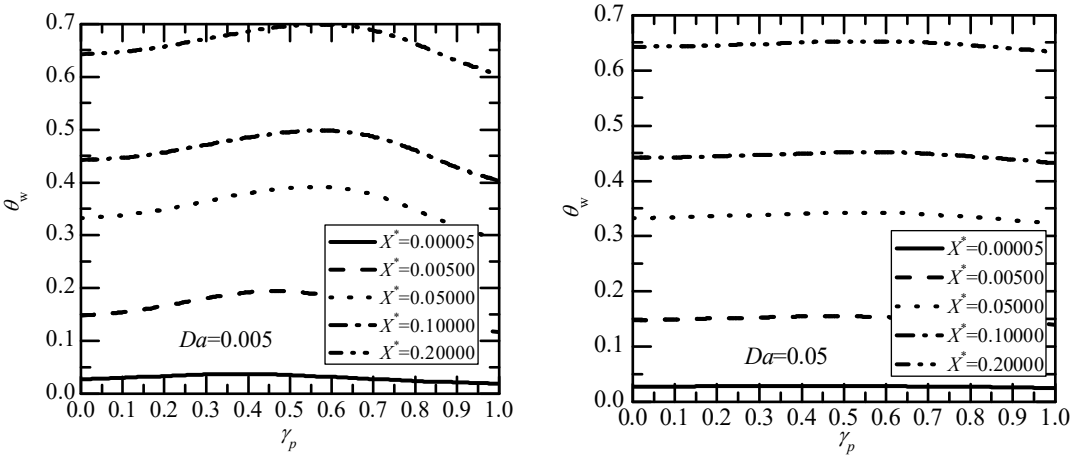

Fig. 5.5: Non dimensional wall temperature θ_w with porous fraction γ_p for different X^* for (a) Da = 0.005 and (b) Da = 0.05.

5.4.3 Local Nusselt Number

Variation of the local Nusselt numbers, Nu_{px} with X^* for different Darcy numbers, Da = 0.001, 0.005, 0.010, 0.050 and 0.100 and for different porous fractions γ_p = 0, 0.2, 0.4, 0.6, 0.8 and 1.0 is shown in Figs. 5.6(a) to 5.6(f). From Figs. 5.6(a) to 5.6(f), It can be observed that the local Nusselt number Nu_{px} decreases as X^* increases, for all porous fractions and for all Darcy numbers. This fact is well known (Nield et al. [57], Satyamurty and Bhargavi [158] and Pavel and Mohammad [187]) for the channel fully filled with porous and clear fluid regions, as also for different arrangements of porous inserts in channels. From, Figs. 5.6(b) to 5.6(d), it is observed that local Nusselt number Nu_{px} increases as Darcy number, Da increases at any X^*. But, for γ_p = 0.8 and 1.0 {Figs. 5.6(e) and 5.6(f)}, Nu_{px} decreases as Darcy number, Da increases. This is may be due to the fact that the porous region is dominating in a channel partially filled with a porous medium at high porous fractions. This fact is given in chapter 2, § 2.5 for fully developed Nusselt numbers. Also, as Darcy number increases, Nu_{px}, for a fully filled porous medium {Fig. 5.6(f)} is the same as Nu_{px} for clear fluid channel {5.6(a)}, which is independent of Darcy number. This means at higher Da, the porous region behaves like a clear fluid region. Comparison between analytical and numerical values of fully developed Nusselt numbers is shown in Table 5.5 for all porous fractions and at Da = 0.005 and 0.050. From Table 5.5, it is found to be in good agreement, and also with those $\{\gamma_p = 0$ and $\gamma_p = 1.0\}$ values available in the literature.

Table 5.5: Comparison between Numerical Values of Nusselt numbers with Analytical Values (Chapter 2) of Nusselt numbers at Fully Developed Length X^*= 0.4.

γ_p	Da = 0.005		Da = 0.050	
	Numerical value	Analytical value	Numerical value	Analytical value
0.0	8.2420	8.2352	8.2420	8.2352
0.2	7.8022	7.7939	8.1780	8.1715
0.4	7.0065	6.9962	8.0018	7.9945
0.6	6.6787	6.6681	7.9346	7.9272
0.8	7.5938	7.5869	8.1544	8.1483
1.0	9.8087	9.8155	8.5991	8.5968

A comparison of the present values of Nu_x for clear fluid channel($\gamma_p = 0$) with the values available in Shah and London [18], p. 181 are given in Table 5.6. The present results shown in Table 5.6 are obtained after neglecting axial conduction. The agreement of the present values with experimental values is good.

Table 5.6: A Comparison of the Present Values of Nu_x for the clear fluid channel ($\gamma_p = 0$) with the Values Available in the Literature

X^*	0.0004	0.0020	0.0080	0.0203	0.0402	0.1250	0.2000	0.3000	0.4000
Present	32.1560	19.1100	12.6100	9.9902	8.8040	8.2459	8.2356	8.2355	8.2353
Shah and London	32.1530	19.1130	12.6040	9.9878	8.8031	8.2458	8.2353	8.2353	8.2353

5.4.4 Comparison with experimental results for γ_p = 1.0

Jiang et al. [188] conducted experimental investigation on heat transfer in parallel plate channels filled with sintered bronze. The dimensional heat transfer coefficients for water and air systems have been presented at different Reynolds numbers. This type of comparison is available in Bhargavi [186].

The dimensional graphical results available in Fig. 5(a) of Jiang et al. [188] have been converted to correspond to the present non-dimensional system as follows.

$Nu_x = h_x(2H)/k_{ef}$; $X^* = X/D_ePe$, where Pe the Peclet number is the product of Re, as given in Jiang et al.[188] and the Prandtl number for water is taken as 7. D_e has been taken as 0.02 m and k_e has been taken as 2.012 W/(m C), as given in Table 3 of Jiang et al. [188]. The Peclet numbers for the experimental conditions of Jiang et al. [188] ranged from 910 to 17675 for water system. Regardless of the conditions very near the entry, the Peclet number range allows neglecting the axial conduction in the energy equation; even if included, there is no much difference in the numerical values. A comparison of Nu_{px} for Da = 0.005 with the values obtained in the present computations is shown in Fig. 5.7 for water system. The agreement for the water system is good though the present numerical prediction is an average of four different Reynolds numbers presented in Jiang et al. [188]. The difference in the Nusselt number values between the present numerical values and the experimental results of Jiang et al. [188] may be due to the assumption of fully developed flows in the computations whereas, the flow is developing graphically in the experiments which explains the dependence of the Nusselt number on the Reynolds number even in a plot with X^*.

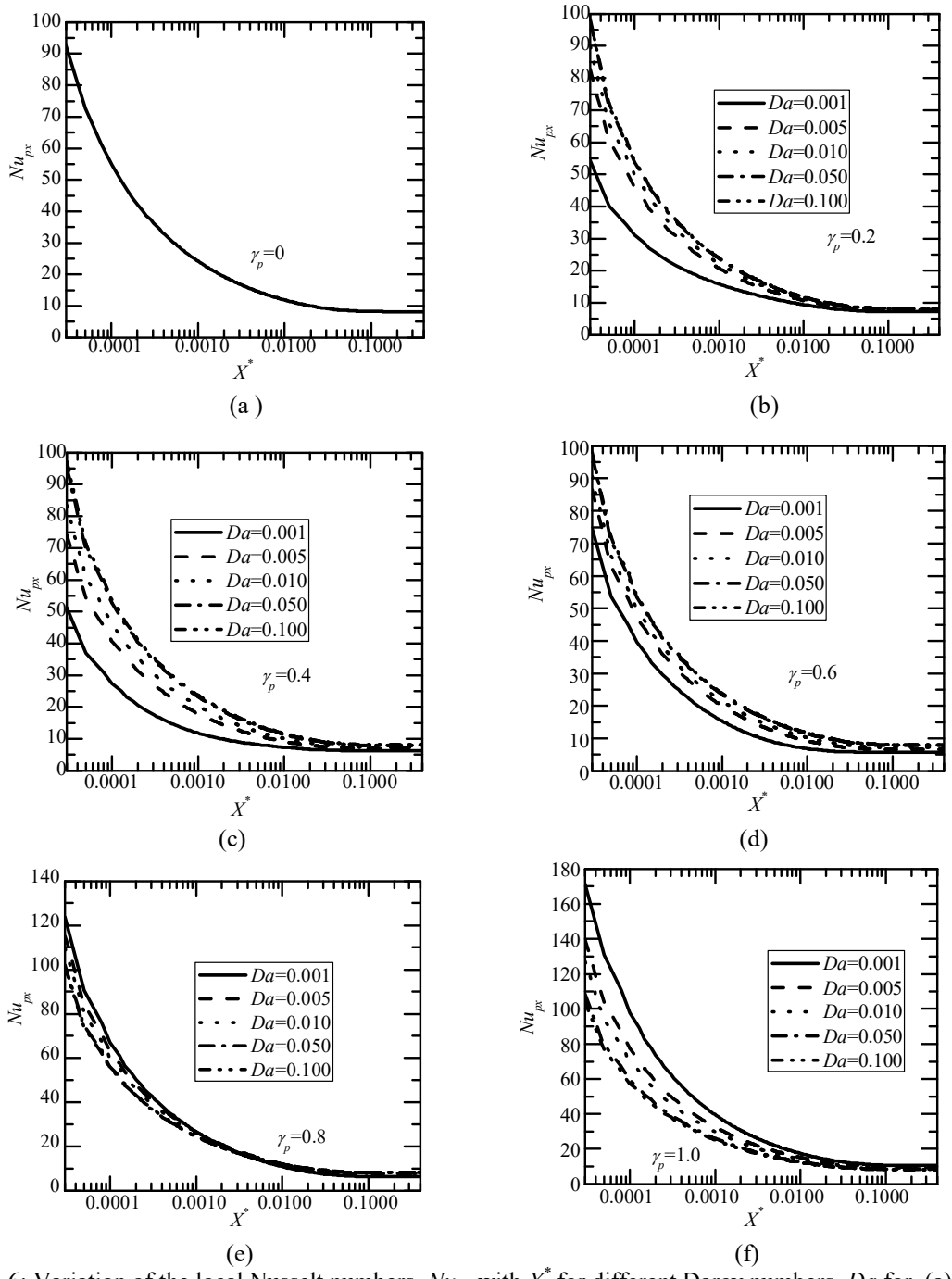

Fig. 5.6: Variation of the local Nusselt numbers, Nu_{px} with X^* for different Darcy numbers, Da for (a) $\gamma_p = 0$ (b) $\gamma_p = 0.2$ (c) $\gamma_p = 0.4$ (d) $\gamma_p = 0.6$ (e) $\gamma_p = 0.8$ and (f) $\gamma_p = 1.0$.

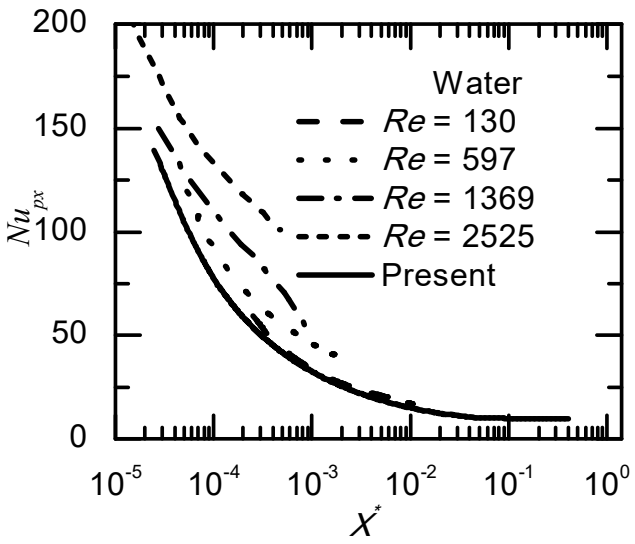

Fig. 5.7: Nu_{px} with X^* for different Re, for γ_p = 1.0 and Da = 0.005 for water particle diameter (not a parameter in the experiment).

The variation of Nu_{px} with γ_p for different values of X^* is shown in Figs. 5.8(a) and 5.8(b) for Darcy numbers, Da = 0.005 and 0.050 respectively. It is observed that Nu_{px} attains minimum value at $\gamma_p \approx 0.6$ at lower Da for a given X^*.

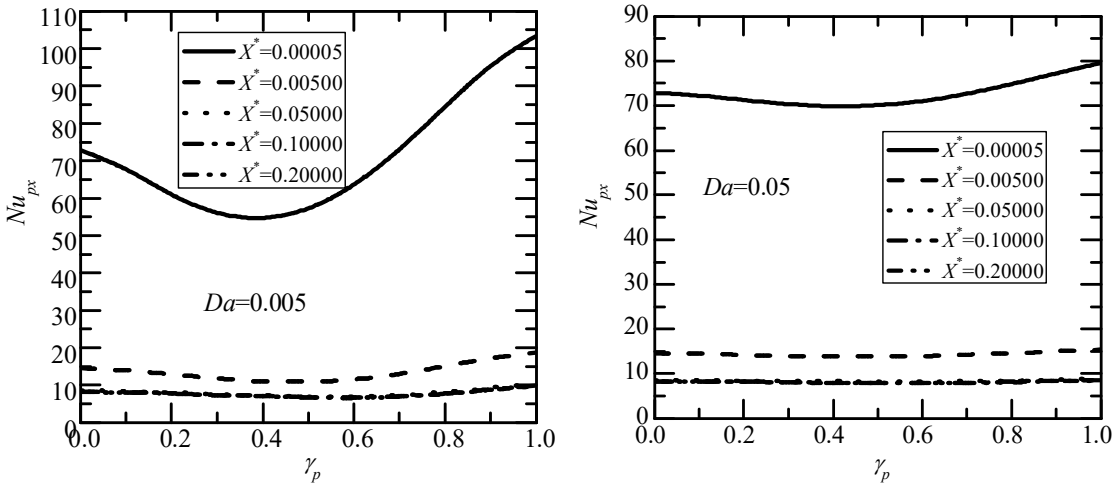

(a) (b)

Fig. 5.8: Variation of the local Nusselt number Nu_{px} with porous fraction γ_p for different values of X^* for (a) Da = 0.005 and (b) Da = 0.050.

5.5 Conclusions

Laminar forced convection in the thermally developing region of parallel plate channels partially filled with a porous material has been studied numerically. The parallel plates have been subjected to constant wall heat flux. The flow field has been assumed to be fully developed. Axial conduction is neglected in the conservation of the thermal energy equation. The problem is characterized by the Darcy number, Da and the porous fraction, γ_p. Numerical solutions have been obtained for $0 \leq \gamma_p \leq 1.0$ and Da = 0.001, 0.005, 0.010, 0.050, and 0.100, employing Successive Acceleration Replacement (SAR) scheme (Ramjee and Satyamurty [15] and Satyamurty and Bhargavi [158]). When axial conduction is neglected, Peclet number does not appear explicitly in the conservation of the thermal energy equation expressed in terms of the normalized non-dimensional axial distance X^*.

- The non-dimensional temperature at the wall, θ_w attains maximum value at a certain porous fraction. With this feature, it is envisaged that the local Nusselt number at the wall attains a minimum for some, $0 < \gamma_p < 1.0$. In the context of constant wall heat flux condition, this implies that the transfer of a given heat flux takes place with a lower temperature difference between the wall and the fluid.

- Non-dimensional bulk mean temperature, θ^*, increases as X^* increases. The values of the local Nusselt numbers when the channel is a clear fluid channel and when the channel is fully filled with a porous material agree well with the values available in Shah and London [18] and Nield et al. [57 and 58]. The local Nusselt number Nu_{px} decreases as X^*

increases for all γ_p and Da, and reaches the fully developed values for $X^* = 0.4$. Nu_{px} is at a minimum when $\gamma_p \approx 0.6$ at low $Da = 0.005$. Thus, there exists an optimum porous fraction to attain minimum enhancement in the Nusselt numbers.

Chapter 6

Effect of Axial Conduction in the Thermally Developing Region of the Channel Partially Filled with a Porous Medium: Constant Wall Heat Flux

6.1 Introduction

In this chapter, the effect of axial conduction on forced convection in a channel partially filled with a porous medium subjected to constant wall heat flux, has been investigated. The walls of the channel have been subjected to constant heat flux. In the studies undertaken, it has been assumed that the flow field is fully developed. The flow field in the channel partially filled with porous material is characterized by the Darcy number, *Da* and the porous fraction, γ_p. In addition, the problem is characterized by the Peclet number, *Pe*, when the axial conduction is included in the conservation of thermal energy equation.

Numerical solutions for two dimensional energy equations in both the fluid and porous regions have been obtained using successive accelerated replacement (SAR) numerical scheme (Ramjee and Satyamurty [15], Satyamurty and Bhargavi [158] and Jagadeesh and Satyamurty [179]). The effects of important relevant parameters on

temperature, bulk mean temperature, temperature based on bulk mean temperature and local Nusselt number have been studied.

6.2 Mathematical Formulation

The physical model and the coordinate system(refer to Fig. 5.1) are the same as those considered in chapter 5, § 5.2. The usual assumptions of isotropic and homogeneous porous medium, Newtonian fluid and local equilibrium have been made. The relevant expressions for a fully developed velocity profile can be obtained in Eqs. (2.26) and (2.29) of chapter 2, § 2.3.

Governing Equations

In the present Chapter effect of axial conduction (F_1) is considered and viscous dissipation(F_2) effects are neglected. i.e F_1 =1 and F_2 = 0. Substituting, F_1 =1 and F_2 = 0 in Eqs. (5.2) and (5.4) of Chapter 5 § 5.2, then the conservation of thermal energy equations in fluid and porous regions respectively, given by,

Fluid Region:

$$u_f \frac{\partial T_f}{\partial x} = \frac{k_f}{\rho C_p}\left(\frac{\partial^2 T_f}{\partial x^2} + \frac{\partial^2 T_f}{\partial y^2}\right) \tag{6.1}$$

In Eq. (6.1), u_f is the velocity in the fluid region, T_f is the temperature in the fluid region ρ, C_p and k_f are the density, the specific heat and the thermal conductivity of the fluid respectively.

Porous Region:

$$u_p \frac{\partial T_p}{\partial x} = \frac{k_{eff}}{\rho C_p}\left(\frac{\partial^2 T_p}{\partial x^2} + \frac{\partial^2 T_p}{\partial y^2} \right) \tag{6.2}$$

In Eq. (6.2), u_p is the velocity in the porous region, T_p is the temperature in the porous region and k_{eff} is the effective thermal conductivity of the porous medium. k_{eff} can be calculated from Catton [21] as,

$$k_{eff} = (1-\varphi)\, k_s + \varphi\, k_f \tag{6.3}$$

In Eq. (6.3), φ is the porosity and k_s is the thermal conductivity of the solid in the porous matrix.

Eqs. (6.1) and (6.2), applicable for the fluid region and porous region respctively, are subjected to the following boundary and interfacial conditions.

Boundary and Interfacial Conditions

$$u_p = 0 \quad , \quad -k_{eff} \frac{\partial T_p}{\partial y} = q \quad \text{at} \quad y = -H/2 \tag{6.4}$$

$$u_f = u_p = u_i \quad , \quad \mu_{eff} \frac{du_p}{dy} = \mu_f \frac{du_f}{dy} \qquad \text{at interface} \quad y = -\frac{H}{2} + \frac{l_p}{2} \tag{6.5}$$

$$T_f = T_p = T_i \, , \quad k_f \left(\partial T_f / \partial y \right) = k_{eff} \left(\partial T_p / \partial y \right) \qquad \text{at interface} \quad y = -\frac{H}{2} + \frac{l_p}{2} \tag{6.6}$$

$$\frac{du_f}{dy} = 0, \; \frac{\partial T_f}{\partial y} = 0 \quad \text{at} \quad y = 0 \quad \{\text{Symmetry boundary conditions}\} \tag{6.7}$$

$$T_f = T_p = T_e \qquad \text{at} \qquad x = 0 \; , \quad -\frac{H}{2} \le y \le 0 \quad \text{(Inlet condition)} \tag{6.8}$$

$$\frac{\partial}{\partial x}\left(\frac{T-T_w}{T_b-T_w}\right)=0 \quad \text{at} \quad -\frac{H}{2}\le y\le\frac{H}{2} \quad \{\text{downstream condition}\} \tag{6.9}$$

Non-dimensionalization

Governing equations {Eqs. (6.1) and (6.2)} are rendered non-dimensional by introducing the following non-dimensional variables.

$$\left.\begin{aligned} &X=x/H,\ Y=y/H,\ U_f=u_f/u_{ref},\ U_i=u_i/u_{ref},\ U_p=u_p/u_{ref},\ P=p/\rho\,u_{ref}^2,\\ &\theta_f=(T_f-T_e)/(qH/k_f),\theta_p=(T_p-T_e)/(qH/k_f) \end{aligned}\right\} \tag{6.10}$$

In Eq. (6.10), X and Y are the non-dimensional coordinates. U and P are the non-dimensional velocity and pressure. The subscripts f and p refer to fluid and porous regions. θ,{ θ_f in the fluid region and θ_p in the porous region}, is the non-dimensional temperature. u_{ref} is the average velocity through the channel. u_{ref} is related to u_p and u_f and is given by,

$$\frac{2}{H}\left[\int_{-H/2}^{-\frac{H}{2}+\frac{l_p}{2}} u_p\,dy+\int_{-\frac{H}{2}+\frac{l_p}{2}}^{0} u_f\,dy\right]=u_{ref} \tag{6.11}$$

In addition, the non-dimensional porous layer thickness γ_p, which shall be referred to as porous fraction is defined by,

$$\gamma_p=l_p/H \tag{6.12}$$

On introducing the non-dimensional variables given in Eq. (6.10), the governing equations for conservation of momentum and energy equations applicable in the fluid and porous regions in non-dimensional form become,

Fluid Region

$$U_f \frac{\partial \theta_f}{\partial X^*} = A_c \frac{1}{Pe^2} \frac{\partial^2 \theta_f}{\partial X^{*2}} + \frac{\partial^2 \theta_f}{\partial Y^2} \tag{6.13}$$

In Eq. (6.13), Pe is the Peclet number and X^* is the normalized X, defined by,

$$Pe = u_{ref} H / \alpha_f \tag{6.14}$$

$$X^* = X / Pe \tag{6.15}$$

Porous Region

$$U_p \frac{\partial \theta_p}{\partial X^*} = \frac{1}{\eta} \left(A_c \frac{1}{Pe^2} \frac{\partial^2 \theta_p}{\partial X^{*2}} + \frac{\partial^2 \theta_p}{\partial Y^2} \right) \tag{6.16}$$

In Eq. (6.16) , η are defined by,

$$\eta = k_f / k_{eff} \tag{6.17}$$

When A_c = 1, in Eqs. (6.13) and (6.16) axial conduction is included, and when A_c = 0, axial conduction is neglected. When A_c = 0, the solutions to Eqs. (6.13) and (6.16)in

terms of X^* do not depend on *Pe*. Eqs. (6.13) and (6.16) are subjected to the following boundary conditions.

Non-dimensional Boundary and Interfacial Conditions

$$\theta_{f,p}(0,Y) = 0 \quad \text{for} \quad -\frac{1}{2} \le Y \le 0 \ \{\text{inlet condition}\} \tag{6.18}$$

$$\frac{dU_f}{dY} = 0,\ \frac{\partial \theta_f}{\partial Y} = 0 \quad \text{at} \quad Y = 0 \ \{\text{symmetry condition}\} \tag{6.19}$$

$$U_f = U_p = U_i,\ \frac{dU_f}{dY} = \frac{1}{\varepsilon}\frac{dU_p}{dY} \quad \text{at the interface} \quad Y = -\frac{1}{2} + \frac{\gamma_p}{2} \tag{6.20}$$

$$\theta_f = \theta_p = \theta_i,\ \frac{\partial \theta_f}{\partial Y} = \frac{1}{\eta}\frac{\partial \theta_p}{\partial Y} \quad \text{at the interface} \quad Y = -\frac{1}{2} + \frac{\gamma_p}{2} \tag{6.21}$$

$$U_p = 0,\ \frac{\partial \theta_p}{\partial Y} = -\eta \quad \text{at} \quad Y = -1/2 \tag{6.22}$$

$$\frac{\partial \theta_b}{\partial X^*} = 0 \Rightarrow \frac{\partial \theta_{f,p}}{\partial X^*} = \frac{\theta_{f,p}}{\theta^*}\frac{\partial \theta^*}{\partial X^*} \quad \text{at} \quad X^* \ge X^*_{fd} \quad \text{for} \quad -1/2 \le Y \le 1/2 \ \{\text{downstream condition}\} \tag{6.23}$$

In Eq. (6.23), θ_b is the non-dimensional temperature based on the bulk mean temperature defined by

$$\theta_b = \frac{T - T_e}{T_b - T_e} = \frac{\theta}{\theta^*} \tag{6.24}$$

Further, the conditions given in Eq. (6.20) ensure the continuity of the velocity and the shear stress as given in Bhargavi and Satyamurty [108] and Satyamurty and Bhargavi [158] at the interface.

6.3 Numerical Scheme: Successive Accelerated Replacement (SAR)

Numerical solutions to Eqs. (6.13) and (6.16) along with the boundary conditions on θ given in Eqs. (6.18) to (6.23) have been obtained employing the successive accelerated replacement (SAR) scheme as described in Ramjee and Satyamurty [15] and Satyamurty and Bhargavi [158]. This iterative scheme was originally derived to solve systems of non-linear algebraic equations by Lieberstein [168], these equations being mildly nonlinear elliptic partial differential equations. This scheme has been used extensively to solve nonlinear ordinary differential equations arising in compressible flows Lew [167] and Dellinger [169]. The scheme is basically the Gauss Siedel Successive Over-relaxation scheme, see, Antia [189]. The terminology of SAR has been used by Dellinger [169].

6.3.1 Application of the SAR Scheme

Non Uniform:

Non-uniform grids described in Chapter 5, § 5.3.3 have been employed in the axial direction. Let *MD* and *ND* be the number of divisions in *X* and *Y* direction and ΔX and

ΔY be the width in *X* and *Y* direction respectively. When the terms in energy Eqs. (6.13) and (6.16)are expressed in finite difference form, the errors $\tilde{\theta}_f, \tilde{\theta}_p$ are given by,

$$\begin{aligned}\tilde{\theta}_f(M,N) &= U_f(N)\left[\frac{\theta_f(M,N)-\theta_f(M-1,N)}{X(M)-X(M-1)}\right] \\ &- A_c\frac{1}{Pe^2}\left[\frac{\begin{array}{l}\big(X(M-1)-X(M-2)\big)\theta_f(M,N)+\big(X(M-2)-X(M)\big)\theta_f(M-1,N)\\ +\big(X(M)-X(M-1)\big)\theta_f(M-2,N)\end{array}}{\big(X(M)-X(M-1)\big)^2\big(X(M-1)-X(M-2)\big)}\right] \\ &-\left[\frac{\theta_f(M,N+1)-2\theta_f(M,N)+\theta_f(M,N-1)}{(\Delta Y)^2}\right]\end{aligned} \tag{6.25}$$

$$\begin{aligned}\tilde{\theta}_p(M,N) &= \eta U_p(N)\left[\frac{\theta_p(M,N)-\theta_p(M-1,N)}{X(M)-X(M-1)}\right] \\ &- A_c\frac{1}{Pe^2}\left[\frac{\begin{array}{l}\big(X(M-1)-X(M-2)\big)\theta_p(M,N)+\big(X(M-2)-X(M)\big)\theta_p(M-1,N)\\ +\big(X(M)-X(M-1)\big)\theta_p(M-2,N)\end{array}}{\big(X(M)-X(M-1)\big)^2\big(X(M-1)-X(M-2)\big)}\right] \\ &-\left[\frac{\theta_p(M,N+1)-2\theta_p(M,N)+\theta_p(M,N-1)}{(\Delta Y)^2}\right]\end{aligned} \tag{6.26}$$

To correct the profile for θ_f and θ_p, according to the SAR scheme, the following derivatives become necessary

$$\frac{\partial\tilde{\theta}_f(M,N)}{\partial\theta_f(M,N)} = \frac{U_f(N)}{X(M)-X(M-1)} - A_c\frac{1}{Pe^2\left[X(M)-X(M-1)\right]^2} + \frac{2}{(\Delta Y)^2} \tag{6.27}$$

$$\frac{\partial\tilde{\theta}_p(M,N)}{\partial\theta_p(M,N)} = \frac{\eta\, U_p(N)}{X(M)-X(M-1)} - A_c\frac{1}{Pe^2\left[X(M)-X(M-1)\right]^2} + \frac{2}{(\Delta Y)^2} \tag{6.28}$$

Boundary conditions:

$$\theta_f(M,N)=\frac{4\theta_f\left(M,N-1\right)-\theta_f\left(M,N-2\right)}{3} \qquad \text{at} \quad N=\frac{ND}{2}+1 \tag{6.29}$$

$$\theta_p(M,N)=\frac{2\eta\ \Delta Y-\theta_p\left(M,N+2\right)+4\theta_p\left(M,N+1\right)}{3} \qquad \text{at} \quad N=1 \tag{6.30}$$

Let *NP* be a grid number corresponding to the interface. It is assumed that the interface coincides with one of the grid planes in the *Y* direction. When a large number of *ND*'s are used, the error involved is not likely to be significant even if the interface does not exactly correspond to an integer *NP*. Boundary conditions given by Eq. (6.21) on θ_f and θ_p in finite difference form become,

$$\theta_f(M,NP)=\theta_p(M,NP) \qquad \text{at} \quad NP=\left(\frac{\gamma_p}{2}\right)ND+1 \tag{6.31}$$

$$\theta_f(M,NP)=\theta_f(M,NP-1)+\frac{1}{\eta}\left[\theta_p(M,NP+1)-\theta_p(M,NP)\right] \qquad \text{at} \quad NP=\left(\frac{\gamma_p}{2}\right)ND+1 \tag{6.32}$$

Inlet condition

$$\theta_p(0,N)=0 \qquad \text{for} \qquad 1\le N\le\left(\frac{\gamma_p}{2}\right)ND+1 \tag{6.33}$$

$$\theta_f(0,N)=0 \qquad \text{for} \qquad \left(\frac{\gamma_p}{2}\right)ND+1\le N\le\frac{ND}{2}+1 \tag{6.34}$$

The downstream boundary conditions {Eq. (6.23)} are expressed in finite difference form as follows

$$\theta_p(MD+1,N)=\frac{\theta^*(MD+1)\left\{[1+(\Delta X^*_{MD-2}/\Delta X^*_{MD-1})]^2\theta_p(MD,N)-\theta_p(MD-1,N)\right\}}{\left\{[1+(\Delta X^*_{MD-2}/\Delta X^*_{MD-1})]^2\theta^*(MD)-\theta^*(MD-1)\right\}}$$

$$\text{for } 1\le N\le NP \quad \text{for } X^*>X^*_{fd}$$

$$\theta_f(MD+1,N)=\frac{\theta^*(MD+1)\left\{[1+(\Delta X^*_{MD-2}/\Delta X^*_{MD-1})]^2\theta_f(MD,N)-\theta_f(MD-1,N)\right\}}{\left\{[1+(\Delta X^*_{MD-2}/\Delta X^*_{MD-1})]^2\theta^*(MD)-\theta^*(MD-1)\right\}} \qquad (6.35)$$

$$\text{for } NP\le N\le ND \quad \text{for } X^*>X^*_{fd}$$

Further, in Eq. (6.35),

$$\Delta X^*_M=X^*(M+1)-X^*(M) \qquad (6.36)$$

When the axial conduction is neglected, i.e., $A_c = 0$ in Eqs. (6.13) and (6.16), the condition given by Eq. (6.35) need not be applied since the governing equations become parabolic. Several numerical trials have been made to establish grid independence, suitable number of grids in X^* and Y directions, error tolerence, ε_t and acceleration factor, ω. Numerical trials are given in chapter 5. $\omega \le 1$ has been chosen, lower values being associated with higher *Pe*. $\varepsilon_t = 10^{-5}$, $X^*_{fd} = 0.4$, $MD = 1000$ and $ND = 90$ have been found to be satisfactory.

6.3.2 Local Nusselt Number

The heat transfer coefficient h_{px}, at the plate $y = -H/2$ adjacent to the porous medium is defined by

$$-k_{eff}\frac{dT_p}{dy}\Big|_{y=-\frac{H}{2}} = h_{px}(T_w - T_b) \tag{6.37}$$

Upon non-dimensionalizing (using Eq. (6.10)), the Nusselt number at $Y = -1/2$, Nu_{px} is given by

$$Nu_{px} = \frac{h_{px}(2H)}{k_f} = \frac{2}{\theta_w - \theta^*} \tag{6.38}$$

6.4 Result and Discussion

It has been assumed that $\varepsilon = \mu_f/\mu_{eff} = 1$ and $\eta = k_f/k_{eff} = 1$. Numerical solutions to the conservation of thermal energy equation applicable in the porous and fluid regions employing the fully developed velocity profile have been obtained for $0 \leq \gamma_p \leq 1.0$, Pe = 5, 10, 25, 50 and 100 and Da = 0.001, 0.005, 0.01, 0.05 and 0.1 by the successive accelerated replacement (SAR) scheme which has been extensively used for this class of problems (Ramjee and Satyamurty[15] and Satyamurty and Bhargavi [158]).

6.4.1 Thermal Field

Variation with porous fraction γ_p:

Non-dimensional temperature in excess of wall temperature, $\theta_w - \theta_p, \theta_w - \theta_f$, profiles at different axial locations for Da = 0.005 and Pe = 5, 100 are shown in Figs. 6.1(a) to 6.1(f) and Figs. 6.2(a) to 6.2(f) for γ_p = 0, 0.2, 0.4, 0.6, 0.8 and 1.0 respectively. It can be

noticed that $\theta_w - \theta_p, \theta_w - \theta_f$ profiles are symmetric about $Y = 0$ when $\gamma_p = 0$ and $\gamma_p = 1.0$, in (a) and (f) of Figs. 6.1 and 6.2. From Figs. 6.1(a) to 6.1(f) and 6.2(a) to 6.2(f), as X^* increases, $\theta_w - \theta_p$, $\theta_w - \theta_f$ increase in both the fluid and porous regions for all porous fractions. If X^* is large (say, = 0.4) and the Peclet number is large too say, $Pe \geq 100$, $\theta_w - \theta_p$, $\theta_w - \theta_f$ tend to fully developed profiles for all porous fractions and Darcy numbers, as given in chapter 2. From Fig. 6.2(a){for $\gamma_p = 0$} and 6.2(f) {for $\gamma_p = 1.0$} for large X^* (say = 0.4), $\theta_w - \theta_f$ tends to be fully developed profiles given in Kays, Crawford and Weigand [185].

Variation of θ profiles with Peclet number, *Pe* :

The non-dimensional temperature in excess of wall temperature $\theta_w - \theta_p, \theta_w - \theta_f$ profiles at different axial locations for $Da = 0.005$ and $\gamma_p = 0.4$ are shown in Figs. 6.3(a) to 6.3(f) respectively, for Peclet numbers, Pe = 5, 10, 25, 50, 100 and $A_c = 0$, i.e., when axial conduction is neglected. From Fig. 6.3, as X^* increases, $\theta_w - \theta_p$, $\theta_w - \theta_f$ increase in both the fluid and porous regions for all Peclet numbers. Fig. 6.3(e) {Pe = 100} and Fig. 6.3(f) { $A_c = 0$} are almost identical except for very small X^* values, indicating that the effect of axial conduction is negligible when $Pe \geq 100$. That is, if X^* is larger (say, = 0.4), $\theta_w - \theta_p$, $\theta_w - \theta_f$ tend to be fully developed profiles, as given in chapter 2, § 2.5 when $Pe \geq 100$.

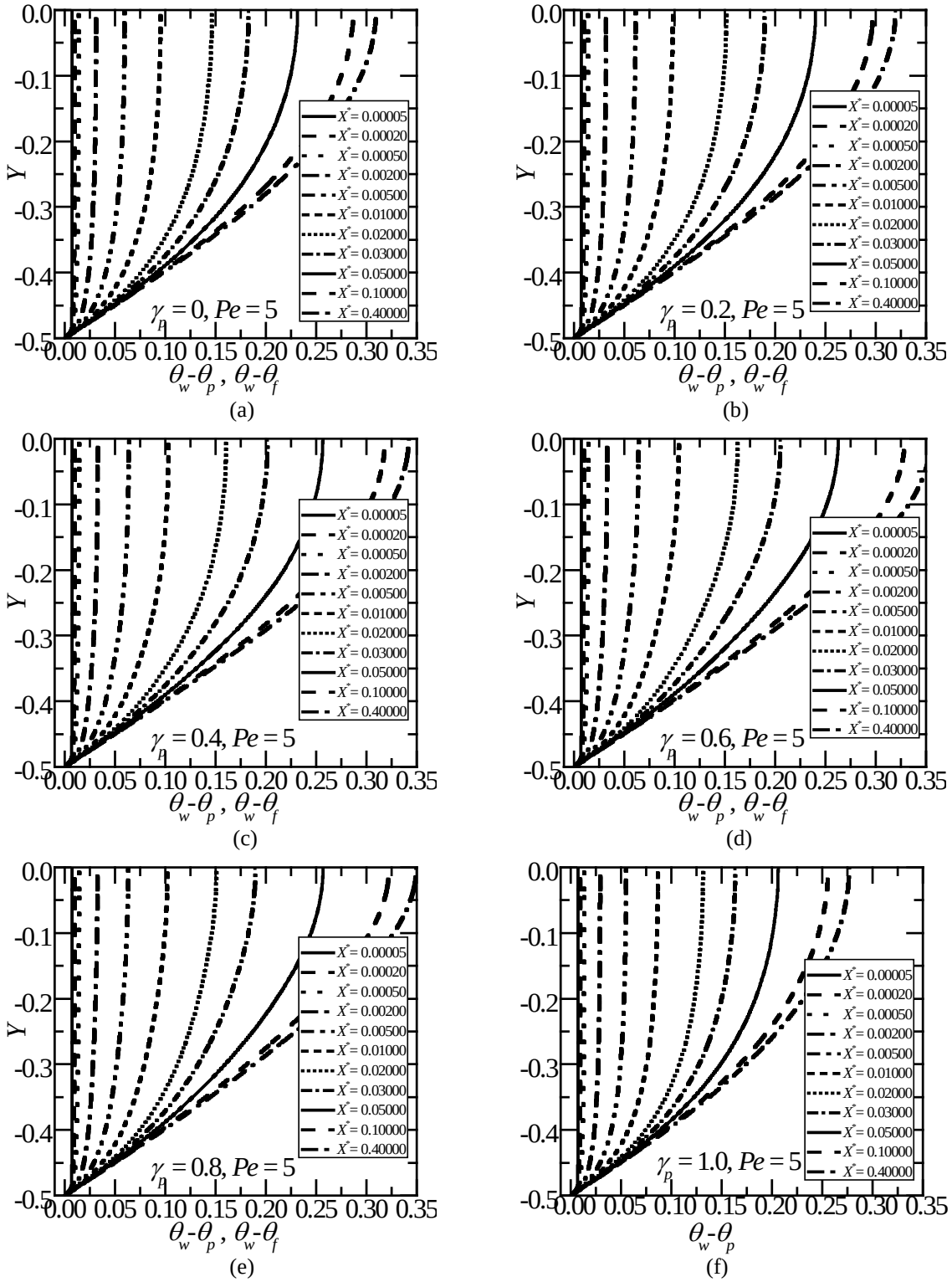

(a) (b) (c) (d) (e) (f)

Fig. 6.1: Variation of $\theta_w - \theta_p$, $\theta_w - \theta_f$ profiles for different X^* values for Da = 0.005 and Pe = 5 for (a) $\gamma_p = 0$ (b) $\gamma_p = 0.2$ (c) $\gamma_p = 0.4$ (d) $\gamma_p = 0.6$ (e) $\gamma_p = 0.8$ and (f) $\gamma_p = 1.0$.

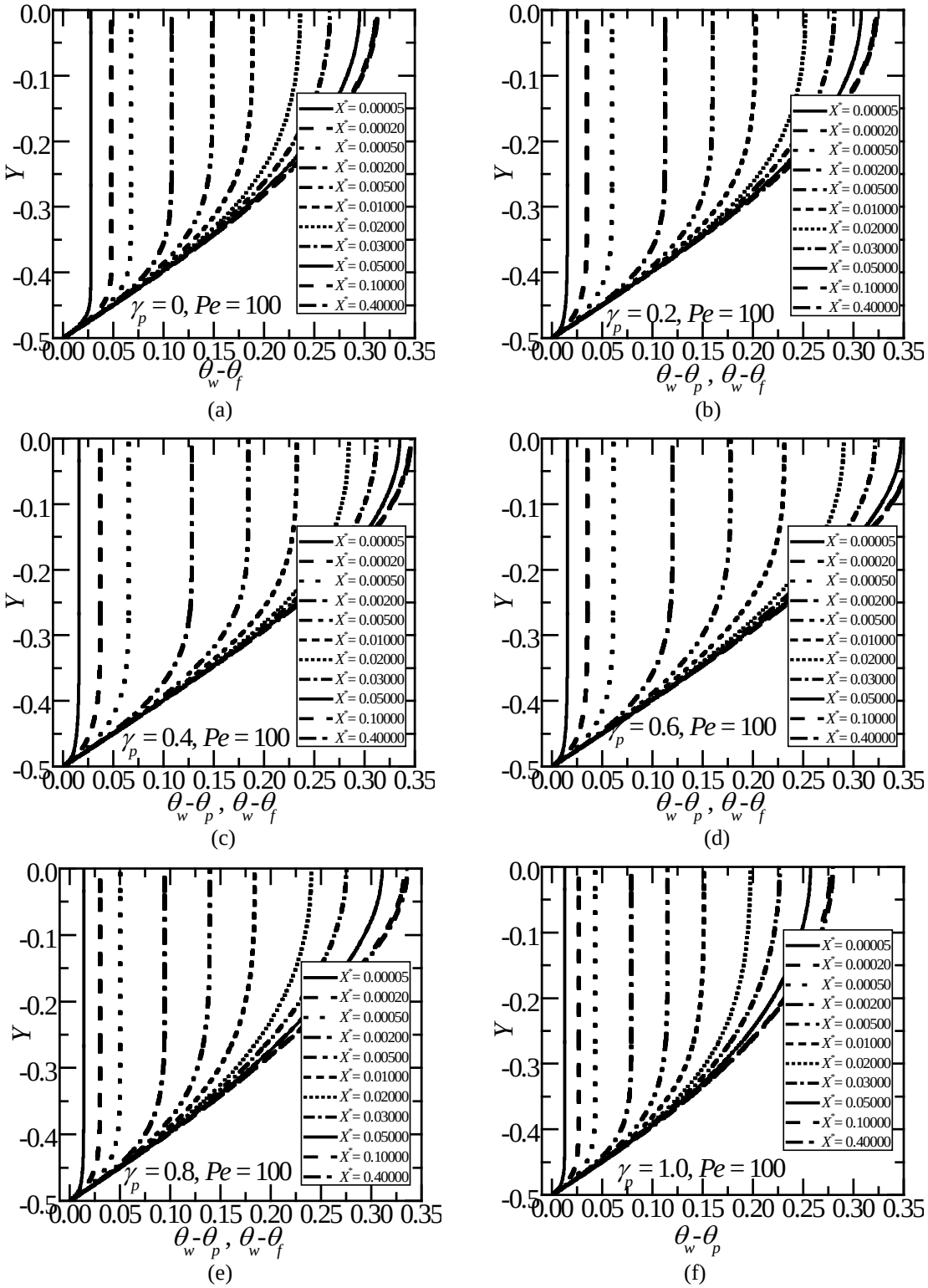

Fig. 6.2: Variation of $\theta_w - \theta_p$, $\theta_w - \theta_f$ profiles for different X^* values for *Da* = 0.005 and *Pe* = 100 for (a) $\gamma_p = 0$ (b) $\gamma_p = 0.2$ (c) $\gamma_p = 0.4$ (d) $\gamma_p = 0.6$ (e) $\gamma_p = 0.8$ and (f) $\gamma_p = 1.0$.

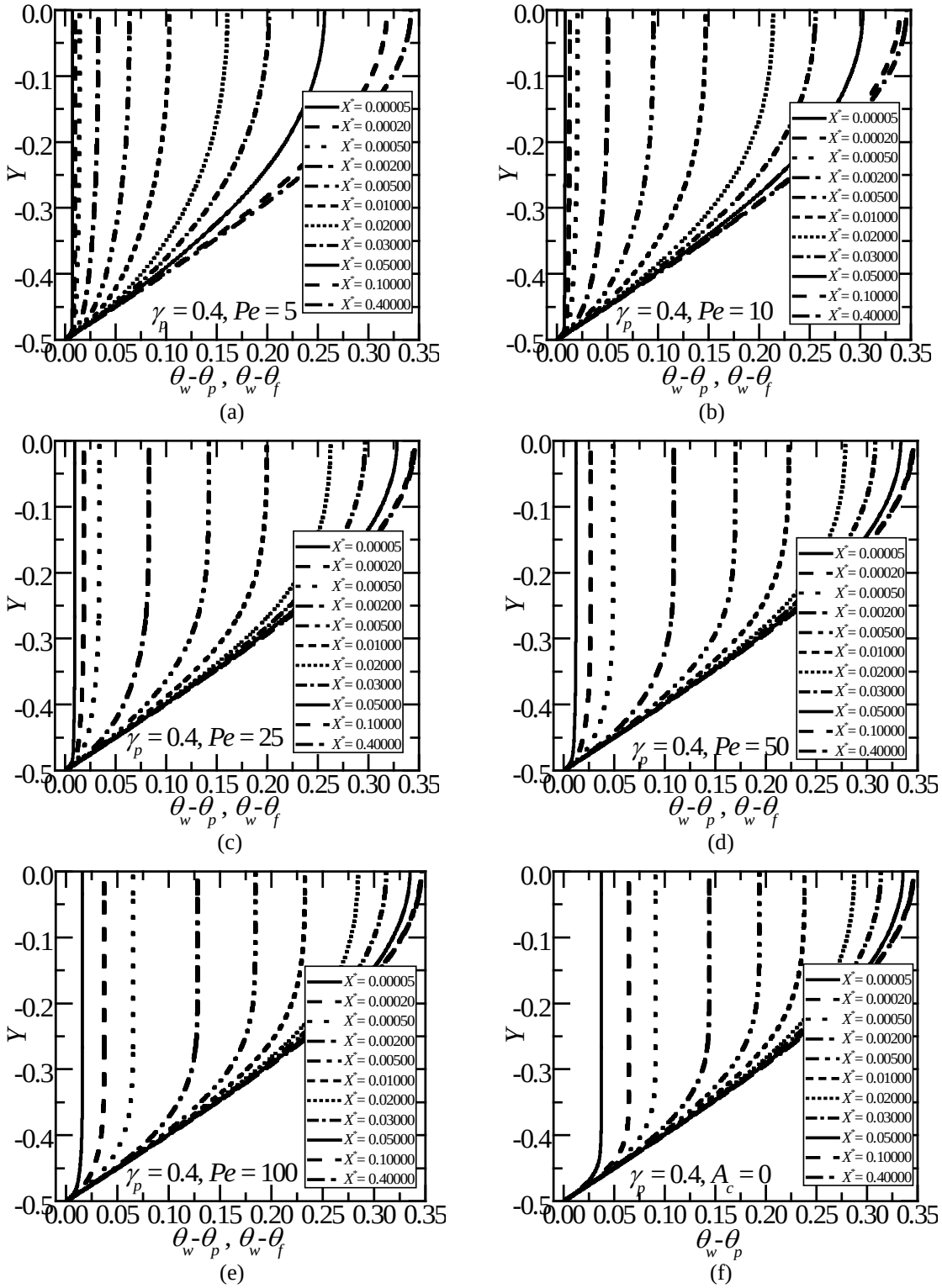

Fig. 6.3: Variation of $\theta_w - \theta_p$, $\theta_w - \theta_f$ profiles for different X^* values for *Da* = 0.005 and $\gamma_p = 0.4$ for (a) *Pe* = 5 (b) *Pe* = 10 (c) *Pe* = 25 (d) *Pe* = 50 (e) *Pe* = 100 and (f) A_c = 0, i.e., when axial conduction is neglected.

Non dimensional temperature based on bulk mean temperature:

θ_b {the non-dimensional temperature based on bulk mean temperature defined by Eq. (6.24)} profiles at different axial locations are shown in Figs. 6.4(a) to 6.4(f) for γ_p = 0{the clear fluid channel}, 0.2, 0.4, 0.6, 0.8 and γ_p = 1.0{the channel fully filled with porous material}, for *Da* = 0.005, *Pe* = 25 . As noted with reference to $\theta_w - \theta_{p,f}$ profiles in Figs. 6.1 and 6.2, θ_b profiles are also symmetric about *Y* = 0, for two cases of the clear fluid channel (γ_p = 0) and the channel fully filled with the porous material(γ_p = 1.0). θ_b is dependent on the Darcy number and approaches that of clear fluid profile for large *Da*. For $\gamma_p \neq 0$ and 1.0, θ_b profiles are not symmetric about *Y* = 0. Axial conduction effect decreases for larger X^*, where θ_b profiles are almost the same for all *Pe*. The plots in Fig. 6.4 also confirm that $\partial\theta_b / \partial X^* \rightarrow 0$ for large X^*.

6.4.2 Non Dimensional Bulk Mean Temperature

Non dimensional bulk mean temperature in excess of wall temperature, $\theta_w - \theta^*$ with X^*, for different Peclet numbers, *Pe* = 5, 10, 25, 50 and 100 for *Da* = 0.05 for γ_p = 0, 0.2, 0.4, 0.6, 0.8 and 1.0 are presented in Figs. 6.5(a) to 6.5(f). From Fig. 6.5, the effect of Peclet number can be accessed. For all X^*, $\theta_w - \theta^*$ is lower for lower *Pe*. The effect of axial conduction thus results in the fluid getting less heated or less cooled. From Figs. 6.5(a) to 6.5(f), as X^* increases, $\theta_w - \theta^*$ increases for all Peclet numbers and porous fractions. As Peclet number increases, $\theta_w - \theta^*$ increases with X^* values for all porous fractions.

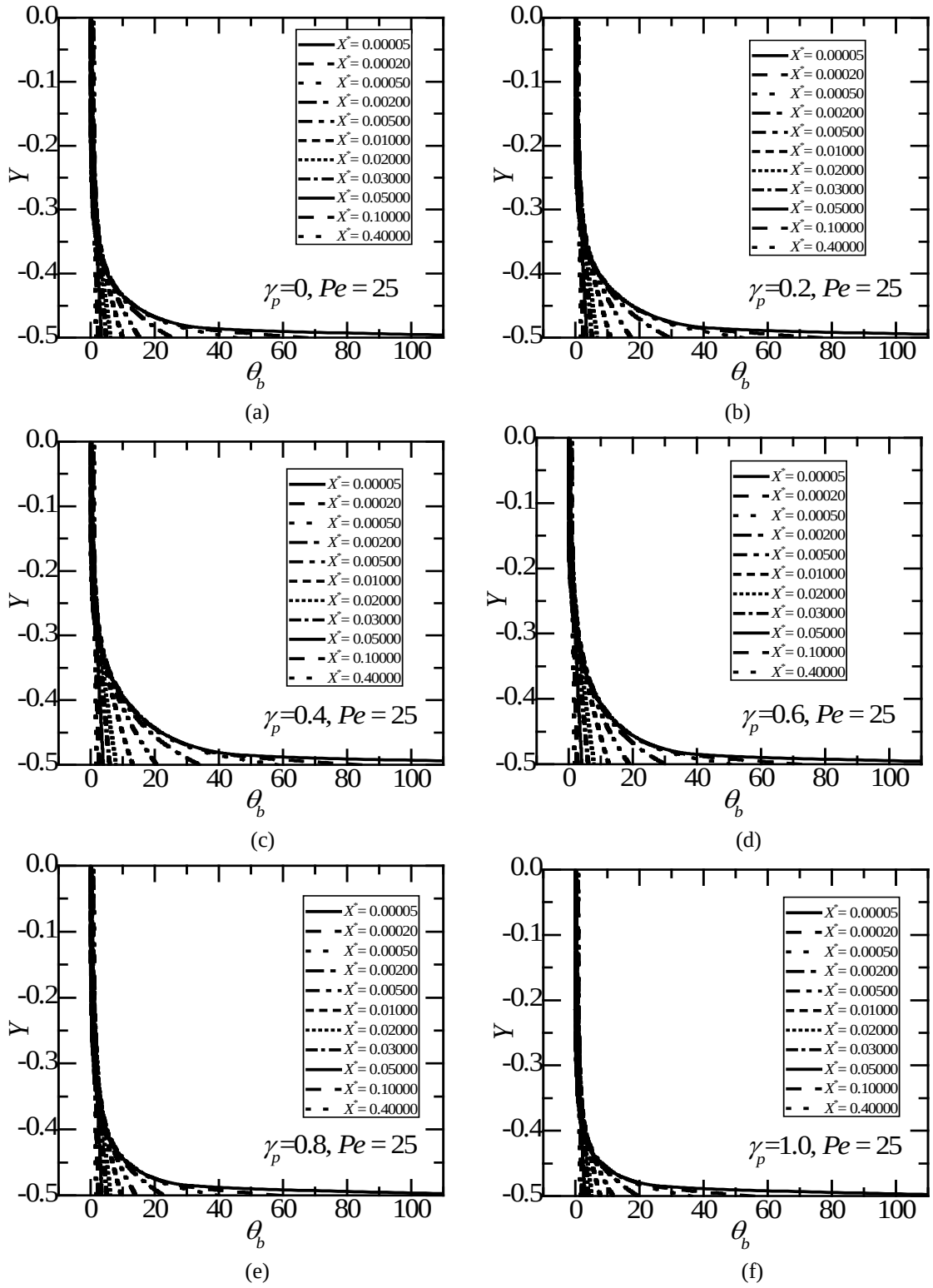

Fig. 6.4: Variation of non dimensional temperature based on Bulk mean temperature, θ_b profiles for different X^* values for Da = 0.005 and Pe = 25 for (a) $\gamma_p = 0$ (b) $\gamma_p = 0.2$ (c) $\gamma_p = 0.4$ (d) $\gamma_p = 0.6$ (e) $\gamma_p = 0.8$ and (f) $\gamma_p = 1.0$.

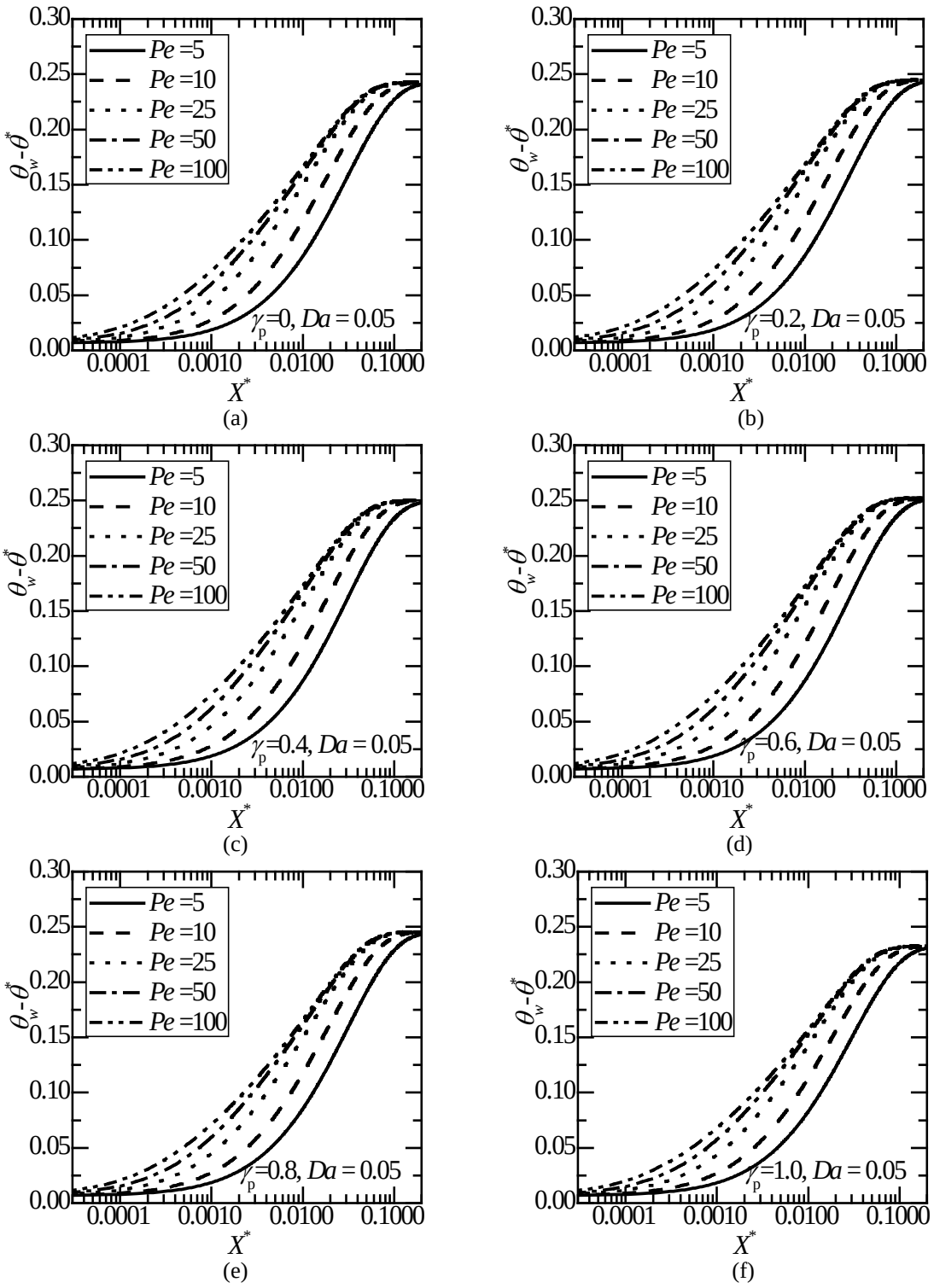

Fig. 6.5: Variation of Non dimensional bulk mean temperature $\theta_w - \theta^*$ with X^* values for different Peclet numbers, *Pe* and Darcy number, *Da* = 0.05 for (a) $\gamma_p = 0$ (b) $\gamma_p = 0.2$ (c) $\gamma_p = 0.4$ (d) $\gamma_p = 0.6$ (e) $\gamma_p = 0.8$ and (f) $\gamma_p = 1.0$.

6.4.3 Local Nusselt number

6.4.3.1 Comparison and Experimental Validation:

Table 6.1: A Comparison of the Present Values of Nu_{px} for Peclet number, Pe =100 for the Clear Fluid Channel ($\gamma_p = 0$) with the Values Available in the Literature [18].

X^*	0.002	0.008	0.02	0.04	0.125	0.2	0.3	0.4
Present	20.732	12.859	10.063	8.832	8.249	8.236	8.235	8.235
Shah and London [17]	19.113	12.604	9.988	8.803	8.246	8.235	8.235	8.235

A comparison of the present values of Nu_{px} for clear fluid channel($\gamma_p = 0$) with the values available in Shah and London [18] is given in Table 6.1. The present results shown in Table 6.1 are obtained for Pe . The agreement of the present values with the values in literature is good. A comparison of the present values of Nu_{px} for $\gamma_p = 1.0$ with the experimental results available in chapter 5 is also given in Fig. 5.7 of chapter 5 for the case of axial conduction neglected.

Variation of Nu_{px} with X^* for Darcy number, Da = 0.001 is shown in Figs. 6.6(a) to 6.6(f) for all porous fractions, γ_p = 0, 0.2, 0.4, 0.6, 0.8 and 1.0, for the different Peclet numbers, Pe. Similar plots are given in Figs. 6.7(a) to 6.7(f) for Darcy numbers, Da = 0.01. The trends in the variation of Nu_{px} with X^* for the channel partially filled with porous material are similar to the well reported trends for channels with clear fluid flow or channels fully filled with porous material. From Figs. 6.6(a) to 6.6(f) and Figs. 6.7(a) to 6.7(f), as Pe increases, Nu_{px} decreases with X^* for all porous fractions. As X^* increases, Nu_{px} decreases for all Peclet numbers and porous fractions. For all X^*, Nu_{px} is lower for higher Pe. The features that (i) Nu_{px} decreases as X^* increases and reaches the fully

developed values (ii) Nu_{px} is higher at lower Peclet numbers, (iii) Axial conduction effects are negligible for $Pe \geq 100$, are displayed. In addition, when $\gamma_p \neq 0$ or $\gamma_p \neq 1.0$, Nu_{px} tends to different constant values for large X^*. These values obviously differ from the fully developed values for the clear fluid channel and the channel fully filled with porous material. Further, it can be expected that the fully developed values of Nu_{px} depends on the porous fraction and Darcy number because of the coupling between the porous and clear fluid regions. It has been found that $Nu_{px} \rightarrow 8.2353$ for $Da > 0.1$, i.e., the channel behaves like a clear fluid channel.

Effect of Axial Conduction

The plots of Nu_{px} vs. X^* and Nu_{px} vs. X are shown in Figs. 6.8(a) and 6.8(b) for different Peclet numbers Pe = 5, 10, 25, 50, 100 and $A_c = 0$ for $Da = 0.05$ and $\gamma_p = 0.2$. Plots of Nu_{px} vs. X^* and Nu_{px} vs. X are shown in Figs. 6.9(a) and 6.9(b) for different Peclet numbers Pe = 5, 10, 25, 50, 100 and $A_c = 0$ for $Da = 0.05$ and $\gamma_p = 0.8$. From Figs. 6.8 and 6.9, Nu_{px}, increases as Pe decreases at a fixed X^*, whereas, Nu_{px} decreases as Pe decreases at a fixed $X = X^*.Pe$. This feature is similar to that followed by clear fluid channel.

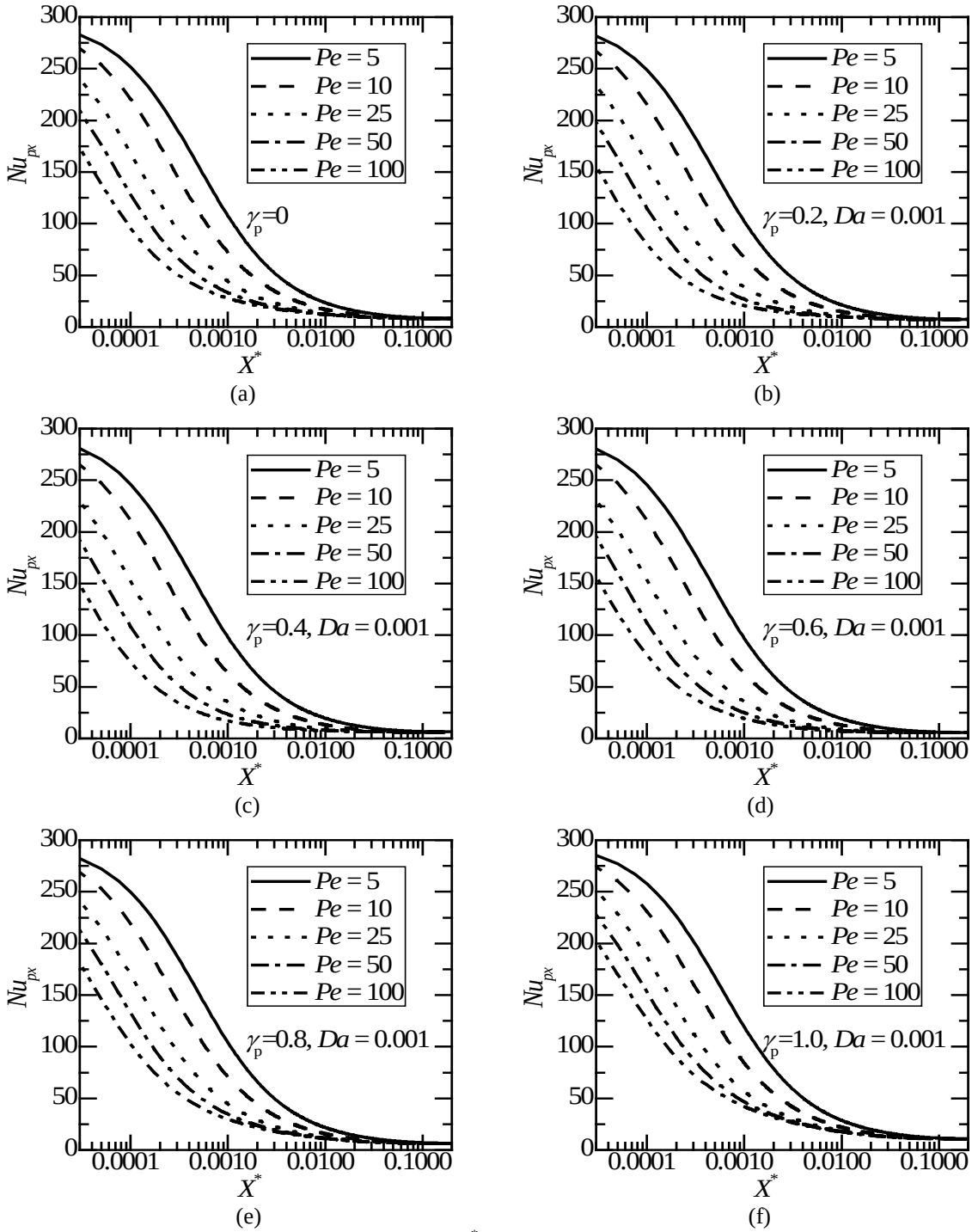

Fig. 6.6: Variation of Nusselt number, Nu_{px} with X^* values for different Peclet numbers, Pe and Da = 0.001 for (a) $\gamma_p = 0$ (b) $\gamma_p = 0.2$ (c) $\gamma_p = 0.4$ (d) $\gamma_p = 0.6$ (e) $\gamma_p = 0.8$ and (f) $\gamma_p = 1.0$.

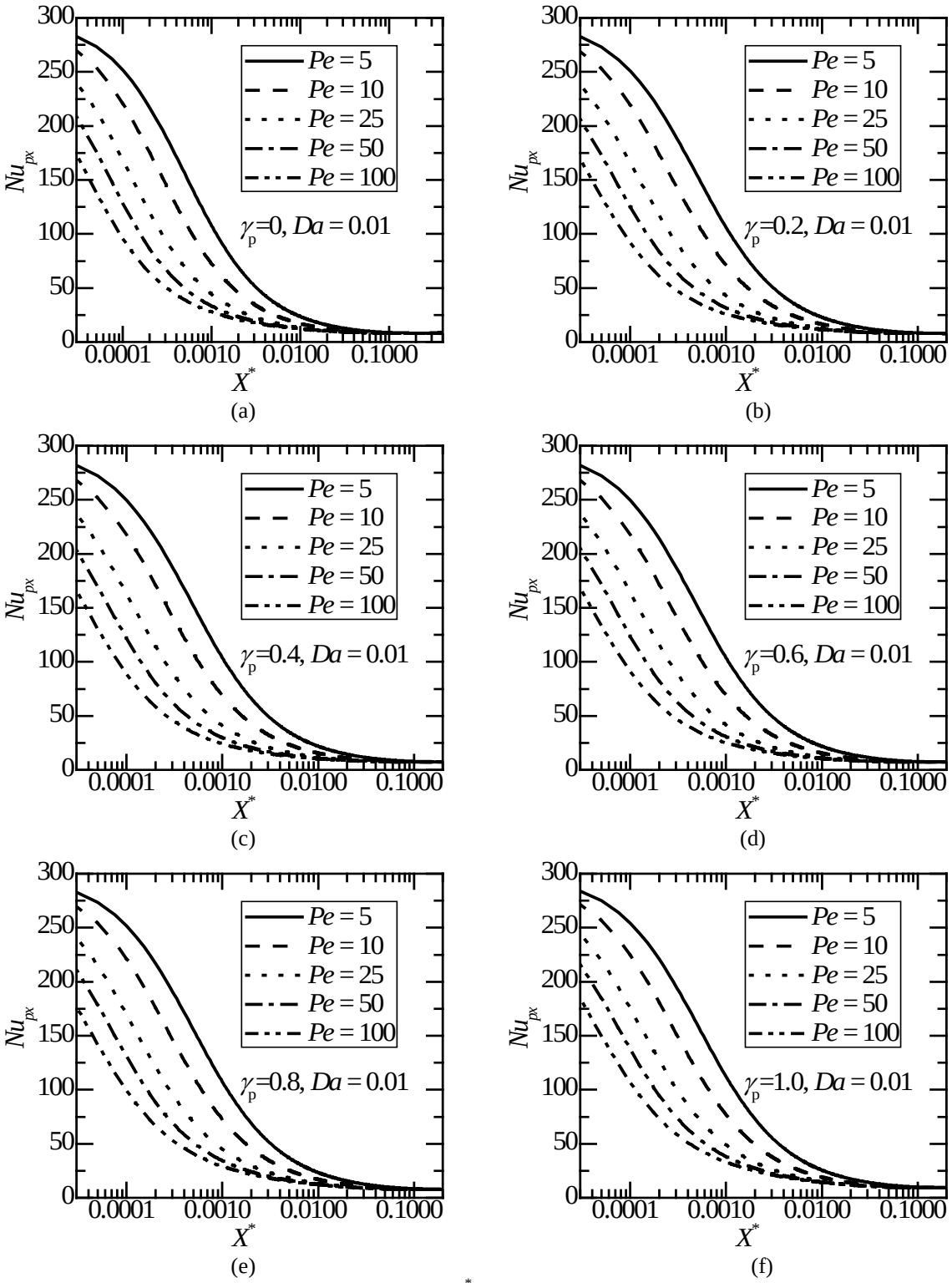

Fig. 6.7: Variation of Nusselt number, Nu_{px} with X^* values for different Peclet numbers, Pe and Da = 0.01 for (a) $\gamma_p = 0$ (b) $\gamma_p = 0.2$ (c) $\gamma_p = 0.4$ (d) $\gamma_p = 0.6$ (e) $\gamma_p = 0.8$ and (f) $\gamma_p = 1.0$.

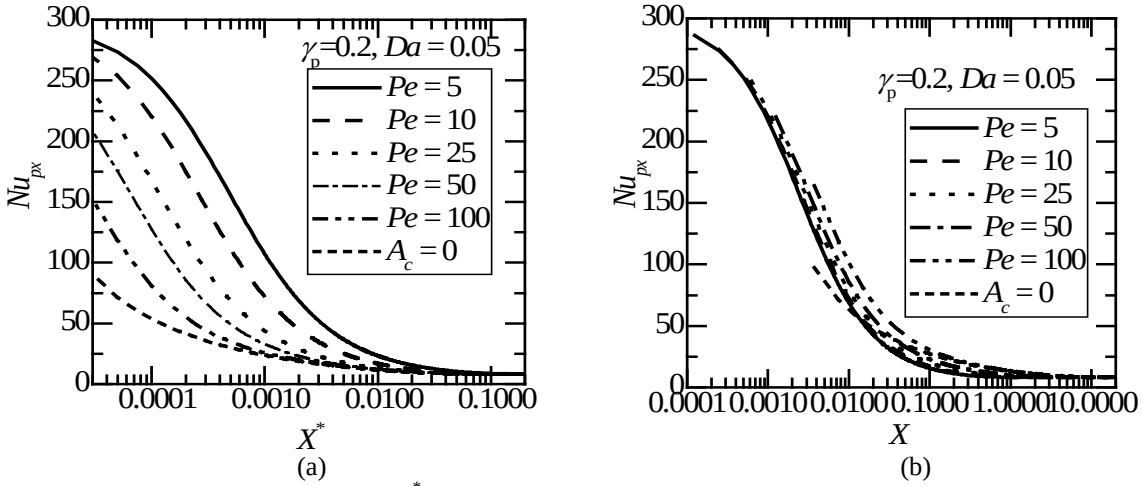

Fig. 6.8: Variation of (a) Nu_{px} vs. X^* (b) Nu_{px} vs. X for different Peclet numbers, Pe and Da = 0.05 for $\gamma_p = 0.2$.

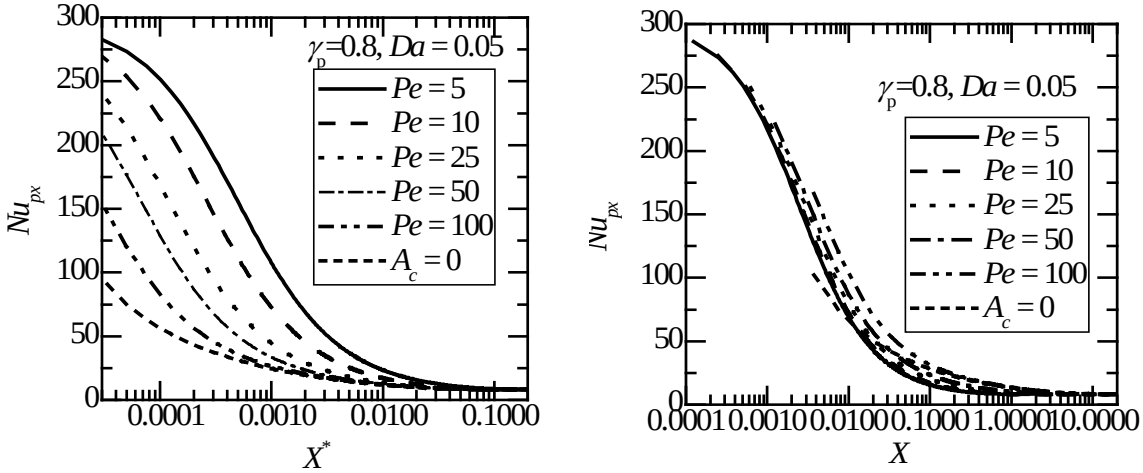

Fig. 6.9: Variation of (a) Nu_{px} vs. X^* (b) Nu_{px} vs. X for different Peclet numbers, Pe and Da = 0.05 for $\gamma_p = 0.8$.

To examine further, a plot of Nu_{px} with γ_p for different Da values at (a) X^* = 0.005, (b) X^* = 0.01, (c) X^* = 0.05 and (d) X^* = 0.1 for Pe = 5 and 50 are shown in Fig. 6.10 and Fig. 6.11 respectively.

It is clear from Figs. 6.10 and 6.11, that the variation of Nu_{px} with γ_p depends on *Da*. Nu_{px} clearly increases as *Da* increases when $\gamma_p < 0.8$, whereas for $\gamma_p > 0.8$, Nu_{px} decreases as *Da* increases. Nu_{px}, decreases as *Da* increases for $\gamma_p = 1.0$, becoming equal to the clear fluid channel value for large *Da*. This fact is observed in thesis of Bhargavi [186] for different channel geometry in Chapter 3. Also, Nu_{px} decreases as *Pe* increases with porous fraction, γ_p for all Darcy numbers. The minimum value of Nu_{px} depends on *Da* but is independent of *Pe* and X^*.

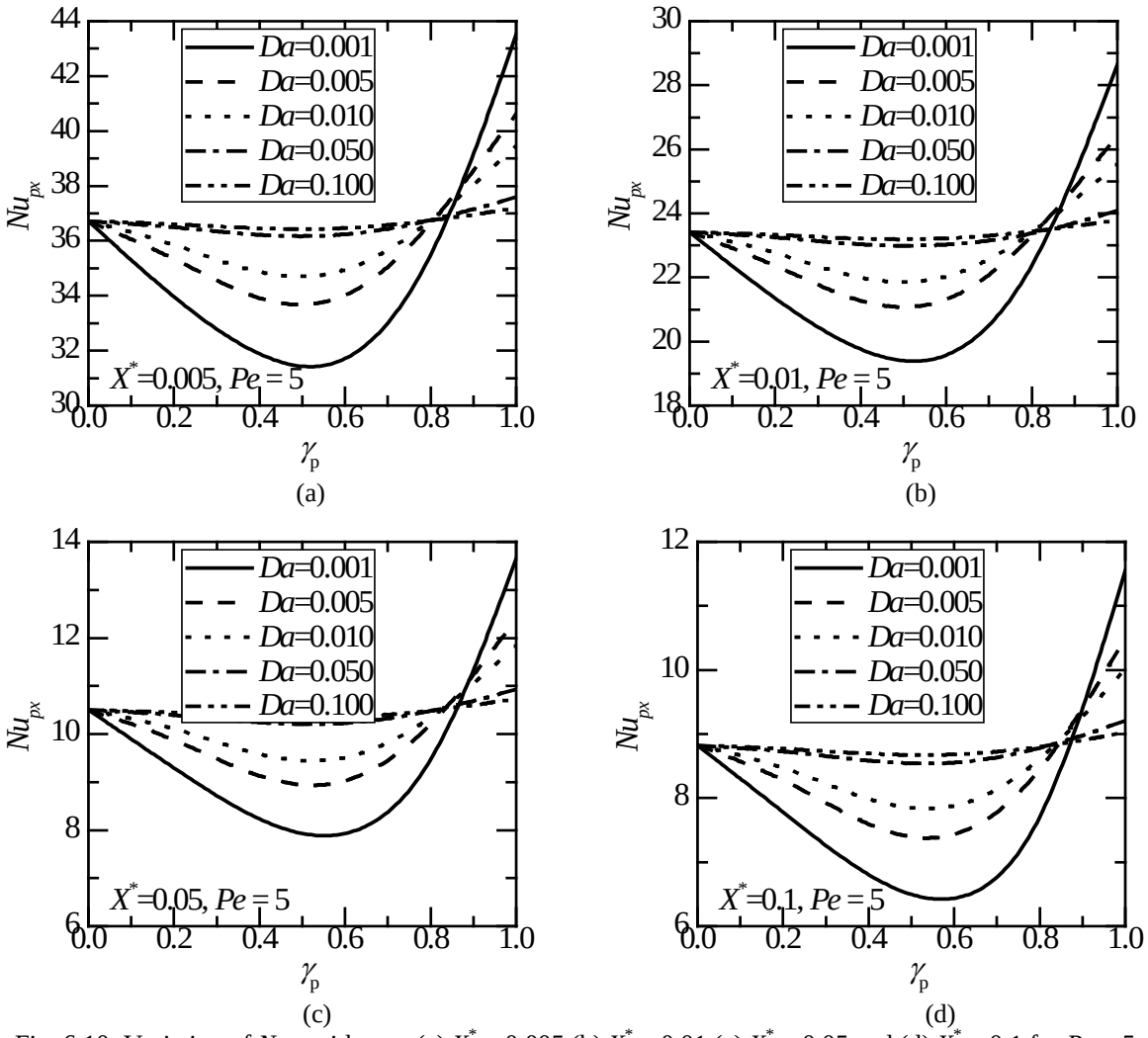

Fig. 6.10: Variation of Nu_{px} with γ_p at (a) $X^* = 0.005$ (b) $X^* = 0.01$ (c) $X^* = 0.05$ and (d) $X^* = 0.1$ for $Pe = 5$ at different Darcy numbers.

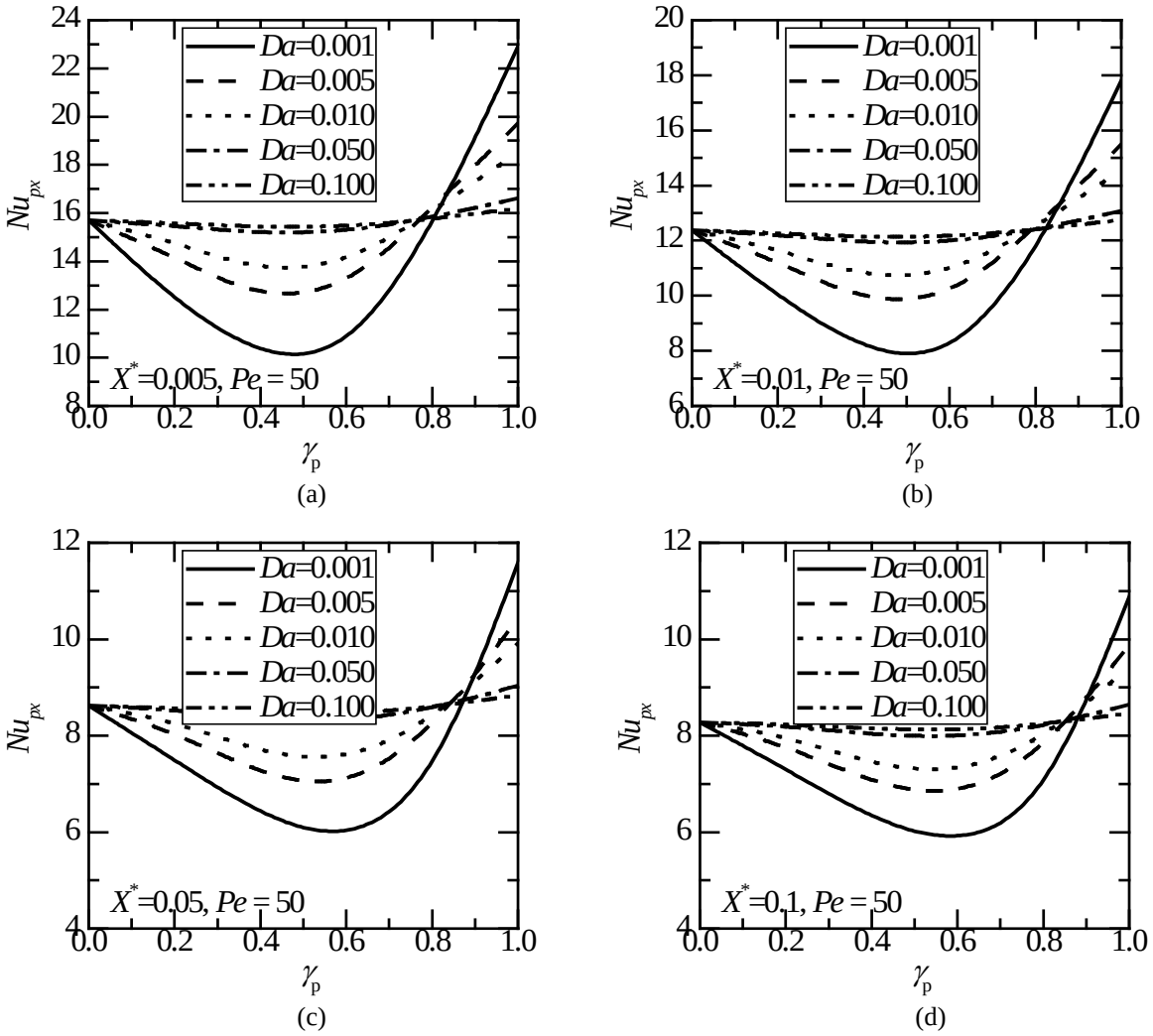

Fig. 6.11: Variation of Nu_{px} with γ_p at (a) $X^* = 0.005$ (b) $X^* = 0.01$ (c) $X^* = 0.05$ and (d) $X^* = 0.1$ for $Pe = 50$ at different Darcy numbers.

6.5 Conclusions

The effect of axial conduction in the thermally developing region of parallel plate channels partially filled with a porous material has been numerically studied. The parallel plates were subjected to constant heat flux. The flow field has been assumed to be fully developed. The problem is characterized by Darcy number, *Da*, Peclet number, *Pe*, and the porous fraction, γ_p. Numerical solutions have been obtained for $0 \leq \gamma_p \leq 1.0$, $5 \leq Pe \leq$

100 and Da = 0.001, 0.005, 0.01, 0.05 and 0.1, employing successive acceleration replacement (SAR) scheme (Ramjee and Satyamurty [15] Satyamurty and Bhargavi [158]). When axial conduction is neglected, Peclet number does not appear explicitly in the conservation of thermal energy equation expressed in terms of the normalized non-dimensional axial distance X^*.

It has been concluded that the non-dimensional temperature profiles become independent of the Peclet number for $Pe \geq 100$ indicating that the effect of axial conduction has become negligible. The downstream condition satisfied by the clear fluid ducts, $\partial\theta_b / \partial X^* \rightarrow 0$, has been found to be valid for parallel plate channels partially filled with porous material also. This feature assumes importance since the flow and thermal fields are not symmetric when the channel is partially filled with porous material. Non-dimensional bulk mean temperature excess of wall temperature, $\theta_w - \theta^*$, increases as X^* increases. $\theta_w - \theta^*$ decreases as Peclet number decreases. This indicates that a stronger axial conduction effect present at lower Peclet numbers makes the fluid get less heated or less cooled compared to when axial conduction is neglected.

The values of the local Nusselt numbers when the channel is a clear fluid channel agree well with the values available in Shah and London [18]. The local Nusselt number Nu_{px} decreases as X^* increases for all γ_p and then reaches as the fully developed values for $X^* \geq 0.4$. Similarly, Nu_{px} increases as Pe decreases for a given X^*. However, at a given X, Nu_{px} decreases as Pe decreases. For $Pe \geq 100$, the axial conduction effect becomes negligible except very close to entrance.

Nu_{px} is a minimum when $\gamma_p \approx 0.6$ at low $Da = 0.001$ increasing to $\gamma_p \approx 0.8$ when $Da = 0.1$. Nu_{px} attains a minimum almost independent of Peclet number and X^*. Thus, there exists an optimum porous fraction to attain deterioration in the Nusselt numbers. In the context of constant wall heat flux condition, this implies that transfer of a given heat flux takes place with higher temperature difference between the wall and the fluid in the present channel geometry.

Chapter 7

Effect of Viscous dissipation and Axial Conduction in the Thermally Developing Region of the Channel Partially Filled with a Porous Material Subjected to Constant Wall Heat Flux

7.1 Introduction

Studies on steady two-dimensional laminar forced convection in hydrodynamically developed and thermally developing flow between parallel plates partially filled with the porous material including viscous dissipation have been presented in this chapter. The channel walls have been kept at constant wall heat flux. The non-dimensional governing conservation of thermal energy equations {same as Eqs. (6.13) and (6.16) of Chapter 6} in the fluid and porous regions are elliptic when axial conduction is included. The non-dimensional temperature profiles in the conduction limit obtained in Chapter 4 are used as the downstream boundary condition needed to solve the governing equations.

In this chapter, numerical solutions to the governing conservation of thermal energy equation including dissipation and axial conduction in the fluid and porous regions have been obtained employing the SAR {Ramjee and Satyamurty[15] and Satyamurty and Bhargavi [158]} scheme. The solutions have been obtained with and without axial conduction terms for $0 \leq \gamma_p \leq 1.0$, $0.005 \leq Da \leq 0.01$, Pe = 5, 25, 100 and

$-1.0 \leq Br \leq 1.0$. The influence of dissipation at different porous fractions, Darcy numbers and Peclet numbers on local Nusselt numbers has been studied.

7.2 Mathematical Formulation

With reference to the physical model already described in Chapter 5 (Fig. 5.1, § 5.2), the governing equations in non-dimensional form for the temperature, including dissipation and axial conduction in the fluid and porous regions in non-dimensional form are given below. Two dissipation functions, i) due to Bejan [49] commonly referred to as, Darcy model and ii) due to Al-Hadhrami, Elliott and Ingham [135 and 136], referred to as, clear fluid comparable model have been evaluated. The assumptions are that $\varepsilon = \mu_f/\mu_{eff} = 1$ and $\eta = k_f / k_{eff} = 1$ have been made.

Governing Equations

In the present Chapter effects of axial conduction (F_1) and viscous dissipation(F_2) effects are considered. i.e $F_1 = 1$ and $F_2 = 1$. Substituting, $F_1 = 1$ and $F_2 = 1$ in Eqs. (5.2) and (5.4) of Chapter 5 § 5.2, then the conservation of thermal energy equations in fluid and porous regions respectively, given by,

Fluid Region:

$$\rho C_p u_f \frac{\partial T_f}{\partial x} = k_f \left(\frac{\partial^2 T_f}{\partial x^2} + \frac{\partial^2 T_f}{\partial y^2} \right) + \mu_f \left(\frac{du_f}{dy} \right)^2 \qquad (7.1)$$

In Eq. (7.1), T_f is the temperature in the fluid region ρ, C_p and k_f are the density, the specific heat and the thermal conductivity of the fluid respectively.

Porous Region:

$$\rho C_p u_p \frac{\partial T_p}{\partial x} = k_{eff}\left(\frac{\partial^2 T_p}{\partial x^2} + \frac{\partial^2 T_p}{\partial y^2}\right) + \Phi_i \tag{7.2}$$

In Eq. (7.2), Φ_i is dissipation model, for i = 1, the Darcy model due to Bejan [49], for i = 2, clear fluid compatible model due to Al-Hadhrami et al. [135 and 136] given by,

Darcy model:

$$\Phi_1 = \frac{\mu_f}{K} u_p{}^2 \tag{7.3}$$

Clear fluid compatible model:

$$\Phi_2 = \frac{\mu_f}{K} u_p{}^2 + \mu_f \left(\frac{du_p}{dy}\right)^2 \tag{7.4}$$

In Eq. (7.2), T_p is the temperature in the porous region and k_{eff} is the effective thermal conductivity of the porous medium. k_{eff} can be calculated from Catton [21] as,

$$k_{eff} = (1-\varphi)\, k_s + \varphi\, k_f \tag{7.5}$$

In Eq. (7.5), φ is the porosity and k_s is the thermal conductivity of the solid in the porous matrix.

B**oundary and Interfacial Conditions**

$$u_p = 0 \quad , \quad -k_{eff}\frac{\partial T_p}{\partial y} = q \quad \text{at} \quad y = -H/2 \tag{7.6}$$

$$u_f = u_p = u_i \quad , \quad \mu_{eff}\frac{du_p}{dy} = \mu_f \frac{du_f}{dy} \qquad \text{at interface} \quad y = -\frac{H}{2} + \frac{l_p}{2} \tag{7.7}$$

$$T_f = T_p = T_i, \qquad k_f\left(\partial T_f / \partial y\right) = k_{eff}\left(\partial T_p / \partial y\right) \qquad \text{at interface} \quad y = -\frac{H}{2} + \frac{l_p}{2} \tag{7.8}$$

$$\frac{du_f}{dy} = 0, \frac{\partial T_f}{\partial y} = 0 \quad \text{at} \quad y = 0 \quad \{\text{Symmetry boundary conditions}\} \tag{7.9}$$

Inlet condition is:

$$T_p = T_e \qquad \text{at} \qquad x = 0\ , \quad -\frac{H}{2} \le y \le -\frac{H}{2} + \frac{l_p}{2} \tag{7.10}$$

$$T_f = T_e \qquad \text{at} \qquad x = 0\ , \quad -\frac{H}{2} + \frac{l_p}{2} \le y \le 0 \tag{7.11}$$

$$\frac{\partial}{\partial x}\left(\frac{T - T_w}{T_b - T_w}\right) = 0 \text{ at } -\frac{H}{2} \le y \le \frac{H}{2} \ \{\text{downstream condition}\} \tag{7.12}$$

Non-dimensionalization

Governing equations {Eqs. (7.1) and (7.2)} are rendered non-dimensional by introducing the following non-dimensional variables.

$$\left.\begin{aligned} &X = x/H\ , \qquad Y = y/H\ , \qquad U_f = u_f / u_{ref}\ , \qquad U_i = u_i / u_{ref}\ , \quad U_p = u_p / u_{ref}\ , \\ &P = p/\rho\, u_{ref}^2\ , \theta_f = (T_f - T_e)/(qH/k_f)\ , \theta_p = (T_p - T_e)/(qH/k_f) \end{aligned}\right\} \tag{7.13}$$

In Eq. (7.13), *X* and *Y* are the non-dimensional coordinates. *U* and *P* are non-dimensional velocity, and pressure. The subscripts *f* and *p* refer to fluid and porous regions. θ,{ θ_f in the fluid region and θ_p in the porous region}, is the non-dimensional temperature. u_{ref} is the average velocity through the channel. u_{ref} is related to u_p and u_f by,

$$\frac{2}{H}\left[\int_{-H/2}^{-\frac{H}{2}+\frac{l_p}{2}} u_p dy + \int_{-\frac{H}{2}+\frac{l_p}{2}}^{0} u_f dy\right] = u_{ref} \tag{7.14}$$

In addition, the non-dimensional porous layer thickness γ_p, which shall be referred to as porous fraction is defined by,

$$\gamma_p = l_p / H \tag{7.15}$$

when the channel walls are subjected to constant heat flux. Peclet number can be absorbed by defining

$$X^* = X / Pe \tag{7.16}$$

On introducing the non-dimensional variables given by Eq. (7.13), the governing equations for energy applicable in the fluid {Eq. (7.1)}and porous {Eq. (7.2) } regions in non-dimensional form become,

Fluid Region

$$U_f \frac{\partial \theta_f}{\partial X^*} = \frac{1}{Pe^2}\frac{\partial^2 \theta_f}{\partial X^{*2}} + \frac{\partial^2 \theta_f}{\partial Y^2} + Br\left(\frac{dU_f}{dY}\right)^2 \tag{7.17}$$

In Eq. (7.17), *Pe*, Peclet number and *Br*, Brinkman number are defined by,

$$Pe = u_{ref} H / \alpha_f,\ Br = \mu_f {u_{ref}}^2 / qH \tag{7.18}$$

when $Br > 0$ implies that, the fluid is getting cooled while $Br < 0$ represents the fluid is getting heated.

Porous Region

$$U_p \frac{\partial \theta_p}{\partial X^*} = \frac{1}{\eta}\left(\frac{1}{Pe^2} \frac{\partial^2 \theta_p}{\partial X^{*2}} + \frac{\partial^2 \theta_p}{\partial Y^2} \right) + \Psi_i \tag{7.19}$$

In Eq. (7.19) , Ψ_i is non-dimensional dissipation model given by,

Darcy model:

$$\Psi_1 = \frac{Br}{Da} U_p{}^2 \tag{7.20}$$

Clear fluid compatible model :

$$\Psi_2 = Br \left[\frac{U_p{}^2}{Da} + \left(\frac{dU_p}{dY} \right)^2 \right] \tag{7.21}$$

In Eq. (7.19) , ε and η are defined by,

$$\eta = k_f / k_{eff} \tag{7.22}$$

Non-dimensional Boundary Conditions

The boundary and interfacial conditions given by Eqs.(7.6) to (7.12) assume the following non-dimensional form (using Eq.(7.13))

$$\frac{dU_f}{dY} = 0, \frac{\partial \theta_f}{\partial Y} = 0 \quad \text{at} \quad Y = 0 \tag{7.23}$$

$$U_f = U_p = U_i, \quad \frac{dU_f}{dY} = \frac{1}{\varepsilon} \frac{dU_p}{dY} \quad \text{at the interface} \quad Y = -\frac{1}{2} + \frac{\gamma_p}{2} \tag{7.24}$$

$$\theta_f = \theta_p = \theta_i, \quad \frac{\partial \theta_f}{\partial Y} = \frac{1}{\eta} \frac{\partial \theta_p}{\partial Y} \quad \text{at the interface} \quad Y = -\frac{1}{2} + \frac{\gamma_p}{2} \tag{7.25}$$

$$U_p = 0\,, \quad \frac{\partial \theta_p}{\partial Y} = -\eta \quad \text{at} \quad Y = -1/2 \tag{7.26}$$

Inlet conditions

$$\theta_p(0,Y) = 0 \quad \text{for} \quad -\frac{1}{2} \le Y \le -\frac{1}{2} + \frac{\gamma_p}{2} \tag{7.27}$$

$$\theta_f(0,Y) = 0 \quad \text{for} \quad -\frac{1}{2} + \frac{\gamma_p}{2} \le Y \le 0 \tag{7.28}$$

$$\frac{\partial \theta_b}{\partial X^*} = 0 \Rightarrow \frac{\partial \theta_{f,p}}{\partial X^*} = \frac{\theta_{f,p}}{\theta^*}\frac{\partial \theta^*}{\partial X^*} \text{ at } X^* \ge X^*_{fd} \text{ for -1/2} \le Y \le 1/2 \tag{7.29}$$

In Eq. (7.29), θ_b is the non-dimensional temperature based on the bulk mean temperature defined by

$$\theta_b = \frac{T - T_e}{T_b - T_e} = \frac{\theta}{\theta^*} \tag{7.30}$$

7. 3 Numerical Scheme: Successive Accelerated Replacement (SAR)

In order to obtain numerical solutions to Eqs. (7.17) and (7.19), as per the SAR [15 and 158] scheme, (described in § 6.3 of Chapter 6 in detail), the required finite difference expressions and the derivatives have been written similar to Eqs. (6.13) and (6.16) of Chapter 6, § 6.3, with the additional terms arising due to viscous dissipation, associated with the Brinkman number, *Br* in Eqs. (7.17) and (7.19). The number of grids in the axial and normal directions, *MD* and *ND* have been chosen as 1000 and 90 respectively as

indicated in Chapter 5. The axial distance needed X^*_{CL} for the thermal field to reach the conduction limit, has been divided into *MD* divisions. ΔX^*_M , the non-uniform grid in the axial direction has been generated according to Eq. (5.50), § 5.3.3 of Chapter 5 and ΔY = 1/*ND*. Further, the error tolerance limit, $\varepsilon_t = 10^{-5}$ and acceleration factor as per Eqs. (5.53) and (5.54), § 5.3.3, have been factored in the equation.

Eqs. (2.26) and (2.29), § 2.3.1, Chapter 2 have been used to calculate the fully developed velocities in the fluid and porous regions. Numerical solutions have been obtained for, $0.001 \leq Da \leq 1.0$, γ_p = 0, 0.2, 0.4, 0.6, 0.8 and 1.0, $-1.0 \leq Br \leq 1.0$ and *Pe* = 5, 50, 100 and neglecting axial conduction (designated by $A_c = 0$) for the two dissipation models, [49, 135 and 136]. The number of combinations of the parameters is very high; detailed computations have been performed and the results are available with the researcher. However, only select results that are needed to bring out the features arising out of including viscous dissipation have been included.

7. 4 Result and Discussion

7.4.1 Channel fully filled with porous medium

Non-dimensional temperature Profiles

The influence of viscous dissipation can be evaluated using non-dimensional temperature in excess of wall temperature, $\theta_w - \theta_p$ profiles available in Chapter 6, § 6.4.1, {e.g., Fig. 6.1(f) and Fig. 6.2(f)} with the profiles obtained in the present chapter with the two different dissipation models.

Non-dimensional temperature in excess of wall temperature, $\theta_w - \theta_p$ profiles for Da = 0.005 and $\gamma_p = 1.0$ at different axial locations, X^* for (a) $Br = -0.5$ and (b) $Br = 0.5$ for the Darcy model are shown in Fig. 7.1 for Pe = 5 and in Fig. 7.2 for Pe = 100 respectively. Similarly, Non-dimensional temperature in excess of wall temperature, $\theta_w - \theta_p$ profiles for Da = 0.005 and $\gamma_p = 1.0$ at different X^* for (a) $Br = -0.5$ and (b) $Br = 0.5$ for the clear fluid compatible model are shown in Fig. 7.3 for Pe = 5 and in Fig. 7.4 for Pe = 100 respectively.

The non-dimensional temperature in excess of wall temperature, $\theta_w - \theta_p$ profiles for γ_p = 1.0 obtained using Darcy model [49] given in Figs. 7.1 and 7.2 {Eq. (7.20) applied for $-0.5 \leq Y \leq 0$ because of symmetry of the channel} are not similar to those shown in Figs. 7.3 and 7.4 for clear fluid compatible model [135 and 136]{Eq. (7.21)}. The difference in the $\theta_w - \theta_p$ profiles for the two dissipation models can be found even when Da is high. The difference in the profiles shown in Figs. 7.1, 7.2 and Figs. 7.3, 7.4 emerge from the dissipation function employed, for the Darcy model and the clear fluid compatible model.

It is clear that Pe = 5 (lowest of the values computed) represents the strongest axial conduction effect while Pe = 100, shows almost negligible axial conduction effect.

On examining Figs. 7.1 and 7.2 for the Darcy model and Figs. 7.3 and 7.4 for clear fluid compatible model, the following conclusions emerge by comparing $\left(\theta_w - \theta_p\right)_{Br\neq 0}$ with $\left(\theta_w - \theta_p\right)_{Br=0}$ {Chapter 6},

$$\left(\theta_w - \theta_p\right)_{Br<0} > \left(\theta_w - \theta_p\right)_{Br=0} \quad \text{and} \quad \left(\theta_w - \theta_p\right)_{Br>0} < \left(\theta_w - \theta_p\right)_{Br=0} \tag{7.31}$$

The relation given in Eq. (7.31) is satisfied for Darcy model.

$$\left(\theta_w - \theta_p\right)_{Br<0} < \left(\theta_w - \theta_p\right)_{Br=0} \quad \text{and} \quad \left(\theta_w - \theta_p\right)_{Br>0} > \left(\theta_w - \theta_p\right)_{Br=0} \tag{7.32}$$

The relation given in Eq. (7.32) is satisfied for clear fluid compatible model.

The limiting value of $\left(\theta_w - \theta_p\right)_{Br\neq 0}$, i.e., $\left(\theta_w - \theta_{p,CL}\right)_{Br\neq 0}$ {given in Chapter-4, Eqs.(4.67), (4.69)} and the values of $\left(\theta_w - \theta_p\right)_{Br\neq 0}$ at the entry region of the channel, depend on the Brinkman number for both the dissipation models. As per our definition, $Br > 0$ represents fluid getting cooled and dissipation prevents the fluid from cooling down to wall temperature, leaving $\left(\theta_w - \theta_p\right)_{Br>0} < 0$. Similarly when $Br < 0$, the fluid is getting heated and the fluid exceeds the wall temperature making $\left(\theta_w - \theta_p\right)_{Br<0} > 0$ for the Darcy model. Whereas, in the case of clear fluid compatible dissipation model, $\left(\theta_w - \theta_p\right)_{Br>0} > 0$ for $Br > 0$ and $\left(\theta_w - \theta_p\right)_{Br<0} < 0$ for $Br < 0$.

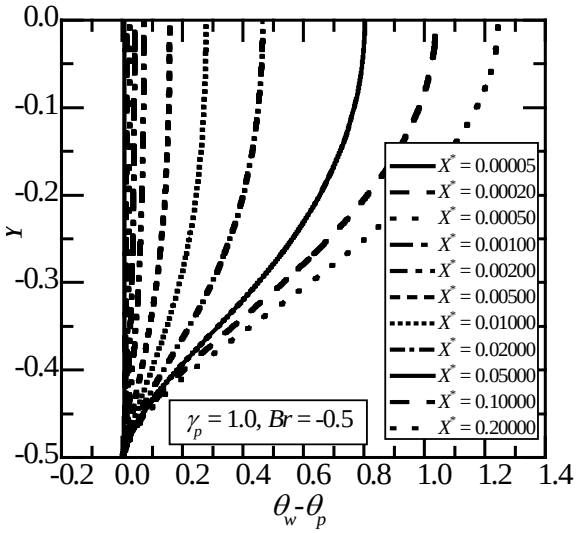

(a)

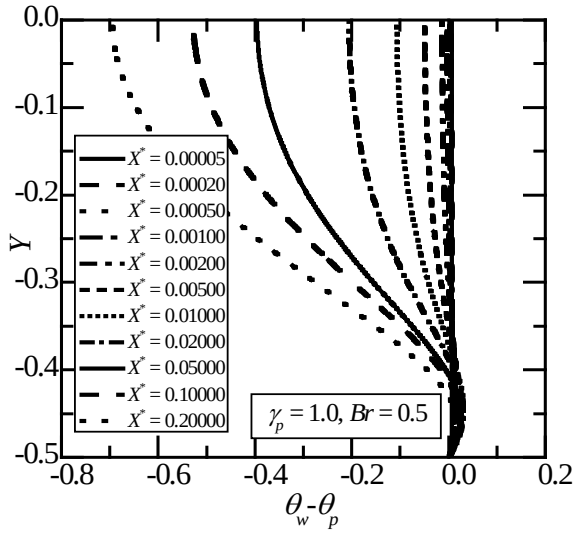

(b)

Fig. 7.1: Variation of non-dimensional temperature excess of wall temperature $\theta_w - \theta_p$ profiles for Da = 0.005 and $\gamma_p = 1.0$ for Pe = 5 at different X^* for (a) $Br = -0.5$ and (b) $Br = 0.5$ for Darcy model.

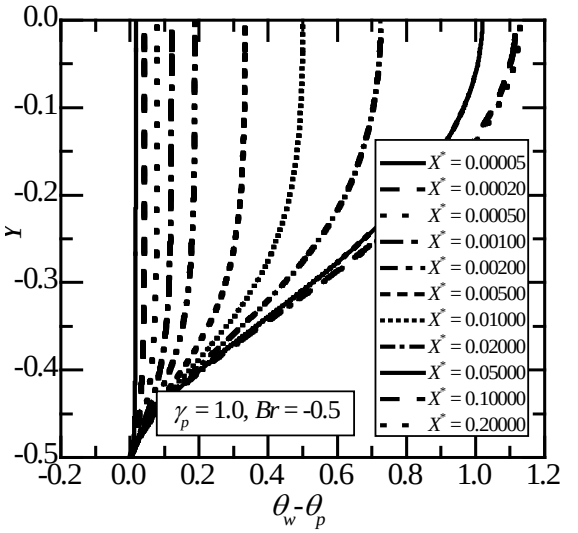

(a)

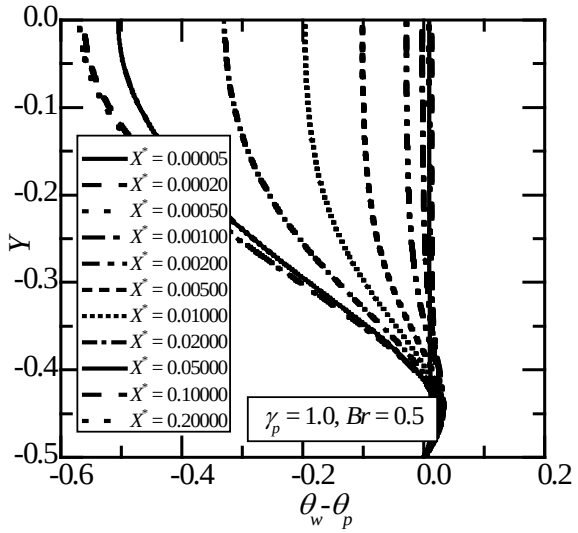

(b)

Fig. 7.2: Variation of non-dimensional temperature excess of wall temperature $\theta_w - \theta_p$ profiles for Da = 0.005 and $\gamma_p = 1.0$ for Pe = 100 at different X^* for (a) $Br = -0.5$ and (b) $Br = 0.5$ for Darcy model.

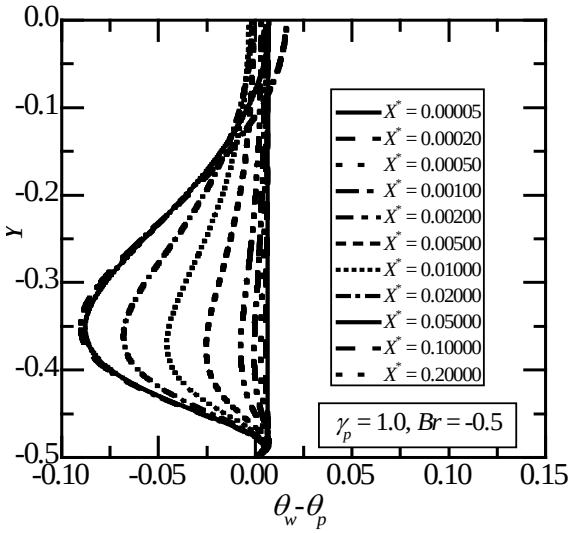

(a)

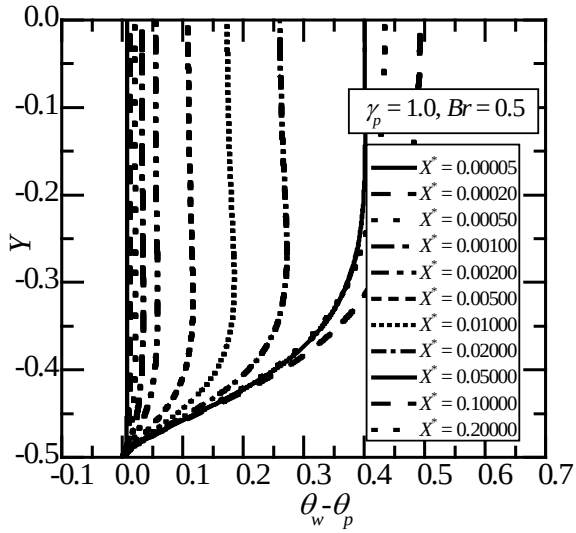

(b)

Fig. 7.3: Variation of non-dimensional temperature excess of wall temperature $\theta_w - \theta_p$ profiles for *Da* = 0.005 and $\gamma_p = 1.0$ for *Pe* = 5 at different X^* for (a) $Br = -0.5$ and (b) $Br = 0.5$ for the clear fluid compatible model.

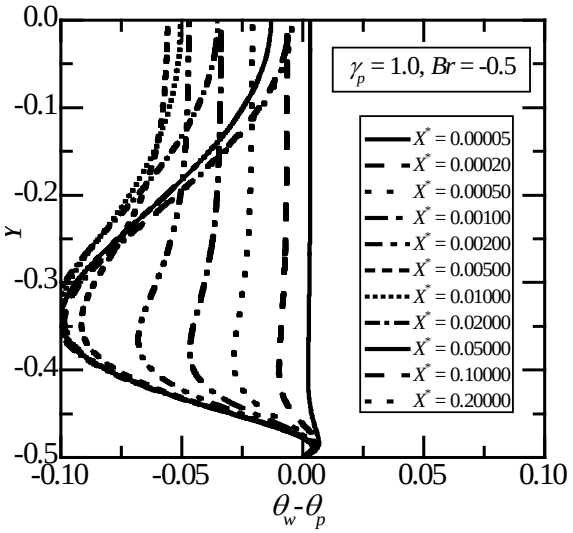

(a)

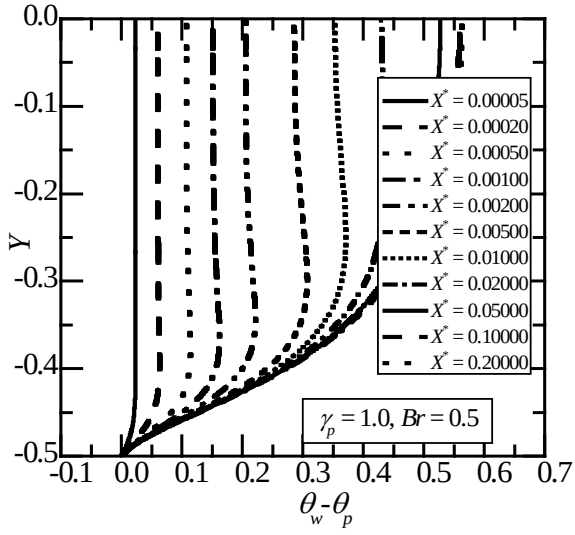

(b)

Fig. 7.4: Variation of non-dimensional temperature excess of wall temperature $\theta_w - \theta_p$ profiles for *Da* = 0.005 and $\gamma_p = 1.0$ for *Pe* = 100 at different X^* for (a) $Br = -0.5$ and (b) $Br = 0.5$ for the clear fluid compatible model.

Plots of $\theta_w - \theta_p$ vs. *Br* are shown in Fig. 7.5 for (a) Darcy model (b) clear fluid compatible model for *Pe* = 5, when axial conduction has been included at X^* = 0.0005 for different *Y* = -0.4, -0.3, -0.2, -0.1 and 0.0 for *Da* = 0.005 for γ_p = 1.0. From Fig. 7.5, $\theta_w - \theta_p$ does vary linearly with *Br* for both the models. This fact is also true when axial conduction is neglected.

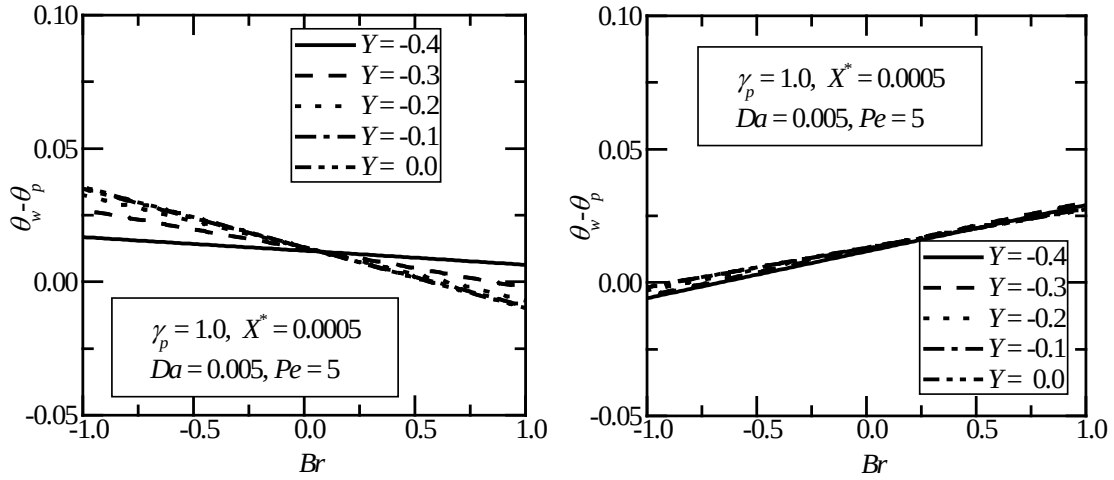

(a) Darcy model (b) Clear fluid compatible model

Fig.7.5 : Variation of non-dimensional temperature excess of wall temperature $\theta_w - \theta_p$ profiles vs. *Br* for *Da* = 0.005 and $\gamma_p = 1.0$ for *Pe* = 5 at X^* = 0.0005 for (a) the Darcy model and (b) the clear fluid compatible model

Local Nusselt number

Variation of local Nusselt number with X^* for (a) $Br \leq 0$ and (b) $Br \geq 0$ for the Darcy model and the clear fluid compatible model are shown in Fig. 7.6 and Fig. 7.7 respectively for *Da* = 0.005 when the axial conduction is neglected (A_c = 0).

From Figs. 7.6 and 7.7, it is apparent that Nu_{px} displays an unbounded swing for *Br* > 0 at, say, X^*_{sw} for the Darcy model. On the other hand for the clear fluid compatible model, Nu_{px} displays an unbounded swing for *Br* < 0 at X^*_{sw}. Nu_{px} displays an unbounded swing since the bulk mean temperature reaches the wall temperature and

exceeds it because of viscous dissipation . This fact is the same in case of the clear fluid channels ($\gamma_p = 0$) . This fact is reported for $\gamma_p = 0$ when channel walls are subjected to constant temperature {Ramjee and Satyamurty[182] and Jagadeesh kumar [190]}. Also, Nu_{px}, increases as Br increases for the Darcy model when $Br \leq 0$. Whereas, Nu_{px}, decreases as Br increases for the clear fluid compatible model when $Br \geq 0$.

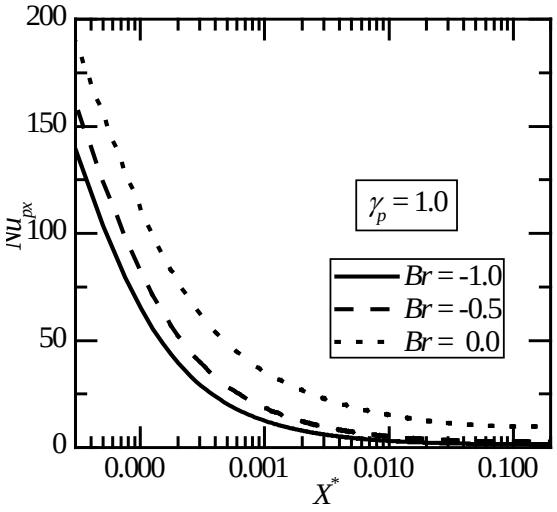

Fig. 7.6: Variation of local Nusselt number with X^* for $\gamma_p = 1.0$ and Da = 0.005 for (a) $Br \leq 0$ (b) $Br \geq 0$ for Darcy model when axial conduction neglected(A_c = 0).

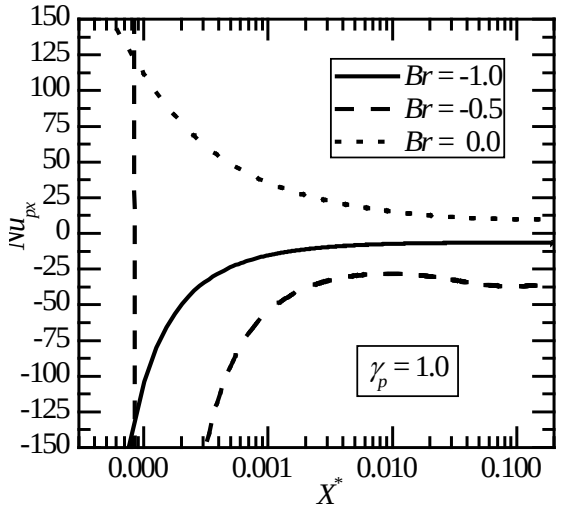

Fig. 7.7: Variation of local Nusselt number with X^* for $\gamma_p = 1.0$ and Da = 0.005 for (a) $Br \leq 0$ (b) $Br \geq 0$ for clear fluid compatible model when axial conduction neglected(A_c = 0).

Variation of local Nusselt number with X^* for Da = 0.005 and $\gamma_p = 1.0$ for different Peclet numbers, Pe = 5, 25 and 100 for (a) $Br = -0.5$ and (b) $Br = 0.5$, are shown in Fig. 7.8 and Fig. 7.9 for the Darcy model and the clear fluid compatible model respectively.

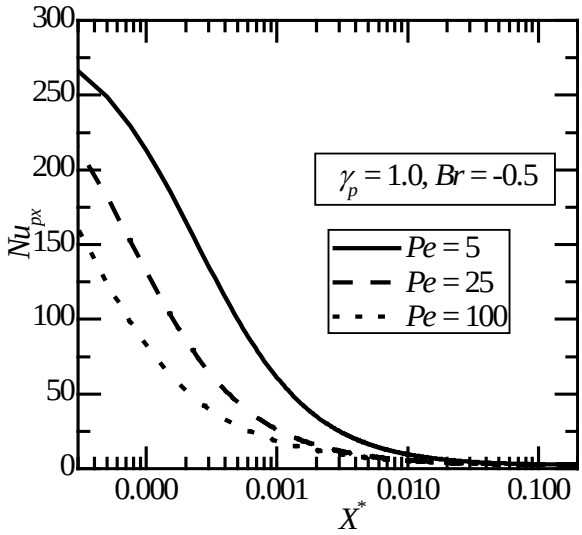

(a)

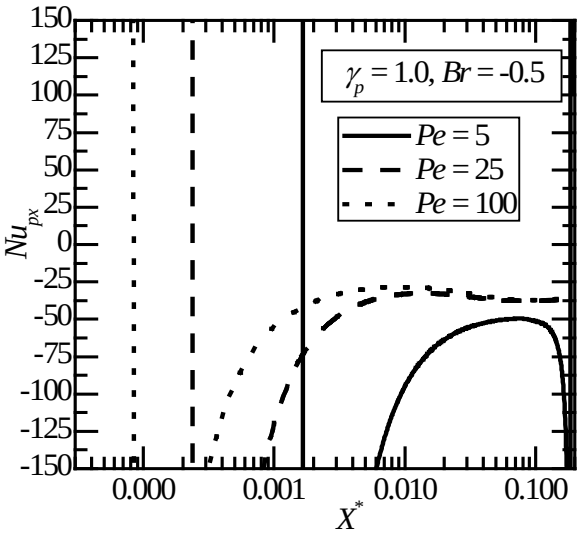

(a)

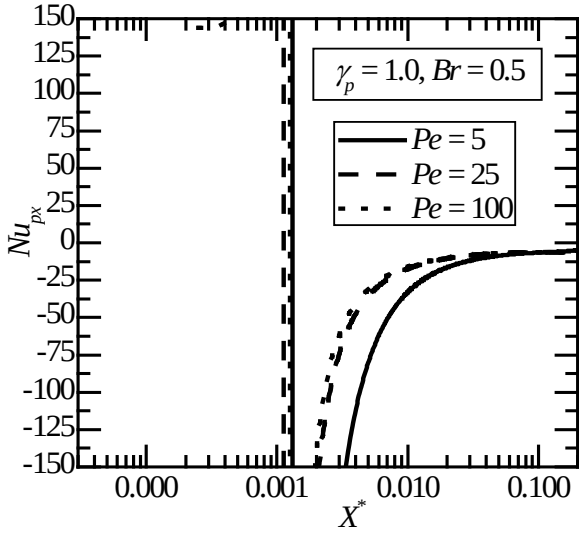

(b)

Fig. 7.8: Variation of local Nusselt number with X^* for Da = 0.005 for different Peclet numbers, Pe at (a) $Br = -0.5$ (b) $Br = 0.5$ for Darcy model.

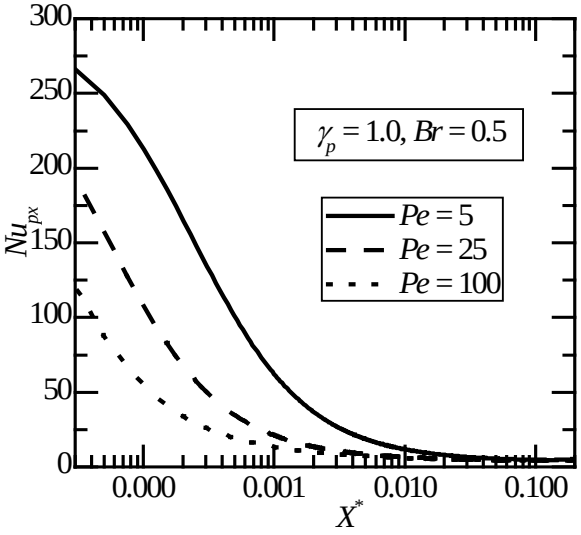

(b)

Fig. 7.9: Variation of local Nusselt number with X^* for Da = 0.005 for different Peclet numbers, Pe at (a) $Br = -0.5$ (b) $Br = 0.5$ for the clear fluid compatible model.

From Fig. 7.8 and Fig. 7.9, Nu_{px} displays an unbounded swing, X^*_{sw} for $Br > 0$ for Darcy model. Whereas, for the clear fluid compatible model, Nu_{px} displays an unbounded swing, X^*_{sw} for $Br < 0$. For both the models, at low Peclet number, the value of the X^*_{sw} is high. Also Nu_{px}, decreases as *Pe* increases for Darcy model when $Br < 0$. But for the clear fluid compatible model, Nu_{px}, decreases as *Pe* increases when $Br > 0$. This model is consistent with the clear fluid channel in the behavior of Nusselt number with X^* for all *Da* and *Pe*.

7.4.2 Channel Partially filled with porous medium

Non-dimensional temperature profiles

Non-dimensional temperature excess of wall temperature profiles, $\theta_w - \theta_p, \theta_w - \theta_f$, for $Da = 0.005$, $Pe = 5$ and $Br = -0.5,\ 0,\ 0.5$ at $X^* = 0.005$ for (a) $\gamma_p = 0.2$ and (b) $\gamma_p = 0.8$ are shown in Fig. 7.10 and Fig. 7.11 for the Darcy and the clear fluid compatible model respectively.

On examining Figs. 7.10(a) and 7.10(b) for the Darcy model and Figs. 7.11(a) and 7.11(b) for the clear fluid compatible model, the following conclusions emerge by comparing $\left(\theta_w - \theta_{f,p}\right)_{Br\neq 0}$ with $\left(\theta_w - \theta_{f,p}\right)_{Br=0}$ {Chapter 6},

$$\left(\theta_w - \theta_{f,p}\right)_{Br<0} < \left(\theta_w - \theta_{f,p}\right)_{Br=0} \quad \text{and} \quad \left(\theta_w - \theta_{f,p}\right)_{Br>0} > \left(\theta_w - \theta_{f,p}\right)_{Br=0} \qquad (7.33)$$

$$\left(\theta_w - \theta_{f,p}\right)_{Br<0} > \left(\theta_w - \theta_{f,p}\right)_{Br=0} \quad \text{and} \quad \left(\theta_w - \theta_{f,p}\right)_{Br>0} < \left(\theta_w - \theta_{f,p}\right)_{Br=0} \qquad (7.34)$$

The relations given in Eqs. (7.33) and (7.34) are valid for all porous fraction in the fluid region and porous regions respectively for both the models.

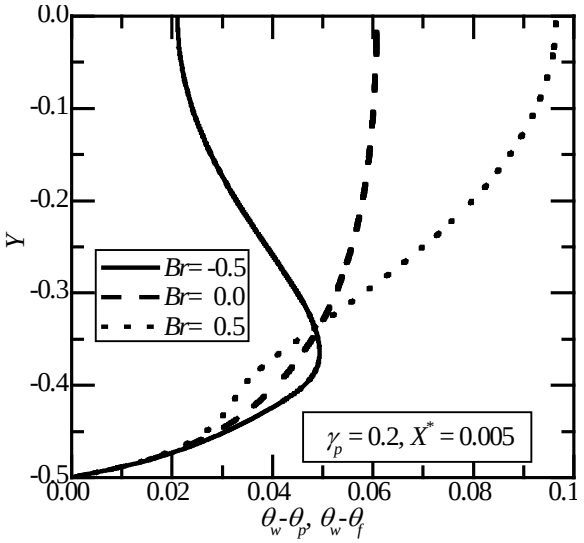

(a)

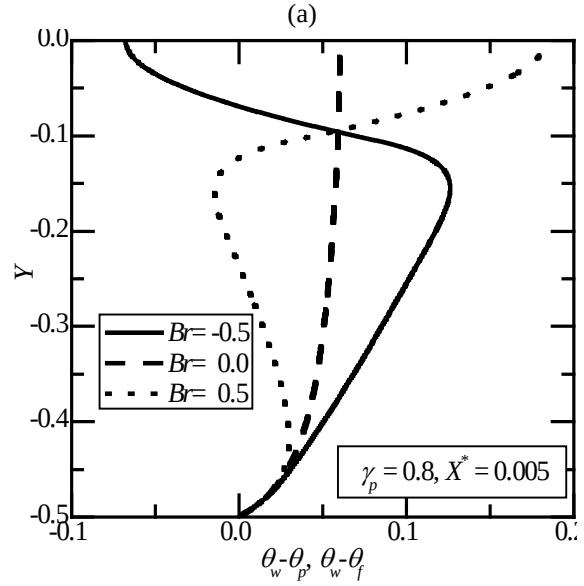

(b)

Fig. 7.10: Variation of non-dimensional temperature excess of wall temperature $\theta_w - \theta_p, \theta_w - \theta_f$ profiles for *Da* = 0.005, *Pe* = 5 and $Br = -0.5,\ 0,\ 0.5$ at X^* = 0.005 for (a) $\gamma_p = 0.2$ and (b) $\gamma_p = 0.8$ for Darcy model.

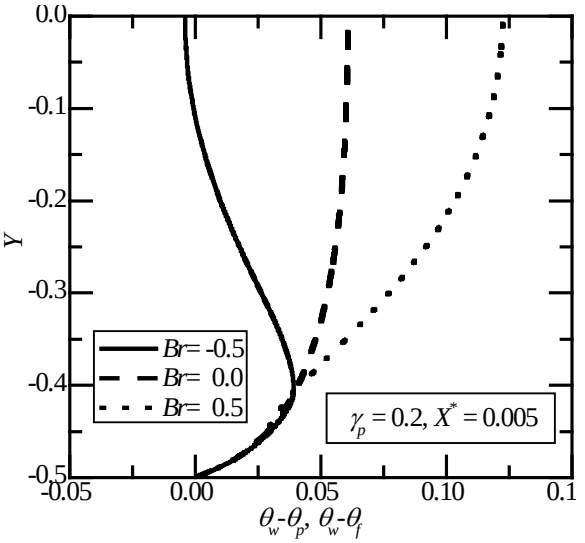

(a)

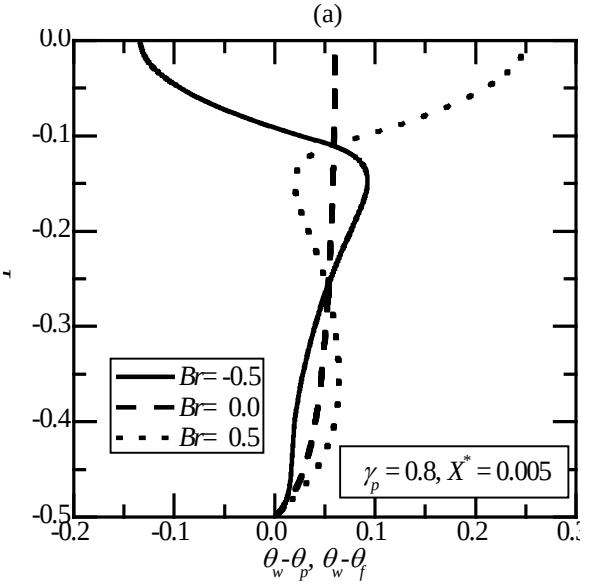

(b)

Fig. 7.11: Variation of non-dimensional temperature excess of wall temperature $\theta_w - \theta_p, \theta_w - \theta_f$ profiles for *Da* = 0.005, *Pe* = 5 and $Br = -0.5,\ 0,\ 0.5$ at X^* = 0.005 for (a) $\gamma_p = 0.2$ and (b) $\gamma_p = 0.8$ for the clear fluid compatible model.

Plots of $\theta_w - \theta_{f,p}$ vs. *Br* are shown in Fig. 7.12 for the Darcy model and Fig. 7.13 for the clear fluid compatible model for *Pe* = 5, when axial conduction has been included at X^* = 0.0005 for different *Y* = -0.4, -0.3, -0.2, -0.1 and 0.0 for *Da* = 0.005 for (a) γ_p = 0.2 and (b) γ_p = 0.8. From Figs. 7.12 and 7.13, $\theta_w - \theta_p$ does vary linearly with *Br* for both the models. This fact is true even when axial conduction is neglected.

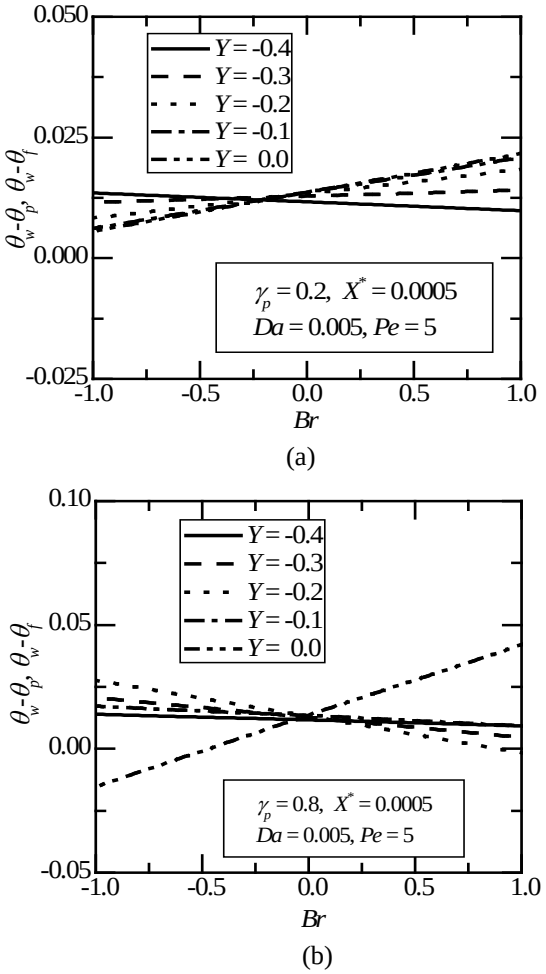

Fig. 7.12: Variation of non-dimensional temperature excess of wall temperature $\theta_w - \theta_p, \theta_w - \theta_f$ profiles vs. *Br* for *Da* = 0.005 for *Pe* = 5 at X^* = 0.0005 for (a) $\gamma_p = 0.2$ and (b) $\gamma_p = 0.8$ for the Darcy model.

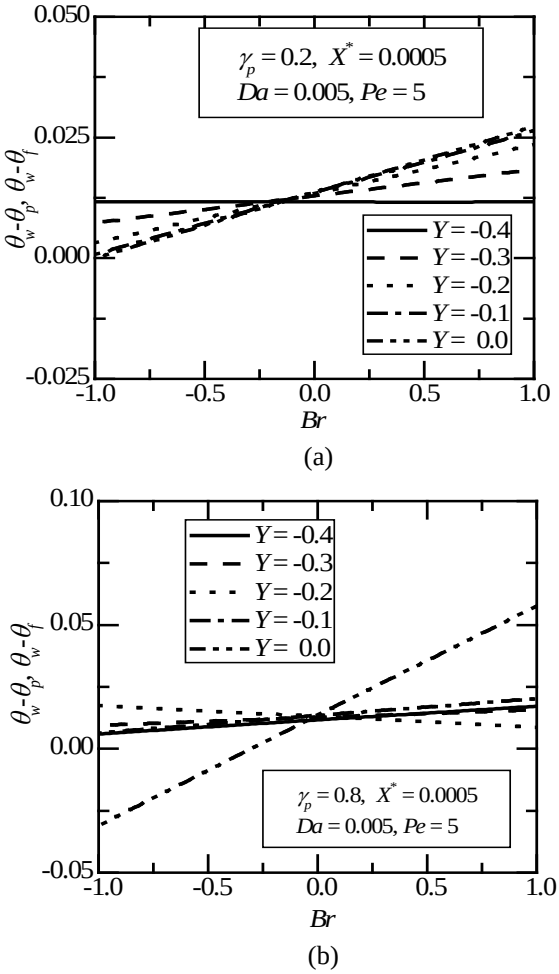

Fig. 7.13: Variation of non-dimensional temperature excess of wall temperature $\theta_w - \theta_p, \theta_w - \theta_f$ profiles vs. *Br* for *Da* = 0.005 for *Pe* = 5 at X^* = 0.0005 for (a) $\gamma_p = 0.2$ and (b) $\gamma_p = 0.8$ for the clear fluid compatible model.

Local Nusselt Numbers

Variation of local Nusselt number with X^* for Da = 0.005, $\gamma_p = 0.2$ and Pe = 5 for (a) $Br \le 0$ and (b) $Br \ge 0$ is shown in Figs. 7.14 and 7.15 for Darcy and clear fluid compatible models respectively. Similarly, variation of local Nusselt number with X^* for Da = 0.005, $\gamma_p = 0.8$ and Pe = 5 for (a) $Br \le 0$ and (b) $Br \ge 0$ is shown in Figs. 7.16 and 7.17 for Darcy and clear fluid compatible model respectively.

From Fig. 7.14 to Fig. 7.17, for both the models, Nu_{px} reveals an unbounded swing for Br < 0 at say, X^*_{sw}. This unbounded swing X^*_{sw} happens for the porous fraction, $\gamma_p \le 0.8$. Also, for both the models, Nu_{px} decreases as Br increases when Br > 0 for the porous fractions with $\gamma_p \le 0.8$. As porous fraction increases, X^*_{sw} increases for the Darcy model. whereas X^*_{sw} decreases as porous fraction increases in the clear fluid compatible dissipation model,

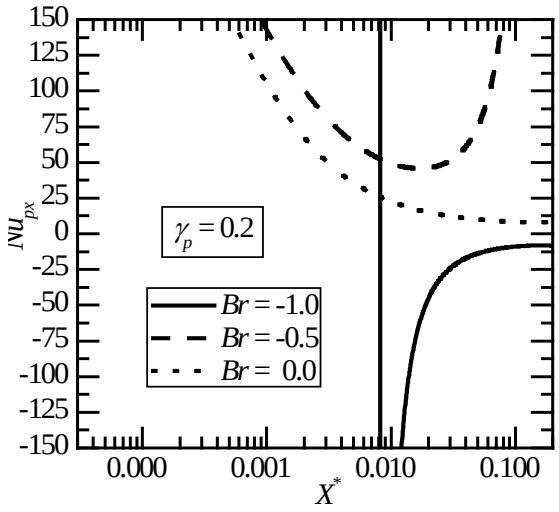

(a)

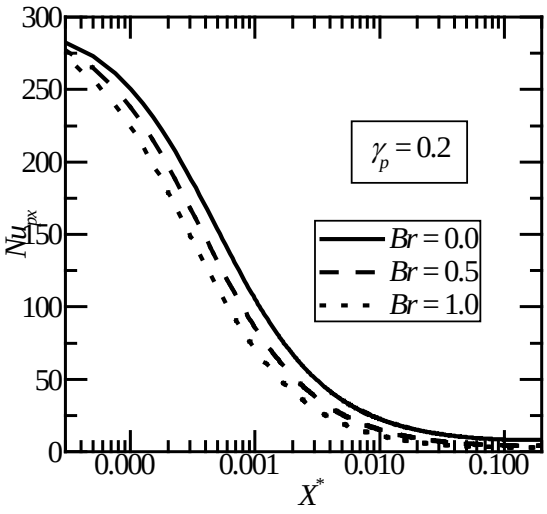

(b)

Fig. 7.14: Variation of the local Nusselt number with X^* for *Da* = 0.005, $\gamma_p = 0.2$ and *Pe* = 5 for (a) $Br \leq 0$ and (b) $Br \geq 0$ for Darcy model .

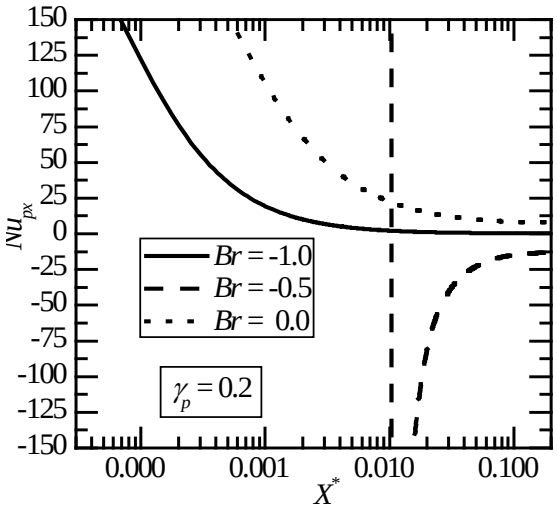

(a)

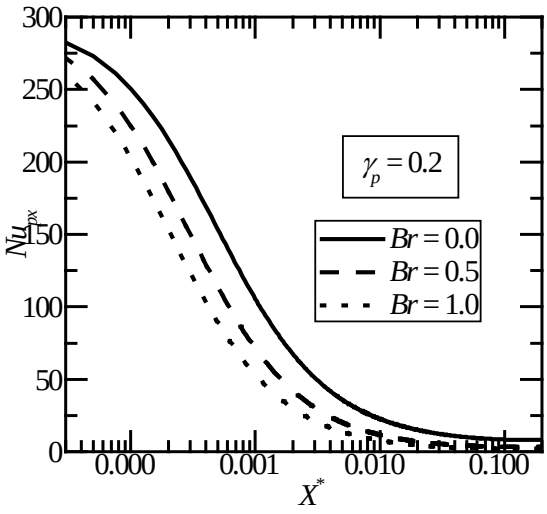

(b)

Fig. 7.15: Variation of the local Nusselt number with X^* for *Da* = 0.005, $\gamma_p = 0.2$ and *Pe* = 5 for (a) $Br \leq 0$ and (b) $Br \geq 0$ for clear fluid compatible model .

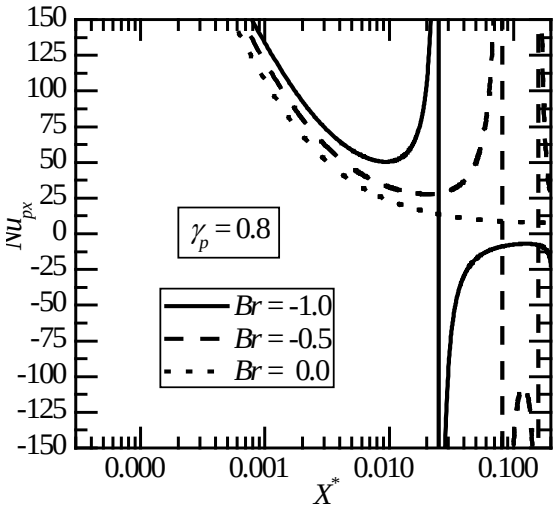

(a)

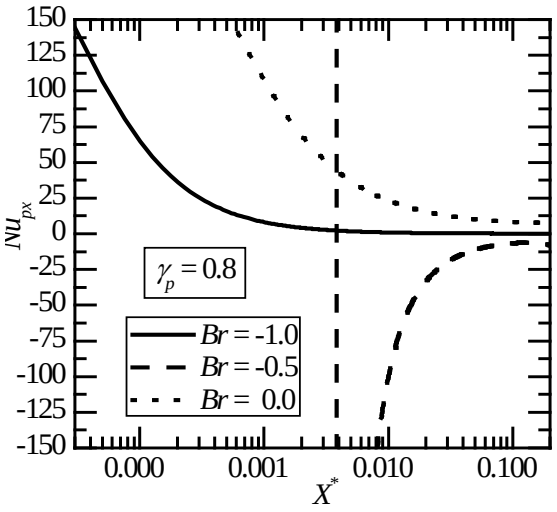

(a)

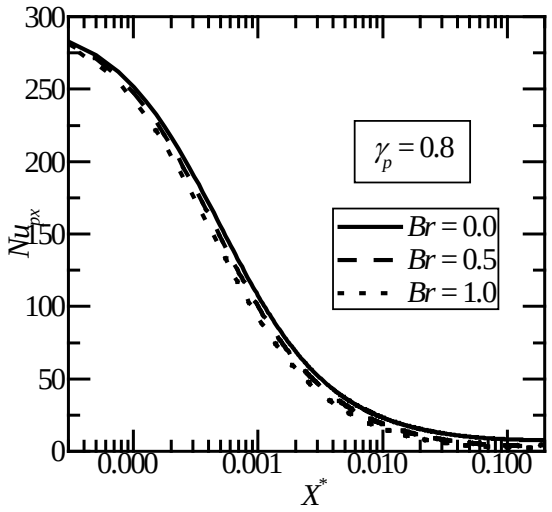

(b)

Fig. 7.16: Variation of local Nusselt number with X^* for Da = 0.005, $\gamma_p = 0.8$ and Pe = 5 for (a) $Br \le 0$ and (b) $Br \ge 0$ for Darcy model.

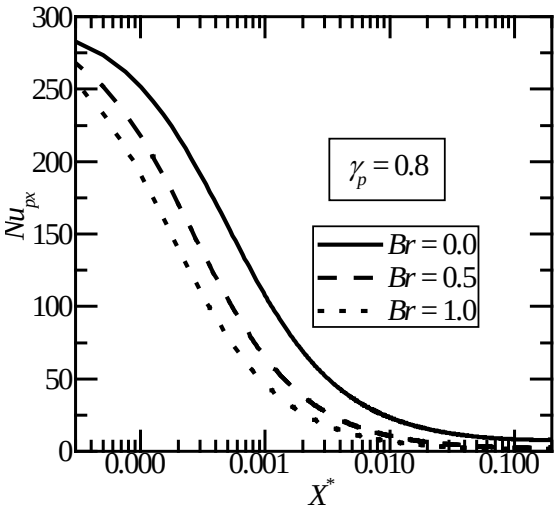

(b)

Fig. 7.17: Variation of local Nusselt number with X^* for Da = 0.005, $\gamma_p = 0.8$ and Pe = 5 for (a) $Br \le 0$ and (b) $Br \ge 0$ for Clear fluid compatible model.

Nusselt Number Changes with Porous Fraction

To examine the changes of the local Nusselt number with porous fraction, plots are given at the entry locations of the channel. Variation of the local Nusselt number, Nu_{px} with γ_p, for different Darcy numbers, Da = 0.005, 0.01 for Pe = 5 for $Br = 0.5$ at (a) X^*= 0.0005

and at (b) X^*= 0.005 is shown in Fig. 7.18 for Darcy model. From Fig. 7.18, it is clear that there is no maximum or minimum in local Nusselt number at a given porous fraction other than γ_p, = 0 and 1.0. Hence we cannot have enhancement or reduction in the local Nusselt number at a given porous fraction in the case of Darcy model.

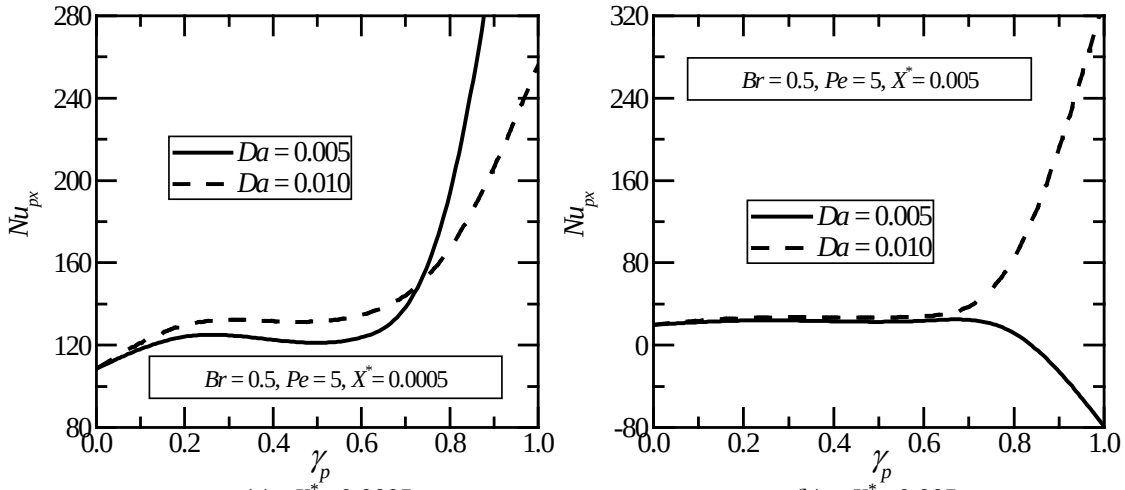

(a) X^*= 0.0005 (b) X^*= 0.005

Fig. 7.18: Variation of local Nusselt number with γ_p, for different Darcy numbers, *Da* = 0.005, 0.01 and *Pe* = 5 at (a) X^*= 0.0005 and (b) X^*= 0.005 for $Br = 0.5$ for the Darcy model.

Variation of the local Nusselt number, Nu_{px} with γ_p, for different Darcy numbers, *Da* = 0.005, 0.01 for *Pe* = 5 for $Br = 0.5$ at (a) X^*= 0.0005 and at (b) X^*= 0.005 is shown in Fig. 7.19 for the clear fluid compatible model. It can be seen from Figs. 7.19(a) and 7.19(b), that the maximum value in local Nusselt number occurs at $\gamma_p \approx 0.2$ while the minimum occurs in Nu_{px} for $\gamma_p \approx 0.6$. The minimum and maximum values do not depend on the axial location of X^*.

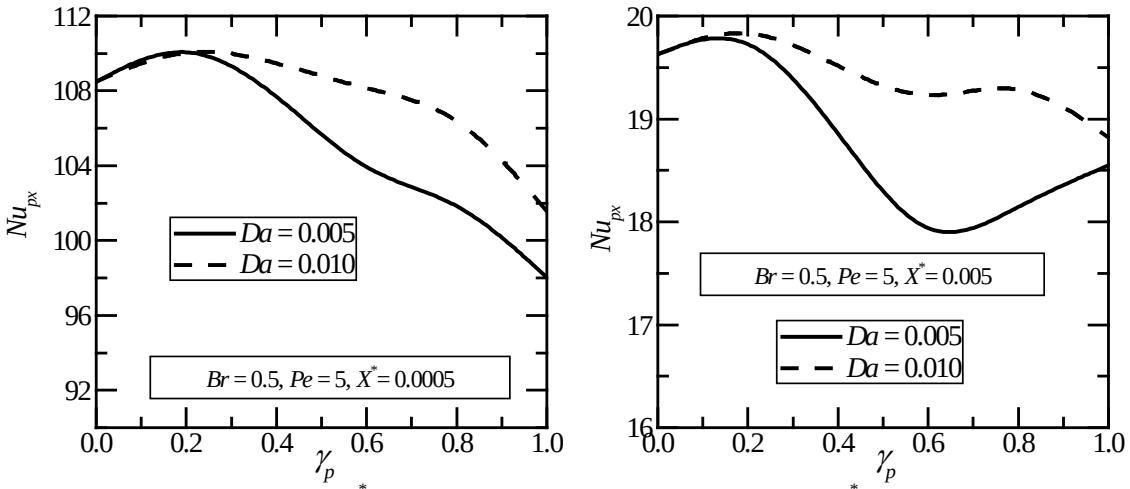

(a) X^* = 0.0005 (b) X^* = 0.005

Fig. 7.19: Variation of local Nusselt number with γ_p, for different Darcy numbers, Da = 0.005, 0.01 and Pe = 5 at (a) X^* = 0.0005 and (b) X^* = 0.005 for $Br = 0.5$ for the clear fluid compatible model.

7.5 Conclusions

Laminar forced convection including axial conduction and viscous dissipation in the thermally developing region of parallel plate channels partially filled with porous material has been numerically studied in the present chapter. The parallel plates have been subjected to constant wall heat flux. The flow field has been assumed to be fully developed. Two dissipation models, namely, a) Darcy model due to Bejan [49] and b) the clear fluid compatible model due to Al-Hadhrami et al. [135 and 136] have been employed in the porous region. The conventional dissipation function {see, Schlichting and Gersten [137]} has been employed in the fluid region. Brinkman number, Br, characterizes the viscous dissipation. As defined in the present thesis, $Br > 0$ represents fluid getting cooled while $Br < 0$, indicates the fluid getting heated.

Numerical solutions have been obtained employing the Successive Acceleration Replacement (SAR) scheme [15 and 158] for both cases, after i) neglecting axial conduction and ii) including axial conduction terms in the energy equation for Pe = 5, 25 and 100. Ranges for the other parameters are $0 \leq \gamma_p \leq 1.0$, $0.005 \leq Da \leq 0.01$, and $-1.0 \leq Br \leq 1.0$.

Nusselt number displays an unbounded swing at some $X^* = X^*_{sw}$ when $Br < 0$. X^*_{sw}, decreases as Br decreases, i.e., for larger negative values of Br. The limiting values of the Nusselt numbers (for large X^*) on the fluid and porous sides, Nu_{px} are dependent on Br for all $Br \neq 0$ in the developing region also. These limiting values depend on the porous fraction too. Nu_{px}, decreases as X^* increases for all porous fractions when $Br > 0$. Nu_{px}, decreases as Br increases for all porous fractions when $Br > 0$. These results are true for both the models when the channel is partially filled with porous material. When fully filled with porous material channels, Nu_{px} increases as Br increases for $Br < 0$ in Darcy model. On the contrary, in the case of the clear fluid compatible model, Nu_{px}, decreases as Br increases for $Br > 0$. The qualitative behavior of Nu_{px}, in the channels partially filled with porous material ($0 < \gamma_p < 1.0$) and the channel fully filled with porous material ($\gamma_p = 1.0$) for the clear fluid compatible model [Eq. (7.21)] is the same as that of clear fluid channel ($\gamma_p = 0$). This fact is reported in { Ramjee and Satyamurty [182] and Mohan Jagadeesh Kumar [190]} for ducts subjected to the constant wall temperature. However, this qualitative behavior of Nu_{px} is not the same in the Darcy model when compared with clear fluid channel. Hence clear fluid compatible dissipation model is more suitable for porous region than Darcy model.

Chapter 8
Summary and Conclusions

Flows and heat transfer through porous media find several applications in diverse fields and circumstances such as compact heat exchangers, packed beds, aerosol transport, geophysics, thermal insulation and heat storage oil and gas extraction, filtration of fluids and seepage of water in river beds, movement of underground water and oil, seepage under a dam, etc. Due to various applications of porous media, the effects of such media on the motion of the fluid have been studied by many investigators.

The conditions to be satisfied at the porous-fluid interface for a class of problem identified in the present study are dealt with here. Slip boundary condition walls were first studied by Beavers and Joseph [37]. Later, Neale and Nader [39] extended this study to include the effect of porous medium. Detailed literature survey on slip condition has been given by Nield and Bejan [48]. Vafai and Kim [41] studied fluid flow in a duct using Darcy Brinkman Forchheimer equation.

A general review of dissipation models applicable for porous media is available in Nield and Bejan [48]. Five forms of the dissipation functions due to Bejan [49], Takhar, Soundalgekar and Gupta [138], Murthy and Singh [139], Nield [140] and Al-Hadhrami, Elliott and Ingham [135 and 136] are available in the literature for flow

through porous media. After identifying the lacunae in the studies available in the literature, pertaining to laminar forced convection in thermally developing region of channels partially filled with porous material, the present study has been undertaken.

The flow field has been assumed to be fully developed governed by Poiseuille equation in the fluid region and by Darcy-Brinkman equation in the porous region. The walls of the channel have been subjected to uniform heat flux. The thermal field has been considered to be developing. After examining the plausible forms for the dissipation function for two-dimensional flow and thermal fields, in general, dissipation effect on the thermal field and heat transfer has been examined. Two models, i) Darcy model [49] and ii) clear fluid compatible dissipation model [135 and 136] to describe dissipation have been considered.

The following is a summary of the results of the studies and the conclusions drawn in Chapters 2 to 7. Certain key points appearing in Chapters 2 to 7 have been reproduced here for completeness.

Analytical or numerical solutions have been obtained in Chapters 2 to 7 of the thesis for the following values of the parameters characterizing the different problems studied. Porous fraction: γ_p = 0, 0.2, 0.4, 0.6, 0.8 and 1.0. Darcy number: Da = 0.001, 0.005, 0.01, 0.05, 0.1 and 1.0. When magnetic field is considered, Hartman number: M = 1, 2, 5 and 10. When axial conduction is considered, Peclet number: Pe = 5, 10, 25, 50 and 100. When axial conduction is neglected, designated by A_c = 0, Pe is absorbed in X^* and does not appear explicitly. When viscous dissipation is included, the Brinkman number: Br =

0, ±0.5 and ±1.0 and selected small values. Analytical solutions to governing equations for the problems studied in Chapters 2, 3 and 4. Numerical solutions to the governing equations for the problems studied in Chapters 5, 6 and 7 have been obtained employing the Successive Accelerated Replacement (SAR) scheme. The methodology of SAR scheme can be found in [15, 158 and 179]. The subject matter dealt with, in Chapters 2 to 7 is summarized below.

Fluid flow and heat transfer in parallel plate channels partially filled with porous medium has been studied in Chapter 2, assuming there is fully developed flow and there are temperature fields. The given amount of porous material has been distributed equally at the two walls. The channel walls are subjected to constant wall heat flux.

Analytical expressions for the non-dimensional velocity and temperature profiles in the porous and clear fluid regions have been obtained. From the velocity and temperature expressions, the fully developed skin friction coefficients and the Nusselt numbers on the porous wall have been obtained analytically. It has been shown that the analytical expressions yield the standard values for a clear fluid channel and for fully porous material filled channels when the porous fraction γ_p is equal to 0 and 1.0 respectively. The porous fraction where the minimum value of Nusselt number occurs decreases as Darcy number increases.

The effects of forced convection and magnetic field for fully developed flow of Newtonian fluid in a parallel plate channel partially filled with porous material have been

studied in Chapter 3. Analytical solution has been obtained and closed form expressions have been derived for velocity, skin friction coefficient and temperature profiles in the porous and fluid regions and for the Nusselt number in the porous region. It has been shown that the analytical expressions yield standard values for Hartmann number, $M = 0$ {absence of the magnetic field)} for all porous fractions γ_p , $0 \leq \gamma_p \leq 1.0${Chapter 2}. Nusselt number and the net change in the Nusselt number increase with Hartmann number, M for all porous fractions, γ_p. Hence the effect of the magnetic field may be considered to enhance the heat transfer in the channels partially filled with porous medium.

Enhancement in the fully developed Nusselt number for parallel plate channel flow subjected to constant wall heat flux and constant wall temperature with porous inserts distributed equally at the two walls of the channel for the three dissipation models has been studied at the conduction limit in Chapter 4. The three dissipation models, namely, 1) the Darcy model [49], 2) form drag model [140] and 3) clear fluid compatible model [135 and 136] in the porous region are employed in the porous region.

Case (i): Subjected to constant wall heat flux

Both the wall heating and wall cooling cases can be examined from the given plots for all values of Brinkman numbers. Limiting temperature profile and limiting Nusselt number plots are given and these depend on the Brinkman number for constant wall heat flux boundary condition. Maximum value of Nusselt number and net change in the Nusselt number occur only at $\gamma_p = 1.0$. For small Darcy number, the difference between these

models in limiting temperatures and limiting Nusselt numbers is negligible, but for larger Darcy number, the difference is significant. Heat transfer enhancement is better in clear fluid compatible model compared with Darcy and form drag model.

Case (ii): Subjected to constant wall temperature

It has been found that the non-dimensional temperature and the bulk mean temperature when viscous dissipation is included are linearly proportional to Brinkman number at the conduction limit. Nusselt numbers in the conduction limit have been found to be independent of Brinkman number, a feature well reported for clear fluid channels, see Barletta [4]. The three models that describe dissipation yield comparable Nusselt number values when *Da* is small (say, $Da < 0.01$) for a channel partially filled with a porous material also.

Laminar forced convection in the thermally developing region of parallel plate channels partially filled with a porous material has been studied numerically in Chapter 5. The parallel plates have been subjected to constant wall heat flux. Axial conduction is neglected in the conservation of thermal energy equation. The non-dimensional temperature at the wall, θ_w attains maximum value at a certain porous fraction. With this feature, it is envisaged that the local Nusselt number at the wall attains a minimum for some $0 < \gamma_p < 1.0$. In the context of constant wall heat flux condition, this implies that the transfer of a given heat flux takes place with a lower temperature difference between the wall and the fluid.

Effect of axial conduction in the thermally developing region of parallel plate channels partially filled with a porous material has been numerically studied in Chapter 6. The parallel plates have been subjected to constant heat flux. It has been concluded that the non-dimensional temperature profiles become independent of the Peclet number for $Pe \geq 100$ indicating that the effect of axial conduction has become negligible. Non-dimensional bulk mean temperature in excess of wall temperature, $\theta_w - \theta^*$, increases as X^* increases. $\theta_w - \theta^*$ decreases as Peclet number decreases. This indicates that a stronger axial conduction effect being present at lower Peclet numbers that makes the fluid less heated or less cooled compared to when axial conduction is neglected. Nu_{px} is a minimum when $\gamma_p \approx 0.6$ at low Da = 0.001 increasing to $\gamma_p \approx 0.8$ when Da = 0.1. Nu_{px} attains a minimum almost independent of Peclet number and X^*.

Laminar forced convection including axial conduction and viscous dissipation in the thermally developing region of parallel plate channels partially filled with porous material has been numerically studied in Chapter 7. The parallel plates have been subjected to constant wall heat flux. Two dissipation models are employed in the porous region. Brinkman number, Br, characterizes the viscous dissipation. As defined in the present thesis, $Br > 0$ represents fluid getting cooled and $Br < 0$, shows fluid getting heated.

Nusselt number displays an unbounded swing at some $X^* = X^*_{sw}$ when $Br < 0$. X^*_{sw}, decreases as Br decreases, i.e., for larger negative value for Br. The limiting values of the Nusselt numbers (for large X^*) on the fluid and porous sides, Nu_{px} are dependent on Br for all $Br \neq 0$ in the developing region also. These limiting values depend on the

porous fraction also. Nu_{px}, decreases as X^* increases for all porous fractions when $Br > 0$. Nu_{px}, decreases as Br increases for all porous fractions when $Br > 0$. These results are true for both models when the channel is partially filled with porous material. For fully filled channels with porous material, Nu_{px}, increases as Br increases when $Br < 0$ for Darcy model. On the other hand, in the case of clear fluid compatible model, Nu_{px}, decreases as Br increases for $Br > 0$. The qualitative behavior of Nu_{px}, in the channels partially filled with porous material ($0 < \gamma_p < 1.0$) and the channel fully filled with porous material ($\gamma_p = 1.0$) for the clear fluid compatible model {Eq. (7.21)} is same that of clear fluid channel($\gamma_p = 0$).

Some Potential Applications (Mohamad [191] and Yucel and Guven [192]):

1. Heat transfer enhancements in heat transfer devices, such as heat exchangers
2. Heat transfer enhancements for single and multiphase flows such as vortex generators and mixers.
3. Cooling of heat-generating obstacles mounted on adiabatic walls in a parallel-plate channel.

Scope for Future Work

The following investigations may be undertaken in future as an extension of the present study:

1. An evaluation of the relative performance of the porous inserts attached to both the walls or placed at the center of the channel as well as the present arrangement when the flow and thermal fields are simultaneously developing may be undertaken with different boundary conditions.

2. Similar evaluation for pipes and annuli partially filled with porous material leads to a desirable configuration given that there are no constraints in choosing the duct size. Investigations may be earned out to establish conditions under which a desirable configuration is obtained.

3. Studies on flow and heat transfer through, ducts, partially filled with porous material considering anisotropic and heterogeneous porous media are warranted for some of the newer applications.

References

1	Hatton, A. P., and Turton, J. S., 1962, "Heat Transfer in the Thermal Entry Length with Laminar Flow between Parallel Walls at Unequal Temperatures", Int. J. Heat Mass Transfer, **5**, pp. 673-679.
2	Mitrovic, J., Maletic, B., and Baclic, B. S., 2006, "Some Peculiarities of the Asymmetric Graetz Problem", Int. J. Engg. Sc., **44**, pp. 436-455.
3	Nield, D. A., 2004, "Forced Convection in a Parallel Plate Channel with Asymmetric Heating", Int. J. Heat Mass Transfer, **47**, pp. 5609-5612.
4	Barletta, A., 1998, "Laminar Mixed Convection with Viscous Dissipation in a Vertical Channel", Int. J. Heat Mass Transfer, **41**, pp. 3501-3513.
5	Sparrow, E. M., and Patankar, S. V., 1977, "Relationships among Boundary Conditions and Nusselt Number for Thermally Developed Duct Flows", ASME J. Heat Transfer, **99**, pp. 483-485.
6	Pins, J. A., Mulder, J. and Schenk, J., 1951, "Heat Transfer in Laminar Flow between Parallel Plates", App. Sci. Res., **A2**, pp. 431-438.
7	Weigand, B., Kanzamar, M., and Beer, H., 2001, "The Extended Graetz Problem with Piecewise Constant Wall Heat Flux for Pipe and Channel Flows", Int. J. Heat and Mass Transfer, **44**, pp. 3941-3952.
8	Cheng, K. C., and Wu, R. S., 1976, "Viscous Dissipation Effects On Convective Instability And Heat Transfer In Plane Poiseuille Flow Heated From Below", App. Sci. Res., **32**, pp. 327-346.
9	Barletta, A., 1999, "Laminar Convection in a Vertical Channel with Viscous Dissipation and Buoyancy Effects", Int. Comm. Heat Mass Transfer, **26**, pp. 153-164.
10	Nguyen, T. V., 1991, "Low Reynolds Number Simultaneously Developing Flows in the Entrance Region of Parallel Plates", Int. J. Heat Mass Transfer, **34**, pp. 1219-1225.
11	Peaceman, D. W., and Rachford, H. H., 1955, "The Numerical Solution of Parabolic and Elliptic Differential Equations", J. Soc. Ind. Appl. Math., **3**, pp. 28-41.
12	Douglas Jr. J., 1955, "On the Numerical Integration of $\partial^2 u/\partial x^2 + \partial^2 u/\partial y^2 = \partial u/\partial t$ by Implicit Methods", J. Soc. Ind. Appl. Math., **3**, pp. 42-65.
13	Leonard, B. P., 1979, "A stable and accurate modeling procedure based on quadratic interpolation", Comput. Methods Appl. Mech. Engrg., **19**, pp. 58-98.
14	Ramjee Repaka, 2008, "Laminar Forced Convection with Viscous Dissipation in Hydrodynamically Developing Flow between Parallel Plates at Unequal Temperatures", Ph.D thesis, I.I.T Kharagpur, India

15	Ramjee Repaka and Satyamurty, V. V., 2010, “Local and Average Heat Transfer in the Thermally Developing Region of an Asymmetrically Heated Channel”, Int. J. Heat Mass Transfer, **53**, pp. 1654-1665.
16	Ramjee Repaka and Satyamurty, V. V., 2010, “Limiting Nusselt Numbers for Viscous Dissipative Flow between Parallel Plates Kept at Unequal Temperatures”, Int. Comm. Heat Mass Transfer, **37**, pp. 1251-1254.
17	Satyamurty, V. V., and Ramjee Repaka, 2011, “Superposition Relations for Forced Convective Local Nusselt Numbers for Flow through Asymmetrically Heated Parallel Plate Channels”, Heat Transfer Engineering, **32**, No. 6, pp. 476-484.
18	Shah, R. K., and London, A. L., 1978, "Laminar Flow Forced Convection in Ducts, Advances in Heat Transfer", Supplement 1, Academic Press., New York, p.172, 1978.
19	Stanek, V., and Szekely, J., 1974, “Three Dimensional Flow of Fluids through Non-Uniform Packed Beds”, AIChE Journal, **20**, pp. 974-980.
20	Slattery, J., 1967, “Flow of Viscoelastic Fluids Though Porous Media”, AICHE Journal, **13**, pp. 1066-1071.
21	Catton, I., 1985, “Natural Convection Heat Transfer in Porous Media, Natural Convection: Fundamentals and Applications W. Aung, S. Kakac and R. Viskanta”, Eds., Hemisphere, New York, pp. 514-547.
22	Givler, R. C., and Altobellis, A., 1994, “A Determination of the Effective Viscosity for the Brinkman-Forchheimer Flow Model”, J. Fluid Mech. **258**, pp. 355-370.
23	Kaviany, M., 1985, “Laminar Flow through a Porous Channel Bounded by Isothermal Parallel Plates”, Int. J. Heat Mass Transfer, **28**, pp. 851-858.
24	Vafai, K., and Kim, S. J., 1989, “Forced Convection in a Channel Filled with a Porous Medium: an Exact Solution”, ASME J. Heat Transfer, **111**, pp. 1103-1106.
25	Nield, D. A., Junqueira, S. L. M., and Lage, J. L., 1996, “Forced Convection in a Fluid-Saturated Porous-Medium Channel with Isothermal or Isoflux Boundaries”, J. Fluid Mech., **322**, pp. 201-214.
26	Bear, J., 1972, "Dynamics of Fluids in Porous Media", Elsevier, New York.
27	Greenkorn, R. A., 1983, "Flow Phenomena in Porous Media", Marcel Dekker, New York.
28	Rogers, F. T., Schilberg, L. E., and Morrison, H. L., 1951, “Convective Currents in Porous Media, IV. Remarks on the Theory”, J. Applied Physics, **22**, pp. 1476-1479.
29	Wooding, R. A., 1963, “Convection in a Saturated Porous Medium at large Reynolds Number or Peclet number”, J. Fluid Mechanics, **15**, pp. 527-544.

30	Elder, J. W., 1967, "Steady Free Convection in a Porous Medium Heated from Below", J. Fluid Mechanics, **27**, pp. 29-48.
31	Elder, J. W., 1967, "Transient Convection in a Porous Medium", J. Fluid Mechanics, **27**, pp. 609- 623.
32	Lapwood, E. R., 1948, "Convection of Fluid in a Porous Medium", Proceedings of the Cambridge Philosophical Society, **44**, pp. 508-521.
33	Katto, Y., and Masuoka, T., 1967, "Criterion for the Onset of Convective Flow in a Fluid in a Porous Medium", Int. J. Heat Mass Transfer, **10**, pp. 297-309.
34	Vafai, K., and Tien, C. L., 1981, "Boundary and Inertia Effects on Flow and Heat Transfer in Porous Media", Int. J. Heat Mass Transfer, **24**, pp. 195-203.
35	Lage, J. L., 1992, "Effect of the Convective Inertia Term on Benard Convection in a Porous Medium", Numerical Heat Transfer, Part A, **22**, No. 4, pp. 469-485.
36	Manole, D. M., and Lage, J. L., 1993, "The Inertial Effect on the Natural Convection Flow within a Fluid-Saturated Porous Medium", Int. J. Heat fluid flow, **14**, No. 4, pp. 376-384.
37	Beavers, G. S., and Joseph, D. D., 1967, "Boundary Conditions at a Naturally Permeable Wall", J. Fluid Mechanics, **30**, 197-207.
38	Saffman, P. G., 1971, "On the Boundary Condition at the Surface of a Porous Media", Stud. Appl. Math., **50**, pp. 93–101.
39	Neale, G., and Nader, W., 1974, "Practical Significance of Brinkman's Extension of Darcy's Law: Coupled Parallel Flows within a Channel and a Bounding Porous Medium", Can. J. Chem. Eng., **52**, pp. 475-478.
40	Vafai, K., and Thiyagaraja, R., 1987, "Analysis of Flow and Heat Transfer at the Interface Region of a Porous Medium", Int. J. Heat Mass Transfer, **30**, pp. 1391-1405.
41	Vafai, K., and Kim, S. J., 1990, "Fluid Mechanics of the Interface Region between a Porous Medium and a Fluid Layer-an Exact Solution", Int. J. Heat Fluid Flow, **11**, pp. 254-256.
42	Sahraoui, M., and Kaviany, M., 1992, "Slip and No-Slip Velocity Boundary Conditions at Interface of Porous, Plain-Media", Int. J. Heat Mass Transfer, **35**. No. 4, pp. 927-943.
43	Chandesris, M., and Jamet, D., 2006, "Boundary Conditions at a Planar Fluid-Porous Interface for a Poiseuille Flow", Int. J. Heat Mass Transfer, **49**, pp. 2137–2150.
44	Prathap Kumar, J., Umavathi, J.C ., and Ali J. Chamkha., 2013, " Steady Solute Dispersion in Composite Porous Medium Between Two Parallel Plates", J. Porous Media, 16, pp.1087-1105.

45	Bhargavi, D., Satyamurty, V.V., and Raja Sekhar, G.P., "Effect of Porous Fraction and Stress Jump on Skin Friction and Heat Transfer in Flow Through a Channel Partially Filled with Porous Material", J. Porous Media., vol 12, pp.1065-1082, 2009.
46	Bejan, A., Dincer, I., Lorente, S., Miguel, A. F., and Reis, A. H., 2004, "Porous and Complex Flow Structures in Modern Technologies", Springer, New York.
47	Kaviany, M., 1991, "Principles of Heat Transfer in Porous Media", Springer, New York.
48	Nield, D. A., and Bejan, A., 2006, "Convection in Porous Media", 3rd Edition, Springer, New York.
49	Bejan, A., 2004, "Convection Heat Transfer", 3rd Edition, Wiley, New York.
50	Edited by Vafai, K., 2005, "Handbook of Porous Media", Taylor and Francis, New York.
51	Poulikakos, D., and Renken, K., 1987, "Forced Convection in Channel Filled with Porous Medium, Including the Effects of Flow Inertia, Variable Porosity, and Brinkman Friction", ASME J. Heat Transfer, **109**, pp. 880-888.
52	Marpu, D. R., 1993, "Non-Darcy Flow and Axial Conduction Effects on in Porous Material Filled Pipes", Warme-und Stoffubertragung, **29**, pp. 51-58.
53	Mitrovic, J., and Maletic, B., 2006, "Effect of Thermal Asymmetry on Laminar Forced Convection Heat Transfer in a Porous Annular Channel", Chem. Eng. Technol., **29**, No. 6, pp. 750-760.
54	Satyamurty, V. V., and Marpu, D. R., 1989, "Numerical Study of Forced Convection Heat Transfer in the Developing Region of a Porous Channel", Proceedings of V International Symposium on Numerical Methods in Engineering, Switzerland, pp. 729-734.
55	Hwang, G. J., Wu, C. C., and Chao, C. H., 1995, "Investigation of Non-Darcian Forced Convection in an Asymmetrically Heated Sintered Porous Channel", Trans. of ASME, Journal of Heat Transfer, **117**, No. 3, p. 725-732.
56	Xiong, M., and Kuznetsov, A. V., 2000, "Forced Convection in a Couette Flow in a Composite Duct: An Analysis of Thermal Dispersion and Non-Darcian Effects", J. Porous Media, **3**, pp. 245-255.
57	Nield, D. A., Kuznetsov, A. V., and Xiong, M., 2003, "Thermally Developing Forced Convection in Porous Medium: Parallel-Plate Channel or Circular Tube with Walls at Constant Heat Flux", J. Porous Media, **6**, No. 3, pp. 203-212.
58	Nield, D. A., Kuznetsov, A. V., and Xiong, M., 2004, "Thermally Developing Forced Convection in Porous Medium: Parallel-Plate Channel or Circular Tube with Isothermal Walls", J. Porous Media, **7**, No.1, pp. 19-27.
59	Haji-Sheikh, A., and Vafai, K., 2004, "Analysis of Flow and Heat Transfer in

	Porous Media Imbedded Inside Various Shaped Ducts", Int. J. Heat Mass Transfer, **47**, pp. 1889-1905.
60	Mitrovic, J., and Maletic, B., 2007, "Heat Transfer with Laminar Forced Convection in a Porous Channel Exposed to a Thermal Asymmetry", Int. J. Heat Mass Transfer, **50**, pp. 1106-1121.
61	Marafie, A., and Vafai, K., 2001, "Analysis of Non-Darcian Effects on Temperature Differentials in Porous Media", Int. J. Heat Mass Transfer, **44**, pp. 4401-4411.
62	Hooman, K., Ranjbar-Kani, A. A., 2003, "Forced Convection in a Fluid-Saturated Porous-Medium Tube with Isoflux Wall", Int. Comm. Heat Mass Transfer, **30**, No. 7, pp. 1015-1026.
63	Haji-Sheikh, A., 2004, "Estimation of Average and Local Heat Transfer in Parallel Plates and Circular Ducts Filled with Porous Materials", ASME J. Heat Transfer, **126**, pp. 400-409.
64	Minkowycz, W. J., and Haji-Sheikh, A., "Heat Transfer in Parallel Plates and Circular Porous Passages with Axial Conduction", Int. J. Heat Mass Transfer, **49**, pp. 2381-2390.
65	Hooman, K., and Gurgenci, H., 2007, "A Theoretical Analysis of Forced Convection in a Porous Saturated Circular Tube: Brinkman-Forchheimer Model", Transport in Porous Media, **69**, pp. 289-300.
66	Kuznetsov, A. V., Nield, D. A., 2009, "Thermally Developing Forced Convection in a Porous Medium Occupied by a Rarefied Gas: Parallel Plate Channel or Circular Tube with Walls at Constant Heat Flux", Transp. Porous Med., **76**, pp. 345-362.
67	Huang, X. Y., and Liu, C. Y., 1996, "The Developing Flow in a Channel Filled with Porous Media", Int. Comm. Heat Mass Transfer, **23**, No.1, pp. 123-132.
68	Awartani, M. M., and Hamdan, M. H., "Fully Developed Flow through a Porous Channel Bounded by Flat Plates", Applied Mathematics and Computation, **169**, pp. 749-757.
69	Haji-Sheikh, A., 2006, "Fully Developed Heat Transfer to Fluid Flow in Rectangular Passages Filled with Porous Materials", ASME J. Heat Transfer, **128**, pp. 550-556.
70	Hooman, K., 2008, "A Perturbation Solution for Forced Convection in a Porous-Saturated Duct", J. Computational and Applied Mathematics, **211**, pp. 57- 66.
71	Nield, D.A., and Kuznetsov, A. V., 2000, " Effects of heterogeneity in forced convection in a porous medium: parallel plate channel or circular duct", Int. J. Heat and Mass Transfer, **43**, pp. 4119-4134.
72	Dileep Singh Chauhan and Vikas Kumar, 2010, **"**Three-Dimensional Couette Flow in a Composite Channel Partially Filled with a Porous Medium", Applied Mathematical Sciences, **4**, No. 54, pp. 2683-2695.

73	Banerji, A., Haji-Sheikh, A., and Seiichi Nomura, 2012, " Heat Transfer with Axial Conduction in Triangular Ducts Filled with Saturated Porous Materials", Numerical Heat Transfer, Part A: Applications, **62** ,pp. 1-24.
74	Poulikakos, D., and Kazmierczak, M., 1987, "Forced Convection in a Duct Partially Filled with a Porous Material", ASME J. Heat Transfer, **109**, No.3, pp. 653-662.
75	Cheng, C. H., Kou, H. S., and Huang, W. H., 1989, "Laminar Fully Developed Forced-Convection Flow within an Asymmetrically Heated Horizontal Double-Passage Channel", Applied Energy, **33**, pp. 265-286.
76	Jang, J. Y., and Chen, J. L., 1992, "Forced Convection in a Parallel Plate Channel Partially Filled with a High Porosity Medium", Int. Comm. Heat Mass Transfer, **19**, pp. 263-273.
77	Kuznetsov, A. V., 1996, "Analytical Investigation of the Fluid Flow in the Interface Region between a Porous Medium and a Clear Fluid in Channels Partially Filled with a Porous Medium", Int. J. Heat Fluid Flow, **12**, pp. 269-272.
78	Kuznetsov, A. V., 1997, "Influence of the Stress Jump Condition at the Porous Medium/Clear-Fluid Interface on a Flow at a Porous Wall", Int. Comm. Heat Mass Transfer, **24**, pp. 401- 410.
79	Kuznetsov, A. V., 1998, "Analytical Investigation of Couette Flow in a Composite Channel Partially Filled with a Porous Medium and Partially with a Clear Fluid", Int. J. Heat Mass Transfer, **41**, pp. 2556-2560.
80	Kuznetsov, A. V., 1998, "Analytical Study of Fluid Flow and Heat Transfer during Forced Convection in a Composite Channel Partly Filled with a Brinkman-Forchheimer Porous Medium", Flow, Turbulence and Combustion, **60**, pp. 173-192.
81	Hamdan, M. O., Al-Nimr, M. A., and Alkam, M. K., 2000, "Enhancing Forced Convection by Inserting Porous Substrate in the Core of a Parallel-Plate Channel", Int. J. Numerical Methods for Heat Fluid Flow, **10**, No. 5, pp. 502-518.
82	Alkam, M. K., Al-Nimr, M. A., and Hamdan, M. O., 2002, "On Forced Convection in Channels Partially Filled with Porous Substrates", Heat Mass Transfer, Springer-Verlag, **38**, No. 4-5, pp. 337-342.
83	Jen, T. C., and Yan, T. Z., 2005, "Developing Fluid Flow and Heat Transfer in a Channel Partially Filled with Porous Medium", Int. J. Heat Mass Transfer, **48**, pp. 3995-4009.
84	Rudraiah, N., 1985, "Coupled Parallel Flows in a Channel and a Bounding Porous Medium of Finite Thickness," ASME J. Fluids Eng., **107**, No. 3, pp.322-329.
85	Vafai, K., and Kim. S. J., 1990, "Analysis of Surface Enhancement by a Porous Substrate", ASME J. Heat Transfer, **112**, pp. 700-706.
86	Huang, P. C., and Vafai, K., 1994, "Passive Alteration and Control of Convective Heat Transfer Utilizing Alternate Porous Cavity-Block Wafers", Int. J. Heat Fluid Flow, **15**, No. 1, pp. 48-61.

87	Huang, P. C., and Vafai, K., 1994, "Analysis of Forced Convection Enhancement in a Channel Using Porous Blocks", J. Thermophysics Heat transfer, **8**, No. 3, pp. 563-573.
88	Huang, P. C., and Vafai, K., 1994, "Analysis of Flow and Heat Transfer over an External Boundary Covered with a Porous Substrate", ASME J. Heat transfer, **16**, pp. 768-771.
89	Huang, P. C., and Vafai, K., 1994, "Internal Heat Transfer Augmentation in a Channel Using an Alternate Set of Porous Cavity-Block Obstacles", Numerical Heat Transfer, Part A, Taylor and Francis, **25**, pp. 519-539.
90	Vafai, K., and Huang, P. C., 1994, "Analysis of Heat Transfer Regulation and Modification Employing Intermittently Emplaced Porous cavities", ASME J. Heat Transfer, **116**, pp. 604-613.
91	Chang, W. J., and Chang, W. L., 1996, "Mixed Convection in a Vertical Parallel-Plate Channel Partially Filled with Porous Media of High Permeability", Int. J. Heat Mass Transfer, **39**, No.7, pp. 1331-1342.
92	Guo, Z., Young Kim, S., and Jin Sung, H., 1997, "Pulsating Flow and Heat Transfer in a Pipe Partially Filled with a Porous Medium", Int. J. Heat Mass Transfer, **40**, No. 17. pp. 4209-4218.
93	Chang, W. J., Dai, W. L., and Chang, W. L., 1996, "The Reynolds Number and Prandtl Number Effects on Developing Convection of Vertical Tube Partially Filled with Porous Medium", Int. Comm. Heat Mass Transfer, **23**, No. 4, pp. 531-542.
94	Alkam, M. K., and Al-Nimr, M. A., 1999, "Improving the Performance of Double-Pipe Heat Exchangers by using Porous Substrates", Int. J. Heat Mass Transfer, **42**, pp. 3609-3618.
95	Kuznetsov, A. V., and Xiong, M., 2000, "Numerical Simulation of the Effect of Thermal Dispersion on Forced Convection in a Circular Duct Partly Filled with a Brinkman-Forchheimer Porous Medium", Int. J. Numerical Methods for Heat and Fluid Flow, **10**. No. 5, pp. 488-501.
96	Alkam, M. K., Al-Nimr, M. A., and Hamdan, M. O., 2001, "Enhancing Heat Transfer in Parallel-Plate Channels by Using Porous Inserts", Int. J. Heat Mass Transfer, **44**, pp. 931-938.
97	Abu-Hijleh, B. A., and Al-Nimr, M. A., 2001, "The Effect of the Local Inertial Term on the Fluid Flow in Channels Partially Filled with Porous Material", Int. J. Heat Mass Transfer, **44**, pp. 1565-1572.
98	Habibollah Sayehvand., and Hossein Shokouhmand., 2006, "Study of Forced Convection in a Pipe Partially Filled With a Porous Medium", Proceedings of the 4th WSEAS Int. Conf. on Heat Transfer, Thermal Engineering and Environment, Elounda, Greece, August 21-23, pp. 292-300.
99	Kim, W. T., Hong, K. H., Jhon, M. S., VanOsdol, J. G., and Smith, D. H., 2003,

	"Forced Convection in a Circular Pipe with a Partially Filled Porous Medium", KSME Int. J., **17**, No. 10, pp. 1583-1596.
100	Huang, P. C., Yang, C. F., Hwang, J. J., and Chiu, M. T., 2005, "Enhancement of Forced-Convection Cooling of Multiple Heated Blocks in a Channel using Porous Covers", Int. J. Heat Mass Transfer, **48**, pp. 647-664.
101	Keyhani, M. H., Karimi, G., and Nazari, M., 2006, "Heat Transfer Enhancement in Channel Partially Filled with Porous Material", Proceedings of the 2nd WSEAS *Int. Conf. on Applied and Theoretical Mechanics*, Venice, Italy, November, 20-22.
102	Sayehvand, H., and Shokouhmand, H., 2006, "Study of Forced Convection in a Pipe Partially Filled With a Porous Medium", Proceedings of the 4th WSEAS Int. Conf. on Heat Transfer, Thermal Engineering and Environment, Elounda, Greece, August 21-23, pp. 292-300.
103	Alkam, M. K., and Al-Nimr, M. A., 2001, "Transient Flow Hydrodynamics in Circular Channels Partially Filled with a Porous Material", Heat Mass Transfer, Springer-Verlag, **37**, pp. 133-137.
104	Mohamed, A. Teamah., Wael M. El-Maghlany., and Mohamed, M. Khairat Dawood., 2011, "Numerical Simulation of Laminar Forced Convection in Horizontal Pipe Partially or Completely Filled with Porous Material", Int. J. Thermal Sciences, **50**, pp.1512-1522.
105	Fumei Rong ., Wenhuan Zhang ., Baochang Shi ., and Zhaoli Guo., 2014, "Numerical study of heat transfer enhancement in a pipe filled with porous media by axisymmetric TLB model based on GPU", Int. J. Heat and Mass Transfer, **70** , pp. 1040–1049
106	Hadim, A., 1994, " Forced Convection in a Porous Channel With Localized Heat Sources", J. Heat Transfer ASME, 116, pp. 465-472
107	Kuznetsov, A. V., and Nield, D.A., 2010, "Forced Convection in a Channel Partly Occupied by a Bidisperse Porous Medium: Symmetric Case", Int. J. Heat and Mass Transfer, **53,** pp. 5137-5175.
108	Bhargavi, D., and Satyamurty, V.V., 2011, "Optimum Porous Insert Configurations for Enhanced Heat Transfer in Channels", J. Porous Media, **14,** , pp. 187-203, 2011.
109	Cekmer, O., Mobedi, M., Ozerdem, B. and Pop, I., 2012 "Fully Developed Forced Convection in a Parallel Plate Channel with a Centered Porous Layer", Transp Porous Media, vol93, pp.179–201.
110	Malashetty, M.S., Umavathi, J.C., and Prathap Kumar, J., 2004, "Two fluid flow and heat transfer in an inclined channel containing porous and fluid layer", Heat and Mass Transfer, **40**, pp.871–876.
111	Tien-Chien Jen., and Yan, T.Z., 2005, " Developing fluid flow and heat transfer in a channel partially filled with porous medium", Int. J. Heat and Mass Transfer, **48**, pp.3995-4009.
112	Shokouhmand, H., Jam, F., and Salimpour, M.R., 2011, "The effect of porous insert position on the enhanced heat transfer in partially filled channels", Int.

	Commu. in Heat and Mass Transfer, **38**, pp. 1162-1167.
113	Carlos G. Aguilar-Madera ., Francisco J. Valdés-Parada ., Benoît Goyeau, J., and Alberto Ochoa-Tapia., 2011, "Convective heat transfer in a channel partially filled with a porous medium", Int. J. Thermal Sci., **50**, pp.1355-1368.
114	Maerefat, M., Mahmoudi, S.Y., and Mazaheri, K.,2011, "Numerical simulation of forced convection enhancement in a pipe by porous inserts", Heat Transfer Eng, **32**, pp. 45–61.
115	Raju, K.V.S., Sudhakar Reddy, T., Raju, M.C., Satya narayana, P.V., and Venkataramana, S., 2014, "MHD Convective Flow Through Porous Medium in a Horizontal Channel with Insulated and Impermeable Bottom Wall in the Presence of Viscous Dissipation and Joule Heating", Ain Shams Engineering Journal, **5**, pp.543–551.
116	Sharmilla, K., and Saranya, S., 2017, "Effect of Magnetic Field in a Forced Convective Saturated Porous Duct", Int. J. Research in Emerging Sci. and tech, **4**.
117	Kurzweg, U.H., 1963, "The Stability of Couette Flow in the Presence of an Axial Magnetic Field", Journal of Fluid Mechanics., vol 17, pp. 52–60.
118	Gulab, R. and Mishra, R., 1977, "Unsteady Flow Through Magneto Hydrodynamic Porous Media", Indian J. Pure Appl. Math., vol 8, pp.637, 1977.
119	Raptis, A. A. and Kafousias , N., 1982, "Heat Transfer In flow Through a Porous Medium Bounded By on an Infinite Vertical Plate Under the Action of a Magnetic Field", Int. J. Energy Research., vol 6 , pp. 241–245.
120	Raptis, A. A. and Perdikis, C.P., 1988, "Combined Free and Forced Convection Flow Through a Porous Medium", Int. J. Energy Research, vol 12, pp. 557–560.
121	Manju, A., Vivek, J., Ramesh Yadav and Parul Saxena., 2016, " Investigation of Magneto hydrodynamic Flow in a Channel with Porous Bounding Wall", Int. J. Special topics and reviews in porous media, vol 7, pp. 281-291.
122	Vineet Kumar, V. and Amit Kumar, G., 2017, "Analytical Solution of the Flow in a Composite Cylindrical Channel Partially Filled with Porous Medium in the Effect of Magnetic Field", Int. J. Special topics and reviews in porous media, vol 8, pp. 39-48.
123	Baoku, I. G., Cookey, C.I. and Olajuwon, B.I.,2010 "Magnetic Field and Thermal Radiation Effects on Steady Hydro Magnetic Couette Flow Through a Porous Channel", Surveys in Mathematics and its Applications., vol 5, pp. 215-228.
124	Varshney, G., Katiyar, V.K. and Kumar, S., 2010 "Effect of Magnetic Field on the in Artery having Multiple Stenosis: A Numerical Study", Int. J. Eng, Sci. Tech., vol 2, pp. 67-82.
125	Ashish, T., Satya, D. and Filippov, A., 2012, "Effect of the Magnetic Field on the Hydrodynamic Permeability of a Membrane", Colloid Journal., vol 74, pp. 515–522.
126	Ghofrani, A., Dibaei M.H., Hakim Sima A., and Shafii M.B., 2013, "Experimental Investigation on Laminar Forced Convection Heat Transfer of

	Ferro Fluids Under an Alternating Magnetic Field, Experimental Thermal and Fluid Science", vol 49, pp.193–200.
127	Sheikholeslami, M., Rashidi, M.M. and Ganji, D.D., 2015, "Numerical Investigation of Magnetic Nano Fluid Forced Convective Heat Transfer in Existence of Variable Magnetic Field Using Two Phase Model", J. Molecular Liquids, vol 212, pp.117–126.
128	Sheikhnejad, Y., Hosseini, R. and Majid Saffar, A., 2015, "Laminar Forced Convection of Ferro Fluid in a Horizontal Tube Partially Filled with Porous Media in the Presence of a Magnetic Field", J. Porous Media, vol 18, pp. 437-448.
129	Takhar, H.S., and Beg, O.A., 1997,"Effects of Transverse Magnetic Field, Prandtl Number and Reynolds Number on Non-Darcy Mixed Convective Flow of an Incompressible Viscous Fluid Past a Porous Vertical Flat Plate in A Saturated Porous Medium", Int. J. Energy Research, **21**, pp. 87-100.
130	Barletta, A., Lazzari, S., Magyari, E., and Pop, I., 2008, "Mixed convection with heating effects in a vertical porous annulus with radially varying magnetic field", Int. J. Heat and Mass transfer, **51**, pp. 5777-5784.
131	Guven Komurgoz ., Aytac Arikoglu., and Ibrahim Ozkol., 2012, "Analysis of the Magnetic Effect on Entropy Generation in an Inclined Channel Partially Filled with a Porous Medium", Numerical Heat Transfer, Part A: Applications, **61**, pp. 786-799.
132	Sahar M. Abdel-Gaied., 2013, "Effect of Magnetic Field on Flow in a Porous Medium over a Permeable Stretching Wall in the Presence of Thermal Radiation and Suction/Injection", IOSR Journal of Mathematics (IOSR-JM), 7, pp. 68-73.
133	Srivastava, B.G., and Satya Deo., 2013, " Effect of magnetic field on the viscous fluid flow in a channel filled with porous medium of variable permeability", Applied Mathematics and Computation **219**, pp. 8959–8964.
134	Jhankal, A.K., Jat, R.N., and Deepak Kumar., 2017, "Magnetohydrodynamics (MHD) Forced Convective Flow and Heat Transfer Over a Porous Plate in a Darcy-Forchheimer Porous Medium in Presence of Radiation", IJCRR, 9, pp. 16-23.
135	Al-Hadhrami, A. K., Elliott, L., and Ingham, D. B., 2002, “Combined Free and Forced Convection Channels of Porous Media”, Transp. Porous Med, **49**, pp. 265-289.
136	Al-Hadhrami, A. K., Elliott, L., and Ingham, D. B., 2003, “A New Model for Viscous Dissipation in Porous Media across a Range of Permeability Values”, Transp. Porous Med, **53**, pp. 117-122.
137	Schlichting, H., and Gersten, K., 2007, *Boundary Layer Theory*, Springer-Verlag.
138	Takhar, H. S., Soundalgekar, V. M., and Gupta, A. S., 1990, “Mixed Convection of an Incompressible Viscous Fluid in a Porous Medium Past a Hot Vertical Plate”, Int. J. Non-Linear Mechanics, **25**. No. 6. pp. 723-728.
139	Murthy, P. V. S. N., and Singh, P., 1997, “Effect of Viscous Dissipation on a Non-Darcy Natural Convection Regime”, Int. J. Heat Mass Transfer, **40**, No. 6,

	pp. 1251-1260.
140	Nield, D. A., 2000, "Resolution of a Paradox Involving Viscous Dissipation and Nonlinear Drag in a Porous Medium", Transp. Porous Med, **41**, pp. 349-357.
141	Nield, D. A., 2006, "A Note on a Brinkman-Brinkman Forced Convection Problem", Trans. Porous Media, **64**, pp. 185-188.
142	Ingham, D. B., Pop, I., 1990, "Combined Free and Forced Convection Porous Medium between Two Vertical Walls with Viscous Dissipation", Transp. Porous Med, **5**, pp. 381-398.
143	Murthy, P. V. S. N., 1998, "Thermal Dispersion and Viscous Dissipation Effects on Non-Darcy Mixed Convection in a Fluid Saturated Porous Medium", Heat Mass Transfer, **33**, pp. 295-300.
144	Tashtoush, B., 2000, "Analytical Solution for the Effect of Viscous Dissipation on Mixed Convection in Saturated Porous Media", Transport in Porous Media, **41**, pp. 197-209.
145	Nield, D. A., Kuznetsov, A. V., and Xiong, M., 2003, "Thermally developing forced convection in a porous medium: Parallel plate channel with walls at uniform temperature, with axial conduction and viscous dissipation effects", Int. J. Heat and Mass Transfer, **46**, pp. 641-651.
146	Rees, D. A. S., Magyari E., and Keller, B., 2003, "The Development of the Asymptotic Viscous Dissipation Profile in a Vertical Free Convective Boundary Layer Flow in a Porous Medium", Transport in Porous Media, **53**, pp. 347-355.
147	Nield, D. A., Kuznetsov, A. V., and Xiong, M., 2004, "Effects of Viscous Dissipation and Flow Work on Forced Convection in a Channel Filled by a Saturated Porous Medium", Transp. Porous Med, **56**, pp. 351-367.
148	Hooman, K., and Ranjbar-Kani, A. A., 2004, "A Perturbation Solution for Viscous Dissipative Laminar Flow in a Porous-Saturated Pipe with Uniform Wall Temperature", I. J. Trans. Phenomena, **6**, pp. 307-313.
149	Umavathi, J. C., Kumar, J. P., Chamkha, A. J., and Pop, I., 2005, "Mixed Convection in a Vertical Porous Channel", Transp. Porous Med, **61**, pp. 315–335.
150	Mahmud, S., and Fraser, R. A., 2005, "Flow, Thermal, and Entropy Generation Characteristics Inside a Porous Channel with Viscous Dissipation", Int. J. Thermal Sciences, **44**, pp. 21-32.
151	Hooman, K., and Gorji-Bandpy, M., 2005, "Laminar Dissipative Flow in a Porous Channel Bounded By Isothermal Parallel Plates", Applied Mathematics and Mechanics, **26**, No. 5, pp. 587-593.
152	Morosuk, T. V., 2005, "Entropy Generation in Conduits Filled with Porous Medium Totally and Partially", Int. J. Heat Mass Transfer, **48**, pp. 2548-2560.
153	.Kuznetsov, A.V., Xiong, M., and Nield, D.A., 2003, " Thermally Developing Forced Convection in a Porous Medium: Circular Duct with Walls at Constant

	Temperature, with Longitudinal Conduction and Viscous Dissipation Effects", Transport in Porous Media, **53, pp.** 331–345.
154	Hooman, K., Pourshaghaghy, A., and Ejlali, A., 2006, " Effects Of Viscous Dissipation on Thermally Developing Forced Convection in a Porous Saturated Circular Tube with an Isoflux Wall", Applied Mathematics and Mechanics (English Edition), **27**, pp. 617–626.
155	Hooman, K., and Gurgenci, H., 2007, "Effects of Viscous Dissipation and Boundary Conditions on Forced Convection In a Channel Occupied by a Saturated Porous Medium", Transport Porous Med, **68**, pp.301-319.
156	Shigeru, T., and Ichimiya, K., 2007, " Analysis of laminar dissipative flow and heat transfer in a porous saturated circular tube with constant wall heat flux", Int. J. Heat and Mass Transfer, **50**, pp.2406-2413.
157	Olaseni Taiwo Lamidi., and Philip Oladapo Olanrewaju., 2010, "Analysis of the Effect of Viscous Dissipation on the Temperature Profile of the Laminar Flow in a Channel Filled with Saturated Porous Media", The Pacific Journal of Science and Technology, **11**, pp.37-44.
158	Satyamurty, V.V., and Bhargavi, D.,2010, "Forced Convection in Thermally Developing Region of a Channel Partially Filled with a Porous Material and Optimal Porous Fraction", Int. J. Thermal Sciences, **49**, pp. 319-332.
159	Habchi, S., and Acharya, S., 1986, “Laminar Mixed Convection in a Symmetrically or Asymmetrically Heated Vertical Channel”, Numerical Heat Transfer, **9**, pp. 605-618.
160	Naito, E., and Nagano, Y., 1989, “Combined Forced and Free Upward-Flow Convection in the Entrance Region between Inclined Parallel Plates”, ASME J. Heat Transfer, **111**, pp. 675-682.
161	Nguyen, T. V., 1992, “Laminar heat transfer for thermally developing flow in ducts”, Int. J. Heat Mass Transfer, **35**, **No.** 7, pp. 1733-1741.
162	Patankar, S. V., 1980, Numerical Heat Transfer and Fluid Flow, McGraw-Hill, New York.
163	Jeng, Y. N., Chen, J. L., and Aung, W., 1992, “On the Reynolds-Number Independence of Mixed Convection in a Vertical Channel Subjected to Asymmetric Wall Temperatures with and Without Flow Reversal”, Int. J. Heat and Fluid Flow,” **13**, pp. 329-339.
164	Krishnan, K. N., and Sastri, V. M. K., 1978, “Numerical Solution of Thermal Entry Length Problem with Variable Viscosities and Viscous Dissipation”, Heat and Mass Transfer, **11**, pp. 73-79.
165	Min, T., Choi, H. Y., Yoo, J. Y., and Choi, H., 1997, “Laminar Convective Heat Transfer of a Bingham Plastic in a Circular Pipe-II: Numerical Approach-Hydrodynamically Developing Flow and Simultaneously Developing Flow”, Int. J. Heat Mass Transfer, **40**, pp. 3689-3701.
166	Thomas, L. H., 1949, “Elliptic Problems in Linear Difference Equations over a Network”. Watson Sci. Comput. Lab. Rept., Columbia University, New York.

167	Lew, H. C., 1968, "Method of Accelerated Successive Replacement Applied to Boundary Layer Equations", AIAA journal, **6**, pp. 929-931.
168	Lieberstain, H. M., 1968, *A Course in Numerical Analysis*, Harper and Row, New York.
169	Dellinger, T. C., 1971, "Computations on Non-equilibrium Merged Shock Layer by Successive Accelerated Replacement Scheme", AIAA Journal, **9**, pp. 262-269.
170	Satyamurty, V. V., 1984, "Successive Accelerated Replacement Scheme Applied to Study of Natural Convection Heat Transfer in Porous Cryogenic Insulations", *ASME Paper no. 85-WA/HT-37*.
171	Satyamurty, V. V. and Marpu, D. R., 1988 "Relative Effects of Variable Fluid Properties and Non-Darcy Flow on Convection in Porous Media", *ASME HTD-96*, pp. 613-621.
172	Marpu, D. R., and Satyamurty, V. V., 1989, "Influence of Variable Fluid Density on Free Convection in Rectangular Porous Media", ASME J. Energy Resources Technology, **111**, pp. 214-220.
173	Satyamurty, V. V., and Marpu, D. R., 1989, "Influence of Linear and Non-Linear Variation of Viscosity on Free Convection in Liquid Filled Rectangular Porous Slabs", Chemical Engineering Communications, **88**, pp. 173-185.
174	Marpu, D. R., and Satyamurty, V. V., 1991, "Investigation on the Validity of Boussinesq Approximation on Free Convection in Vertical Porous Annulus", Warme-und Stoffubertragung, **26**, pp. 141-147.
175	Marpu, D. R., 1990, "Studies on Fluid Property Variation and Non-Darcy Flow on Free and Forced Convection in Porous Media", Ph.D. Thesis, IIT Kharagpur, India.
176	Sharma, R. V., 1998, "Studies on Influence of Fluid Density Variation and Non-Darcy Flow on Natural Convection in a Porous Box", Ph.D. Thesis, IIT Kharagpur, India.
177	Prakash Chandra, 2004, "Studies on Convection Heat Transfer in Fluid Filled Saturated Anisotropic Rectangular Porous Slab", Ph.D. Thesis, IIT Kharagpur, India.
178	Satyamurty, V. V., and Prakash Chandra, 2008, "Natural Convection Heat Transfer in Anisotropic Rectangular Porous Slab Subjected to End to End Temperature Difference", *Proceedings of 19th National and 8th ISHMT-ASME Heat and Mass Transfer Conference*, 3-5 January, 2008, Hyderabad, India.
179	Jagadeesh Kumar, M., and Satyamurty, V.V., 2015, " Effect of Entry Temperature on Forced Convection Heat Transfer With Viscous Dissipation in Thermally Developing Region of Concentric Annuli", J. Heat Transfer, 137, pp. 121001(1-8).
180	Chorlton, F., 2004, "Text Book of Fluid Mechanics".

181	Murthy, P.V.S.N., 2001, "Effect of Viscous Dissipation on Mixed Convection in a Non-Darcy Porous Medium", J. porous media, **4**, pp. 23-32.
182	Ramjee, R., and Satyamurty, V. V.,2013, "Effect of Viscous Dissipation on Forced Convection Heat Transfer in Parallel Plate Channels with Asymmetric Boundary Conditions", Proceedings of the ASME , International Mechanical Engineering Congress and Exposition IMECE2013 November 15-21, 2013, San Diego, California, USA.
183	Mahmoudi, Y., Karimi, N. and Mazaheri, K., 2014, "Analytical Investigation of Heat Transfer Enhancement in a Channel Partially Filled with a Porous Material Under Local Thermal Non-Equilibrium Condition: Effects Of Different Thermal Boundary Conditions at The Porous-Fluid Interface", Int. J. Heat Mass Transfer, **70**, pp.875–891.
184	Mahmoudi, Y. and Karimi, N., 2014, "Numerical Investigation of Heat Transfer Enhancement in a Pipe Partially Filled with a Porous Material Under Local Thermal Non-Equilibrium Condition", Int. J. Heat Mass Transfer, 68, pp.161–173.
185	Kays, W. M., Crawford, M. E., and Weigand, B., 2012, "Convective Heat and Mass Transfer", Fourth edition.
186	Bhargavi, D., 2011, "Forced Convection Heat Transfer with Viscous Dissipation in Parallel Plate Channels Partially Filled with Porous material", Ph.D thesis, I.I.T Kharagpur, India
187	Pavel, B.I., and Mohamad, A.A., 2004, "An Experimental and Numerical Study on Heat Transfer Enhancement For Gas Heat Exchangers Fitted with Porous Media", Int. J. Heat Mass Transfer, **47**, pp. 4939–4952.
188	Jiang Pei-Xue., Li Meng., Tian-Jian Lu., Lie Yu and Ze-Pei Ren., 2004, "Experimental research on convection heat transfer in sintered porous plate channels", Int. J. heat and mass transfer, **47**, pp. 2085-2096.
189	Antia, H. M., 1991, "Numerical Methods for Scientists and Engineers", Tata McGraw Hill, New Delhi, India.
190	Jagadeesh Kumar, M., 2016, "Effect of Axial Conduction and Viscous Dissipation on Heat Transfer for Laminar Flow Through a Circular Pipe", Perspectives in Science, **8**, pp. 61-65.
191	Mohamad. A., 2003, "Heat transfer enhancements in heat exchangers fitted with porous media Part I: constant wall temperature", International Journal of Thermal Sciences, **42**, pp. 385–395.
192	Nuri Yucel and Tolga Guven. R., 2007 "Forced-Convection Cooling Enhancement of Heated Elements in a Parallel-Plate Channels using Porous Inserts", Numerical Heat Transfer, Part A, **51**, pp. 293–312.

Appendix

$$A_1 = e^{\frac{\gamma_p}{2}\sqrt{\frac{\varepsilon}{Da}}} - 1$$

$$A_2 = e^{\gamma_p\sqrt{\frac{\varepsilon}{Da}}} + 1$$

$$A_3 = e^{\gamma_p\sqrt{\frac{\varepsilon}{Da}}} - 1$$

$$A_4 = e^{\frac{\gamma_p}{2}\sqrt{\frac{\varepsilon}{Da}}}$$

$$A_5 = e^{\gamma_p\sqrt{\frac{\varepsilon}{Da}}}$$

$$A_6 = e^{-\frac{1}{2}\sqrt{\frac{\varepsilon}{Da}}}$$

$$A_7 = e^{\frac{1}{2}\sqrt{\frac{\varepsilon}{Da}}}$$

$$A_8 = e^{\frac{(1+2\gamma_p)}{2}\sqrt{\frac{\varepsilon}{Da}}}$$

$$A_9 = e^{\frac{(1+\gamma_p)}{2}\sqrt{\frac{\varepsilon}{Da}}}$$

$$A_{10} = e^{\sqrt{\frac{\varepsilon}{Da}}}$$

$$A_{11} = 240Da^{3/2}A_3$$

$$A_{12} = A_3\varepsilon(\gamma_p - 1)^2$$

$$A_{13} = A_2\sqrt{\varepsilon}(\gamma_p - 1)^3$$

$$A_{14} = A_5(\gamma_p - 2) - 4A_4(\gamma_p - 1) + \gamma_p - 2$$

$$A_{15} = -1/\left(\sqrt{\varepsilon}\right)210Dae^{-\frac{(1+2\gamma_p)}{2}\sqrt{\frac{\varepsilon}{Da}}}$$

$$A_{16} = e^{\frac{1}{2}\sqrt{\frac{\varepsilon}{Da}}}(A_5 - A_5{}^3)$$

$$A_{17} = \varepsilon\left(-4A_4(\gamma_p - 2) + 7(\gamma_p - 1)(1 + A_5)\right)$$

$$A_{18} = 2 - 2(2+3\varepsilon)\gamma_p + (2+3\varepsilon){\gamma_p}^2$$

$$A_{19} = \left({A_5}^2(3\gamma_p - 5) + 2A_5(4\gamma_p - 7) - 5 - 12(-1+\gamma_p)(A_4 - A_4^3) + 3\gamma_p \right)$$

$$A_{20} = 2(\gamma_p - 1)^3 + \varepsilon(-6 + 30\gamma_p - 33{\gamma_p}^2 + 11{\gamma_p}^3)$$

$$A_{21} = 12DaA_1^2 + A_2(\gamma_p - 1)^2$$

$$A_{22} = 24DaA_1^2 + A_2(\gamma_p - 1)^2$$

$$A_{23} = -4 + 8\gamma_p - 18\eta\gamma_p - 4{\gamma_p}^2 + 15\eta{\gamma_p}^2$$

$$A_{24} = -8 + (16 - 30\eta)\gamma_p + (-8 + 25\eta){\gamma_p}^2$$

$$A_{25} = -2(-1+\gamma_p)^2 + 3\eta(2 - 8\gamma_p + 5{\gamma_p}^2)$$

$$A_{26} = e^{\gamma_p\sqrt{\frac{\varepsilon(1+DaM^2)}{Da}}}$$

$$A_{27} = e^{\frac{\gamma_p}{2}\sqrt{\frac{\varepsilon(1+DaM^2)}{Da}}}$$

$$A_{28} = \sqrt{1+DaM^2}\left(A_1 + 1 + 2DaM^2A_2\right)\sqrt{\varepsilon}\ \sinh[M(\gamma_p - 1)]$$

$$A_{29} = 2A_1(A_1 - 1)M\cosh[M(\gamma_p - 1)]$$

$$A_{30} = \sqrt{(1+DaM^2)\varepsilon}\left(1 + DaM^2(1+\varepsilon)\right)\gamma_p + \sqrt{(1+DaM^2)}\left(1 - DaM^2(-1+\varepsilon)\right)\gamma_p\left(\frac{A_1 + A_1^{-1}}{2}\right)$$

$$A_{31} = 2\sqrt{Da}\left(-2(DaM^2 - 1)\varepsilon\left(\frac{A_2 - A_2^{-1}}{2}\right) + \left(-1 + DaM^2(-1+\varepsilon)\varepsilon\right)\left(\frac{A_1 - A_1^{-1}}{2}\right)\right)$$

$$A_{32} = -\gamma_p\left(A_1^2 + 1\right)\sqrt{\varepsilon(1+DaM^2)}$$

$$A_{33} = \sqrt{(1+DaM^2)}\left(1 - DaM^2(1+\varepsilon)\right)\sqrt{\varepsilon}\gamma_p + DaM^2\sqrt{(1+DaM^2)\varepsilon}(1+\varepsilon)\gamma_p\left(\frac{A_1 - A_1^{-1}}{2}\right)$$

$$A_{34} = 2\sqrt{Da}\left(2(DaM^2 - 1)\varepsilon\left(\frac{A_2 - A_2^{-1}}{2}\right) - (1 - \varepsilon + DaM^2(1+\varepsilon))\left(\frac{A_1 - A_1^{-1}}{2}\right)\right)$$

$$A_{35} = \left(1 + A_1\left(2 - 2DaM^2(-1+\varepsilon)\right) + DaM^2(1+\varepsilon) + A_1^2\left(1 + DaM^2(1+\varepsilon)\right)\right)$$

$$A_{36} = \left(1 + A_1^2\left(1 - DaM^2(-1+\varepsilon)\right) - DaM^2(\varepsilon - 1) + 2A_1\left(1 + DaM^2(1+\varepsilon)\right)\right)\cosh[M(\gamma_p - 1)]$$

$$A_{37} = (-DaM^2 - 1)\begin{pmatrix} 2 + e^{2M(\gamma_p - 1)}(M(1 + DaM^2(1+\varepsilon))(\gamma_p - 1) - 2) \\ -2e^{2M(\gamma_p - 1)}M(-1 + DaM^2(-1+\varepsilon))(\gamma_p - 1) + M(1 + DaM^2(1+\varepsilon))(\gamma_p - 1) \end{pmatrix}$$

$$A_{38} = 4Da\left(-1 + e^{2M(\gamma_p - 1)}\right)M^2(1 + DaM^2)\left(\frac{A_2 - A_2^{-1}}{2}\right)$$

$$A_{39} = (1 + DaM^2)\begin{pmatrix} 2 + e^{2M(\gamma_p - 1)}(2 + M(-1 + DaM^2(-1+\varepsilon))(\gamma_p - 1)) \\ -2e^{M(\gamma_p - 1)}M(1 + DaM^2(1+\varepsilon))(\gamma_p - 1)\left(\frac{A_1 - A_1^{-1}}{2}\right) + M(-1 + DaM^2(1+\varepsilon)) \end{pmatrix}$$

$$A_{40} = 2\sqrt{Da}(1 + e^{M(\gamma_p - 1)})^2 M\sqrt{\varepsilon(1 + DaM^2)}\left(2DaM^2\left(\frac{A_2 - A_2^{-1}}{2}\right) + \left(\frac{A_1 - A_1^{-1}}{2}\right)\right)$$

$$A_{41} = -1 + e^{2M(\gamma_p - 1)}\left(-1 + DaM^2(-1+\varepsilon)\right) + DaM^2(-1+\varepsilon) - 2e^{M(\gamma_p - 1)}M\left(1 + DaM^2(1+\varepsilon)\right)\left(\frac{A_1 - A_1^{-1}}{2}\right)$$

$$A_{42} = 2e^{M(\gamma_p - 1)}\left(1 - DaM^2(-1+\varepsilon) + (1 + DaM^2(1+\varepsilon))\cosh[M - M\gamma_p]\right)$$

$$A_{43} = \left(A_1 - 2A_2 + 1\right)e^{-\frac{1}{2}\sqrt{\frac{\varepsilon}{Da}(1 + DaM^2)}}$$

$$A_{44} = \frac{2A_2 e^{-\frac{1}{2}\sqrt{\frac{\varepsilon}{Da}(1 + DaM^2)}}(1 + DaM^2)\left(\frac{\sqrt{Da}\tanh[\frac{\gamma_p}{4}\sqrt{\frac{\varepsilon(1 + DaM^2)}{Da}}]}{\sqrt{(1 + DaM^2)\varepsilon}} + \frac{\tanh\left[\frac{M}{2}(1-\gamma_p)\right]}{M}\right)}{\frac{\coth[\frac{\gamma_p}{2}\sqrt{\frac{\varepsilon(1 + DaM^2)}{Da}}]}{\sqrt{Da\varepsilon}} + M\ \tanh\left[\frac{M}{2}(\gamma_p - 1)\right]}$$

$$A_{45} = \frac{\left(1 + A_1\right)\sqrt{\varepsilon}\gamma_p(1 + DaM^2) - 2\sqrt{Da}A_5\sqrt{1 + DaM^2}}{(1 + DaM^2)^{3/2}\varepsilon\gamma_p}$$

$$A_{46} = -8e^{-\sqrt{\frac{\varepsilon}{Da}(1 + DaM^2)}}(A_1 - A_2^3)$$

$$A_{47} = \frac{-Da\left(-4\sqrt{Da}A_5 + A_7\sqrt{1 + DaM^2}\varepsilon\gamma_p\right)p_g}{A_7(1 + DaM^2)^{3/2}\sqrt{\varepsilon}}$$

$$A_{48} = \frac{-2\left(2U_i(e^{M(\gamma_p - 1)} - 1)M^2 + (M - 2 - M\gamma_p + e^{M(\gamma_p - 1)}(2 + M - M\gamma_p))p_g\right)}{(1 + e^{M(\gamma_p - 1)})M^3}$$

$$A_{49} = \left(1 + e^{M(\gamma_p - 1)}\right)(M^2(-4Y^2 + (\gamma_p - 1)^2 - 8)$$

$$A_{50} = \left(1 - e^{2\sqrt{\frac{\varepsilon}{Da}(1+DaM^2)}}\right)\varepsilon$$

$$A_{51} = 8e^{\frac{3}{2}\sqrt{\frac{\varepsilon}{Da}(1+DaM^2)}} - 8e^{\frac{1}{2}\sqrt{\frac{\varepsilon}{Da}(1+DaM^2)}}$$

$$A_{52} = 1 + e^{2\sqrt{\frac{\varepsilon}{Da}(1+DaM^2)}}$$

$$A_{53} = \left(1 + e^{\sqrt{\frac{\varepsilon}{Da}(1+DaM^2)}}\right)\varepsilon\sqrt{(1+DaM^2)}$$

$$A_{54} = 1 + e^{\sqrt{\frac{\varepsilon}{Da}}\gamma_p}$$

$$A_{55} = -1 + e^{\sqrt{\frac{\varepsilon}{Da}}\gamma_p}$$

$$A_{56} = -2 + e^{\sqrt{\frac{\varepsilon}{Da}}\gamma_p}(-2 + \gamma_p) - 4e^{\frac{1}{2}\sqrt{\frac{\varepsilon}{Da}}\gamma_p}(-1 + \gamma_p) + \gamma_p$$

$$A_{57} = \left(-1 + e^{\frac{1}{2}\sqrt{\frac{\varepsilon}{Da}}\gamma_p}\right)^2\left(7 - 2e^{\frac{1}{2}\sqrt{\frac{\varepsilon}{Da}}\gamma_p} + 7e^{\sqrt{\frac{\varepsilon}{Da}}\gamma_p}\right)$$

$$A_{58} = \left(-2 + e^{\frac{1}{2}\sqrt{\frac{\varepsilon}{Da}}\gamma_p} - e^{\frac{3}{2}\sqrt{\frac{\varepsilon}{Da}}\gamma_p} + 2e^{2\sqrt{\frac{\varepsilon}{Da}}\gamma_p}\right)(-1 + \gamma_p)\sqrt{\varepsilon}$$

$$A_{59} = e^{\sqrt{\frac{\varepsilon}{Da}}\gamma_p}(-1 + \gamma_p)^2\varepsilon^2{\gamma_p}^2$$

$$A_{60} = \varepsilon^{3/2}(-1 + \gamma_p)\gamma_p\left(-1 + e^{\sqrt{\frac{\varepsilon}{Da}}\gamma_p}(-1 + \gamma_p) + \gamma_p + 2e^{\frac{1}{2}\sqrt{\frac{\varepsilon}{Da}}\gamma_p}\right)$$

$$A_{61} = 1 - 10\gamma_p - 4\varepsilon^{3/2}e^{\frac{1}{2}\sqrt{\frac{\varepsilon}{Da}}\gamma_p}(-1 + \gamma_p)\gamma_p + 7{\gamma_p}^2 + 2e^{\sqrt{\frac{\varepsilon}{Da}}\gamma_p}(-1 - 6\gamma_p + 3{\gamma_p}^2) + 2e^{2\sqrt{\frac{\varepsilon}{Da}}\gamma_p}(1 - 10\gamma_p + 7{\gamma_p}^2)$$

$$A_{62} = \left(24Da^{3/2} - 6\sqrt{Da}\varepsilon(\gamma_p - 1)^2\right)A_2 + A_1\sqrt{\varepsilon}(\gamma_p - 1)^3 + 12Da\sqrt{\varepsilon}A_3$$

$$A_{63} = \left({A_2}^2 - 48Da^{3/2}A_2\sqrt{\varepsilon}\left(\begin{array}{l} 1 + e^{\sqrt{\frac{\varepsilon}{Da}}}(1 + 3\varepsilon(\gamma_p - 2) - \gamma_p) \\ +3\varepsilon(\gamma_p - 2) - 12e^{\frac{1}{2}\sqrt{\frac{\varepsilon}{Da}}\gamma_p}\varepsilon(\gamma_p - 1) - \gamma_p \end{array}\right)(\gamma_p - 1)^2\right)$$

$$A_{64} = \left(-e^{2\gamma_p \sqrt{\frac{\varepsilon}{Da}}} \right) \varepsilon^{3/2} (\gamma_p - 1)^5$$

$$A_{65} = \sqrt{\varepsilon} A_2 A_3$$

$$A_{66} = e^{2\gamma_p \sqrt{\frac{\varepsilon}{Da}}} \left(4(\gamma_p - 2) + (\gamma_p - 1) \left(6\varepsilon - 8e^{\frac{\gamma_p}{2} \sqrt{\frac{\varepsilon}{Da}}} - 8e^{\frac{3\gamma_p}{2} \sqrt{\frac{\varepsilon}{Da}}} \right) + e^{\sqrt{\frac{\varepsilon}{Da}}} (-8 + 6\varepsilon + 4\gamma_p - 6\varepsilon\gamma_p) \right)$$

$$A_{67} = e^{\gamma_p \sqrt{\frac{\varepsilon}{Da}}} (-28 + 48\gamma_p - 22\gamma_p{}^2) + (-2 + \gamma_p{}^2)(1 + e^{2\gamma_p \sqrt{\frac{\varepsilon}{Da}}}) + 8 \left(e^{\frac{\gamma_p}{2} \sqrt{\frac{\varepsilon}{Da}}} + e^{\frac{3\gamma_p}{2} \sqrt{\frac{\varepsilon}{Da}}} \right) (2 - 3\gamma_p + \gamma_p{}^2)$$

$$A_{68} = \left(-1 + e^{\frac{1}{2} \sqrt{\frac{\varepsilon}{Da}} \gamma_p} \right)^2 \left(7 - 2e^{\frac{1}{2} \sqrt{\frac{\varepsilon}{Da}} \gamma_p} + 7e^{\sqrt{\frac{\varepsilon}{Da}} \gamma_p} \right)$$

$$A_{69} = 8Da^{3/2} A_5 - e^{\sqrt{\frac{\varepsilon}{Da}} \gamma_p} \varepsilon^2 (\gamma_p - 1)^2 \gamma_p{}^2$$

$$A_{70} = \left(-1 + e^{\sqrt{\frac{\varepsilon}{Da}} \gamma_p} \right) A_7$$

$$A_{71} = A_8 - 4e^{\frac{3}{2} \sqrt{\frac{\varepsilon}{Da}} \gamma_p} (-1 + \gamma_p) \gamma_p$$

$$A_{72} = \left(e^{\frac{\gamma_p}{2} \sqrt{\frac{\varepsilon}{Da}}} - e^{\frac{3\gamma_p}{2} \sqrt{\frac{\varepsilon}{Da}}} \right) \varepsilon^{3/2} (\gamma_p - 1) \gamma_p$$

$$A_{73} = \varepsilon^2 (\gamma_p - 1)^2 \gamma_p$$

$$A_{74} = 8Da \left(-1 + e^{\frac{\gamma_p}{2} \sqrt{\frac{\varepsilon}{Da}}} \right)^2 - 4\sqrt{Da\varepsilon} A_2 (\gamma_p - 1) + A_1 \varepsilon (\gamma_p - 2) \gamma_p$$

$$A_{75} = -A_1{}^2 \varepsilon (\gamma_p - 1)^3 \gamma_p$$

$$A_{76} = A_1{}^2 \varepsilon (\gamma_p - 2Y - 1) \gamma_p$$

$$A_{77} = \left(-1 + e^{\frac{\gamma_p}{2} \sqrt{\frac{\varepsilon}{Da}}} \right)^2 \left(-7 + e^{\gamma_p \sqrt{\frac{\varepsilon}{Da}}} (-7 + \varepsilon) + \varepsilon + 2e^{\frac{\gamma_p}{2} \sqrt{\frac{\varepsilon}{Da}}} (1 + \varepsilon) \right)$$

$$A_{78} = \left(-2 + 2e^{2\gamma_p \sqrt{\frac{\varepsilon}{Da}}} + e^{\frac{\gamma_p}{2}\sqrt{\frac{\varepsilon}{Da}}}(1+\varepsilon) - e^{\frac{3\gamma_p}{2}\sqrt{\frac{\varepsilon}{Da}}}(1+\varepsilon) \right)(\gamma_p - 1)$$

$$A_{79} = 1 + \varepsilon(\gamma_p - 1)^2 + 8(\gamma_p - 1)\gamma_p + 3{\gamma_p}^2 - 2\gamma_p(1 + 2\gamma_p)$$
$$+ e^{2\gamma_p \sqrt{\frac{\varepsilon}{Da}}}(1 + \varepsilon(\gamma_p - 1)^2 - 2\gamma_p - {\gamma_p}^2) + 2e^{\gamma_p \sqrt{\frac{\varepsilon}{Da}}}(-1 + 2\gamma_p - 5{\gamma_p}^2 + \varepsilon(-1 + 2\gamma_p + {\gamma_p}^2))$$
$$+ 4\gamma_p(\gamma_p - 1)\left(4e^{\gamma_p \sqrt{\frac{\varepsilon}{Da}}} + 2e^{2\gamma_p \sqrt{\frac{\varepsilon}{Da}}} - e^{\frac{\gamma_p}{2}\sqrt{\frac{\varepsilon}{Da}}}(1+\varepsilon) - e^{\frac{3\gamma_p}{2}\sqrt{\frac{\varepsilon}{Da}}}(1+\varepsilon) \right)$$

$$A_{80} = (\gamma_p - 1)(1+\varepsilon)\left(e^{\gamma_p \sqrt{\frac{\varepsilon}{Da}}} - e^{3\gamma_p \sqrt{\frac{\varepsilon}{Da}}} \right) - 2(-1+\varepsilon)\gamma_p \left(e^{\frac{3\gamma_p}{2}\sqrt{\frac{\varepsilon}{Da}}} - e^{\frac{5\gamma_p}{2}\sqrt{\frac{\varepsilon}{Da}}} \right)$$

$$A_{81} = {A_1}^2 \varepsilon(\gamma_p - 1)^3 \gamma_p$$

$$A_{82} = \left(1 + e^{\gamma_p \sqrt{\frac{\varepsilon}{Da}}}(1 + 3\varepsilon(\gamma_p - 2) - \gamma_p) + 3\varepsilon(\gamma_p - 2) - 12e^{\frac{\gamma_p}{2}\sqrt{\frac{\varepsilon}{Da}}}\varepsilon(\gamma_p - 1) - \gamma_p \right)(\gamma_p - 1)^2$$

$$A_{83} = \left(1 + e^{2\gamma_p \sqrt{\frac{\varepsilon}{Da}}} \right)\varepsilon^{3/2}(\gamma_p - 1)^5$$

$$A_{84} = {A_1}^2 \varepsilon(\gamma_p - 1)^6$$

$$A_{85} = -2 + e^{\sqrt{\frac{\varepsilon}{Da}}\gamma_p}(-2 + \gamma_p) - 4e^{\frac{1}{2}\sqrt{\frac{\varepsilon}{Da}}\gamma_p}(-1 + \gamma_p) + \gamma_p$$

$$A_{86} = e^{2\sqrt{\frac{\varepsilon}{Da}}\gamma_p}(2(\gamma_p - 2) + 3\varepsilon(\gamma_p - 1)) + 2(\gamma_p - 2) + e^{\sqrt{\frac{\varepsilon}{Da}}\gamma_p}(6\varepsilon + 4\gamma_p - 8 - 6\varepsilon\gamma_p)$$
$$- (\gamma_p - 1)\left(16e^{\frac{1}{2}\sqrt{\frac{\varepsilon}{Da}}\gamma_p} + 3\varepsilon \right)$$

$$A_{87} = ({\gamma_p}^2 - 2)\left(1 + e^{2\sqrt{\frac{\varepsilon}{Da}}\gamma_p} \right) + e^{\sqrt{\frac{\varepsilon}{Da}}\gamma_p}(-28 + 48\gamma_p - 22{\gamma_p}^2)$$
$$+ 8(2 - 3\gamma_p + {\gamma_p}^2)\left(e^{\frac{1}{2}\sqrt{\frac{\varepsilon}{Da}}\gamma_p} + e^{\frac{3}{2}\sqrt{\frac{\varepsilon}{Da}}\gamma_p} \right)$$

$$A_{88} = \left(-1 + e^{\frac{\gamma_p}{2}\sqrt{\frac{\varepsilon}{Da}}} \right)^2 \left(-7 + e^{\gamma_p \sqrt{\frac{\varepsilon}{Da}}}(-7 + \varepsilon) + \varepsilon + 2e^{\frac{\gamma_p}{2}\sqrt{\frac{\varepsilon}{Da}}}(1+\varepsilon) \right),$$

$$A_{89} = \left(-2 + 2e^{2\gamma_p \sqrt{\frac{\varepsilon}{Da}}} + e^{\frac{\gamma_p}{2}\sqrt{\frac{\varepsilon}{Da}}}(1+\varepsilon) - e^{\frac{3\gamma_p}{2}\sqrt{\frac{\varepsilon}{Da}}}(1+\varepsilon) \right)(\gamma_p - 1),$$

$$A_{90} = e^{2\gamma_p \sqrt{\frac{\varepsilon}{Da}}}(-1+\varepsilon)\varepsilon^2(\gamma_p - 1)^2 {\gamma_p}^2$$

$$A_{91} = (\gamma_p - 1)(1+\varepsilon)\left(e^{\gamma_p \sqrt{\frac{\varepsilon}{Da}}} - e^{3\gamma_p \sqrt{\frac{\varepsilon}{Da}}} \right) - 2(-1+\varepsilon)\gamma_p \left(e^{\frac{3\gamma_p}{2}\sqrt{\frac{\varepsilon}{Da}}} - e^{\frac{5\gamma_p}{2}\sqrt{\frac{\varepsilon}{Da}}} \right)$$

$$A_{92} = \left(e^{\frac{\gamma_p}{2}\sqrt{\frac{\varepsilon}{Da}}} - e^{\frac{3\gamma_p}{2}\sqrt{\frac{\varepsilon}{Da}}} \right)(-1+\varepsilon)\varepsilon^{3/2}(\gamma_p - 1)\gamma_p$$

$$A_{93} = e^{\gamma_p \sqrt{\frac{\varepsilon}{Da}}}(-1+\varepsilon)\varepsilon^2(\gamma_p - 1)^2 \gamma_p$$

$$A_{94} = -2\sqrt{Da}\left(-1 + e^{\sqrt{\frac{\varepsilon}{Da}}} \right) + \left(1 + e^{\sqrt{\frac{\varepsilon}{Da}}} \right)\sqrt{\varepsilon}$$

$$A_{95} = \left(1 + e^{2\sqrt{\frac{\varepsilon}{Da}}} - 2e^{\sqrt{\frac{\varepsilon}{Da}}}(-2+\varepsilon) \right)$$

$$A_{96} = -12{U_i}^2 \left(Da\left(e^{\gamma_p \sqrt{\frac{\varepsilon}{Da}}} - 1 \right)^2 - \sqrt{Da}\left(e^{2\gamma_p \sqrt{\frac{\varepsilon}{Da}}} - 1 \right)\sqrt{\varepsilon}\gamma_p + e^{\gamma_p \sqrt{\frac{\varepsilon}{Da}}}\varepsilon {\gamma_p}^2 \right)$$

$$A_{97} = 12U_i Da\left(e^{\frac{\gamma_p}{2}\sqrt{\frac{\varepsilon}{Da}}} - 1 \right)\left(\begin{array}{l} 6Da\left(e^{\frac{\gamma_p}{2}\sqrt{\frac{\varepsilon}{Da}}} - 1 \right)\left(e^{\frac{\gamma_p}{2}\sqrt{\frac{\varepsilon}{Da}}} + 1 \right)^2 - 2\sqrt{Da}\left(\begin{array}{l} 1 + 2e^{\frac{\gamma_p}{2}\sqrt{\frac{\varepsilon}{Da}}} + \\ 2e^{\gamma_p \sqrt{\frac{\varepsilon}{Da}}} + e^{\frac{3\gamma_p}{2}\sqrt{\frac{\varepsilon}{Da}}} \end{array} \right)\sqrt{\varepsilon}\gamma_p \\ + e^{\frac{\gamma_p}{2}\sqrt{\frac{\varepsilon}{Da}}}\left(e^{\frac{\gamma_p}{2}\sqrt{\frac{\varepsilon}{Da}}} - 1 \right)\varepsilon {\gamma_p}^2 \end{array} \right) p_g$$

$$A_{98} = -Da\left(e^{\frac{\gamma_p}{2}\sqrt{\frac{\varepsilon}{Da}}} - 1 \right)^2 \sqrt{\varepsilon}\gamma_p \left(\begin{array}{l} 36Da^{3/2}\left(e^{\gamma_p \sqrt{\frac{\varepsilon}{Da}}} - 1 \right) + \left(e^{\frac{\gamma_p}{2}\sqrt{\frac{\varepsilon}{Da}}} + 1 \right)^2 \sqrt{\varepsilon}(\gamma_p - 1)^3 \\ -6Da\left(1 + 4e^{\frac{\gamma_p}{2}\sqrt{\frac{\varepsilon}{Da}}} + e^{\gamma_p \sqrt{\frac{\varepsilon}{Da}}} \right)\sqrt{\varepsilon}\gamma_p \end{array} \right) {p_g}^2$$

$$A_{99} = \left(e^{\frac{\gamma_p}{2}\sqrt{\frac{\varepsilon}{Da}}} - 1 \right)^2 \varepsilon\gamma_p$$

$$A_{100} = \left(e^{\frac{(5\gamma_p - 2)}{2}\sqrt{\frac{\varepsilon}{Da}}} - e^{(2\gamma_p - 1)\sqrt{\frac{\varepsilon}{Da}}} \right) \gamma_p$$

$$A_{101} = Da^2 \left(e^{\frac{\gamma_p}{2}\sqrt{\frac{\varepsilon}{Da}}} - 1 \right)^2$$

$$A_{102} = -2Dae^{(\gamma_p - 1)\sqrt{\frac{\varepsilon}{Da}}}$$

$$A_{103} = \left(1 + 4e^{\frac{\gamma_p}{2}\sqrt{\frac{\varepsilon}{Da}}} + e^{\gamma_p\sqrt{\frac{\varepsilon}{Da}}} \right) \varepsilon$$

$$A_{104} = \sqrt{Da} \left(-2\sqrt{Da} \left(e^{\gamma_p\sqrt{\frac{\varepsilon}{Da}}} - 1 \right) + \left(e^{\gamma_p\sqrt{\frac{\varepsilon}{Da}}} + 1 \right) \sqrt{\varepsilon}\gamma_p \right)$$

$$A_{105} = 24Da^{3/2} \left(e^{\frac{\gamma_p}{2}\sqrt{\frac{\varepsilon}{Da}}} - 1 \right)^2 \sqrt{\varepsilon}\gamma_p + \left(e^{\gamma_p\sqrt{\frac{\varepsilon}{Da}}} - 1 \right) \varepsilon\gamma_p \left((\gamma_p - 1)^3 - 6Da\gamma_p \right)$$

$$A_{106} = \frac{6U_i{}^2 \left(Da \left(e^{\gamma_p\sqrt{\frac{\varepsilon}{Da}}} - 1 \right)^2 (1+\varepsilon) - \sqrt{Da} \left(e^{2\gamma_p\sqrt{\frac{\varepsilon}{Da}}} - 1 \right) \sqrt{\varepsilon}(1+\varepsilon)\gamma_p - e^{\gamma_p\sqrt{\frac{\varepsilon}{Da}}} (\varepsilon - 1)\varepsilon\gamma_p{}^2 \right)}{Da \left(e^{\gamma_p\sqrt{\frac{\varepsilon}{Da}}} - 1 \right)^2 \varepsilon\gamma_p}$$

$$A_{107} = 6U_i \left(e^{\frac{\gamma_p}{2}\sqrt{\frac{\varepsilon}{Da}}} - 1 \right) \left(\begin{array}{l} 2Da \left(e^{\frac{\gamma_p}{2}\sqrt{\frac{\varepsilon}{Da}}} - 1 \right) \left(e^{\frac{\gamma_p}{2}\sqrt{\frac{\varepsilon}{Da}}} + 1 \right)^2 (\varepsilon - 3) - 2\sqrt{Da\varepsilon} \left(e^{\frac{\gamma_p}{2}\sqrt{\frac{\varepsilon}{Da}}} + 1 \right) \left(\begin{array}{l} e^{\gamma_p\sqrt{\frac{\varepsilon}{Da}}} (\varepsilon - 1) + \varepsilon \\ -e^{\frac{\gamma_p}{2}\sqrt{\frac{\varepsilon}{Da}}} (\varepsilon + 1) - 1 \end{array} \right) \gamma_p \\ + e^{\frac{\gamma_p}{2}\sqrt{\frac{\varepsilon}{Da}}} \left(e^{\frac{\gamma_p}{2}\sqrt{\frac{\varepsilon}{Da}}} - 1 \right) (\varepsilon - 1)\varepsilon\gamma_p{}^2 \end{array} \right) p_g$$

$$A_{108} = \frac{1}{2}(\gamma_p - 1)^3 \, p_g{}^2$$

$$A_{109} = \frac{3Da}{\left(1 + e^{\frac{1}{2}\sqrt{\frac{\varepsilon}{Da}}} \right)^2 \sqrt{\varepsilon}} \left(2\sqrt{Da} \left(e^{\gamma_p\sqrt{\frac{\varepsilon}{Da}}} - 1 \right) (\varepsilon - 3) - \left(e^{\gamma_p\sqrt{\frac{\varepsilon}{Da}}} + 2e^{\frac{\gamma_p}{2}\sqrt{\frac{\varepsilon}{Da}}} (\varepsilon - 2) - 1 \right) \sqrt{\varepsilon}\gamma_p \right) p_g{}^2$$

$$A_{110} = \left(e^{\frac{3\gamma_p}{2}\sqrt{\frac{\varepsilon}{Da}}} - e^{\gamma_p\sqrt{\frac{\varepsilon}{Da}}} \right) (\varepsilon + 1)\gamma_p$$

$$A_{111} = e^{\gamma_p\sqrt{\frac{\varepsilon}{Da}}} - 2e^{\frac{3\gamma_p}{2}\sqrt{\frac{\varepsilon}{Da}}} + e^{2\gamma_p\sqrt{\frac{\varepsilon}{Da}}}$$

$$A_{112} = \left(e^{\frac{1}{2}\sqrt{\frac{\varepsilon}{Da}}} - 1\right)^2 \left(1 + e^{\gamma_p\sqrt{\frac{\varepsilon}{Da}}} - 2e^{\frac{\gamma_p}{2}\sqrt{\frac{\varepsilon}{Da}}}(\varepsilon - 2)\right)\varepsilon$$

$$A_{113} = \left(24Da^{3/2} - 6\sqrt{Da}\varepsilon(\gamma_p - 1)^2\right)\left(e^{\gamma_p\sqrt{\frac{\varepsilon}{Da}}} - 1\right) + \left(e^{\gamma_p\sqrt{\frac{\varepsilon}{Da}}} + 1\right)\sqrt{\varepsilon}(\gamma_p - 1)^3$$
$$+ 12Da\sqrt{\varepsilon}\left(\left(e^{\gamma_p\sqrt{\frac{\varepsilon}{Da}}} + 1\right)(\gamma_p - 2) - 4e^{\frac{\gamma_p}{2}\sqrt{\frac{\varepsilon}{Da}}}(\gamma_p - 1)\right)$$

$$A_{114} = 12U_i^2 \begin{pmatrix} \sqrt{Da}\left(e^{(\gamma_p-1)\sqrt{\frac{\varepsilon}{Da}}} - e^{(3\gamma_p-1)\sqrt{\frac{\varepsilon}{Da}}}\right) + 2e^{(2\gamma_p-1)\sqrt{\frac{\varepsilon}{Da}}}\sqrt{\varepsilon}\gamma_p \\ -24U_i Da\left(e^{\frac{\gamma_p}{2}\sqrt{\frac{\varepsilon}{Da}}} - 1\right)^2\left(\sqrt{Da}\left(e^{(\gamma_p-1)\sqrt{\frac{\varepsilon}{Da}}} - e^{(2\gamma_p-1)\sqrt{\frac{\varepsilon}{Da}}}\right) + e^{\frac{(3\gamma_p-2)}{2}\sqrt{\frac{\varepsilon}{Da}}}\sqrt{\varepsilon}\gamma_p\right)p_g \end{pmatrix}$$

$$A_{115} = Dae^{(\gamma_p-1)\sqrt{\frac{\varepsilon}{Da}}} \begin{pmatrix} 72Da^{3/2}\left(e^{\frac{\gamma_p}{2}\sqrt{\frac{\varepsilon}{Da}}} - 1\right)^3\left(e^{\frac{\gamma_p}{2}\sqrt{\frac{\varepsilon}{Da}}} + 1\right) + \left(e^{\gamma_p\sqrt{\frac{\varepsilon}{Da}}} - 1\right)^2\sqrt{\varepsilon}(\gamma_p - 1)^3 \\ -12Da\left(e^{\frac{\gamma_p}{2}\sqrt{\frac{\varepsilon}{Da}}} - 1\right)^2\left(1 + 4e^{\frac{\gamma_p}{2}\sqrt{\frac{\varepsilon}{Da}}} + e^{\gamma_p\sqrt{\frac{\varepsilon}{Da}}}\right)\sqrt{\varepsilon}\gamma_p \end{pmatrix} p_g{}^2$$

$$A_{116} = 15\left(e^{3\gamma_p\sqrt{\frac{\varepsilon}{Da}}} - 1\right) + 32\left(e^{\frac{\gamma_p}{2}\sqrt{\frac{\varepsilon}{Da}}} - e^{\frac{5\gamma_p}{2}\sqrt{\frac{\varepsilon}{Da}}}\right) + 79\left(e^{2\gamma_p\sqrt{\frac{\varepsilon}{Da}}} - e^{\gamma_p\sqrt{\frac{\varepsilon}{Da}}}\right)$$

$$A_{117} = \left(e^{\gamma_p\sqrt{\frac{\varepsilon}{Da}}} + e^{2\gamma_p\sqrt{\frac{\varepsilon}{Da}}}\right)(39 - 9\gamma_p) + (\gamma_p - 1)\left(7 + 64e^{\frac{3\gamma_p}{2}\sqrt{\frac{\varepsilon}{Da}}} + 7e^{3\gamma_p\sqrt{\frac{\varepsilon}{Da}}}\right)$$

$$A_{118} = 3\sqrt{Da}\left(e^{\gamma_p\sqrt{\frac{\varepsilon}{Da}}} - 1\right)\left(e^{\gamma_p\sqrt{\frac{\varepsilon}{Da}}} + 1\right)^2\varepsilon(\gamma_p - 2)\gamma_p - 2e^{\gamma_p\sqrt{\frac{\varepsilon}{Da}}}\left(e^{\gamma_p\sqrt{\frac{\varepsilon}{Da}}} + 1\right)\varepsilon^{3/2}(\gamma_p - 3)\gamma_p{}^2$$

$$A_{119} = \left(e^{\frac{\gamma_p}{2}\sqrt{\frac{\varepsilon}{Da}}} - 1\right)^2\left[11\left(1 + e^{\frac{3\gamma_p}{2}\sqrt{\frac{\varepsilon}{Da}}}\right) + 27\left(e^{\frac{\gamma_p}{2}\sqrt{\frac{\varepsilon}{Da}}} + e^{\gamma_p\sqrt{\frac{\varepsilon}{Da}}}\right)\right]$$

$$A_{120} = \left(e^{\gamma_p\sqrt{\frac{\varepsilon}{Da}}} + e^{2\gamma_p\sqrt{\frac{\varepsilon}{Da}}} - e^{\frac{\gamma_p}{2}\sqrt{\frac{\varepsilon}{Da}}} - e^{\frac{3\gamma_p}{2}\sqrt{\frac{\varepsilon}{Da}}}\right)\varepsilon^{3/2}(\gamma_p - 3)\gamma_p{}^2$$

$$A_{121} = 3\sqrt{Da}\left(e^{\frac{\gamma_p}{2}\sqrt{\frac{\varepsilon}{Da}}}+1\right)\varepsilon\gamma_p\left[(\gamma_p-2)\left(1+e^{\frac{\gamma_p}{2}\sqrt{\frac{\varepsilon}{Da}}}+e^{\frac{3\gamma_p}{2}\sqrt{\frac{\varepsilon}{Da}}}+e^{2\gamma_p\sqrt{\frac{\varepsilon}{Da}}}\right)+2e^{\gamma_p\sqrt{\frac{\varepsilon}{Da}}}(5\gamma_p-6)\right]$$

$$A_{122} = \left(e^{\frac{\gamma_p}{2}\sqrt{\frac{\varepsilon}{Da}}}-1\right)\sqrt{\varepsilon}\left[11(\gamma_p-1)\left(1+e^{2\gamma_p\sqrt{\frac{\varepsilon}{Da}}}\right)+e^{\frac{\gamma_p}{2}\sqrt{\frac{\varepsilon}{Da}}}(41\gamma_p-14)\right]$$

$$A_{123} = 17\left(e^{2\gamma_p\sqrt{\frac{\varepsilon}{Da}}}-1\right)+8\left(e^{\frac{3\gamma_p}{2}\sqrt{\frac{\varepsilon}{Da}}}-e^{\frac{\gamma_p}{2}\sqrt{\frac{\varepsilon}{Da}}}\right)$$

$$A_{124} = \left(e^{\frac{\gamma_p}{2}\sqrt{\frac{\varepsilon}{Da}}}-1\right)\left(e^{\frac{\gamma_p}{2}\sqrt{\frac{\varepsilon}{Da}}}+1\right)^3\varepsilon(\gamma_p-1)^4$$

$$A_{125} = \left(e^{\gamma_p\sqrt{\frac{\varepsilon}{Da}}}-1\right)\varepsilon\gamma_p\left[3(\gamma_p-2)+3e^{\gamma_p\sqrt{\frac{\varepsilon}{Da}}}(\varepsilon-2)-8e^{\frac{\gamma_p}{2}\sqrt{\frac{\varepsilon}{Da}}}(\gamma_p-1)\right]$$

$$A_{126} = \left(e^{\frac{\gamma_p}{2}\sqrt{\frac{\varepsilon}{Da}}}+1\right)^2\left(e^{\gamma_p\sqrt{\frac{\varepsilon}{Da}}}+1\right)\varepsilon^{3/2}(\gamma_p-2)(\gamma_p-1)^3\gamma_p$$

$$A_{127} = (4+29\gamma_p)\left(e^{2\gamma_p\sqrt{\frac{\varepsilon}{Da}}}+1\right)+8(4+11\gamma_p)\left(e^{\frac{\gamma_p}{2}\sqrt{\frac{\varepsilon}{Da}}}+e^{\frac{3\gamma_p}{2}\sqrt{\frac{\varepsilon}{Da}}}\right)+6e^{\gamma_p\sqrt{\frac{\varepsilon}{Da}}}(31\gamma_p-12)$$

$$A_{128} = \left(2-6\gamma_p+(\varepsilon-2){\gamma_p}^2(\gamma_p-3)\right)\left(e^{2\gamma_p\sqrt{\frac{\varepsilon}{Da}}}+1\right)+4\varepsilon(\gamma_p-3){\gamma_p}^2\left(e^{\frac{\gamma_p}{2}\sqrt{\frac{\varepsilon}{Da}}}+e^{\frac{3\gamma_p}{2}\sqrt{\frac{\varepsilon}{Da}}}\right)$$
$$+2e^{\gamma_p\sqrt{\frac{\varepsilon}{Da}}}\left(-2+6\gamma_p+(\varepsilon+2){\gamma_p}^2(\gamma_p-3)\right)$$

$$A_{129} = 8Da\left(e^{\frac{\gamma_p}{2}\sqrt{\frac{\varepsilon}{Da}}}-1\right)^2-4\sqrt{Da}\left(e^{\gamma_p\sqrt{\frac{\varepsilon}{Da}}}-1\right)\sqrt{\varepsilon}(\gamma_p-1)+\left(e^{\gamma_p\sqrt{\frac{\varepsilon}{Da}}}+1\right)(\gamma_p-1)^2$$

$$A_{130} = 15\left(e^{\gamma_p\sqrt{\frac{\varepsilon}{Da}}}+1\right)(\gamma_p-1)^6{p_g}^2$$

$$A_{131} = Da\left(e^{\gamma_p\sqrt{\frac{\varepsilon}{Da}}}-1\right)^2-\sqrt{Da}\left(e^{2\gamma_p\sqrt{\frac{\varepsilon}{Da}}}-1\right)\sqrt{\varepsilon}\gamma_p+e^{\gamma_p\sqrt{\frac{\varepsilon}{Da}}}\varepsilon{\gamma_p}^2$$

$$A_{132} = 6Da\left(e^{\frac{\gamma_p}{2}\sqrt{\frac{\varepsilon}{Da}}}-1\right)\left(e^{\frac{\gamma_p}{2}\sqrt{\frac{\varepsilon}{Da}}}+1\right)^2 - 2\sqrt{Da}\left(1+2e^{\frac{\gamma_p}{2}\sqrt{\frac{\varepsilon}{Da}}}+2e^{\gamma_p\sqrt{\frac{\varepsilon}{Da}}}+e^{\frac{3\gamma_p}{2}\sqrt{\frac{\varepsilon}{Da}}}\right)\sqrt{\varepsilon}\gamma_p$$
$$+e^{\frac{\gamma_p}{2}\sqrt{\frac{\varepsilon}{Da}}}\left(e^{\frac{\gamma_p}{2}\sqrt{\frac{\varepsilon}{Da}}}-1\right)\varepsilon{\gamma_p}^2$$

$$A_{133} = 144Da^{3/2}\left(e^{\gamma_p\sqrt{\frac{\varepsilon}{Da}}}-1\right)\eta\gamma_p$$

$$A_{134} = \left(1+e^{\gamma_p\sqrt{\frac{\varepsilon}{Da}}}+2e^{\frac{\gamma_p}{2}\sqrt{\frac{\varepsilon}{Da}}}\right)\begin{pmatrix}4\gamma_p(1-\eta)-1-6{\gamma_p}^2(1-2\eta)\\+4{\gamma_p}^3(1-3\eta)+{\gamma_p}^4(4\eta-1)-24Da\eta{\gamma_p}^2\end{pmatrix}-48Da\eta{\gamma_p}^2e^{\frac{\gamma_p}{2}\sqrt{\frac{\varepsilon}{Da}}}$$

$$A_{135} = -24Da^{3/2}\left(e^{\gamma_p\sqrt{\frac{\varepsilon}{Da}}}-1\right)+12Da\sqrt{\varepsilon}\left(1+e^{\gamma_p\sqrt{\frac{\varepsilon}{Da}}}+2e^{\frac{\gamma_p}{2}\sqrt{\frac{\varepsilon}{Da}}}(\gamma_p-1)\right)$$
$$-\left(e^{\gamma_p\sqrt{\frac{\varepsilon}{Da}}}+1\right)\sqrt{\varepsilon}(\gamma_p-1)^3$$

$$A_{136} = 8Da\left(e^{\frac{\gamma_p}{2}\sqrt{\frac{\varepsilon}{Da}}}-1\right)^2 - 4\sqrt{Da}\left(e^{\gamma_p\sqrt{\frac{\varepsilon}{Da}}}-1\right)\sqrt{\varepsilon}(\gamma_p-1)+\left(1+e^{\gamma_p\sqrt{\frac{\varepsilon}{Da}}}\right)(\gamma_p-1)^2$$

$$A_{137} = \left(e^{\gamma_p\sqrt{\frac{\varepsilon}{Da}}}-1\right)\left(24Da^{3/2}-6\sqrt{Da}\varepsilon(\gamma_p-1)^2\right)+\left(e^{\gamma_p\sqrt{\frac{\varepsilon}{Da}}}+1\right)\sqrt{\varepsilon}(\gamma_p-1)^3$$
$$+12Da\sqrt{\varepsilon}\left((\gamma_p-2)\left(e^{\gamma_p\sqrt{\frac{\varepsilon}{Da}}}+1\right)-4e^{\frac{\gamma_p}{2}\sqrt{\frac{\varepsilon}{Da}}}(\gamma_p-1)\right)$$

$$A_{138} = 8Da\left(e^{\frac{\gamma_p}{2}\sqrt{\frac{\varepsilon}{Da}}}-1\right)^2 - (\gamma_p-1)\left(4\sqrt{Da}\left(e^{\gamma_p\sqrt{\frac{\varepsilon}{Da}}}-1\right)\sqrt{\varepsilon}+\left(1+e^{\gamma_p\sqrt{\frac{\varepsilon}{Da}}}\right)(\gamma_p-1)\right)$$

$$A_{139} = 192Da^2\left(e^{\frac{\gamma_p}{2}\sqrt{\frac{\varepsilon}{Da}}}-1\right)^2\eta - 96Da^{3/2}\left(e^{\gamma_p\sqrt{\frac{\varepsilon}{Da}}}-1\right)\sqrt{\varepsilon}\eta(\gamma_p-1)$$

$$A_{140} = \left(e^{\gamma_p\sqrt{\frac{\varepsilon}{Da}}}+1\right)\varepsilon\left(-1-4(\eta(1+12Da)-1)\gamma_p+6(2\eta(1+2Da)-1){\gamma_p}^2\right.$$
$$\left.+(4-12\eta){\gamma_p}^3+(4\eta-1){\gamma_p}^4\right.$$

$$A_{141} = -12Dae^{\frac{(1+2\gamma_p)}{2}\sqrt{\frac{\varepsilon}{Da}}}\left(e^{\frac{\gamma_p}{2}\sqrt{\frac{\varepsilon}{Da}}}-1\right)\left(2\sqrt{Da}\left(e^{\frac{\gamma_p}{2}\sqrt{\frac{\varepsilon}{Da}}}-1\right)-\left(e^{\frac{\gamma_p}{2}\sqrt{\frac{\varepsilon}{Da}}}+1\right)\sqrt{\varepsilon}(\gamma_p-1)\right)$$

$$A_{142} = 16Da\left(e^{\frac{\gamma_p}{2}\sqrt{\frac{\varepsilon}{Da}}}-1\right)^2\left(e^{\gamma_p\sqrt{\frac{\varepsilon}{Da}}}+1\right)$$

$$A_{143} = -2\sqrt{Da}\left(e^{\gamma_p\sqrt{\frac{\varepsilon}{Da}}}-1\right)\sqrt{\varepsilon}\left(3(\gamma_p-1)\left(1+e^{\gamma_p\sqrt{\frac{\varepsilon}{Da}}}\right)+2\gamma_p e^{\frac{\gamma_p}{2}\sqrt{\frac{\varepsilon}{Da}}}\right)$$

$$A_{144} = \varepsilon\gamma_p\left((\gamma_p-2)\left(1+e^{2\gamma_p\sqrt{\frac{\varepsilon}{Da}}}\right)+e^{\gamma_p\sqrt{\frac{\varepsilon}{Da}}}(6\gamma_p-8)\right)$$

$$A_{145} = 96Da^{5/2}e^{\frac{(1+2\gamma_p)}{2}\sqrt{\frac{\varepsilon}{Da}}}\left(e^{\frac{\gamma_p}{2}\sqrt{\frac{\varepsilon}{Da}}}-1\right)^2\left(9+9e^{\gamma_p\sqrt{\frac{\varepsilon}{Da}}}+2e^{\frac{\gamma_p}{2}\sqrt{\frac{\varepsilon}{Da}}}\right)$$

$$A_{146} = -4\sqrt{Da}e^{\frac{1+2\gamma_p}{2}\sqrt{\frac{\varepsilon}{Da}}}\left(e^{\gamma_p\sqrt{\frac{\varepsilon}{Da}}}-1\right)^2\varepsilon(\gamma_p-1)^4$$

$$A_{147} = -\varepsilon^{3/2}\gamma_p(\gamma_p-2)(\gamma_p-1)^3\left(e^{\left(\frac{1+2\gamma_p}{2}\right)\sqrt{\frac{\varepsilon}{Da}}}-e^{\left(\frac{1+6\gamma_p}{2}\right)\sqrt{\frac{\varepsilon}{Da}}}\right)$$

$$A_{148} = 24Da^{3/2}e^{\left(\frac{1+2\gamma_p}{2}\right)\sqrt{\frac{\varepsilon}{Da}}}\left(e^{\frac{\gamma_p}{2}\sqrt{\frac{\varepsilon}{Da}}}\right)^2\varepsilon\gamma_p\left((\gamma_p-2)\left(1+e^{\gamma_p\sqrt{\frac{\varepsilon}{Da}}}\right)-2e^{\gamma_p\sqrt{\frac{\varepsilon}{Da}}}(\gamma_p-1)\right)$$

$$A_{149} = -48Da^2e^{\left(\frac{1+2\gamma_p}{2}\right)\sqrt{\frac{\varepsilon}{Da}}}\left(e^{\gamma_p\sqrt{\frac{\varepsilon}{Da}}}-1\right)\sqrt{\varepsilon}\left((3\gamma_p+1)\left(1+e^{\gamma_p\sqrt{\frac{\varepsilon}{Da}}}\right)+e^{\frac{\gamma_p}{2}\sqrt{\frac{\varepsilon}{Da}}}(4\gamma_p-2)\right)$$

$$A_{150} = -4Dae^{\left(\frac{1+2\gamma_p}{2}\right)\sqrt{\frac{\varepsilon}{Da}}}\left(e^{\gamma_p\sqrt{\frac{\varepsilon}{Da}}}-1\right)\sqrt{\varepsilon}\begin{pmatrix}2+4e^{\frac{\gamma_p}{2}\sqrt{\frac{\varepsilon}{Da}}}(\gamma_p-1)^3-2\gamma_p(3-3\gamma_p+{\gamma_p}^2)\\-\varepsilon{\gamma_p}^2(3-\gamma_p)+e^{\gamma_p\sqrt{\frac{\varepsilon}{Da}}}\begin{pmatrix}2-6\gamma_p\\-(\varepsilon-2){\gamma_p}^2(3-\gamma_p)\end{pmatrix}\end{pmatrix}$$

$$A_{151} = -12{U_i}^2\begin{pmatrix}-\sqrt{Da}\left(e^{2\gamma_p\sqrt{\frac{\varepsilon}{Da}}}-1\right)(1+\varepsilon)-2e^{\gamma_p\sqrt{\frac{\varepsilon}{Da}}}(\varepsilon-1)\sqrt{\varepsilon}\gamma_p\\+24U_iDa\left(e^{\frac{\gamma_p}{2}\sqrt{\frac{\varepsilon}{Da}}}-1\right)^2(\varepsilon-1)\left(\sqrt{Da}\left(e^{\gamma_p\sqrt{\frac{\varepsilon}{Da}}}-1\right)-e^{\frac{\gamma_p}{2}\sqrt{\frac{\varepsilon}{Da}}}\sqrt{\varepsilon}\gamma_p\right)p_g\end{pmatrix}$$

$$A_{152} = Da\begin{pmatrix} -24Da^{3/2}\left(e^{\frac{\gamma_p}{2}\sqrt{\frac{\varepsilon}{Da}}}-1\right)^3\left(e^{\frac{\gamma_p}{2}\sqrt{\frac{\varepsilon}{Da}}}+1\right)(\varepsilon-3)+\left(e^{\gamma_p\sqrt{\frac{\varepsilon}{Da}}}-1\right)^2 \\ -12Da\left(e^{\frac{\gamma_p}{2}\sqrt{\frac{\varepsilon}{Da}}}-1\right)^2\left(1+e^{\gamma_p\sqrt{\frac{\varepsilon}{Da}}}-2e^{\frac{\gamma_p}{2}\sqrt{\frac{\varepsilon}{Da}}}(\varepsilon-2)\right)\sqrt{\varepsilon}\gamma_p \end{pmatrix} {p_g}^2$$

$$A_{153} = 15(1+\varepsilon)\left(1+e^{2\gamma_p\sqrt{\frac{\varepsilon}{Da}}}\right)-2(\varepsilon-47)e^{\gamma_p\sqrt{\frac{\varepsilon}{Da}}}-32(1+\varepsilon)\left(e^{\frac{\gamma_p}{2}\sqrt{\frac{\varepsilon}{Da}}}+e^{\frac{3\gamma_p}{2}\sqrt{\frac{\varepsilon}{Da}}}\right)$$

$$A_{154} = e^{\frac{(2+3\gamma_p)}{2}\sqrt{\frac{\varepsilon}{Da}}}\left(e^{\gamma_p\sqrt{\frac{\varepsilon}{Da}}}-1\right)\left(e^{\gamma_p\sqrt{\frac{\varepsilon}{Da}}}+1\right)^2\varepsilon(1+\varepsilon)(\gamma_p-2)\gamma_p$$

$$A_{155} = 2\left(e^{\frac{(2+5\gamma_p)}{2}\sqrt{\frac{\varepsilon}{Da}}}+e^{\frac{(2+7\gamma_p)}{2}\sqrt{\frac{\varepsilon}{Da}}}\right)(\varepsilon-1)\varepsilon^{3/2}(\gamma_p-3){\gamma_p}^2$$

$$A_{156} = 2Dae^{\frac{(2+3\gamma_p)}{2}\sqrt{\frac{\varepsilon}{Da}}}\sqrt{\varepsilon}\begin{bmatrix} 32e^{\frac{3\gamma_p}{2}\sqrt{\frac{\varepsilon}{Da}}}(\varepsilon-2)(\gamma_p-1)-7(\varepsilon+1)(\gamma_p-1)\left(1+e^{3\gamma_p\sqrt{\frac{\varepsilon}{Da}}}\right) \\ +\left(9\gamma_p-39+9\varepsilon(\gamma_p+1)\right)\left(e^{\gamma_p\sqrt{\frac{\varepsilon}{Da}}}+e^{2\gamma_p\sqrt{\frac{\varepsilon}{Da}}}\right) \end{bmatrix}$$

$$A_{157} = 6Da^{3/2}e^{\sqrt{\frac{\varepsilon}{Da}}}\left(e^{\frac{\gamma_p}{2}\sqrt{\frac{\varepsilon}{Da}}}+1\right)\left(e^{\gamma_p\sqrt{\frac{\varepsilon}{Da}}}-e^{\frac{\gamma_p}{2}\sqrt{\frac{\varepsilon}{Da}}}\right)^3\left(5\varepsilon-11-16e^{\frac{\gamma_p}{2}\sqrt{\frac{\varepsilon}{Da}}}+e^{\gamma_p\sqrt{\frac{\varepsilon}{Da}}}(5\varepsilon-11)\right)$$

$$A_{158} = e^{(1+2\gamma_p)\sqrt{\frac{\varepsilon}{Da}}}\left(e^{\frac{\gamma_p}{2}\sqrt{\frac{\varepsilon}{Da}}}-1\right)^2\left(e^{\gamma_p\sqrt{\frac{\varepsilon}{Da}}}+1\right)(\varepsilon-1)\varepsilon^{3/2}(\gamma_p-3){\gamma_p}^2$$

$$A_{159} = \left(e^{\frac{(2+7\gamma_p)}{2}\sqrt{\frac{\varepsilon}{Da}}}+e^{\frac{(2+5\gamma_p)}{2}\sqrt{\frac{\varepsilon}{Da}}}\right)\left(9\gamma_p-10-\varepsilon(\gamma_p-2)\right)-(\varepsilon-1)(\gamma_p-2)\begin{pmatrix} e^{\frac{(2+3\gamma_p)}{2}\sqrt{\frac{\varepsilon}{Da}}} \\ -e^{\frac{(2+9\gamma_p)}{2}\sqrt{\frac{\varepsilon}{Da}}} \end{pmatrix}$$
$$+(\varepsilon+1)(\gamma_p-2)\left(e^{(1+2\gamma_p)\sqrt{\frac{\varepsilon}{Da}}}-e^{(1+4\gamma_p)\sqrt{\frac{\varepsilon}{Da}}}\right)$$

$$A_{160} = -(7\varepsilon - 11)(\gamma_p - 1)\left(e^{\frac{(2+3\gamma_p)}{2}\sqrt{\frac{\varepsilon}{Da}}} + e^{\frac{(2+9\gamma_p)}{2}\sqrt{\frac{\varepsilon}{Da}}} \right) + \left(23\gamma_p - 53 + \varepsilon(25 - 7\gamma_p)\right)\left(e^{\frac{(2+5\gamma_p)}{2}\sqrt{\frac{\varepsilon}{Da}}} + e^{\frac{(2+7\gamma_p)}{2}\sqrt{\frac{\varepsilon}{Da}}} \right)$$

$$+ \left(19\gamma_p + 8 + \varepsilon(7\gamma_p - 16)\right)\left(e^{(1+2\gamma_p)\sqrt{\frac{\varepsilon}{Da}}} + e^{(1+4\gamma_p)\sqrt{\frac{\varepsilon}{Da}}} \right) + 2e^{(1+3\gamma_p)\sqrt{\frac{\varepsilon}{Da}}}\left(56 - 53\gamma_p + \varepsilon(7\gamma_p - 16)\right)$$

$$A_{161} = e^{\sqrt{\frac{\varepsilon}{Da}}}\left(1 + e^{\frac{\gamma_p}{2}\sqrt{\frac{\varepsilon}{Da}}} \right)\left(e^{\gamma_p\sqrt{\frac{\varepsilon}{Da}}} - e^{\frac{\gamma_p}{2}\sqrt{\frac{\varepsilon}{Da}}} \right)\left((11\varepsilon - 85)\left(1 + e^{\gamma_p\sqrt{\frac{\varepsilon}{Da}}} \right) + 8e^{\frac{\gamma_p}{2}\sqrt{\frac{\varepsilon}{Da}}}(\varepsilon - 5) \right)$$

$$A_{162} = e^{\frac{(2+3\gamma_p)}{2}\sqrt{\frac{\varepsilon}{Da}}}\left(e^{\gamma_p\sqrt{\frac{\varepsilon}{Da}}} - 1 \right)^3 \varepsilon(\gamma_p - 1)^4$$

$$A_{163} = e^{\frac{(2+3\gamma_p)}{2}\sqrt{\frac{\varepsilon}{Da}}}\left(e^{\gamma_p\sqrt{\frac{\varepsilon}{Da}}} - 1 \right)^2\left(e^{\gamma_p\sqrt{\frac{\varepsilon}{Da}}} + 1 \right)\varepsilon^{3/2}(\gamma_p - 2)(\gamma_p - 1)^3\gamma_p$$

$$A_{164} = (\varepsilon - 3)(\gamma_p - 2)\left(e^{\frac{(2+9\gamma_p)}{2}\sqrt{\frac{\varepsilon}{Da}}} - e^{\frac{(2+3\gamma_p)}{2}\sqrt{\frac{\varepsilon}{Da}}} \right) + \left(22 - 19\gamma_p + \varepsilon(\gamma_p - 2)\right)\left(e^{\frac{(2+7\gamma_p)}{2}\sqrt{\frac{\varepsilon}{Da}}} - e^{\frac{(2+5\gamma_p)}{2}\sqrt{\frac{\varepsilon}{Da}}} \right)$$

$$+ 2\left(10 - 7\gamma_p + \varepsilon(\gamma_p - 2)\right)\left(e^{(1+2\gamma_p)\sqrt{\frac{\varepsilon}{Da}}} + e^{(1+4\gamma_p)\sqrt{\frac{\varepsilon}{Da}}} \right)$$

$$A_{165} = \left(6\gamma_p - 2 + 3(\varepsilon - 2){\gamma_p}^2 - (\varepsilon - 2){\gamma_p}^3\right)\left(e^{\frac{(2+3\gamma_p)}{2}\sqrt{\frac{\varepsilon}{Da}}} + e^{\frac{(2+9\gamma_p)}{2}\sqrt{\frac{\varepsilon}{Da}}} \right)$$

$$+ \left(2 - 6\gamma_p + 3(2 - 5\varepsilon + 4\varepsilon^2){\gamma_p}^2 + (5\varepsilon - 2 - 4\varepsilon^2){\gamma_p}^3\right)\left(e^{\frac{(2+5\gamma_p)}{2}\sqrt{\frac{\varepsilon}{Da}}} + e^{\frac{(2+7\gamma_p)}{2}\sqrt{\frac{\varepsilon}{Da}}} \right)$$

$$+ 2\left(2 - 6\gamma_p + (6 + 3\varepsilon - 3\varepsilon^2){\gamma_p}^2 + (\varepsilon^2 - \varepsilon - 2){\gamma_p}^3\right)\left(e^{(1+2\gamma_p)\sqrt{\frac{\varepsilon}{Da}}} + e^{(1+4\gamma_p)\sqrt{\frac{\varepsilon}{Da}}} \right)$$

$$+ 4e^{(1+3\gamma_p)\sqrt{\frac{\varepsilon}{Da}}}\left(6\gamma_p - 2 + (2 - \varepsilon + \varepsilon^2){\gamma_p}^2\left(\gamma_p - 3\right)\right)$$

$$A_{166} = 6\left(5\gamma_p + 4 + \varepsilon(\gamma_p - 4)\right)\left(e^{(1+2\gamma_p)\sqrt{\frac{\varepsilon}{Da}}} + e^{(1+4\gamma_p)\sqrt{\frac{\varepsilon}{Da}}} \right) - 3\left(5\gamma_p + 4 + \varepsilon(\gamma_p - 4)\right)\left(e^{\frac{(2+5\gamma_p)}{2}\sqrt{\frac{\varepsilon}{Da}}} + e^{\frac{(2+7\gamma_p)}{2}\sqrt{\frac{\varepsilon}{Da}}} \right)$$

$$+ e^{\frac{(2+3\gamma_p)}{2}\sqrt{\frac{\varepsilon}{Da}}}\left(29\gamma_p + 4 + \varepsilon(4 - 7\gamma_p)\right) + 4e^{(1+3\gamma_p)\sqrt{\frac{\varepsilon}{Da}}}\left(52 - 49\gamma_p + \varepsilon(11\gamma_p - 20)\right)$$

$$A_{167} = Da\left(e^{\gamma_p\sqrt{\frac{\varepsilon}{Da}}}-1\right)^2(\varepsilon+1)-\sqrt{Da}\left(e^{2\gamma_p\sqrt{\frac{\varepsilon}{Da}}}-1\right)(\varepsilon+1)\sqrt{\varepsilon}\gamma_p-(\varepsilon-1)e^{\gamma_p\sqrt{\frac{\varepsilon}{Da}}}{\gamma_p}^2$$

$$A_{168} = 2Da\left(e^{\frac{\gamma_p}{2}\sqrt{\frac{\varepsilon}{Da}}}-1\right)\left(e^{\frac{\gamma_p}{2}\sqrt{\frac{\varepsilon}{Da}}}+1\right)^2(\varepsilon-3)+2\sqrt{Da}\left(\begin{array}{l}e^{\frac{\gamma_p}{2}\sqrt{\frac{\varepsilon}{Da}}}(\varepsilon-1)\\+(\varepsilon+1)\left(1-e^{\frac{\gamma_p}{2}\sqrt{\frac{\varepsilon}{Da}}}\right)\end{array}\right)\gamma_p$$
$$+e^{\frac{\gamma_p}{2}\sqrt{\frac{\varepsilon}{Da}}}\left(e^{\frac{\gamma_p}{2}\sqrt{\frac{\varepsilon}{Da}}}-1\right)(\varepsilon-1)\varepsilon{\gamma_p}^2$$

$$A_{169} = Da^{3/2}\eta\gamma_p\left(e^{\gamma_p\sqrt{\frac{\varepsilon}{Da}}}-1\right)(48\varepsilon-144)-48Dae^{\frac{\gamma_p}{2}\sqrt{\frac{\varepsilon}{Da}}}\varepsilon^{3/2}\eta{\gamma_p}^2+\sqrt{\varepsilon}$$

$$A_{170} = 2Da\left(e^{\frac{\gamma_p}{2}\sqrt{\frac{\varepsilon}{Da}}}-1\right)\left(e^{\frac{\gamma_p}{2}\sqrt{\frac{\varepsilon}{Da}}}+1\right)^2(\varepsilon-3)-2\sqrt{Da}\left(e^{\frac{\gamma_p}{2}\sqrt{\frac{\varepsilon}{Da}}}+1\right)\sqrt{\varepsilon}\left(\begin{array}{l}\left(1+e^{\gamma_p\sqrt{\frac{\varepsilon}{Da}}}\right)(\varepsilon-1)\\-(\varepsilon+1)e^{\frac{\gamma_p}{2}\sqrt{\frac{\varepsilon}{Da}}}\end{array}\right)\gamma_p$$
$$+e^{\frac{\gamma_p}{2}\sqrt{\frac{\varepsilon}{Da}}}\left(e^{\frac{\gamma_p}{2}\sqrt{\frac{\varepsilon}{Da}}}-1\right)(\varepsilon-1)\varepsilon{\gamma_p}^2$$

List of Published Papers

1. D. Bhargavi and J. Sharath Kumar Reddy, "**Analytical Investigation of Laminar Forced Convection with Viscous Dissipation In Parallel Plate Channels Partially Filled With Porous Material: Constant Wall Heat Flux** ", Published in *Special Topics and Reviews in Porous Media: International Journal*, Volume 8, Issue 1, pp. 1-16, 2017.

2. D. Bhargavi and J. Sharath Kumar Reddy, "**Effect of Heat Transfer in the Thermally Developing Region of the Channel Partially Filled with a Porous Medium: Constant Wall Heat Flux**", *Published in International Journal of Thermal Sciences* , Volume 130, pp. 484-495, 2018.

3. D. Bhargavi and J. Sharath Kumar Reddy, "**Analytical Study of Forced Convection In a Channel Partially Filled with a Porous Material with Effect of Magnetic Field: Constant Wall Heat Flux**" *Published in Special Topics and Reviews in Porous Media: International Journal*, Volume 9, pp. 201-216, 2018.

4. D. Bhargavi and J. Sharath Kumar Reddy, "**Analytical Investigation of Laminar Forced Convection with Viscous Dissipation in Parallel Plate Channels Partially Filled with a Porous Material: Constant Wall Heat Flux**", *Published in Journal of Nanofluids*, Volume 8, pp. 1-14, 2019.

5. J. Sharath Kumar Reddy and D. Bhargavi, "**Couette Flow and Heat Transfer in a Channel Partially Filled with Porous Material: Constant Wall Heat Flux**", *Published in International Journal of Pure and Applied Mathematics*, Volume 113, issue 9, pp. 148-156, 2017.

6. J. Sharath Kumar Reddy and D. Bhargavi, "**Numerical Study of Fluid Flow in a Channel Partially Filled with Porous Medium with Darcy Brinkman Forchheimer Equation**" *Published in Special Topics and Reviews in Porous Media: International Journal*, Volume 9, pp. 301-312, 2018.

7. J. Sharath Kumar Reddy and D. Bhargavi, "**Analytical Study of Fluid Flow in a Channel Partially Filled with Porous Medium with Darcy-Brinkman Equation**", **Published in Lecture Notes in mechanical Engineering**, **NHTFF** Book, pp. 489-496, 2018.

List of Communicated Papers

8. J.Sharath Kumar Reddy and D.Bhargavi, **"Analytical Study of Laminar Forced Convection in Parallel Plate Channels Partially Filled with Porous Material with Viscous Dissipation at the Conduction Limit",** Communicated *to International Journal of Heat and Technology*.

9. J. Sharath Kumar Reddy and D. Bhargavi, "**Effect of Axial Conduction in the Thermally Developing Region of the Channel Partially Filled with a Porous Medium: Constant Wall Heat Flux ",** Communicated to *International Information and Engineering Technology Association*.

10. D.Bhargavi and J.Sharath Kumar Reddy "**Effect of Axial Conduction and Viscous dissipation in the Thermally Developing Region of the Parallel Plate Channel Partially Filled with a Porous medium: Constant Wall Heat Flux",** Yet to Communicate.